Ventilation Control and Ventilation Performance of Multi-zone Air Conditioning Systems

Sun Zhongwei

A thesis submitted in partial fulfillment of the requirements for the Degree of Doctor of Philosophy

Department of Building Services Engineering

The Hong Kong Polytechnic University

2010

CERTIFICATE OF ORIGINALITY

I hereby declare that this thesis is my own work and that, to the best of my knowledge and belief, it reproduces no material previously published or written, nor material that has been accepted for the award of any other degree or diploma, except where due acknowledgement has been made in the text.

Signature: _____

Name: Sun Zhongwei

Department of Building Services Engineering

The Hong Kong Polytechnic University

Hong Kong, China

August 2010

ABSTRACT

Abstract of thesis entitled: Ventilation Control and Ventilation performance of Multi-zone Air Conditioning Systems

Submitted by : Sun Zhongwei

For the degree of : Doctor of Philosophy

at The Hong Kong Polytechnic University in August, 2010.

The indoor air quality (IAQ) and energy consumption of buildings have received increasing concern over the last twenty years. The optimal ventilation control of multi-zone VAV Air-conditioning (HVAC) systems provides great potential in reducing energy consumption while ensuring acceptable IAQ and satisfactory thermal comfort. In the last two decades, a number of ventilation control strategies with different degrees of promise have been developed for multi-zone air-conditioning systems. However, most of them cannot always maintain satisfying ventilation performance due to variable indoor thermal comfort and pollution sources of different ventilation zones. Another important issue is that the modeling of the space ventilation usually uses perfect mixing models in conventional dynamic ventilation simulations to test and evaluate the control of air-conditioning systems. However, the complete-mixing air model fails to consider the impact of non-uniform air temperature stratifications on the ventilation performance.

Therefore, the aim of this study is to develop an online ventilation optimal control strategies for multi-zone air-conditioning systems to minimize the overall system

energy consumption while maintaining satisfactory IAQ. A CFD-based virtual ventilation test system is also developed to evaluate the dynamic ventilation performance by taking account of indoor air stratification phenomena using a CFD-based space temperature offset model. The aim is achieved through addressing the following objectives. (1) Develop a CO_2-based adaptive Demand Controlled Ventilation (DCV) strategy, (2) Develop an indoor air temperature set point reset strategy for critical zones, (3) Develop a model-based indoor air temperature set point resetting strategy for critical zones, and (4) Develop a model-based outdoor air flow rate optimal control strategy for a full air system with primary air handling units. In addition, a CFD-based ventilation test method is developed to test the indoor air ventilation performance in a simulated environment.

The CO_2-based adaptive DCV strategy and the indoor air temperature reset strategy are developed to optimize the outdoor air flow rate to satisfy the coincident ventilation and thermal load requirements of different zones. The DCV strategy is further implemented and validated using an independent Intelligent Building Management and Integration platform (IBmanager) in a super high-rise building in Hong Kong by comparing with the original fixed outdoor air flow rate control strategy. Both the site tests and simulation tests showed that this DCV strategy can help to reduce the system energy cost while still maintaining acceptable indoor air quality.

The model-based indoor air temperature set point resetting strategy for critical zones is developed to reduce the unbalance among the required outdoor air fractions of all

the zones and to further optimize the indoor air temperature set point of the critical zones. The thermal comfort, indoor air quality and total energy consumption are considered simultaneously. The indoor air temperature set point is optimized using the Genetic Algorithm (GA) based on the trade-offs among the indoor air CO_2 concentration, index of predicted mean vote (PMV) and total system energy consumption in the format of a system response-based cost function.

The model-based outdoor air flow rate optimal control strategy is developed to reduce the system energy consumption and to optimize the outdoor air flow rate for the full air system with a primary air handling unit. The energy consumption of the primary fan and the energy consumption for cooling outdoor air are considered simultaneously. The outdoor air flow rate set point is optimized based on the trade-offs among the energy consumption of the primary fan and the energy consumption for cooling outdoor air in the system response-based cost function.

A simulation package developed on the Transient Simulation Program (TRNSYS) is used as the simulation platform to validate and evaluate the performance of the proposed different ventilation optimal control strategies. The test results showed that about 1.01%~17.7% energy in the system under investigation can be saved when using these optimal control strategies when compared with the conventional ventilation control strategies.

The CFD-based virtual ventilation test method is developed for control and optimization of the indoor environment by combining a ventilated room with a ventilation control system. It is demonstrated to be a feasible evaluation tool for the

ventilation systems for investigating the ventilation control performance in a simulated environment. A data-based space temperature offset model is developed using the data generated by the CFD model and then used as a virtual temperature sensor in the CFD-based virtual test method. The validated virtual sensor is used to compensate the air temperature non-uniform stratification in occupied rooms and improve thermal comfort in a mechanical ventilated room efficiently.

Keywords: Ventilation control; demand-controlled ventilation; adaptive control; critical zone identification; occupancy detection; optimal control; genetic algorithm; building automation systems; computational fluid dynamics.

PUBLICATIONS ARISING FROM THIS STUDY

Journal papers

Zhongwei Sun, Shengwei Wang. A CFD-based test method for control of indoor environment and space ventilation. Building and Environment, 45, (3), 2010, pp: 1441-1447.

Zhongwei Sun, Shengwei Wang, Qulan Zhou, Shi'en Hui. Experimental study on desulfurization efficiency and gas-liquid mass transfer in a new liquid-screen desulfurization system. Applied Energy, 87, (5), 2010, pp: 1505-1512.

Zhongwei Sun, Shengwei Wang and Zhenjun Ma. In-situ implementation and Validation of a CO_2-based Adaptive demand-controlled ventilation strategy in a Multi-zone Office Building. Building and Environment, 46, (3), 2011, pp: 124-133.

Xinhua Xu, Shengwei Wang, Zhongwei Sun, Fu Xiao. A model-based optimal ventilation control strategy of multi-zone VAV air-conditioning systems. Applied Thermal Engineering, 29, (1), 2009, pp: 91-104.

Conference papers

Zhongwei Sun, Shengwei Wang, Fu Xiao. Modeling indoor temperature stratification dynamics in a ventilated room using a simplified physical model, The 6th International Symposium on Heating, Ventilating and Air Conditioning (ISHVAC09), Nanjing, China, 2009.

Zhongwei Sun, Shengwei Wang, Fu Xiao. Determination of CO_2 concentration

stratification in a ventilated room using a simplified physical model based on CFD simulation, The 1st International Postgraduate Conference on Infrastructure and Environment, Hong Kong, China, 2009.

Zhongwei Sun, Shengwei Wang, Qulan Zhou, Shi'en Hui. Gas-liquid flow characteristics and desulfurization mass transfer performance in a liquid-screen fuel gas desulfurizing tower, International Conference on Applied Energy, Singapore, 2010.

Submitted

Zhongwei Sun and Shengwei Wang, Model-based optimal control of outdoor air flow rate of an Air-Conditioning system with primary air handling unit, submitted to <*Indoor and Built Environment*>.

Zhongwei Sun, Shengwei Wang and Gongsheng Huang. A model-based Set Point Scheme for Space Temperature Control of Improved Accuracy and Thermal Comfort, submitted to <*Building Services Engineering Research and Technology*>.

ACKNOWLEDGEMENTS

First and foremost, I wish to express my greatest gratitude and appreciation to my Chief Supervisor, Chair Professor Wang Shengwei. Without his continuous guidance, encouragements and supports during the entire course of my research work, the thesis would not be finished.

I would like to express my deepest appreciations to my Co-Supervisor Dr. Linda Xiao Fu for her invaluable assistance and constant encouragement, not only in my study, but also in my life.

I further express my appreciations to my colleagues in the Building Automation and Energy Management research group for their company and support throughout the PhD study.

My heartfelt appreciation goes to my beloved parents, for their unconditional love, supports, understanding and encouragements.

Finally I want to thank everyone who directly or indirectly offered his/her help and support to this thesis.

TABLE OF CONTENTS

LIST OF FIGURES

LIST OF TABLES

NOMENCLATURE

Symbols	Description	Unit
M	Air mass flow rate	kg/s
C	CO_2 concentration	ppm
V	Air volume flow rate	m^3/s
G	Moisture generation rate	kg/s
S	CO_2 generation rate	m^3/s
Q	Indoor air sensible heat change	kJ/s
D	Indoor air humidity change	kg/s
Cp	Heat capacity	J/(kg K)
m	Supply air mass exchange	kg/s
v	Supply air volume exchange	m^3/s
$\Gamma_{\Phi,eff}$	Effective coefficient	kg/(m s)
P	Air pressure in each zone	Pa
ρ	Air density of zone	kg/m^3
C_d	Coefficient of power law	ND
A	Area of the interface boundary	m^2
S_Φ	Source term of the general flow property	ND
T	Temperature of zone	℃
R	Gas constant of air	J/(mol K)
Eac	Air change effectiveness	ND

R_P	Target outdoor air requirements per person	$m^3/(s\ p)$
R_b	Target outdoor air requirements per unit area	$m^3/(s\ m^2)$
X	Uncorrected outdoor air fraction	
Z	Required greatest outdoor air fraction	
Y	Corrected outdoor air fraction	
$U_{Aa,T}$	Sensible heat transfer coefficient at air side	kW/℃
$U_{Aa,h}$	Mass transfer coefficient at air side	kg/s
U_{Aw}	heat transfer coefficient at water side	kW/℃
T_b	Equivalent coil surface temperature	℃
h	Enthalpy	kJ/kg
h_b	Saturated air enthalpy	kJ/kg
G_b	Saturated air moisture content	kg/kg
W	Power input	kW
U_{PID}	PID control output of the space temperature controller	
Kp	Proportional gain	
$\hat{Y}$	Output of the model	
e	Model error	
COP	Coefficient of performance including the pump and the chiller	ND
C_f	Dimensionless flow coefficient	ND
Ch	Dimensionless pressure coefficient	ND
RVS	Rotational speed	n/s

D	Diameter of blades	m
C_η	Fan efficiency	ND
P_{rise}	Pressure head of fan.	Pa
N_{floor}	Number of floors	
$\Gamma_{\Phi,eff}$	Effective coefficient	kg/(m s)
S_Φ	Source term of the general flow property	ND
G_k	Generation of turbulence kinetic energy due to the mean velocity gradients	kg/(m s^3)
G_b	Generation of turbulence kinetic energy due to buoyancy	kg/(m s^3)
ω	Parameter	
$S\kappa$, $S\varepsilon$	User-defined source terms	
f_{off}	Nonlinear function	
ΔT_{of}	Temperature offset	℃
y	True value of the measured temperature	℃
y'	Measured value of the variable	
T_c	Time constant.	
T_i	Integral time	

T_d	Derivative time	
U_k	Output of PID controller.	
I_{error}	Performance index	
$e(t)$	Relative system error	
J	Cost function	
PMV	Predicted mean vote	

Greek

dt	Sampling interval	s
n	Flow exponent	ND
θ	Unknown parameter	
k,ε	Inverse effective Prandtl number	ND
λ	Forgetting factor	ND
β	Model parameters to be identified	ND
γ	Model parameters to be identified	ND
ω	Parameter to be estimated	ND
Δt_{smp}	Sampling interval	s
α	Coefficient accounting for the heat flow through building envelopes and internal mass	ND
g	Gravitational acceleration	m/s^2
u	Air velocity in the x direction	m/s
v	Air velocity in the y direction	m/s
w	Air velocity in the z direction	m/s
μ	Air viscosity	Pa **s**

β	Thermal expansion coefficient of air	1/K
k	Air conductivity	W/(m k)

Subscript	**Description**
s	Supply air
i,j	One space
source	Air mass source in zone
sink	Air mass sink in zone
ref	Reference value
out	Outdoor air
R	Indoor air
tot	Total air
sen,	Sensible
cond	Condensation
a,	Air
in,	Inlet
w	Water
k	Current sampling instants
k-1	Previous sampling instants
set	Set-point
pred	Prediction
sim	Simulation
max	Maximum
min	Minimum

P	Proportional factor
I	Integral factor
D	Derivative factor
est	Estimated value
meas	Measured value
cz	Critical zone
virt	Virtual temperature sensor
sens	Actual temperature sensor
rtn	Return air

Note: ND= No dimensions.

CHAPTER 1 INTRODUCTION

1.1 Motivation

Heating, Ventilation and Air-conditioning (HVAC) systems are the major energy consumers in buildings. According to the statistics provided by the DOE (2003), the energy consumption of HVAC systems in industrial and commercial buildings constituted 12% of the United State primary energy consumption. In Hong Kong, the energy consumption of air-conditioning systems contributed about 50% of the annual energy budgets in most air-conditioned buildings (Yik 1997). The energy efficiency of air-conditioning systems is therefore essential to reduce the global energy consumption of buildings and promote the environmental sustainability. In recent years, another issue which receives wide concern is the indoor air quality (IAQ) because the contribution of IAQ to the total personal exposure to air pollutions is significant. A poor IAQ may be caused if the operation of air-conditioning systems is strongly dynamic and the occupancy schedules or load conditions vary significantly. The set points of air-conditioning systems might significantly deviate from the real optimal values, which will affect health and productivity of occupants because people spend most of their time in indoor environments.

To reduce the energy consumption of the building HVAC systems while maintaining or improving the IAQ for occupants of the building, a large number of researches

have paid significant efforts on designing energy-efficient HVAC component and utilizing the renewable energy sources, such as solar energy and wind energy etc. However, the control and operation of the HVAC systems will mainly affect the system energy usage and IAQ. Among basic controls of air-conditioning systems, the outdoor air ventilation control is essential to ensure the IAQ and thermal comfort with less energy consumption of the multi-zone air-conditioning systems. Conventional outdoor ventilation control strategies mainly involve constant outdoor airflow rate control or strategies based on maximum return CO_2 measurement in summer, transient, or winter seasons. These strategies often result in either excessive energy waste or poor indoor environmental performance due to improper control and operation of strategies. Therefore, it is significant to develop several advanced ventilation control strategies in our research for ensuring the high ventilation performance of the air-conditioning systems.

Most existing studies on the optimization and control of the outdoor air ventilation for air-conditioning systems were carried out through simulation tests and the field validation on real buildings is still limited or even lacking. In the meantime, the field tests of ventilations control strategies can seldom be implemented properly or effectively because of inadequate control strategies, inappropriate measurement instrumentations, measurement uncertainties/errors and component degradations and faults. The inadequate control strategies and inappropriate sensor instrumentation in multi-zone air-conditioning systems also prevent the implementation of advanced outdoor air ventilation control, particularly those which aim to provide satisfactory indoor environment of each zone by consuming minimum energy. Therefore, this

thesis presents an in-situ implementation and validation of a CO_2-based adaptive DCV strategy in a super high-rise building in Hong Kong. Since the accuracy and reliability of the major measurement instrumentations affect the actual performance of the adaptive DCV strategy significantly, the commissioning and calibration of major measurement instrumentations are presented as well.

Another fundamental function of HVAC systems is to provide building occupants with comfortable thermal conditions. A large amount of research on thermal comfort has been done to improve the indoor thermal environment using the perfect mixing model. However, these studies cannot precisely feedback the spatial variations of controlled variables because the indoor air velocity, temperature, and pollution stratification are uneven in building spaces. The use of perfect mixing model may not be practical when controlled variables vary considerably over distances. The unevenness always causes poor thermal comfort in the occupied zone using the measurements at the sensor locations. The negligence of the indoor air stratification phenomena is one of the main reasons for malfunction of indoor environment control systems, which in turn causes frequent complaints against the poor indoor environment. Therefore, many complicated room models, such as Computational Fluid Dynamics (CFD) model and the zonal model have been developed to predict the indoor air stratification phenomena before the ventilation system is constructed. However, the computational burden is usually heavy, which prevents their online applications. It would be a significant step forward to integrate the simulation of the space ventilation and the indoor thermal stratification phenomena to a real-time ventilation control strategy for ventilation performance test purposes.

1.2 Aim and Objectives

Development, site validation and performance test of online optimal ventilation control strategies for multi-zone air-conditioning systems play significant roles in reducing the overall energy consumption of buildings, and maintaining the satisfactory IAQ and thermal comfort. However, current studies on this issue are far away from being sufficient. Therefore, the development and implementation of the proposed ventilation control strategies and a CFD-based virtual ventilation system test platform for air-conditioning systems for real-time applications is the main aim of this research. The aim is achieved by addressing the following objectives:

1. Develop a CO_2-based adaptive DCV strategy and the indoor air temperature set point reset strategy of critical zones for the multi-zone VAV ventilation systems to achieve the satisfactory indoor environment of individual zones and enhance energy performance during typical summer seasons.
2. Develop a model-based indoor air temperature optimal control strategy for temperature resetting based on the trade off among the thermal comfort, indoor air quality and total energy consumption simultaneously. The temperature set point of critical zones can be optimized using the system response-based cost function to reduce the unbalance among the required outdoor air fractions of all the zones.
3. Present a model-based optimal control of outdoor air flow rate of full air system with primary air handling unit based on the trade-offs among the energy consumption of the PAU fan system and the energy consumption for cooling

outdoor air. This strategy is a preferable choice while the outdoor air enthalpy is smaller than the return air enthalpy.

4. Develop the software tools and provide the implementation guidelines for applying online the proposed supervisory and optimal control strategy in practice.
5. Perform field implementation and validation of the adaptive DCV strategy and enthalpy-based ventilation control strategy. To ensure the acceptable performance, the major measurement instrumentations, including the CO_2 sensor, air flow rate meters, are calibrated.
6. Develop a CFD-based ventilation test method to integrate the simulation of the space ventilation and the indoor thermal stratification phenomena to a real-time ventilation control strategy for ventilation performance test purposes. A space temperature offset model is also developed to compensate the indoor air stratification phenomena to optimal indoor ventilation performance.

1.3 Organization of This Thesis

The thesis is organized into ten chapters as below.

Chapter 1 presents the motivations of this research, the aim and objectives, and the organization of this thesis.

Chapter 2 presents a literature review on the simulation and practical implementation studies of conventional ventilation control strategies, the

conventional models of indoor air such as the well-mixed models, the multi-zone models, CFD models, and zonal models.

Chapter 3 introduces the major parameter estimation techniques, the basic control loops of air-conditioning systems and system optimization techniques for nonlinear optimization processes, which will be used in this thesis. These techniques are essential for ensuring the HVAC systems to operate with a better or optimized performance with optimal set-points. The parameter estimation technique is also important to ensure the components' models in HVAC systems to continuously provide reliable estimations.

Chapter 4 presents a CO_2-based adaptive DCV strategy for multi-zone air-conditioning systems, which employs an online occupancy identification using the dynamic multi-zone ventilation equation and zone temperature set point reset strategy of critical zones. The energy and environmental performances of the adaptive DCV strategy is validated and evaluated by comparing with other typical ventilation strategies under various weather conditions in TRNSYS environment.

Chapter 5 presents a model-based indoor air temperature set point resetting strategy for critical zones of the multi-zone HVAC system aiming at reducing the unbalance among the required outdoor air fractions of all the zones. The performances of the strategy is tested and evaluated by comparing with a conventional ventilation control strategy using the simulation-assisted method.

Chapter 6 presents a model-based optimal control of outdoor air flow rate of full air system with primary air handling unit aiming at optimizing the outdoor air flow rate by compromising the energy consumption of the primary fan and the energy consumption for cooling outdoor air. Case studies are carried out to evaluate the system performance using the simulation-assisted test method in a typical spring season.

Chapter 7 describes a data-based space temperature offset model as a virtual temperature sensor in temperature control to compensate the temperature non-uniform stratification and hence to improve the indoor thermal comfort in occupied rooms. Case studies are carried out to validate the accuracy and reliability of the CFD modeling method using experimental measurements. The effect of the virtual temperature sensor on the zone temperature control performance is tested in a CFD-based virtual ventilation test method.

Chapter 8 presents a CFD-based virtual ventilation test method for control and optimization of indoor environment by combining a ventilated room with a ventilation control system. The data-based space temperature offset model is integrated as a component of the ventilation control system. Case studies are carried out to evaluate the control accuracy and reliability of the CFD-based virtual ventilation test method.

Chapter 9 presents the site implementation of a CO_2-based adaptive DCV strategy in a super high-rise building. The performance of this DCV strategy is practically implemented and validated by comparing with that of an original used fixed outdoor

air flow rate control strategy. The test results, implementation architectures and the commissioning and calibration of major measurement instrumentations are presented as well.

Chapter 10 summarizes the work reported in this thesis, and gives some recommendations for future application and research.

CHAPTER 2 LITERATURE REVIEW

This chapter mainly presents various conventional ventilation control approaches for multi-zone VAV ventilation systems. Section 2.1 briefly introduces the significance of the ventilation control in HVAC systems, the ventilation performance of conventional ventilation strategies mainly for the DCV strategies, and the practical ventilation application case studies. Section 2.2 presents the significance of indoor air environment control for analyzing the indoor air stratification phenomena and the kinds of conventional room models, mainly including the well-mixed room model, multi-zone room model, CFD room model, zonal room model, and the new data-based mechanistic model presented in Chapter 7.

2.1 Conventional Ventilation Control Approaches

2.1.1 Importance of Building Ventilation Control

People spend most of their time in the indoor environments. Therefore, healthy indoor environments are critical to the healthy of people. Indoor air quality (IAQ) can be enhanced by proper ventilation control, which dilutes and removes the moisture, CO_2, and other pollutants in the ventilated rooms.

Outdoor air ventilation control is one of the key factors affecting the air quality in the ventilated spaces. All the harmful contaminants need to be exhausted by using the outdoor air flow. Therefore, the main aim of building ventilation is not only to

reduce the energy consumption of buildings, but also to provide occupants with a better indoor air quality. At the same time, it is necessary to ensure a minimum outdoor air control value provided for the occupants. Therefore, how much outdoor air should be designed as the minimum value is important as well. This value should be decided using a proper ventilation control strategy to maintain a satisfactory indoor air environment.

2.1.2 Demand-Controlled Ventilation Control

The indoor quality of buildings and the associated energy use have been of growing significantly concern over the last 20 years. Sufficient outdoor air intake is essentially important to ensure acceptable indoor air quality (Elovitz 1995, Chan 2005, Liu and Liu 2005). Demand-Controlled Ventilation (DCV), proposed by Kusuda (1976) in 1976, attempts to achieve acceptable indoor air quality with reduced energy cost by controlling the outdoor air ventilation rate based on certain measured variable. In DCV control, carbon dioxide concentration (CO_2) is often used as an important parameter for ventilation control while carbon dioxide is a reliable surrogate for bioeffluents from occupancy and not a contaminant of concern in buildings (ASHRAE 1996, Chao and Hu 2004, Mui and Wong et al. 2006). However, many studies (Persily 1993, ASHRAE 1996) pointed out that the CO_2-based DCV control strategy cannot adequately satisfy the ventilation demand in a space in many situations since CO_2 concentration provides no information on the adequacy of ventilation rate relative to sources of other contaminants in the room, such as those generated by building materials.

Therefore, ASHRAE (1996) proposed a revised version of the ventilation standard (62-1989R) for public review, suggesting that the minimum requirement on the outdoor air ventilation rate should be determined by not only the actual occupancy, but also the occupied area. This approach provides a way to consider the non-occupant-generated pollutants. However, the standards (ASHRAE 1999, 2001) proposed that the minimum outdoor air rate is determined only by the actual occupancy together with the target outdoor air rate per person in different situations. In the latest standard (ASHRAE 2004), it is restated that the design outdoor air ventilation rate is determined by occupancy and occupied area accounting for people-related sources and area-related sources.

Using these standards to determine minimum outdoor air rate, the actual occupancy for a space has to be quantified in advance. ASHRAE (62-1989R, 1999) proposed a steady-state method to detect the actual space occupancy and then to determine the outdoor air ventilation rate. This steady-state occupancy detection is based on steady-state mass balance equations, yet the assumptions are far from the real process resulting in large lag of occupancy detection (Persily 1993, Wang and Jin 1998). Therefore, many researchers proposed dynamic occupancy detection methods to detect the variable occupancy (Ke and Mumma 1997, Wang and Jin 1998). In the methods, CO_2 concentration derivative term in the mass balance equation is approximated using the current and previous samplings of CO_2 concentration. The sensors' noise and dynamic derivative term may results in unstable occupancy detection. Wang et al. (Wang et al 1999) further developed robust filters to alleviate these effects. The test results of simulation and field experiments demonstrated the

filters can improve the stability greatly of the dynamic algorithm. Since the volume of carbon dioxide sensors is increasing and the prices are decreasing, CO_2 sensors are economically justified for more practical applications of effective outdoor air ventilation control (Jones et al. 1997, ASHRAE 2003).

It is very common that one air handling system serves many zones in modern commercial office buildings. Different zones have different occupancy and thermal loads. Therefore, the outdoor air fractions (the ratio of outdoor airflow rate to supply airflow rate) of each zone may differ greatly from other to satisfy the coincident ventilation and thermal load requirements. Ordinarily, the minimum outdoor air intake rate is designed based on the total design occupancy. In this situation, the identical outdoor air fraction results in over-ventilation in some zones while under-ventilation in other zones. Another alternative is that the minimum outdoor air intake rate is designed to satisfy the zone with most outdoor air needs while other zones keeping over-ventilation. To ensure enough ventilation for all the zones while minimizing energy use, the unvitiated outdoor air in the over-ventilated zones can be counted as outdoor air to reduce the direct outdoor air intake from outside. ASHRAE (1996, 1999, 2001) proposed a multiple zone equation to correct the outdoor air fraction for outdoor air flow rate design under design condition.

Under full and partial occupancy load conditions, Mumma and Bolin (1994) presented energy performance of zone-level ventilation control with the multiple zone equation. The performance evaluation was based on scheduled supply air temperature, supply air flow rate, outdoor air requirement at each zone on the basis

of an hour of static state for design condition and off-design condition. Nassif et al. (2005) presented a supply CO_2-based Demand-Controlled Ventilation control strategy for multi-zone air conditioning systems to reduce system energy use while maintaining the indoor IAQ at each zone. This strategy is based on the multiple zone equation and estimated supply CO_2 concentration set point. The supply CO_2 concentration set point was determined on the basis of steady state mass balance. This makes the set point deviate from it real (optimal) value. Additionally, the strategy used the scheduled occupancy ratio to calculate the outdoor air fraction of the critical zone and the other zones statically. In fact, the critical zone varies from time to time depending on the thermal load and occupancy profiles of all the zones. Even in the critical zone, the occupancy may be partial instead of full. Ketter (2003) pointed out that, the multiple space equation is mainly for design purposes. When it is used for control, the actual number of occupancy should be counted in advance. On the other hand, proper online control should be assured.

2.1.3 Enthalpy-based Ventilation Control

The optimal control of the outdoor air is significant to provide an acceptable indoor air quality with less energy consumption under dynamic HVAC systems. In summer seasons, the DCV strategy has been validated to be an effective approach to maintain a satisfactory ventilation performance. However, the outdoor air with lower temperature might provide much more cooling into HVAC systems to reduce the cooling load accordingly. In this case, more outdoor air can result in better indoor air quality and energy efficiency of the HVAC systems. Various ways of outdoor air

flow rate optimal control have been studied to determine the quantity of outdoor air into air-handling units (Park 1984, Wang 2000, ASHRAE 2004, Spitler 1987). ASHRAE (2004) compared different temperature-based air-side economizer. When the outdoor air temperature was greater than the return air temperature, the outdoor air dampers were controlled at their minimum positions. However, the influence of the outdoor air latent heat on air-conditioning system was neglected in these temperature-based control strategies. Therefore the temperature-based control strategy might be prohibited in the very hot and humid climate zones, such as Hong Kong.

To consider the effect of air latent heat on the system energy efficiency, the enthalpy-based outdoor air control strategies (Zaheer-uddin 2000, Ardehali 1997, Spitler 1987, Hydeman 2003, GSA 2003) were developed to determine the outdoor air flow rate, especially in highly humid climates. In these studies, the outdoor air flow rate was set to be its lower limit when the return air enthalpy was smaller than the outdoor air enthalpy. Otherwise, the outdoor air flow rate was set to its maximum value and the cooling valve was regulated to control the supply air at its set point. It is worthy noticing that the above enthalpy-based strategies failed to minimize the coil load for certain outdoor air conditions. Therefore, Seem (2009) presented an optimization-based enthalpy control strategy to optimize the outdoor air flow rate when mechanical cooling was required. The minimized coil load could be obtained using the system current operating conditions. This strategy, therefore, was able to determine the outdoor air fraction by calculating the coil load of air-conditioning systems in any climates. However, the minimum outdoor air flow rate was a fixed

value in this study. It might result in over ventilation when the occupancy ratio is low and insufficient ventilation when the occupancy ratio is higher than design maximum occupancy.

In addition, the outdoor air of air-conditioning systems was ordinarily induced using the air handling unit (AHU) not a primary air unit (PAU). Outdoor air flow rate was controlled by coupling the outdoor air, exhaust air and recirculation air dampers (Zhao 1998), coupling the outdoor air and recirculation dampers, or leaving the outdoor air damper widely open(Krakow et al. 2000, Xu et al 2004). These approaches were only suitable for outdoor air flow rate control in air-conditioning systems without installing the PAUs. However, the PAUs as the energy consuming components of air-conditioning systems are installed in some particular HVAC systems when induced outdoor ventilation systems are not available or the outdoor air quality is not satisfied, especially in some super high-rise buildings in Hong Kong. The primary fan is adopted to supply the required outdoor air to air-conditioning systems in the building. When the outdoor air enthalpy is smaller than the return air enthalpy, more outdoor air may reduce the load of cooling system. However, it will result in the increasing energy consumption of primary fan in this system accordingly. It is significant to develop a new outdoor air flow rate optimal control strategy for the air-conditioning system with the primary air handling unit. However, no sufficient research has been studied on this local outdoor ventilation control of the air conditioning system.

2.1.4 Performance Tests and Practical Applications

Some site installations using the CO_2-based DCV strategies were also studied to evaluate the energy saving potential by comparing with other types of control in various buildings, such as office buildings (Haghighat F et al. 1992), conference rooms (Fleury 1992), school buildings (Janssen and Hill 1982), banks (Gabel and Janssen et al. 1986), auditoriums (Zamboni M, Berchtold 1991, Fehlmann and Wanner et al. 1993).

Sodergen (1982) performed the study of the CO_2-based DCV strategy in office buildings of in Helsinki. The CO_2 control system was compared with the constant outdoor air and timer-based control, and plots of CO_2 concentrations were generated. The outdoor air control algorithm was not described in this study. Gabel et al. (1986) presented a study in a bank in Pasco, Washington. The project involved the measurement of energy consumption and indoor air quality. Occupant responses to the IAQ were also surveyed. The IAQ was monitored in winter, spring, and summer seasons, with one week under normal operation followed by one week of CO_2-based DCV. When the CO_2 set point was set to be 1000ppm, it can be found that air leakage through the closed damper was large enough to keep the CO_2 concentration below the set point. The savings in energy consumption were calculated to be 7.8% when the CO_2 control strategy was implemented. According to the questionnaire, the occupants were not able to detect any differences in air quality at CO_2 levels of 300 and 1000ppm. A comprehensive study of CO_2-based DCV was performed in Montreal (Donnini et al. 1991) on two floors of an office building. One floor was

equipped with a CO_2-based DCV system, while the other floor served as a control. The CO_2 control algorithm was set so that the outdoor damper was closed at concentrations below 600ppm, and opened at concentrations above 600ppm, with the maximum opening occurring at 1000ppm. In addition to measuring the CO_2 concentration, the study measured formaldehyde, particles, ventilation system performance, thermal comfort and energy demand. The outdoor air dampers were kept closed most of the year because there were not enough people raising the CO_2 concentration above the limit. The thermal comfort was generally adequate on both floors. Occupants of the DCV floor complained significantly more about the indoor environment than those occupants of the control floor. The DCV strategy can obtain about 12% annual energy saving. Davidge (1991) presented a CO_2-based controlled DCV in a 30,000m^2 office building. According to his study, the system never controlled the ventilation rate because the outdoor air temperatures during the winter were not low enough to allow free-cooling. During the summer, however, the damper leakage was more than enough to control the CO_2 level. Fleury (1992) performed a study on the performance of a CO_2-based DCV in a conference room. According his study, the fan motor speed was adjusted based on the CO_2 concentration. Occupants rated the air quality in the conference room from good to excellent. The measured CO_2 concentration in the space was between 350ppm and 850ppm. Pavlovas (2004) presented that the DCV has a positive influence on the heating energy demand and confirmed in several aspects findings in previous studies. However, some aspects may be added regarding the negative influence on indoor climate from different DCV strategies and rather demanding occupant loads.

Buildings nowadays are mostly equipped with comprehensive building automation systems (BASs) and building energy management control systems (EMCS) that allow the possibility of site implementation and application of advanced DCV strategies in real buildings to enhance and optimize the operation and control of their HVAC systems (Kroner 1997, Degw 1995, Bien 2002, Arkin 1997, Wang 2004, Wang 2007). However, the BASs systems in buildings are usually not implemented properly or not used effectively because of inadequate control strategies, inappropriate instrumentation, measurement uncertainties/errors and component degradations and faults. The insufficient and inappropriate sensor instrumentation air-conditioning systems also prevented the implementations of advanced ventilation control particularly those providing satisfactory indoor environment using minimum energy. Since reliable and accurate ventilation control strategy and sensor measurements are essential, Chapter 9 presents the site implementation and validation of a CO_2-based adaptive DCV strategy for multi-zone ventilation systems in a super high-rise building. Considering that the measurement instrumentations play a significant role in ensuring the success of the DCV strategy, the calibration and commissioning of major measurement instrumentations are presented as well. The actual control performance, energy and environmental benefits due to the use of the CO_2-based adaptive DCV strategy are tested and evaluated by comparing with the originally implemented fixed outdoor air flow rate control strategy.

2.2 Introduction of Conventional Room Models on the Indoor Air Stratification

2.2.1 Influence of Room Air Stratification on Indoor Air Environment

The relationships between indoor air environment and human comfort have been widely investigated. The occupant evaluated the indoor climate mainly by its air quality and thermal conditions. The air quality within a building perceived by the occupants is a function of indoor air pollution. The thermal comfort is mainly determined by the indoor air flow pattern, temperature and relative humidity. However, individual occupants, especially located in the occupied zones will have varying requirements for their comfort level and the indoor air quality. Although environmental control systems are in use in various buildings, complaints about indoor climate are still common (Jaakkola 1994; Brightman et al. 1997).

The distribution of air within rooms and among rooms is inextricably linked to indoor air environment. Airflow within a room affects the indoor air thermal distribution and the emission rate at which contaminants emit into the air from sources within the room. These indoor thermal plume and air pollutions are transported primarily by the room airflow within a room or among rooms. The amount of air introduced into the room, the air temperature and the air quality, the conditions of indoor air heat and pollution sources and the way of the air diffused into the room are all important factors determining the indoor air thermal and quality conditions. People's perceptions of indoor air quality and their thermal comfort are affected by air speed, temperature and humidity distribution. Therefore a large

number of researches have been studied on the indoor air stratification problems to attain the desirable indoor air environments.

2.2.2 Approaches of Determining Indoor Air Quality

A large number of room air flow modeling techniques have been developed and applied to building problems for system test and optimal control to maintain the satisfied indoor air thermal environment over the past 40 years. Measurement is difficult and costly, and can only give results under prevailing weather and building conditions. Mathematical models, on the other hand, can determine and predict air flow patterns and concentrations for all possible combinations of building leakage and weather conditions.

As long as mechanistic modeling of indoor air flow distribution is concerned, two types of approaches can be identified, which are integral (macro) and differential (micro) approaches. Both of them are classified simply as four groups, for example the simple well-mixed models, multi-zone models, zonal models, and Computational Fluid Dynamics (CFD) models. These models are illustrated in details as follows.

2.2.2.1 Well-mixed Room Models

The simple well-mixed models with one air node representing the whole air volume in the room are commonly used to study the energy consumption of HVAC system in buildings (TRNSYS1996, DOE1989).

The air density, flow field, temperature and pollution are assumed to be well mixed in each ventilated zone. For example, the temperature sensor measurements can represent the indoor air temperature based on the concept of the well-mixed models. For each zone, the indoor air energy balance, moisture balance and pollutant balance can be expressed as Equation 2.1 to Equation 2.3 respectively.

$$M_i c_p \frac{dT_i}{dt} = m_{s,i} c_p (T_s - T_i) + Q_{sen,i} \tag{2.1}$$

$$M_i \frac{dG_i}{dt} = m_{s,i} (G_s - G_i) + D_i \tag{2.2}$$

$$V_i \frac{dC_i}{dt} = v_{s,i} (C_s - C_i) + S_i \tag{2.3}$$

where M is the air mass, C is the CO_2 concentration, V is the volume, G is the moisture generation rate, S_i is the CO_2 generation rate, $Q_{sen,i}$ is the indoor air sensible heat change, D_i is the indoor air humidity change, dt is the sampling interval, C_p is the heat capacity, m is the supply air mass exchange, v is the supply air volume exchange, subscripts s indicates supply air, i indicates one space.

However, it is well known that the air temperature, air velocity and pollution concentration distribution are uneven in ventilated spaces. The unevenness always causes poor thermal comfort and IAQ in the occupied zone using the measurements at the sensor locations. The negligence of indoor air distribution is one of the main reasons for malfunction of indoor environment control systems, which in turn causes frequent complaints against the poor indoor environment.

2.2.2.2 Multi-zone Room Models

Multi-zone models can present the airflows and pollutant dispersion in a building. They represent a building as a network of well-mixed spaces, or zones, connected by the discrete flow paths such as doors, windows, wall cracks, fans, ducts, and so on. Within a multi-zone model, the user describes a building by assembling various component models, each representing a zone, a point outside the building, or one of a number of types of flow paths. The model then predicts the system's behavior based on the interaction of the assembled components, for example, the typical multi-zone offices of a commercial building mentioned in Chapter 4. A multi-zone model of this building would link the different zones using models of the buildings, cracks and ventilation system components.

Multi-zone models can be used with time-varying input or boundary conditions to predict variations in conditions over the period of interest. Assuming that air flow patterns are unaffected by any indoor sources, the energy and mass balance calculation in each zone at each time step can be included in a multi-zone model to predict the variation of concentrations against time. Examples of this type of models, which are in widespread used are COMIS and CONTAM (Feustel, H.E., 1992, Feustel, H.E., 1999, Walton, G., 1997).

Actually the indoor temperature, pressure and pollution concentration field might vary dynamically. But the multi-zone models typically treat each room as well-mixed air and are limited to cope with variations in indoor flow rates, temperature and air pollution concentrations. No existing program provides

multi-zone model with facilities to model detailed variations within the ventilated rooms (Haghighat and Megri, 1996). Usually, the study of detailed indoor air flow, temperature and pollution distribution is conducted using the Computational Fluid Dynamics (CFD) methods (Haghighat F.,1999; Xu W.et al,2001a and 2001b).

2.2.2.3 CFD Room Models

CFD methods are used to numerically model physical processes within a fluid using the solutions of a set of non-linear partial differential equations, such as the continuity, momentum, energy and pollution conservations. These differential equations express the fundamental physical laws that govern the conservation of these equations. For room air motion, the driving forces are pressure differences, which are caused by the wind, thermal buoyancy, mechanical ventilation systems or combinations of these. In this case, the indoor air flow velocity may be low with high turbulence intensity. Therefore, CFD models have been widely used in the analysis of indoor airflow, temperature, and contaminant distribution in a ventilated room (Haghighat et al. 1992). These models have been validated under different flow conditions and geometry (Chen and Xu, 1998; Nielsen, 1998; Topp 1999).

An analytical solution of the coupled, non-linear, partial differential equations for a three dimensional, turbulent flow field is not possible. The numerical methods are necessary to discrete the flow field using finite difference methods to calculate the complicated flow problems (Fluent 2005). CFD models are commonly used to simulate fluid flows, particularly in complex environment. It is well known that the CFD method can generate realistic model without more costly experimental

investment. So the CFD method is now popularly employed for ventilation field to provide precise information including the distribution of indoor air flow, temperature, and pollution transports.

Despite the sufficiency of the simulated results with detailed information considering the indoor air flow and temperature field, CFD models suffer from huge computation load. It is widely known that the running of a complicated CFD simulation might consume much more computing time. An important restriction for the use of the CFD model is that the solution of the system of equations converges to a 'steady-state' result. Since many of the energy and contaminant transport conditions might be transient or dynamic, this is a serious drawback for the use of CFD models. The trade-off between the number of grid cells used and therefore the grid size and the time needed for the computation can not be neglected during the simulation periods. Therefore, the complicated CFD models will not be suitable for the dynamic ventilation control system in most cases.

2.2.2.4 Zonal Room Models

A zonal model is an intermediate approach between the CFD and the well-mixed room models. In zonal models, the ventilated space in question is divided into a number of macroscopic zones similarly in the multi-zone approach. According to the different ventilation strategies, the ventilated space can be divided into different zones which are identified as specific (driven) flow and standard (current) zones (Inard et al, 1996) and mixed zone (Haghighat et al, 2001; Musy et al, 2002). The specific flow zones are those zones, which are within the reach of jets, plumes and

thermal boundary layers. All the other zones outside the influence of specific flows are collectively called current zones, which are mostly found within the occupied region of the room. Mixed zones are combinations of specific and standard zones. Contrary to CFD models, only the conservation equations of mass and energy are solved. The Navier-Stokes equations are not considered. The air flow between the sub-volumes has to be calculated using empirical correlations or other simplified methods (pressure calculation) (Haghighat et al, 2001). For each zone (or sub-volume), the mass balance and thermal energy balance can be written as Equation (2.4) and (2.5).

$$\frac{dM_i}{dt} = \sum_{j=1}^{n} M_{ij} + M_{source} + M_{\sin k} = 0 \tag{2.4}$$

$$\frac{dQ_i}{dt} = \sum_{j=1}^{n} Q_{ij} + Q_{source} + Q_{\sin k} = 0 \tag{2.5}$$

where M_i is the mass of air in zone *i*, and M_{ij} is the air mass flow rate from zone *i* to zone *j*, M_{source} is air mass source in zone; $M_{\sin k}$ is air mass sink in zone; Q_i is the heat energy in zone *i*, and Q_{ij} is the rate of heat energy from zone *i* to zone *j*, Q_{source} is the rate of heat energy supplied by the source in the zone, and Q_{sink} is the rate of heat energy removed from the zone.

The pressure at the middle of the zone is assumed to obey the perfect gas law. Zones are rectangular parallelepiped and the mass flow across the common interface boundary of such zones can be expressed as a function of pressure in Equation (2.6).

$$M_{ij} = \varepsilon_{ij}\rho_i C_d A_{ij}\left|P_j - P_i\right|^n = \varepsilon_{ij}\rho_i C_d A_{ij}\left|\Delta P_{ij}\right|^n \tag{2.6}$$

A hydrostatic field assumption has been used to relate the zone pressures with reference pressure shown in Equation (2.7) and Equation (2.8).

$$P_i = \rho_i R T_i \tag{2.7}$$

$$P_i = P_{ref} - \rho g Z \tag{2.8}$$

Power law is applied to calculate the air mass flow rate across the cell interface in Equation (2.9).

$$V_{ij} = C_d \rho \Delta P_{ij}^{\ n} \tag{2.9}$$

where P_i is the pressure in the zone i; P_j is the pressure in the zone j; ρ_i is the air density of zone i; C_d is the coefficient of power law; n is the flow exponent; A_{ij} is the area of the interface boundary; P_{ref} is the reference pressure at bottom of the zone; g is the gravitational acceleration; R is gas constant of air; T_i is the temperature of zone i; ΔP_{ij} is the pressure difference between zone i and zone j.

L. MORA (L. MORA 2002) compared the zonal model and CFD model predictions of indoor airflows under mixed convection conditions to experimental data. The zonal model can give a satisfactory estimation of airflow patterns with specific laws

to model momentum added to air by the jet. The zonal model is a suitable tool to estimate thermal comfort in ventilated room. However it can not get more detailed air flows patterns and if it is accurate in the 3 dimensional space. Laret (Laret 1980) developed an analytical model based on steady state conditions, which was able to calculate the temperature profile at the centre of the room. During H. (During H. 1994) studied the use of zonal model for transient conditions. The number of sub-volume is increased to 12. Transient analysis was focused on long time periods. Short time dynamics, important in controller studies, have not been treated and the dynamic phenomenon is mainly dynamics of envelope elements. Hutter (Hutter E. 1981) presented a zonal model for natural convection. The model uses a variable number of air layers and represents also the zones of natural convection near the walls. Brent Griffith. (Brent Griffith. 2003) developed a momentum-zonal model based on Euler equation to enhance building load and energy simulations by predicting indoor air flow and temperatures. The model has been coupled to the heat balance model and tested on load calculations. Total computation times for load calculations were two orders of magnitude higher using the momentum-zonal model compared to traditional complete-mixing. The zonal models predict the air flow pattern reasonably for natural ventilation (Wurtz et al. 1999a, Haghighat et al. 2001). This is because the airflow in nature convection results mainly due density difference. However, the zonal models have shown obvious discrepancies for predicting the recirculation flow pattern in a ventilated space with forced convection (Haghighat et al. 2001, Mora et al. 2003). Since the power-law model is applied in the standard zone, it is the main reason resulting in the deviation of zonal models.

Some attempts have been made to improve the accuracy of zone models. Wurtz et al. (1999a) investigated the effect of using different values of flow coefficient on the prediction of indoor airflow and temperature distribution for natural convection. The relationship between the airflow rate and temperature at some positions within room and varying flow coefficient are illustrated. Griffith and Chen (2003) adopted the micro-approach to develop an alternative model, named the momentum-zonal model. This model can give good prediction of temperature stratification in a natural ventilated space mainly driven by the buoyancy. All these zonal models are limited to one specific case and are not generic as well for other ventilated rooms. Therefore conventional zonal models are very rarely used to simulate the indoor thermal environment stratification phenomena based on the online feedback control for control purposes of ventilation systems.

2.2.2.5 Data-based Mechanistic Models

Most existing models mentioned above are mechanistic models, such as the conventional zonal models and CFD models. Mechanistic models describe the system based on the priori defined physical, mechanical and chemical mechanisms. These models are developed based on a number of assumptions and differential equations, which result in their exceptional complexity and time consuming of computation. It is a main disadvantage to adopt for ventilation system control purposes.

A data-based mechanistic model can provide a physically meaningful description of indoor dynamics of heat and mass transfer in the ventilated space with non-uniform

stratifications, while providing low order models. The advantage of this model is that it not only considers the indoor air physical mechanism but also owns the compact expression and accurate performance. Therefore, it is an ideal basis for design of the model-based ventilation control system.

2.3 Summary

Ventilation control is essential for improving the indoor quality of buildings and reducing the associated energy use of HVAC systems. Various ventilation control strategies are reviewed in this chapter, such as the various DCV strategies, enthalpy-based ventilation control strategies. At the same time, the research on the indoor air stratification phenomena is presented as well, including the significance of study on indoor air stratification, the current research approaches and its limitations. All these research outcomes will provide a significant theoretical basis and guidance for my PhD studies.

CHAPTER 3 PARAMETER ESTIMATION, CONTROL AND OPTIMIZATION TECHNIQUES OF HVAC SYSTEMS

This chapter mainly presents the online process parameters identification of dynamic models, the local and supervisory control, and the optimization algorithms of HVAC systems. Section 3.1 briefly introduces the main parameters estimation approaches, including the least squares estimated algorithm, the recursive least square (RLS) algorithm, the time-varying parameters estimated algorithm and exponential forgetting RLS estimated algorithm. Section 3.2 presents the significance and approaches of the local and supervisory control of the HVAC systems. The nonlinear optimization techniques for local and supervisory controls of HVAC systems, including the direct search method, sequential quadratic programming (SQP), conjugate gradient method, branch and bound (B&B), genetic algorithm (GA), and evolutionary programming are illustrated in Section 3.3**.**

3.1 Parameter Estimation

Online identification of process parameters is a key technique in the development and control of various components' models in the HVAC system. The least squares method (Astrom et al. 1989) is a basic approach for parameter estimation. With the exponential forgetting algorithm (Astrom et al. 1989), this method can also be

applied to systems with slow varying parameters. Various studies concerning the HVAC modeling, parameter estimation, and system identification highlight the feasibility and advantages of using the least square method in the whole HVAC system.

3.1.1 Least Squares Estimated Algorithm

Assume that a continuous process is describe as

$$y(t) = \sum_{i=1}^{n} \Phi_i(t)\theta_i \tag{3.1}$$

where *y(t)* is an observed variable that is a function of time *t*, Φ_i is the known functions named the regression variables or the regressors, the θ_i is the unknown parameters. In most applications, there are *k* values of the observed variables. To accommodate these observations, the relation in Equation (3.1) is expressed in matrix form as Equation (3.2).

$$Y = \Phi\theta \tag{3.2}$$

where *Y* is an array with dimension *k*, Φ is a *k***n* matrix, and θ is an array with dimension *n*. The variables of Y, Φ and θ are expressed in Equation (3.3)

$$Y = \begin{bmatrix} y(1) \\ y(2) \\ \cdot \\ \cdot \\ y(k) \end{bmatrix}_{k\times 1}, \Phi = \begin{bmatrix} \Phi^T(1) \\ \Phi^T(2) \\ \cdot \\ \cdot \\ \Phi^T(k) \end{bmatrix} = \begin{bmatrix} \Phi_1(1) & \Phi_2(1) & \cdots & \Phi_n(1) \\ \Phi_1(2) & \Phi_2(2) & \cdots & \Phi_n(2) \\ \cdot & \cdot & \cdot & \cdot \\ \cdot & \cdot & \cdot & \cdot \\ \Phi_1(k) & \Phi_2(k) & \cdots & \Phi_n(k) \end{bmatrix}_{k\times n}, and \theta = \begin{bmatrix} \theta_1 \\ \theta_2 \\ \cdot \\ \cdot \\ \theta_n \end{bmatrix}_{n\times 1} \tag{3.3}$$

The problem is to determine the parameters in such a way that the outputs computed from the model in Equation (3.2) agree well with the measured variables *y(i)* in the sense of least squares. This means that the error of Equation (3.4) should be minimized, where the error is shown in Equation (3.5). The symbol $\hat{}$ denotes the estimated variables.

$$V(\theta,k)=\frac{1}{2}\sum_{i=1}^{k}\varepsilon(i)^2=\frac{1}{2}\sum_{i=1}^{k}(y(i)-\Phi^T(i)\hat{\theta})^2=\frac{1}{2}E^TE=\frac{1}{2}\|E\|^2 \tag{3.4}$$

$$E=Y-\hat{Y}=Y-\Phi\hat{\theta} \tag{3.5}$$

The least-squares estimation proves that the function of Equation (3.4) is minimal for estimated parameters $\hat{\theta}$ such that

$$\Phi^T\Phi\hat{\theta}=\Phi^TY \tag{3.6}$$

If the matrix $\Phi^T\Phi$ is nonsingular, the minimum is unique and is given by Equation (3.7).

$$\hat{\theta}=(\Phi^T\Phi)^{-1}\Phi^TY \tag{3.7}$$

$$P(k)=(\Phi^T\Phi)^{-1}=\left(\begin{bmatrix}\Phi_1(k) & \Phi_2(k) & \cdots & \Phi_n(k)\end{bmatrix}\begin{bmatrix}\Phi_1(k)\\ \Phi_2(k)\\ \cdot\\ \cdot\\ \cdot\\ \Phi_1(k)\end{bmatrix}\right)^{-1}=\left(\sum_{i=1}^{k}\Phi(i)\Phi^T(i)\right)^{-1} \tag{3.8}$$

On the basis of Equation (3.8), the Equation (3.7) can be rewritten as Equation (3.9). The unknown parameters are then given using Equation (3.9) with *P(k)* given by Equation (3.8).

$$\hat{\theta} = P(k)\left(\sum_{i=1}^{k} \Phi(i) y(i)\right) \tag{3.9}$$

3.1.2 Recursive Least Square (RLS) Algorithm

Many real-world applications, such as adaptive control, adaptive filtering, and adaptive prediction, require a system model to be available online while the system is in operation. Recursive Estimation is a method to estimate models for batches of input-output data. In the adaptive controllers, the investigations are obtained sequentially in real time. It is necessary to make the computation recursively to save computation time and to reduce the space to store the historical data. In preparation for the recursive computations, Equation (3.8) can be rewritten as Equation (3.10).

$$P(k)^{-1} = \sum_{i=1}^{k} \Phi(i)\Phi^{T}(i) = \sum_{i=1}^{k-1} \Phi(i)\Phi^{T}(i) + \Phi(k)\Phi^{T}(k) = P(k-1)^{-1} + \Phi(k)\Phi^{T}(k) \tag{3.10}$$

The Equation (3.9) can be expressed as Equation (3.11). The error is written as Equation (3.12).

$$\hat{\theta} = \hat{\theta}(k-1) + K(k)\varepsilon(k) \tag{3.11}$$

$$\varepsilon(k) = y(k) - \Phi^{T}(k)\hat{\theta}(k-1) \tag{3.12}$$

$$K(k) = P(k)\Phi(k) = P(k-1)\Phi(k)\left[I + \Phi^T(k)P(k-1)\Phi(k)\right]^{-1} \quad (3.13)$$

$$P(k) = P(k-1)\left[I - K(k)\Phi^T(K)\right] \quad (3.14)$$

where I is a n dimensional identity matrix. The parameters of Equation (3.11) to Equation (3.14) can be estimated recursively.

3.1.3 Time-Varying Parameters Estimated Algorithm

As mentioned in Section 3.1.1 and 3.1.2, the identified parameters are assumed to be constant in each predicting step. However, in some cases, the parameters vary significantly against the time. It needs to consider this situation in which the parameters are time-varying. Due to the parameters of the state equations are varying slowly with the time, the estimated parameter is named the slowly time-varying parameter. Therefore the Equation (3.4) can be rewritten as Equation (3.15)

$$V(\theta, k) = \frac{1}{2}\sum_{i=1}^{k} \lambda^{k-i}\left(y(i) - \varphi^T(i)\theta\right)^2 \quad (3.15)$$

where λ is the forgetting factor ($0 < \lambda \leqslant 1$).

3.1.4 Exponential Forgetting RLS Estimated Algorithm

When a time varying system is concerned, the RLS algorithm with constant exponential forgetting factor may not obtain satisfactory estimation under near steady-state conditions due to no savings of earlier data. In this case, the value of the

forgetting factor in Equation (3.15) can set to be close to 1. Much earlier data will save with the increasing of the λ value. The data obtained at the previous n sampling time can be set to be λn. This method is named exponential forgetting RLS method accordingly. On the basis of above calculations, the exponential forgetting RLS estimated method is expressed from Equation (3.16) to Equation (3.17).

$$\hat{\theta}(k) = \hat{\theta}(k-1) - K(k)\left(y(k) - \varphi^T(k)\hat{\theta}(t-1)\right) \tag{3.16}$$

$$K(k) = P(k)\varphi(k) = P(k-1)\varphi(k)\left(\lambda I + \varphi^T(k)P(k-1)\varphi(k)\right)^{-1} \tag{3.17}$$

$$P(k) = \left(I - K(k)\varphi^T(k)\right)P(k-1)/\lambda \tag{3.18}$$

3.2 Control of Air-conditioning Systems

There are several factors that influence indoor air quality and thermal comfort. These factors are air temperature, air velocity, relative humidity, radiant environment and activity level. Air temperature is the most common measurement of comfort, and the one that is most widely understood. An air-conditioning system provides the controlled environment in which the following parameters are maintained within desired ranges: temperature, humidity, air distribution and indoor air quality in order to build up a comfortable and healthy indoor environment for people to work or live in. Thermal comfort and minimum health requirement must be achieved by the basic controls of system, while the control of air-conditioning systems aims at providing satisfying thermal comfort and indoor air quality with minimum energy consumption.

To save energy consumption and improve indoor environment, various measures, such as DCV control, supply air temperature reset control, VAV supply air static pressure control, etc., are used in Chapter 4, 5, and 6. In a typical VAV system, the local loop controls and supervisory controls are listed as follows.

Local loop controls include: a) AHU supply air temperature control; b) static pressure control; c) zone temperature control or zone air flow rate control; d) outdoor air flow rate control; e) supply fan and return fan control.

Supervisory controls include: *A)* outdoor air flow rate set point reset; *B)* Static pressure set point reset; *C)* AHU supply air temperature set point reset.

The local loop is essential for the system to operate properly to provide the comfortable and healthy indoor environment, while the supervisory controls allow that system operates with a better or optimized performance. The outdoor air flow set point reset affects the energy consumption, mainly for the coil load and the indoor air quality. The static pressure reset affects the energy consumption of the fan only if it does go to improper range. It is set too low, the critical zone may not be provided with insufficient airflow. When it is set too high, noise problem might occur. The AHU supply temperature reset will affect the thermal comfort and energy use of the system, mainly for fan energy consumption.

The on-line global control should optimize the overall performance not simply to minimize the energy cost or simply maximize the controlled indoor environment quality. Instead, it should find the proper compromise among the costs and quality.

The main variables affecting the energy consumption and environment quality include the zone air temperature, zone humidity, zone air pollution concentrations, ventilation rate and the entire system power consumption, etc.

3.3 Optimization Techniques

3.3.1 Significance of Optimization Techniques in HVAC System

Optimization techniques are widely of concern in HVAC fields. The critical issues of control optimization problems (optimizing control set points) are to employ appropriate optimization algorithm to search for the optimal set point(s) according the system responses. In general, the optimization techniques developed in the optimal control field could be summarized into two categorizes: linear optimization techniques and nonlinear optimization techniques. The linear optimization technique is a simple and straightforward technique since there is always a unique optimum in a linear optimization problem. The linear optimization technique includes direct method, recursive method, iterative method, etc. Compared to the linear optimization technique, the nonlinear optimization technique is complex and sophisticated since many local optimums exist in a nonlinear optimization problem. It is also difficult to find the global optimum.

Therefore, searching for the optimal values of the set points of HVAC systems is usually a nonlinear optimization process. The local and supervisory optimization techniques are required for the performance evaluation of HVAC system. A number of studies have been carried out on the development and application of various

nonlinear optimization techniques in HVAC systems, such as the direct search method (Hooke 1961) , conjugate gradient method (Nizet et al. 1984), sequential quadratic programming Olson et al. 1990, Sun et al. 2005, Chang 2004, Bassily et al. 2005), branch and bound (B&B) method, genetic algorithm (Wang et al. 2002, Chang 2005, Xu et al. 2007b), and evolutionary programming (Beyer 2001).

3.3.2 Direct Search Method

Direct search method (Hooke 1961) is a nonlinear optimization method that neither requires nor explicitly approximates derivatives for the problem to be solved. Instead, a set of trial points is generated and their function values are compared with the best solution previously obtained at each iteration. This information is then used to determine the next set of trial points. This general description encompasses a wide variety of techniques, including the provably convergent pattern search methods, together with other approaches such as random search methods and genetic algorithms. It is not reasonable to apply this method if the derivatives of the loss function are easily available with low computational efforts. Although the direct search method does not require the deviations to exist, higher performance can be expected in smooth functions.

3.3.3 Sequential Quadratic Programming (SQP)

Since its popularization in the late 1970s, Sequential Quadratic Programming (SQP) has become the most successful method for solving nonlinearly constrained optimization problems. As with most optimization methods, SQP is not a single

algorithm, but rather a conceptual method from which numerous specific algorithms have evolved. Backed by a solid theoretical and computational foundation, both commercial and public domain SQP algorithms have been developed and used to solve a remarkably large set of important practical problems. Recently large scale versions have been devised and tested with promising results.

Its basic idea is to linearize the constraints and set up a quadratic objective function to form a quadratic program (QP). The basic structure of an SQP includes four steps (Reklaitis et al. 1983): (1) Set up and solve a QP sub-problem, and yield a search direction; (2) Test for convergence--if it is satisfied, then stop; (3) Take a step along the search direction to a new point and (4) Update the approximated Hessian matrix H used in the QP and return to step (1).

3.3.4 Conjugate Gradient Method

The conjugate gradient method is an effective method for symmetric positive definite systems. It is the oldest and best known of the no stationary methods discussed here. The method proceeds by generating vector sequences of iterations (*i.e.*, successive approximations to the solution), residuals corresponding to the iteration, and search directions used in updating the iteration and residuals. Although the length of these sequences can become large, only a small number of vectors need to be kept in memory. Two inner products are performed in order to compute update scalars that are defined to make the sequences satisfy certain orthogonal conditions in iterations. On a symmetric positive definite linear system, these conditions imply that the distance to the true solution is minimized in certain norm.

This method is based on conjugate search directions and the spirit of the Steepest Descent method. It is used to find the nearest local minimum of a function of n variables, which presupposes that the gradient of the function can be computed. It uses conjugate directions instead of the local gradient for going downhill (Golub 1989).

3.3.5 Branch and Bound (B&B)

Branch and bound (B&B) is a general algorithm for finding optimal solutions of various optimization problems, especially in discrete and combinatorial optimization. It consists of a systematic enumeration of all candidate solutions, where large subsets of fruitless candidates are discarded by using upper and lower estimated bounds of the quantity being optimized. The method was first proposed by A. H. Land et al. (1960) for linear programming.

3.3.6 Genetic Algorithm (GA)

Genetic algorithms (GA) are search algorithms based on the mechanics of Darwin's natural selection. They combine survival of the fittest among string structures with a structured yet randomized information exchange to form a search algorithm with some of the innovative flair of human search (Holland 1975). Since their introduction by Holland (David et al. 1989), GA has been applied to a diverse range of scientific, engineering, and economic search problems. The robustness of genetic algorithms is due to their capability to locate the global optimum in a multimodal landscape. Examples of applications of GA in the science and engineering fields

include optimization of neural network structure and weights, solution of optimal control problems, and design of structures and image feature recognition (Lee et al. 1995, Katz et al. 1994). The potential of GA for use in process control and control of air-conditioning systems has also been studied (Wang and Wang 2002, Chang 2005, Xu and Wang 2007b).

A GA is a search procedure based on the Darwin's natural selection rather than a simulated reasoning process. Domain knowledge is embedded in the abstract representation of a candidate solution called a chromosome. Usually, the chromosome is constructed by a binary string. Chromosomes are grouped into sets called population. Successive populations are called generations. The GA commences by generating randomly a initial population, *G(0)*. The population *P* of *n* individuals $\{I_1,\cdots, I_n]$ interacts with an environment *E* which returns a fitness $f_1,\cdots, f_n$ for an individual. Corresponding to each individual I_j ($j= i,\cdots,n$) is a chromosome c_j which encodes the individual's genetic information. The basic operation of a GA is to evolve a new population *P'* from *P* by the operations of selection, crossover, and mutation. The selection operation picks individuals from *P* based on some relative fitness criterion. The crossover operation takes pairs of selected individuals as parents and allows them to produce children containing genetic information from both parents. The mutation operation changes some random portion of the chromosome of an individual. Successive generations will produce increasingly fit individuals.

An abstract view of the GA method is listed as follows (Davis 1991): (i) Generate initial population, *G(0)*; (ii) Evaluate *G(0)*; (iii) *t=0*; (iv) Repeat; (v) *c = t+1*; (vi) Generate *G(t)* using *G(t-1)*; (vii) Evaluate *G(t)*.

This process continues until solution is found. There are basically two methods for generating a new population *P'* from *P*. The first method needs the selection operator to select pairs for crossover. The children of this crossover, sometimes with mutation involved according to its probability, replace a pair of individuals in *P*. This method is called steady-state replacement. The other method is called generational replacement. A new population with the same number of individuals in *P* is created by using selection, crossover, and mutation, for a sufficient number of times to fill up the new population.

3.3.7 Evolutionary Programming

For EA in general, there are three major paradigms-evolution strategy (ES), evolutionary programming (EP) and genetic algorithm (GA). Their major differences lie in the data representation, importance of recombination and mutation, and the approach of selection. Generally for GA, the representation of the individuals is binary; recombination (or crossover) is essential; and mutation has less importance and selection is stochastic. For EP, the representation is real-valued, mutation is essential, recombination is not included, and the selection is stochastic. For ES, the representation is also real-valued, both mutation and recombination are important, but the selection is deterministic.

Many optimization problems were handled by EA technique (Back et al. 2000, Beyer 2001, Fogel 1994, Fong et al. 2006, Fong et al. 2008), such as EP and ES. EP in effect has similar feature in the stochastic selection as that of GA, but it is not necessary to be encoded in binary representation for processing, since EP can directly handle the real-valued individuals and mutate them with a suitable variation operator. There are four main stages in this evolutionary programming: Initialization, Evaluation, Selection and Variation. The flow chart of the developed EP algorithm is shown in Figure 3.1

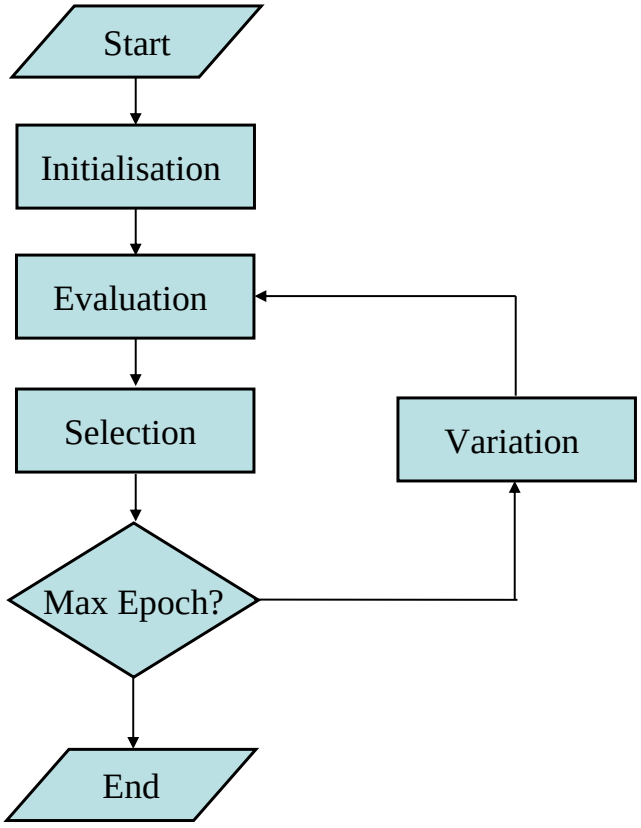

Figure 3.1 Algorithm of evolutionary programming

3.4 Summary

In Section 3.1, we briefly discuss the typical parameters estimated algorithms to learn unknown parameters of a given mathematical model. These algorithms will form the basics and guidance of various models' approximation of the HVAC systems. The application of these estimated algorithms will be discussed in the Chapter 4 to Chapter 8.

Section 3.2 of this chapter summarizes the typical air side control approaches of the HVAC systems, including the local and supervisory control issues. Reasonable optimal control strategies can significantly affect the indoor environment, energy consumption of the different system components, and overall system performance.

As mentioned in the Section 3.3 of this chapter, the performance of the HVAC system can be improved through the optimization of control set points. The great number of variable problems makes the conventional optimization methods require a sequential, computationally intensive approach to search for the optimal set of solutions. To optimize the overall system performance, the different optimization techniques of the local or supervisor control are illustrated. The generality of the problem restricts the number of available solution methods. The mentioned GA global optimization method called simulated annealing has demonstrated success in solving both combinatorial problems (e.g. mixed integer problems) and functions of continuous variables. The simulated general applicability makes it an appealing method for solving the general HVAC system optimization problems.

CHAPTER 4 AN APTIVE DEMAND CONTROLLED VENTILATION STRATEGY FOR MULTI-ZONES HVAC SYSTEMS

In air-conditioning systems serving multiple zones, conventional ventilation strategies often result in over-ventilation in some zones while under-ventilation in other zones when heating/cooling load and occupancy profiles of zones diversify greatly. This chapter presents an adaptive Demand-Controlled Ventilation (DCV) strategy for multi-zone air-conditioning systems, which employs an online occupancy identification using the dynamic multi-zone ventilation equation and zone temperature set point reset of critical zones. The strategy identifies the critical zones online, and fully considers the outdoor air demand of critical zones and the unvitiated outdoor air in the re-circulated air from other zones. The air temperature reset scheme of critical zones results in the increase of the supply air fraction and therefore the amount of outdoor air delivered to the critical zones. Consequently the total outdoor airflow demand and the overall energy consumption are reduced while the ventilation of critical zones is satisfied. The energy and environmental performances of the adaptive DCV strategy is validated and compared with other typical ventilation strategies under various weather conditions.

4.1 Adaptive DCV Strategy Based On the Dynamic Multi-Zone Ventilation Equation

The multiple zone equation (ASHRAE 1999, 2001) is proposed mainly for design purpose to correct the outdoor air fraction for the calculation of outdoor air flow rate set point with the known critical zone in design phase. When a VAV system serves multiple zones, the outdoor air flow rate requirements as well as outdoor air fraction requirement for different zones are very different due to the different thermal dynamics and different practical occupancy. Therefore, the zone with the required greatest outdoor air fraction (i.e., critical zone) also varies. The preset design outdoor air flow rate is not proper in operation due to the dynamic thermal characteristics, the dynamical occupancy and the ever-changing critical zone. To effectively determine the total outdoor air flow rate set point, the multiple zone equation is transplanted using the online determined outdoor air requirement of each zone and online determined critical zone.

4.1.1 Dynamic Occupancy Detection

Since the steady state occupancy detection produces obvious delay of occupancy profile from the actual one, dynamic occupancy detection (Wang et al. 1999) is used for occupancy detection. For a space with multiple zones served by a single air conditioning system, the CO_2 balance is represented as Equation (4.1). For each zone, the CO_2 balance is represented as Equation (4.2). The occupancy model is one dimensional model. When CO_2 concentration derivative terms in the mass balance equations are approximated using the current and previous samplings of CO_2

concentration, the average occupancy in the total space (P^k) and the occupancy in *i*-th zone ($P^k_{zone,i}$) at the current sampling step are detected by Equation (4.3) and (4.4) respectively. To increase the stability and reliability of the detected occupancy, filters are used to decrease the effects of sensors' noise and dynamic derivative term (Wang et al 1999).

$$P_{tot}S + V_{out}C_{out} - V_{out}C_{rtn} = V\frac{dC_R}{dt} \tag{4.1}$$

$$P_{zone,i}S + V_{s,zone,i}C_s - V_{s,zone,i}C_{zone,i} = V_{zone,i}\frac{dC_{zone,i}}{dt} \tag{4.2}$$

$$P^k_{tot} = \frac{E_{ac}(V^k_{out} + V^{k-1}_{out})(C^k_R - C^k_{out})}{2S} + V\frac{C^k_R - C^{k-1}_R}{S\Delta t} \tag{4.3}$$

$$P^k_{zone,i} = \frac{E_{ac}(V^k_{s,zone,i} + V^{k-1}_{s,zone,i})(C^k_{zone,i} - C^k_s)}{2S} + V_{zone,i}\frac{C^k_{zone,i} - C^{k-1}_{zone,i}}{S\Delta t} \tag{4.4}$$

where V_{out} is the outdoor air volumetric flow rate, C_s is the CO_2 concentration of the supply air, V is the air volume in the conditioned space/zone, C_R is the average CO_2 concentration in the conditioned indoor space, P is the number of occupants, and S is the average CO_2 generation rate of an occupant, *zone,i* indicates the *i*-th zone. E_{ac} is the air change effectiveness.

4.1.2 Identification of the Critical Zone

The critical zone is the zone with the greatest required outdoor air fraction in the supply air, while not the maximum outdoor air flow rate requirement. The outdoor

airflow rate requirement of each zone shall be determined by the outdoor airflow rate related to occupancy and the outdoor air flow rate related to the occupied area as Equation (4.5). With the online measurement of the supply airflow rate of each zone, the greatest required fraction of outdoor air in the supply air is determined as Equation (4.6).

$$V_{out,\,zone,\,i} = P_{zone,\,i} R_P + R_b A_{zone,\,i} \tag{4.5}$$

$$Z = \max\left\{ \frac{V_{out,\,zone,\,i}}{V_{s,\,zone,\,i}} \right\} \tag{4.6}$$

where R_P and R_b is the target outdoor air requirements per person and per unit area respectively as prescribed in the standard (ASHRAE 2004), A is the net floor area, $V_{out,zone,i}$ is the outdoor air requirement of the i-th zone, $V_{s,zone,i}$ is the online measurement of supply air to the i-th zone, Z is the outdoor air fraction of the critical zone.

4.1.3 Dynamic Multi-Zone Ventilation Equation

When the air-conditioning system provides the outdoor air flow rate, which is determined by the total detected occupancy as shown in Equation (4.7) (i.e., uncorrected outdoor air flow rate), some zones are over-ventilated while others under-ventilated. Using the measurement of the total supply air flow rate, the uncorrected outdoor air fraction is calculated as Equation (4.8).

$$V_{out,\,uncorrected} = P_{tot} R_P + R_b A \tag{4.7}$$

$$X = \frac{V_{out,uncorrected}}{V_{s,tot}} \tag{4.8}$$

where $V_{out,uncorrected}$ is the uncorrected outdoor air flow rate, $V_{s,tot}$ is the total supply airflow rate, and X is the uncorrected outdoor air fraction.

When the air-conditioning system provides the supply air with the required greatest outdoor air fraction (Z), the critical zone is supplied with the required outdoor airflow rate while the other zones are supplied with a outdoor air flow rate more than required. This means that there is unvitiated outdoor air in other zones, and the unvitiated outdoor air will return and mix in the total supply air. Therefore, the re-circulated unvitiated outdoor air should be counted when calculating the introduced outdoor air flow rate. The online corrected outdoor air fraction directly from outdoor is calculated as Equation (4.9). The actual corrected outdoor air flow rate directly from outside is calculated as Equation (4.10).

where Y is the corrected outdoor air fraction, $V_{out,corrected}$ is the actual corrected total outdoor air flow rate.

Substituting with Equation (4.5)-(4.9), Equation (4.10) can be written as Equation (4.11).

$$Y = \frac{X}{1 + X - Z} \tag{4.9}$$

$$V_{out,corrected} = Y \times V_{s,tot} \tag{4.10}$$

$$V_{out,corrected} = \frac{\frac{P_{tot}R_P + R_bA}{V_{s,tot}}}{1 + \frac{P_{tot}R_P + R_bA}{V_{s,tot}} - \max\left\{\frac{P_{zone,i}R_P + R_bA_{zone,i}}{V_{s,zone,i}}\right\}} \times V_{s,tot} \qquad (4.11)$$

The corrected outdoor airflow rate from outdoor is calculated using the online measurements of *total supply air flow rate* and *the supply airflow rate to each zone*, and the online "measurements" of total occupancy and occupancy in each zone.

4.2 Introduction of the Indoor Air Temperature Set Point Reset Scheme

4.2.1 Zone Temperature Set Point Reset Scheme

In the adaptive DCV scheme, a zone temperature set point reset scheme is employed to force the demanded outdoor airflow rate ($V_{fr,adp}$) from $V_{fr,corrected}$ towards $V_{fr,uncorrected}$ by resetting (reducing in cooling cases) the zone temperature set point of the identified ventilation critical zones while keeping the critical zones supplied with sufficient outdoor air. The effect of this algorithm in the adaptive DCV scheme is illustrated in Figure 4.1. The zone thermal comfort will normally not be scarified noticeably as the PPD index does not vary significantly over a temperature range. The zone temperature set point reset will result in larger flow rate to these critical zones, less outdoor air fraction required by them and eventually less total outdoor airflow demand.

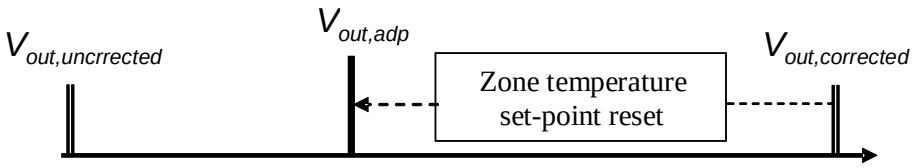

Figure 4.1 Illustration of zone temperature set point reset scheme

4.3 Comparison the Adaptive DCV Strategy with the Conventional Ventilation Strategies

For the conventional control strategies using design occupancy to determine the minimum outdoor air requirement, the acceptable air quality and minimum energy consumption often cannot be achieved in operation because the actual thermal load and occupancy may deviate far that at design conditions. Therefore, in this study, four DCV strategies, including the proposed adaptive DCV strategy, were compared by applying them in a multi-zone VAV system. These four DCV strategies are listed as follows.

Strategy A: *Outdoor air flow rate determined according to detected total occupancy load (e.g. according to Equation (4.7))*

Strategy B: *Outdoor air flow rate determined according to the required outdoor air fraction of the identified critical zone*

Strategy C: *Outdoor air flow rate determined according to the required outdoor air fraction of the identified critical zone using the dynamic multi-zone ventilation equation (e.g. according to Equation (4.11))*

Strategy D: Adaptive DCV using the dynamic multi-zone ventilation equation (Equation (4.11) and critical zone temperature set point reset

Strategy A and Strategy B as well as their basic instrumentation are illustrated in Figure 4.2. Strategy A estimates the total occupancy dynamically as Equation (4.3), using the measurements of return air, outdoor air CO_2 concentrations and outdoor air flow rate. The strategy determines the required outdoor air flow rate according to Equation (4.7).

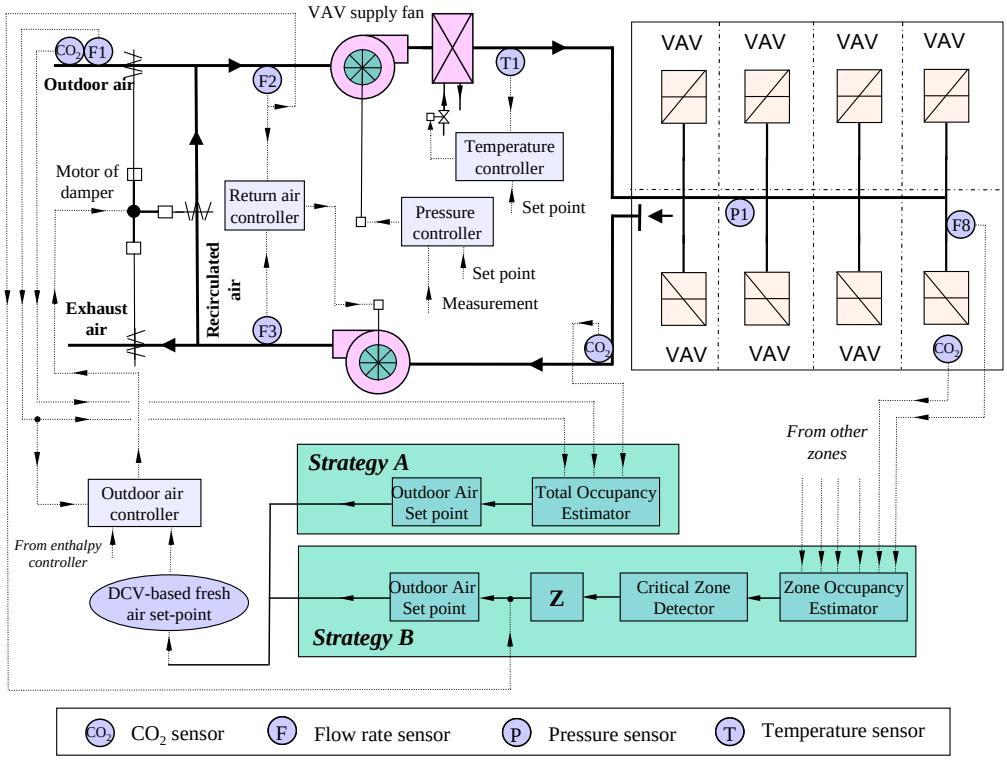

Figure 4.2 Illustration of DCV Strategy A and Strategy B and instrumentation

Strategy B determines the outdoor air flow rate according to the required outdoor air fraction of the critical zone to satisfy the outdoor air requirement of this zone. This strategy des not count the unvitiated outdoor air in the over-ventilated zones. Using

this strategy, as Figure 4.2, the supply air flow rate and the return air CO_2 concentration of each zone are monitored by the control outstation. They are used to estimate the zone occupancy using the zone occupancy estimator as Equation (4.4). Then, the critical zone is identified using Equation (4.5) and (4.6) using the estimated occupancy and the measured supply airflow rate of each zone. Based on the required outdoor air fraction (Z) of the critical zone and the measured of total supply air flow rate, the required total outdoor airflow rate of the system can be determined (i.e., $V_{out,tot} = Z \times V_{s,tot}$).

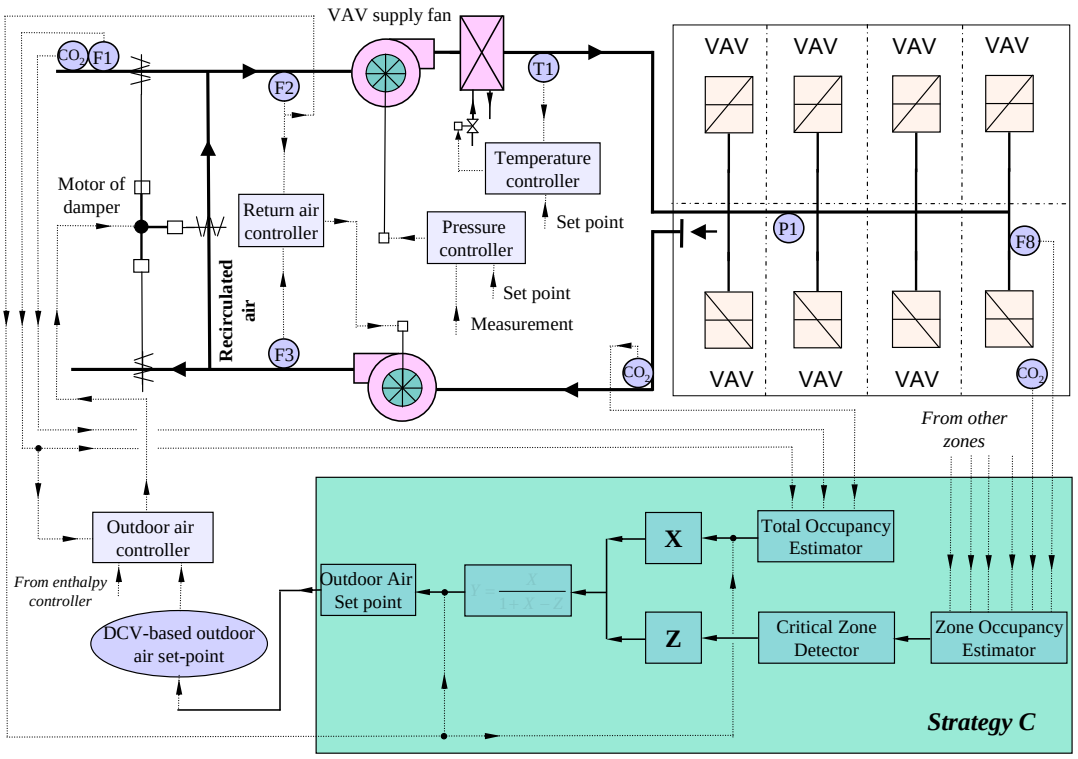

Figure 4.3 Illustration of DCV Strategy C and instrumentation

Strategy C, as illustrated in Figure 4.3, is a trade-off between Strategy A and Strategy B. Using this strategy, the estimated total occupancy and the measured total supply airflow rate are used to determine the uncorrected outdoor air fraction (X) as

Equation (4.7) and (4.8). The required outdoor air fraction (Z) of the identified critical zone is employed to correct the outdoor air fraction (X) using the multi-zone ventilation equation, Equation (4.9). The required outdoor air flow rate is calculated as the product of the corrected outdoor air fraction (Y) and the measured total supply air flow rate as Equation (4.10) or (4.11). This strategy counts the unvitiated outdoor air in the over-ventilated zones.

Strategy D, proposed in this study, is the strategy reducing the total outdoor airflow rate by resetting the air temperature of critical zone on the basis of Strategy C, which is described in detail in the previous section.

4.4 Test and Performance of the Adaptive DCV Strategy

4.4.1 Test System and Environment

The multi-zone VAV air-conditioning system is also illustrated in Figure 4.2. The system serves half of a floor of a high-rise commercial building. Served floor space is divided into eight zones of different usages using partitions as Figure 4.4. Zone 8 is used as a meeting room and other zones are used as office. The ceiling height of the floor is 3.9 meters and the total floor area is 1166 m^2. The concerned floor space faces outside at three orientations. All the conditioned air is delivered to indoor space through VAV boxes. Return air is drawn back through ceiling plenum. The design air flow rate of the VAV system is 6 m^3/s. This system involves two fans of variable pitch angle, a cooling coil and interlocked dampers, etc.

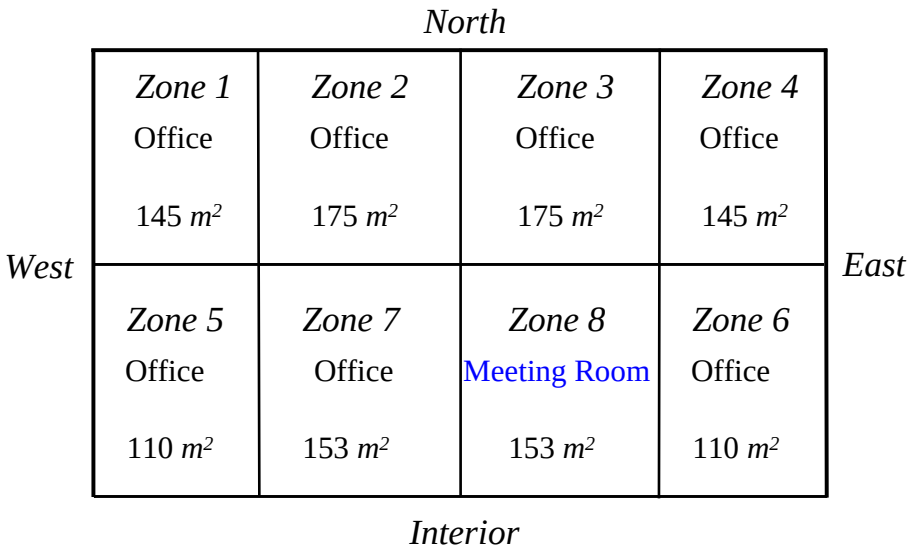

Figure 4.4 Layout of air-conditioned floor of multiple zones

In simulation, all the VAV boxes serving the concerned floor space is represented by eight VAV boxes each serving one zone. The temperature controller controls the outlet temperature of the cooling coil. The pressure controller maintains the supply air static pressure at its set point by modulating the fan pitch angle of the supply fan. The return air controller controls the flow rate difference to maintain a positive pressure in the building. The outdoor air controller controls the outdoor airflow rate by regulating the outdoor air damper. The outdoor air damper, return air damper, and re-circulated air damper are interlocked. Pressure independent VAV boxes are used to control zone temperatures. All the above controllers employ digital PID control.

At high level, the system involves enthalpy control and three supervisory controls. Supply air static pressure set point can be reset by its supervisory controller according to the control status of VAV terminals to reduce the fan energy consumption. Supply air temperature also can be reset according to the control status of VAV terminals to achieve reduced fan energy consumption and to avoid the

indoor temperature out of control. DCV strategy determines an outdoor airflow set point based on estimated indoor occupancy to maintain adequate indoor air quality and reduce energy consumption. Enthalpy control strategy determines if more outdoor air and how much is introduced by comparing the air status of outdoor air and return air to achieve best energy saving. The outdoor airflow supervisor finally chooses the larger one of the set points from the enthalpy control strategy and the DCV strategy. In this study, the four different DCV strategies were employed respectively for comparison purposes.

In practical HVAC systems, most processes are nonlinear. In this study, dynamic models were used to simulate the cooling/heating coils of the nonlinear nature (Wang 1999, Wang and Zheng 2001). The resistance characteristic of the outdoor air damper is nonlinear and was simulated using the Legg's exponential correlation (Legg 1987). The flow characteristics of the heating and cooling coil valves are equal percentage with dead bands (Xu and Wang et al. 2004). Dynamic sensor model was used to simulate the temperature, pressure, flow and CO_2 sensors using time constant method. An actuator model was used to simulate the realistic characteristics of the actuators. The actuator is assumed to accelerate very quickly and then turn at constant speed (Haves and Dexter 1989). A minimum change (e.g. the sensitivity of the actuator) in demanded position is required to restart the actuator. The model also includes the hysteresis in the linkage between actuators and valves or dampers. The detailed description on the models of air-conditioning system and digital controllers can be found in references (Wang 1999).

4.4.2 Test Results and Performance Evaluation

4.4.2.1 Test conditions

In the simulation test, occupancy, lighting and equipment loads in each zone were provided as input data files. The solar gains of each zone transmitted through the windows, sol-air temperature of each zone, the outdoor air temperature, humidity and as well as CO_2 concentration at different weather conditions, were also provided as input data files. The outdoor air CO_2 concentration was 360ppm. The generation rates of CO_2, latent and sensible loads of one person are selected to be $5*10^{-6}m^3/s$, $1.17*10^{-5}$ kg/s and 0.065kW respectively. The internal load and occupancy in each zones remained the same for comparison tests of alternative DCV strategies in different weather conditions. The air-conditioning system worked from 7:50 am to 19:00 pm.

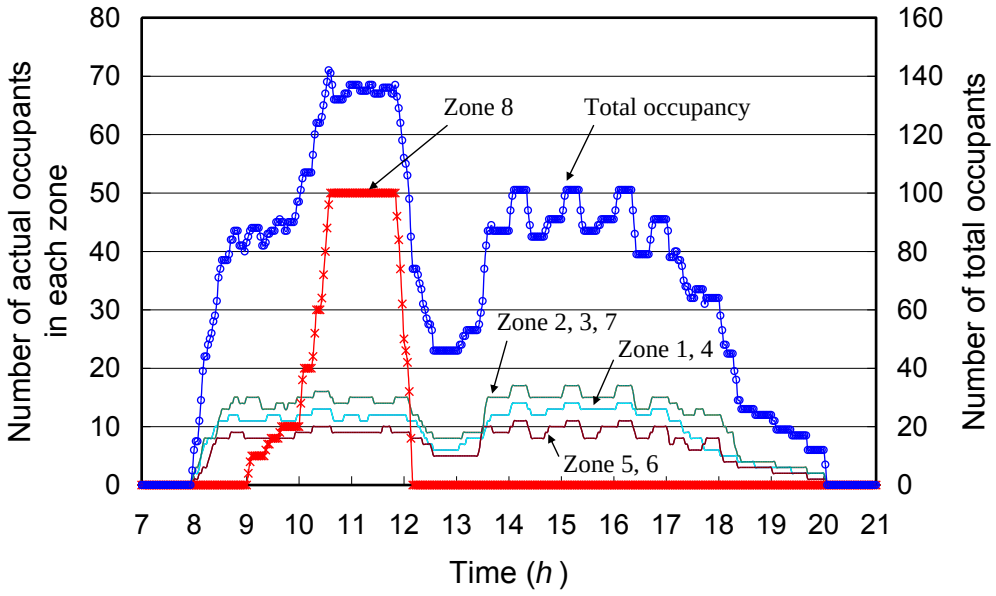

Figure 4.5 Total occupancy profile and occupancy profiles of individual zones

The occupancy profiles of each zone as well as the total occupancy profile are presented in Figure 4.5. The number of occupants varied significantly. For Zone 8 as a meeting room, the occupants enter the meeting room after 9:00am gradually over a period. The occupants reached the maximum about 50 persons at 10:30 am, and left the meeting room at about 12:00 am with a short period. For the zones of office usage from Zone 1 to Zone 7, the maximum density of occupancy is about $10m^2$ per person. The occupancy load varied all the day. Some occupants left the office during lunch hours. At about 6:00 pm, the occupants left the office gradually. However, the air-conditioning system still worked till 7:00 pm for the remaining people. After that, a small number of people still stayed in office for some time and indoor air temperature was maintained by the thermal storage effect of the internal masses.

Many tests were carried out in different weather conditions. The tests of typical sunny summer day and cloudy summer day were presented in the study. Figure 4.6 shows the outdoor air dry-bulb temperatures and humidity in the two test days. The air temperature on the sunny test day varied between 26.1 ℃ and 33.4 ℃. In the sunny summer day, the perimeter zones reached their design thermal load at different times resulting in fully openings of coincident VAV dampers. The air temperature in the mild cloudy summer day varied between 27.6 ℃ and 29.7 ℃ during office hours. In both test days, the weather was very humid. The outdoor air flow was governed by DCV strategy only in both days. The overall solar radiation heat gains of Zone 2, 3, and 4 through windows were the highest among that of all the zones in the morning. In the afternoon, the overall solar radiation heat gain of Zone 1 was is the highest.

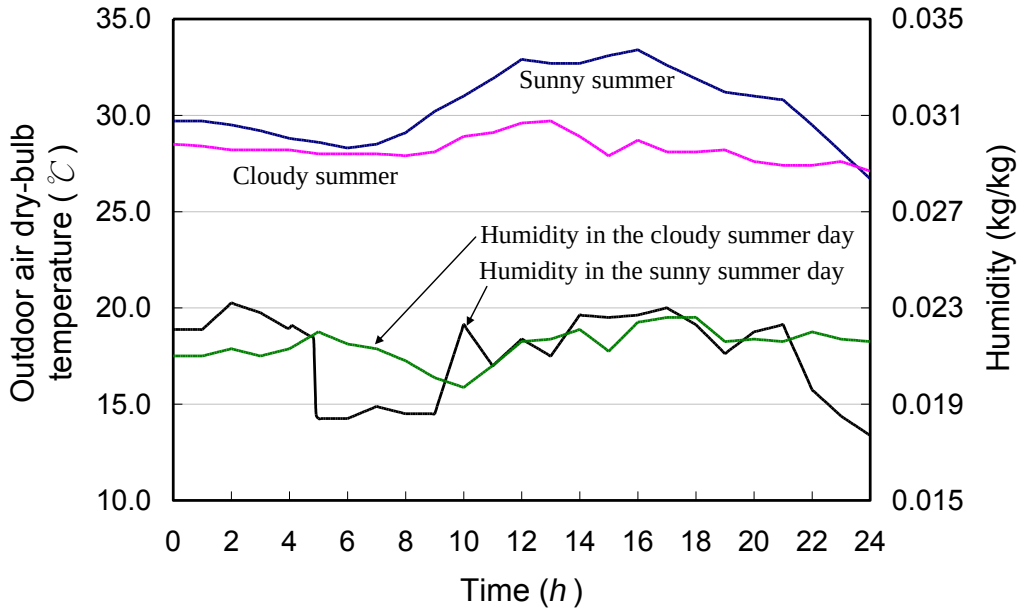

Figure 4.6 Outdoor air dry-bulb temperature and humidity of test days

4.4.2.2 Occupancy detection and control performance

In the evaluation exercise, various tests were conducted to validate the performance of occupancy detection in the alternative strategies at different weather conditions. The occupancy detector performance was similar. The test results in the sunny summer test day using Strategy C were used to demonstrate the performances of the total occupancy estimation and the occupancy estimation of each zone.

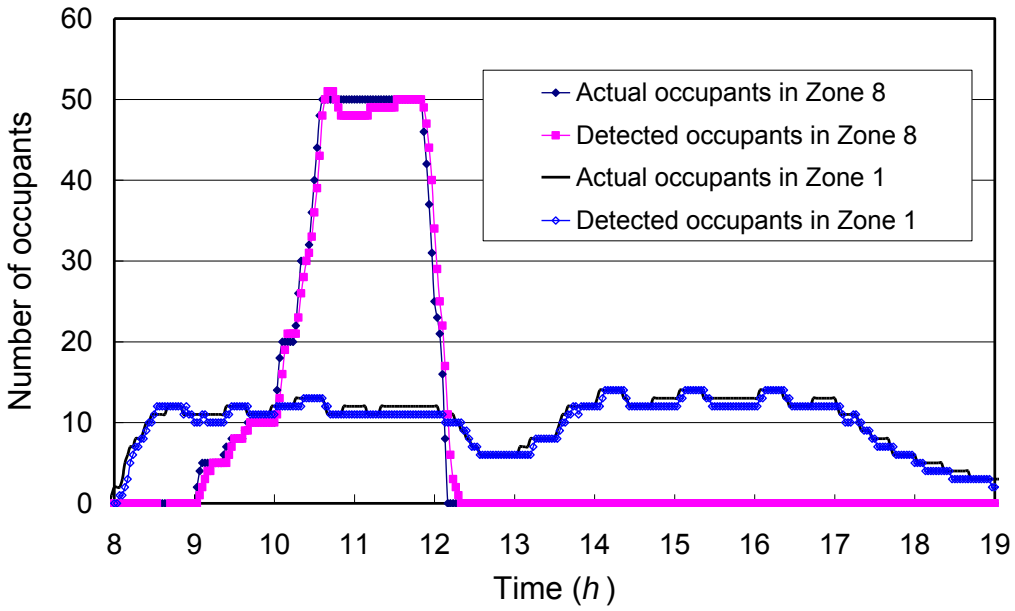

Figure 4.7 Estimated and actual occupancy profiles of Zone 1 and Zone 8

Figure 4.7 presents the estimated and actual occupancy profiles of Zone 1 and Zone 8 respectively. Zone 8 was used for meeting purpose with high occupancy density and sharp changes. It shows that the estimated occupancy profile of Zone 8 followed well the changes of the actual occupancy profile in spite of slight delay and the error of the estimated occupancy was 6.4% which is acceptable. The estimated occupant number of Zone 1 also agreed well with the actual number of occupants. The occupancy estimation performances of other zones were similar as they were used for the same purpose.

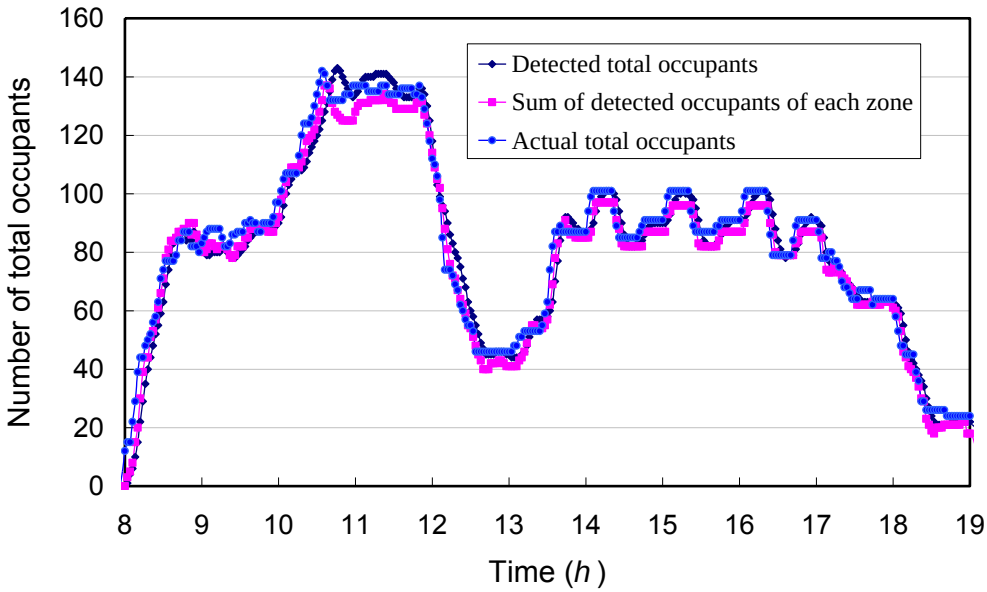

Figure 4.8 Estimated and actual total occupancy profiles

Figure 4.8 presents the actual total number, the estimated total number and the summation of estimated occupant number of eight zones. The figure shows the three profiles matched well. The error of the estimated total occupant number was 7.1% while the error of the summated total occupant number was is 6.4% compared with the actual total occupant number.

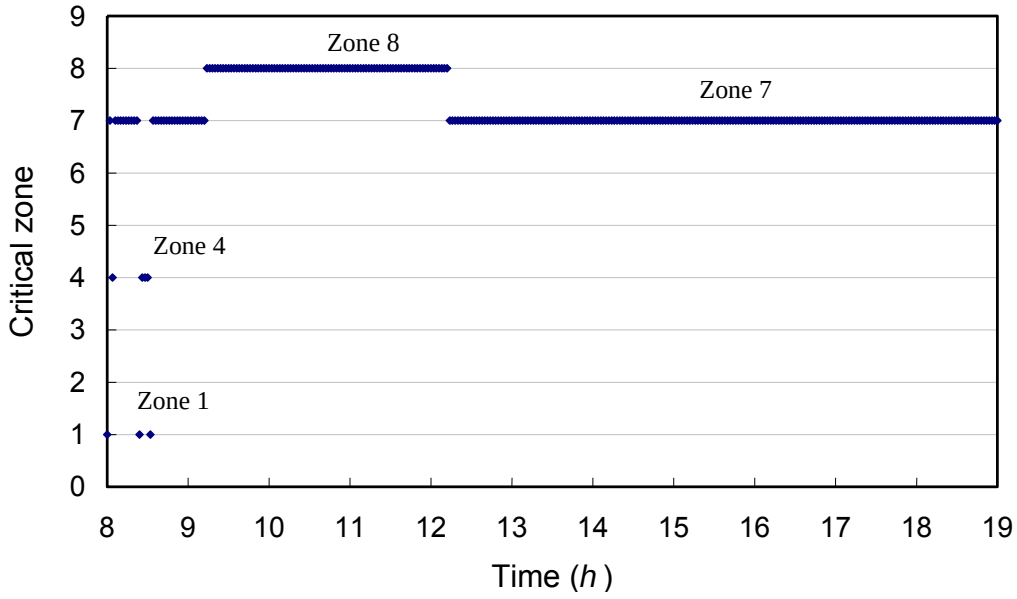

Figure 4.9 Identified critical zones

Figure 4.9 shows the dynamically identified critical zones. In most of the office hour, the critical zone was Zone 7. This zone is an interior zone with relatively less cooling requirement in summer season compared with perimeter zones while the outdoor air requirement is similar to others. When the meeting room (Zone 8) was occupied from 9:00am to 12:00am, the occupants increased greatly resulting in high demand in outdoor air. The critical zone changed from Zone 7 to Zone 8. When the meeting room was unoccupied, the critical zone was returned to Zone 7. Generally, the critical zone varies according to the change of cooling demand and outdoor air flow rate demand of each zone.

As an example, the operation of the system controlled using Strategy C is presented. Figure 4.10 shows the demanded positions (control signals) of outdoor air damper and cooling coil water valve when Strategy C was used.

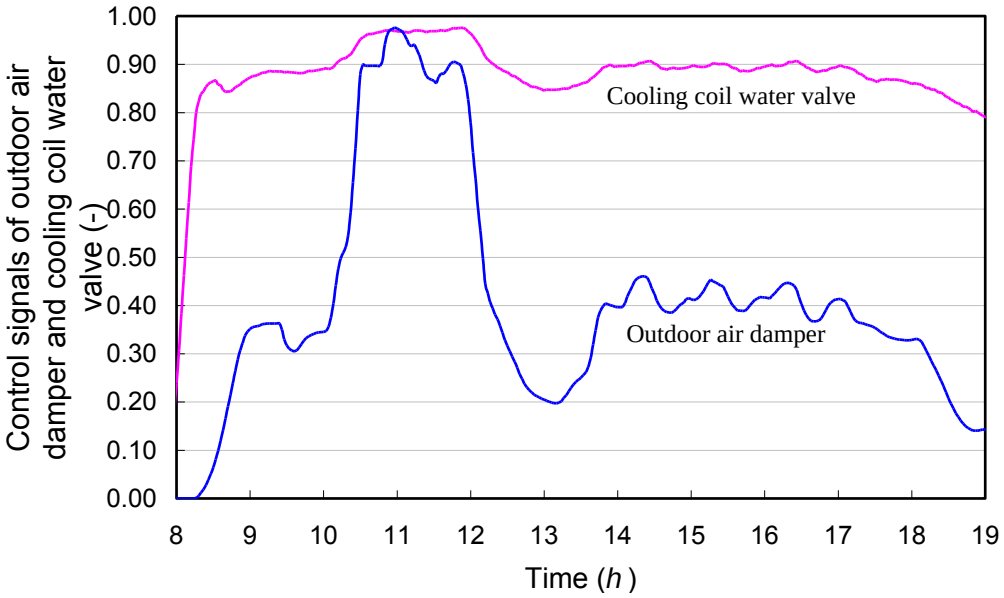

Figure 4.10 Control signals of the water valve and air damper using Strategy C

It can be investigated that the controlled outdoor air damper position increased greatly after 10:00am because of almost fully opening required allowing more outdoor air flow rate introduced to meet the high occupancy load of the meeting room.

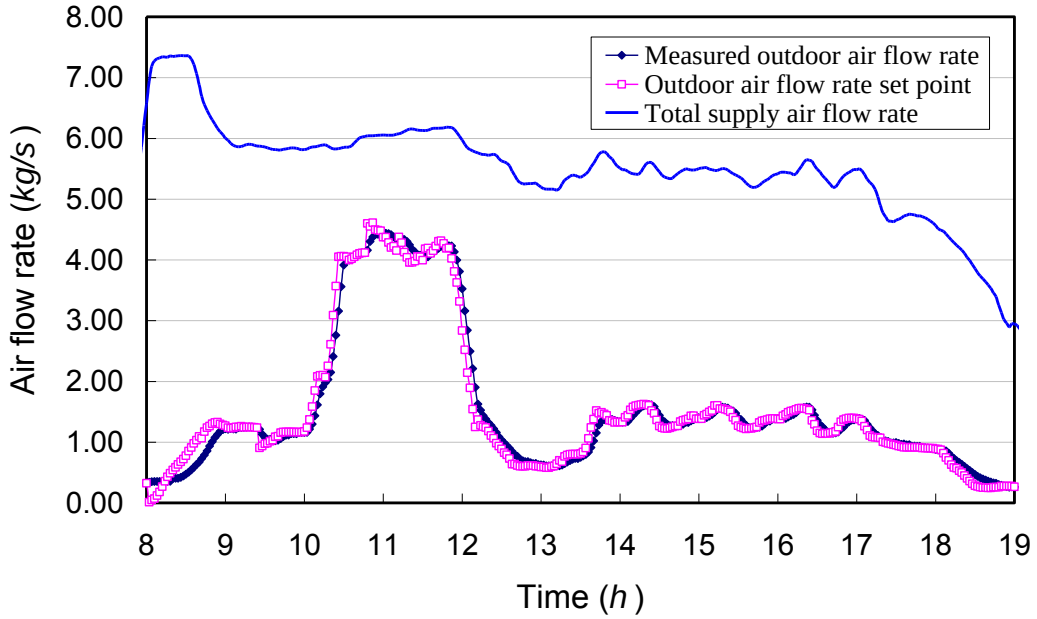

Figure 4.11 Total supply and outdoor air flow rate using Strategy C

Figure 4.11 presents the measured outdoor air flow rate and its set point as well as the measured total supply airflow rate. It shows that demanded outdoor air varied very significantly due to the great changes of occupancy in the meeting room while the total supply air flow rate varied much less according to the total cooling load of the space.

4.4.2.3 Energy and environmental performance

The CO_2 concentration profiles of individual zones using four DCV strategies in the sunny summer test day are presented in Figure 4.12-4.15 respectively.

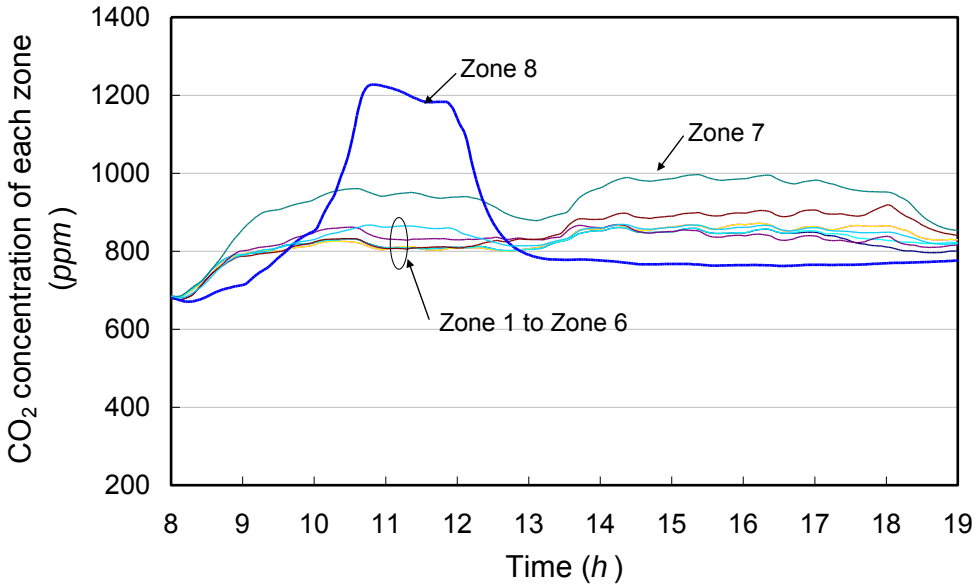

Figure 4.12 CO_2 concentrations of individual zones using Strategy A

When the outdoor air set point was controlled using Strategy A (Figure 4.12), Zone 8 (critical zone) was not supplied with sufficient outdoor air resulting in the maximum CO_2 concentration over 1200ppm and CO_2 concentration over 1000ppm lasting for about two hours when the meeting room was occupied. For the other zones, the CO_2 concentration was almost between 800ppm and 1000ppm. It is obvious that the critical zone is under-ventilated seriously while other zone slightly over-ventilated when the estimated total occupancy was used to determine the total outdoor airflow rate set point.

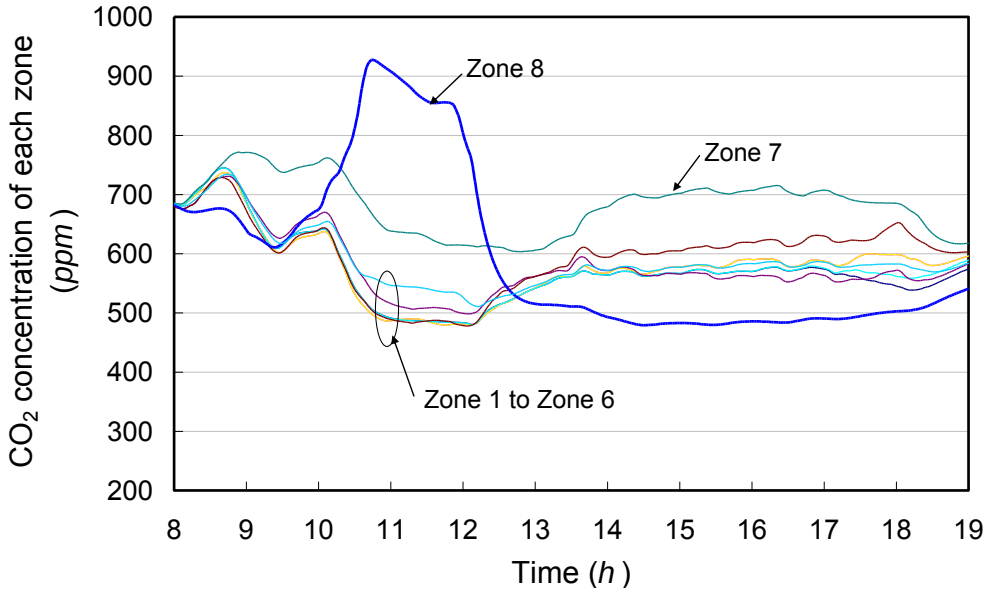

Figure 4.13 CO_2 concentration of each zone using Strategy B

Figure 4.13 shows the CO_2 concentration profiles of individual zones when the outdoor air set point was controlled using Strategy B. The outdoor air set point was much higher than that using Strategy A. All the zones were over-ventilated including the critical zone (Zone 8). The maximum CO_2 concentration of Zone 8 was 927ppm while the average value was very low, 597ppm. The lowest CO_2 concentrations from Zone 1 to Zone 6 were about 500ppm lasting for about one hour. After 12:00am when the occupants left the meeting room, the CO_2 concentrations of zones were still low because of the unvitiated outdoor air. The average values were lower than 600ppm. The average PPD of each zone were desirable, in a range between 5.80 and 7.32 (Table 4.1). This strategy does not count the unvitiated outdoor air when determining the outdoor airflow set point.

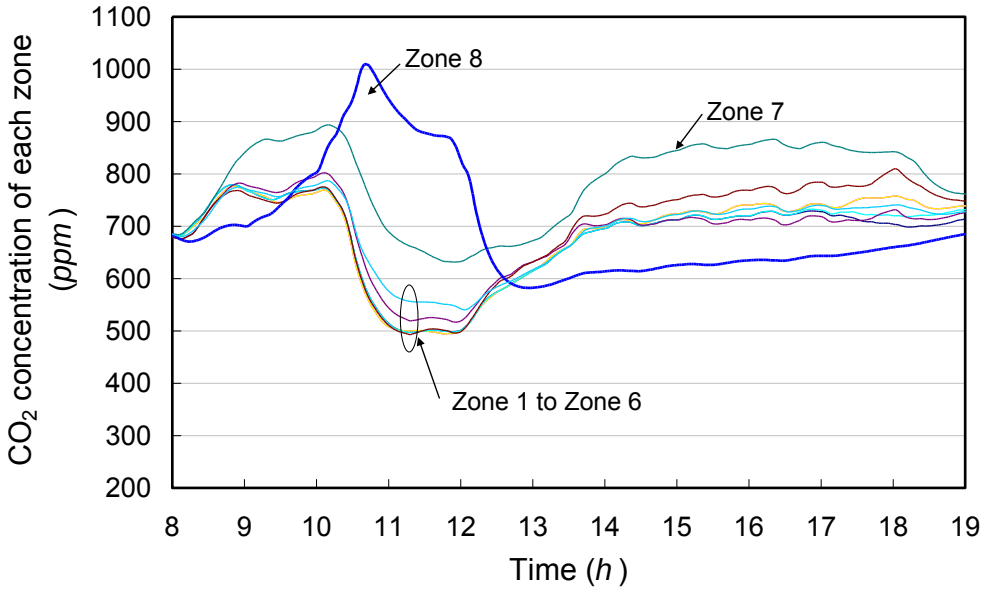

Figure 4.14 CO_2 concentrations of individual zones using Strategy C

Figure 4.14 shows the CO_2 concentrations of each zone using Strategy C. The maximum CO_2 concentration of critical zone (Zone 8) was about 1000ppm lasting for a very short period. The CO_2 concentration was within a range between 800ppm and 1000ppm when this zone was occupied from 10:00am to 12:00am. By counting the unvitiated outdoor air when determining the total supply air flow set point, the CO_2 concentrations from Zone 1 to Zone 6 after 12:00am increased about 150ppm by comparing to the coincident CO_2 concentrations using Strategy B. The average CO_2 concentrations of individual zones in the office hour were between 680ppm to 787ppm. The average PPD of each zone were also desirable from 5.80 to 7.31 as list in Table 4.1. When implementing Strategy C, the outdoor air intake directly from outside was reduced significantly by counting the unvitiated outdoor air.

Although Strategy C can reduce the outdoor air intake directly from outside while maintaining acceptable environmental performance, the CO_2 concentration of

non-critical zones was still very low resulting in high cooling energy consumption when the required outdoor air fractions of zones differ greatly (from 10:00 am to 12:00 am in Figure 4.14). Strategy D can reduce the difference among the required outdoor air fractions of individual zones by resetting the air temperature set point of the critical zone slightly while not scarifying the thermal comfort of the critical zone significantly. In this study, a very simple rule was used to reset the zone temperature set point. When the difference between the required outdoor air fraction of the critical zone (Z) and the uncorrected outdoor air fraction (X) is larger than 0.3, the air temperature of the critical zone is set at 22℃. The air temperature of the critical zone is set at 24℃ (i.e. Original set point) when the difference less than 0.2. The temperature set point is set using simple linear interpolation when the difference is between 0.2 and 0.3.

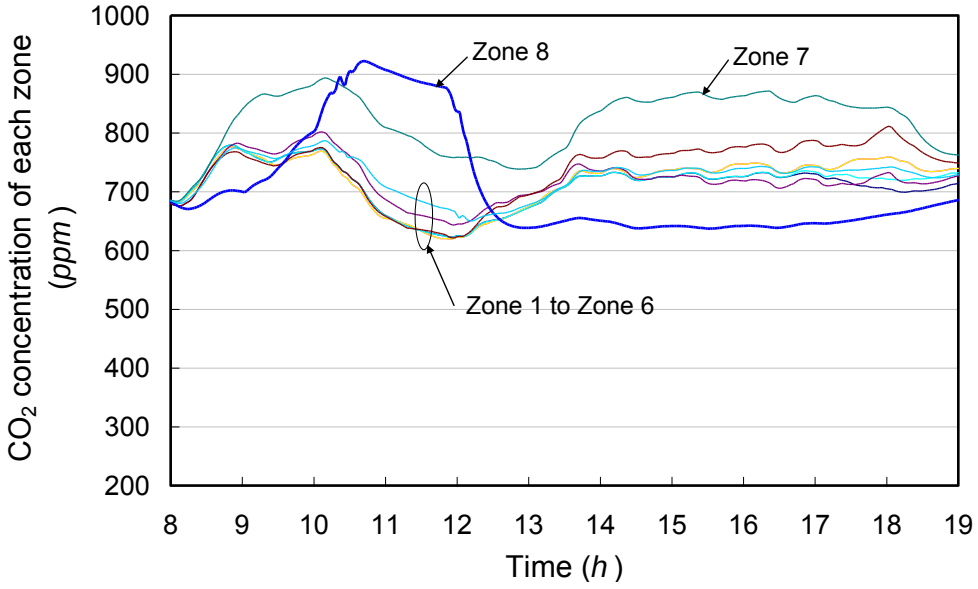

Figure 4.15 CO_2 concentrations of individual zones using Strategy D

Figure 4.15 presents the CO_2 concentrations of individual zones zone using the adaptive DCV strategy (Strategy D). The CO_2 concentration of Zone 8 (as critical zone from 10:00 am to 12:00 am) was about 900ppm while the CO_2 concentrations of other zones at the same period increased more than 100ppm by comparing to that in the coincident period when using Strategy C. In this period, the total outdoor air intake from outside decreased due to the air temperature resetting in the critical zone (Zone 8) which resulted in the decrease of the required outdoor air fraction of this critical zone.

When the air temperature of critical zone was reset, the thermal comfort of individual zones was not affected significantly (PDD of Zone 8 increased from 7.31 to 7.81) as shown in Table 4.1. The average PPD of individual zones was also desirable ranging from 5.84 to 7.81.

Table 4.1 Summary of PPD of each zone in the sunny summer test day using different DCV strategies

Zone		Zone 1	Zone 2	Zone 3	Zone 4	Zone 5	Zone 6	Zone 7	Zone 8
Strategy A	Maximum	17.04	15.60	15.60	17.31	14.44	14.67	11.60	13.20
	Minimum	5.51	5.02	5.02	5.48	5.11	5.00	5.00	5.00
	Average	6.21	5.98	5.98	6.27	5.93	5.92	*5.79*	*7.29*
Strategy B	Maximum	17.04	15.60	15.60	17.31	14.44	14.67	11.60	13.15
	Minimum	5.51	5.02	5.02	5.48	5.11	5.00	5.00	5.00
	Average	6.23	5.98	5.98	6.30	5.92	5.92	*5.80*	*7.32*
Strategy C	Maximum	17.04	15.60	15.60	17.31	14.44	14.67	11.60	13.15
	Minimum	5.51	5.02	5.02	5.49	5.11	5.00	5.00	5.00
	Average	6.22	5.98	5.98	6.28	5.92	5.92	*5.80*	*7.31*
Strategy D	Maximum	17.04	15.60	15.60	17.31	14.44	14.67	11.60	13.29
	Minimum	5.54	5.02	5.02	5.53	5.11	5.00	5.00	5.00
	Average	6.21	5.98	5.98	6.27	5.93	5.92	*5.84*	*7.81*

The energy performance in the sunny summer test day using these four alternative strategies is presented in Table 4.2. When using these strategies, the fan energy consumptions (including VAV supply air fan and return air fan) were almost the same because the total supply air rates, determined by the total cooling load, were not affected by the use of different ventilation strategies. What were very different are the cooling coil energy consumptions due to the cooling load difference of outdoor air when controlled using different ventilation strategies. Using Strategy B, the cooling energy consumption was 51.74% more than that using Strategy A because of a great amount of outdoor air intake, which resulted in serious over-ventilation in non-critical zones as shown in Figure 4.13. When Strategy C, counting the unvitiated outdoor air, was used, the cooling energy consumption was 23.4% more than that using Strategy A while achieving satisfied indoor air quality.

When air temperature of the critical zone was reset slightly lower using Strategy D, the cooling energy consumption was 13.61% more than that using Strategy A while providing satisfied indoor environment quality. Strategy D decreased outdoor air cooling energy consumption greatly although the cooling energy consumption due to lower indoor air temperature increased slightly. This strategy saved about 8% cooling energy when compared with Strategy C. The overall electricity consumptions are also presented in Table 4.2 (assuming overall COP 2.5). The implementation of Strategy D can result in satisfied indoor environment quality by considering the outdoor air fraction demand of critical zone and unvitiated outdoor air in the re-circulated air, as well as resetting the air temperature of critical zones when beneficial.

Table 4.2 Summary of energy performance in the sunny summer test day using different DCV strategies

Strategies	*Strategy A*	*Strategy B*	*Strategy C*	*Strategy D*
VAV fan consumption (*kWh*)	152.69	151.18	151.56	154.82
Return fan consumption (*kWh*)	72.04	73.53	72.72	73.40
Total fan consumption (*kWh*)	224.73	224.71	224.28	228.22
Differential (%)	-	-0.01	-0.20	1.55
Cooling coil consumption (*MJ*)	3321.87	5040.56	4099.07	3774.08
Differential (%)	-	51.74	23.40	13.61
Overall electricity consumption (*kWh*)	593.83	784.77	679.74	647.57
Differential (%)	-	32.16	14.47	9.05

Table 4.3 shows the energy performance in the cloudy summer test day using four DCV strategies. The overall electricity consumption using Strategy B and Strategy C

was 25.25% and 13.56% more than that using Strategy A respectively. Strategy D consumed 7.83% more than that of Strategy A but 5.73% less than Strategy C.

Table 4.3 Summary of energy performance in the cloudy summer test day using different DCV strategies

Strategies	Strategy A	Strategy B	Strategy C	Strategy D
VAV fan consumption (kWh)	112.98	112.70	112.59	113.89
Return fan consumption (kWh)	52.79	53.67	53.23	53.83
Total fan consumption (kWh)	165.77	166.37	165.82	167.72
Differential (%)	-	0.36	0.03	1.18
Cooling coil consumption (MJ)	2711.89	3768.01	3281.56	3023.45
Differential (%)	-	38.94	21.01	11.49
Overall electricity consumption (kWh)	467.09	585.04	530.44	503.66
Differential (%)	-	25.25	13.56	7.83

It is worth noticing that, in some situations, the actual outdoor air cannot follow the outdoor air set point when using Strategy B. As shown in Figure 4.16 for Strategy B in the sunny summer test day, the outdoor airflow rate set point was very high because of considering the outdoor air fraction demand of critical zone only. The actual measured outdoor airflow rate was much less than the set point even if the outdoor air damper was at the fully open position. In fact, in many conventional air-conditioning systems, the supply airflow rate is controlled as priority by modulating supply air fan while outdoor air is controlled by modulating outdoor air damper only.

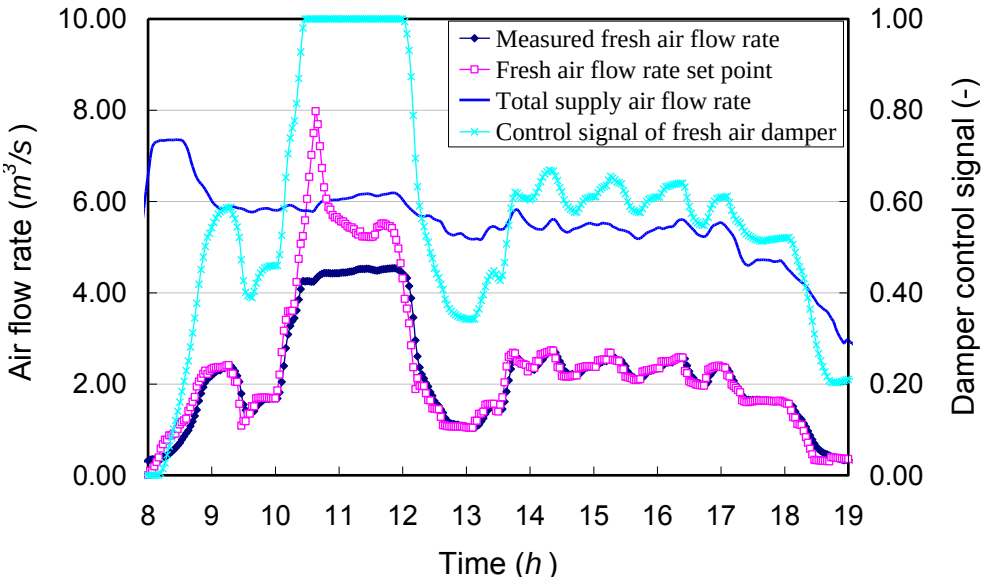

Figure 4.16 Supply/outdoor air flow rates and demanded outdoor air damper position using Strategy B

4.5 Summary

Test results show that the adaptive DCV strategy provides much better energy and environmental performance for multi-zone air-conditioning systems compared with other conventional DCV strategies. This adaptive DCV strategy using dynamic multi-zone ventilation equation and critical zone temperature set point reset can achieve satisfied indoor environment with slightly more energy consumption about 7.8% - 9% in the tested summer conditions in Hong Kong by comparing to the strategy which determines the outdoor air flow rate according to detected total occupancy load. The DCV strategy without adopting using dynamic multi-zone ventilation equation (Strategy B) consumed 25.3% - 32.2% more energy to satisfy the needs of ventilation in critical zones. When the DCV strategy employed the dynamic multi-zone ventilation equation, it consumed 13.6%-14.5% more electricity to satisfy the needs of ventilation in critical zones. The energy saving effect of

adopting dynamic multi-zone ventilation equation was up to 11.7%-17.7%. When adopting the critical zone temperature set point reset, the electrical energy consumption was further reduced by 5.4-5.7%.

The environment and energy performance enhancement of the adaptive DCV strategy is due to the fact that the strategy considers simultaneously the dynamic outdoor air fraction demand of critical zone for better indoor air quality and reuses the unvitiated outdoor air from other zones for energy reduction, and actively reduces the required outdoor air fraction of critical zones using temperature set point resetting without scarifying thermal comfort of these zones. The tests were conducted in the conditions where the thermal load distribution and outdoor air flow distribution mismatch significantly. In practical operations, the actual energy impact will vary significantly. However, it can be concluded that the energy and environmental performance can be improved significantly by adopting the adaptive DCV strategy, i.e. considering the dynamic ventilation needs of critical zones simultaneously, and use of dynamic multi-zone ventilation equation and critical zone temperature set point reset.

CHAPTER 5 MODEL-BASED INDOOR AIR TEMPERATURE SET POINT RESETTING OPTIMAL CONTROL STRATEGY OF CRITICAL ZONES OF MULTI-ZONE HVAC SYSTEMS

This chapter presents a model-based indoor air temperature set point resetting optimal control strategy of critical zones of multi-zone VAV air-conditioning systems aiming at optimizing the total outdoor air flow rate by compromising the thermal comfort, indoor air quality and total energy consumption. Genetic algorithm is used for optimizing the temperature set point of critical zones in the optimization process. This strategy was evaluated in an occupied building and air-conditioning environment introduced in Section 4.4 of Chapter 4 under various weather conditions. The results show that this optimal strategy can achieve significant energy saving while maintaining acceptable thermal comfort and indoor air quality.

5.1 Overview of the Model-based Temperature Optimal Control Strategy

The model-based temperature optimal control strategy is a dynamic temperature set point resetting scheme of critical zones. This strategy is different from the previous studies in that the temperature set point of critical zones is optimized dynamically and automatically, which is adaptive to the ever-changing weather conditions and

indoor condition (mainly occupancy) of each zone. The adaptive multi-zone DCV control strategy presented Chapter 4, is to optimize the total outdoor air flow rate directly from outdoors by considering the outdoor air requirement of the critical zone in multi-zone VAV air conditioning systems, as shown in Figure 5.1. This DCV control strategy aims at counting the unvitiated outdoor air from the over-ventilation zones for reducing the total outdoor air flow rate directly from outdoors in hot seasons when resetting the outdoor air flow rate from outdoors for energy saving.

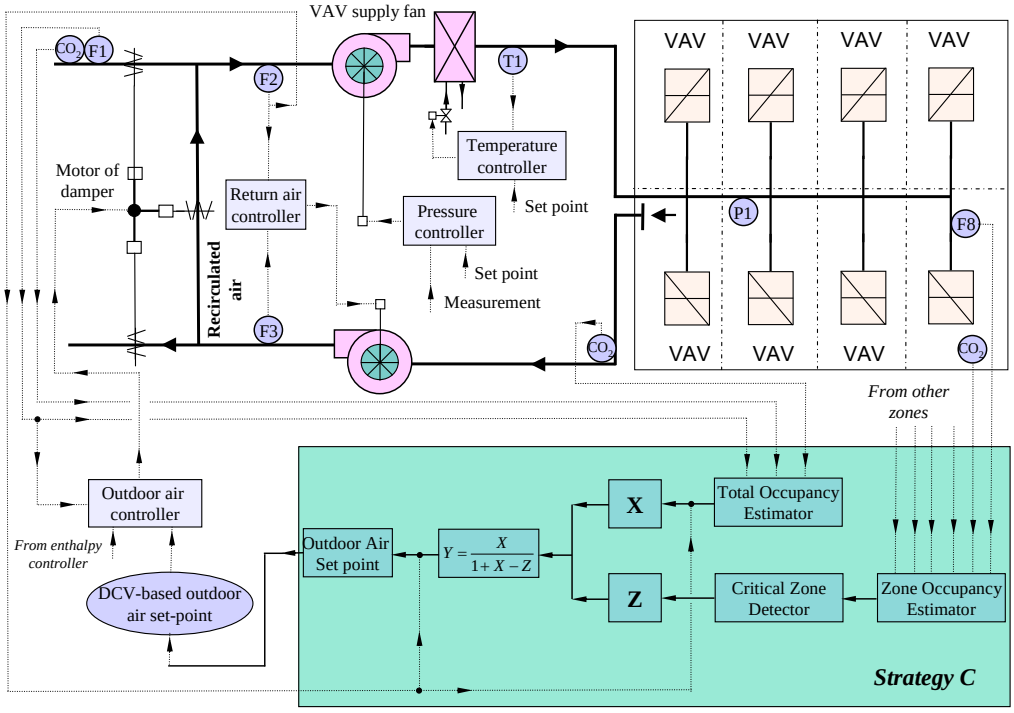

Figure 5.1 Illustration of the dynamic multi-zone ventilation equation scheme and instrumentation

However, when the required outdoor air fractions of zones differ greatly, the capability of the dynamic multi-zone ventilation equation scheme reducing total outdoor air flow rate for energy saving is very limited while maintaining the

acceptable indoor air quality of each zone. If the air temperature set point of the critical zone is reset slightly (e.g. lower in cooling condition) to delivery more air to the critical zones, the required outdoor air fraction of the critical zone decreases resulting the required outdoor air fractions of all the zone tending to be uniform. Eventually, the demanded total outdoor air intake will decrease when the dynamic multi-zone ventilation equation scheme is implemented.

Obviously, the indoor air temperature set point resetting of critical zones will affect the thermal comfort more or less. The dynamic temperature set point resetting scheme is to optimize the temperature set point of critical zones by compromising the indoor thermal comfort, air quality and the total energy consumption. This scheme is based on model prediction and uses genetic algorithm for optimizing the temperature set point of critical zones as shown in Figure 5.2.

5.1.1 Introduction of the Dynamic Temperature Set Point Resetting Strategy

The dynamic temperature set point resetting scheme for critical zones is to the reduce the unbalance of the required outdoor air fractions between the critical zones and other zones aiming at reducing the total energy consumption while maintaining acceptable thermal comfort and indoor air quality in all the zones especially in critical zones. This scheme is illustrated schematically in Figure 5.2, which is parallel to the real process of the multi-zone VAV air conditioning system for online optimizing the temperature set point of critical zones for practical applications. This scheme mainly consists of parameter estimators and genetic algorithm (GA) optimizer. These estimators are developed to identify the parameters of the cooling

coil and fans for their performance predictions, and to identify the source terms (i.e., sensible cooling load, moisture load and CO_2 pollutant load) in each zone for the state prediction of each zone. The parameter identification is based on the online measurements of the real process.

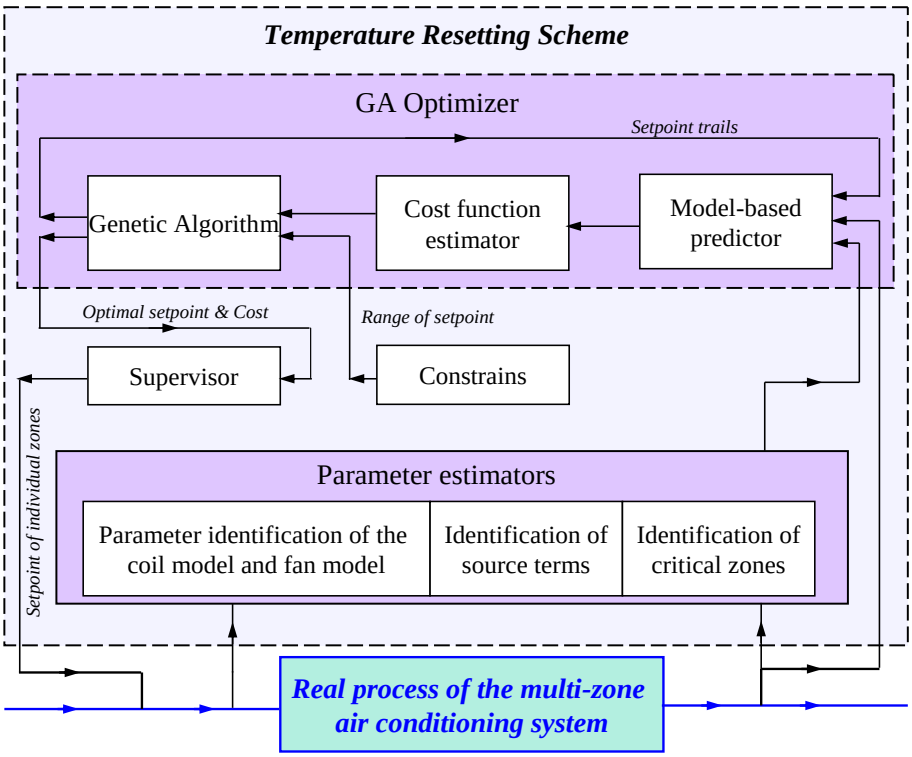

Figure 5.2 Illustration of the dynamic temperature set point resetting scheme of critical zones

In the GA optimizer, a model-based predictor is developed to predict the total energy consumption, thermal comfort and indoor air quality of each zone based on the online identified models and the current states of the real process as well as the temperature set point trails of critical zones. The cost function is calculated based on the predicted performance by compromising total energy consumption, thermal comfort and indoor air quality. Genetic algorithm is employed to optimize the temperature set point of critical zones within the searching range. This optimizer

starts with a group of random set point trails within the allowed range at it first generation. These trails (set point of critical zones) are given to the predictor as inputs for performance prediction. A supervisor determines if the optimal set point is used in the zone temperature controller for practical control. The parameter identification of these simplified models, system performance prediction and temperature optimization of critical zones will be presented respectively.

5.2 Simplified Online Incremental Prediction Model

5.2.1 Parameter Identification for Performance Prediction

For system performance prediction, the parameters of the coil is needed to be identified for thermal performance prediction of the coil in prediction period, and the parameters of fans to be identified for fan power consumption prediction based on predicted air flow rates. The sensible cooling load, moisture load and pollutant load (i.e., source terms) are also needed to be identified online for the state prediction of each zone (i.e., temperature moisture content and pollutant concentration) at the end of the prediction interval.

5.2.2 Incremental Coil Model and Its Parameter Identification

In the prediction period, the cooling coil model needs to predict the required chilled water flow rate and the air moisture at the coil outlet since the inlet air conditions (i.e., air flow rate, moisture content and temperature etc.) is given, the outlet air temperature is set, and the inlet water temperature is given. The cooling coil model needs to be calibrated dynamically in advance using the previous measurements. In

this study, two sets of parameters are assumed to be related to the heat transfer coefficients at water side and air side of the coil respectively. The details are given below.

It is assumed that the Lewis number is equal to one approximately. It is true when the coil works in the normal temperature range. In this case, the Lewis relation is represented as Equation (5.1) (Eckert 1959). The sensible heat transfer rate of a coil can be computed as Equation (5.2) regarding to the Lewis relation. The sensible heat transfer on airside can also be computed as Equation (5.3). The total heat transfer at the air side is computed as Equation (5.4). The water condensation rate on the coil surface can be computed as Equation (5.5). The outlet air moisture content can further be calculated as Equation (5.6) with the known water condensation. As for the water side, the heat transfer has the correlation as Equation (5.7). The transfer coefficients on the water side and air side are the functions of water and air flow rates represented as Equation (5.8) and (5.9) respectively.

$$\frac{UA_{a,T}}{UA_{a,h}} = c_p \tag{5.1}$$

$$Q_{sen} = UA_{a,T}\left(T_{a,in} - T_b\right) = UA_{a,h}\, c_p\left(T_{a,in} - T_b\right) \tag{5.2}$$

$$Q_{sen} = m_a\, c_p\left(T_{a,in} - T_{a,out}\right) \tag{5.3}$$

$$Q_{tot} = UA_{a,h}\left(h_{a,in} - h_b\right) \tag{5.4}$$

$$m_{cond} = UA_{a,h}\left(G_{a,in} - G_b\right) \tag{5.5}$$

$$G_{a,out} = G_{a,in} - \frac{m_{cond}}{m_a} \tag{5.6}$$

$$Q_{tot} = UA_w \left(T_b - T_{w,in}\right) \tag{5.7}$$

$$UA_w = \beta_w \left(m_w\right)^{\gamma_w} \tag{5.8}$$

$$UA_{a,h} = \beta_a \left(m_a\right)^{\gamma_a} \tag{5.9}$$

where $UA_{a,T}$ and $UA_{a,h}$ are the sensible heat transfer coefficient and mass transfer coefficient respectively at air side, UA_w are the heat transfer coefficient at water side, Q is heat flow, G is the moisture content, T is temperature, T_b is the equivalent coil surface temperature, h is enthalpy, h_b and G_b are the saturated air enthalpy and the saturated air moisture content at the equivalent coil surface temperature, m is mass flow rate, c_p is air specific heat, β and γ are model parameters to be identified, subscripts *sen*, *cond* indicate sensible, condensation respectively, subscripts *a*, *in*, *out*, *w* indicate air, inlet, outlet and water respectively.

To identify the parameters of β and γ, the heat transfer coefficients of $UA_{a,h}$ and UA_w need to be calculated while the equivalent coil surface temperature (T_b) is computed in advance using iteration based on the inlet and outlet air states of the coil. To increase the accuracy of the model prediction, the model parameters (i.e., β_a, γ_a, β_w, γ_w) are assumed to be constant within a limited working range. Therefore, they are considered to be slowly-varying parameters. These parameters are estimated using RLS (recursive least square) estimation technique with

exponential forgetting using measurements. Using the heat transfer coefficients calculated at the current and former sampling instants, *RLS* technique is used to estimate and update the parameters of the coil model. With the known parameters, the water flow rate and outlet air moisture content can be computed based on Equation (5.2-5.9) at the prediction period.

5.2.3 Incremental Fan Model and Its Parameter Identification

The power input of fans can be modeled to be approximately proportional to their flow rate cubed as Equation (5.10) when the change of flow rate is in a small range. Since the power input and flow rate are measured, the parameter can be learnt and estimated directly as Equation (5.11) and updated at each sampling instant. A first-order filter is used to filter the effects of the measurement noises on the parameter estimation. With the parameter, the power input of fans can be estimated as Equation (5.10) based on the air flow rates.

$$W = \omega v^3 \tag{5.10}$$

$$\omega^k = \frac{W^k}{\left(v^k\right)^3} \tag{5.11}$$

where W is the power input, v is the air flow rate of the fan, ω is parameter to be estimated. This parameter is assumed to be constant in a prediction period.

5.2.4 Incremental Source Terms of All the Zones

Building sensible cooling load, latent load (i.e., moisture load), and pollutant load are important external disturbances of the air conditioning system. In the optimization process, these loads are needed to know in advance to predict the air state of indoor space for system performance prediction. These loads can not be measured directly. However, they can be estimated based on measurements. For each zones, the energy balance, moisture balance and pollutant balance can be expressed as Equation (5.12-5.14) respectively. In the study, CO_2 concentration is used to indicate IAQ of each zone although VOCs may also be used for the index of indoor air quality. Sensible heat load ($Q_{sen,i}$), moisture load (D_i) and pollutant load (S_i) are called *source terms* since they are the driving forces in these equations. In a prediction period, these three source terms can be considered to be constant, and can computed during a sampling step as Equation (5.15-5.17).

$$M_i c_p \frac{dT_i}{dt} = m_{s,i} c_p (T_s - T_i) + Q_{sen,i} \tag{5.12}$$

$$M_i \frac{dG_i}{dt} = m_{s,i} (G_s - G_i) + D_i \tag{5.13}$$

$$V_i \frac{dC_i}{dt} = v_{s,i} (C_s - C_i) + S_i \tag{5.14}$$

$$Q_{sen,i}^k = M_i c_p \frac{T_i^k - T_i^{k-1}}{\Delta t_{smp}} - m_{s,i}^k c_p \left(T_s^k - T_i^k\right) \tag{5.15}$$

$$D_i^k = M_i \frac{G_i^k - G_i^{k-1}}{\Delta t_{smp}} - m_{s,i}^k \left(G_s^k - G_i^k\right) \tag{5.16}$$

$$S_i^k = V_i \frac{C_i^k - C_i^{k-1}}{\Delta t_{smp}} - v_{s,i}^k \left(C_s^k - C_i^k \right) \tag{5.17}$$

where M is the air mass of one space, C is the CO_2 concentration, V is the volume of one space, D is the moisture generation rate, S the CO_2 generation rate, Δt_{smp} is the sampling interval, subscripts s indicates supply air, superscripts k and $k-1$ represent the current and previous sampling instants respectively.

In the optimization process of the temperature set point of critical zones in one prediction period, this resetting of the set point will result in slightly change of the sensible cooling loads in critical zones due to the heat transfer through building envelopes and the internal mass. Therefore, the originally estimated sensible cooling load of critical zones is needed to corrected, and then is used in the prediction period for system performance prediction. This correction is made approximately as Equation (5.18) according to the sampling indoor air temperature and outdoor air temperature as well as the temperature set point of the critical zones. In the prediction period, the moisture load and pollutant load of each zone are assumed be the same as estimated in the sampling step. The sensible cooling loads of non-critical zones are also assumed to be the same as estimated in the sampling step.

$$Q_{sen,i}^{pred} = (1-\alpha) Q_{sen,i}^k + \frac{\alpha Q_{sen,i}^k}{T_{out}^k - T_i^k} \left(T_{out}^k - T_{set,i} \right) \tag{5.18}$$

where α is a coefficient accounting for the heat flow through building envelopes and internal mass, the subscript *set* indicates set point, the superscript *pred* indicates prediction.

5.3 System Performance Prediction Using GA Optimal Algorithm

5.3.1 System Performance Prediction

System performance prediction includes the prediction of the indoor air states (i.e., temperature, moisture content and pollutant) of all the zones, the supply air flow rate of each zone, the total supply air flow rate, the outlet air state of the cooling coil, the energy consumption of the cooling coil, the power consumption of fans etc. in one prediction period. To accurately predict the dynamic process responses at the end of one prediction period (Δt_{pred}) and within this prediction period, the prediction period is simulated by dividing this period into *N* simulation steps of the time step Δt_{sim} as Equation (5.19). For the performance prediction of the coil, *Section 5.2.2* has given detailed descriptions. During a small simulation time, supply air flow rate and conditions are assumed to be constant. Because sensible heat load ($Q_{sen,i}$), moisture load (D_i), and pollutant (S_i) are slowly-varying variables, they are assumed to be constant during a prediction period. Therefore, Equation (5.12-5.14) can be expressed approximately by replacing the derivative terms with finite difference terms as Equation (5.20-5.22) respectively.

$$\Delta t_{sim} = \frac{\Delta t_{pred}}{N} \tag{5.19}$$

$$T_i^{j+1} = T_i^{j} + \left[\frac{m_{s,i}^{j}}{M_i} \left(T_s^{j} - T_i^{j} \right) + \frac{Q_{sen,i}}{M_i c_p} \right] \Delta t_{sim} \tag{5.20}$$

$$G_i^{j+1} = G_i^j + \left[\frac{m_{s,i}^j}{M_i} \left(G_s^j - G_i^j \right) + \frac{D_i}{M_i} \right] \Delta t_{sim} \tag{5.21}$$

$$C_i^{j+1} = C_i^j + \left[\frac{v_{s,i}^j}{V_i} \left(C_s^j - C_i^j \right) + \frac{S_i}{V_i} \right] \Delta t_{sim} \tag{5.22}$$

where the subscripts *j* and *j+1* represent the current and the next simulation time steps respectively, subscripts *sim* indicates simulation.

Neglecting the delay of the VAV local supply air flow control loop responding to the change of flow rate demand of each zone, the VAV supply air flow rate to each zone at the current simulation time step can be expressed as Equation (5.23) by the prediction of the VAV flow rate set point. Assuming the VAV system can deliver the demanded air flow rates to each zone, the total air flow rate of the VAV system can be expressed as Equation (5.24). The return air flow rate is assumed to be equal to the total supply air flow rate. The return air temperature, moisture and pollutant are assumed to be constant using the values at the current sampling instants although they are changing in the prediction period. The changes of the total supply air flow rate and the outdoor air rate account for the change of the cooling energy consumption of the cooling coil.

$$m_{s,i}^j = m_{s,\min,i} + U_{PID,i}^j \left(m_{s,\max,i} - m_{s,\min,i} \right) \tag{5.23}$$

$$m_s^j = \sum_{i=1}^{I} m_{s,i}^j \tag{5.24}$$

where subscripts *max*, *min* indicate maximum and minimum respectively, $U_{PID,i}^{j}$ is the prediction of the PID control output of the space temperature controller at the current simulation step (*j*).

$U_{PID,i}^{j}$ is computed as Equation (5.25). These three terms of this equation are the proportional term, integral term and derivative term respectively. They can be predicted using Equation (5.26-5.28) for a simulation time step. These terms can be in different forms according to the actual PID algorithm implemented by a manufacturer. E_i is the difference between the zonal air temperature and its set point of the *i*-th zone, and can be expressed as Equation (5.29). At each sampling step, the initial values of integral term and derivative term can be fetched from the relevant storage of the zonal temperature controllers.

$$U_{PID,i}^{j} = U_{P,i}^{j} + U_{I,i}^{j} + U_{D,i}^{j} \tag{5.25}$$

$$U_{P,i}^{j} = K_{P,i} E_i^{j} \tag{5.26}$$

$$U_{I,i}^{j} = \frac{K_{P,i}}{t_{I,i}} \frac{\left(E_i^{j} + E_i^{j-1}\right)}{2} \Delta t_{sim} + U_{I,i}^{j-1} \tag{5.27}$$

$$U_{D,i}^{j} = \frac{K_{P,i} t_{D,i} \frac{\left(E_i^{j} + E_i^{j-1}\right)}{\Delta t_{sim}} + U_{D,i}^{j-1}}{2} \tag{5.28}$$

$$E_i^{j} = T_i^{j} - T_{set,i}^{j} \tag{5.29}$$

where K_p is the proportional gain, the subscripts *P*, *I* and *D* indicate proportional, integral and derivative respectively.

These models for the prediction of state variables (i.e., T_i, D_i, C_i) are needed to be tuned further for increasing accuracy since there may be derivations between the predictions and the real processes. The tuning model as Equation (5.30) is employed to correct the model predictions. At a sampling instant (t^{k-1}), the required measurement data are collected to estimate the source terms as Equation (5.15-5.17). These source terms are used by these models as Equation (5.20-5.22) to estimate the state variables at the next sampling instant (t^k) by the simulation of a few time steps. At the next sampling instant, these state variables are available and the model prediction error (e^k_{meas}) can be measured. To reduce the effects of the measurement uncertainty and model uncertainty, a filter using forgetting factor is used to stabilize the error estimation (e^k_{est}) as Equation (5.31). This error is used to correct the model output at the future next sampling instant (t^{k+1}).

$$\hat{Y} = Y + e \tag{30}$$

$$e^{k+1}_{est} = \lambda\, e^k_{est} + (1-\lambda) e^k_{meas} \tag{5.31}$$

where *Y* is the output of the model (i.e., state variables T_i, D_i, C_i), $\hat{Y}$ is the output of the model after correction, *e* is the correction factor representing the estimated error between model prediction and real process. e_{est} is the model error estimation, e_{meas} is the measured model error, λ is a forgetting factor.

5.3.2 Optimization of Temperature Set Point of Critical Zones

With these models proposed previously, the responses of the building and air-conditioning systems to the changes of the controls (i.e., total outdoor air flow rate and zonal temperature set point) can be predicted in a prediction period. The responses of concern are the air temperature, moisture content, supply air flow rate, pollutant (CO_2) concentration of each zone, total supply air flow rate and outdoor air ventilation rate, outlet temperature and moisture content of the cooling coil, total cooling energy consumption and the power consumption of fans.

In the optimization of the temperature set point of critical zones, three elements, i.e., IAQ (represented using CO_2 concentration) of each zone, the thermal comfort of each zone, and total energy consumption are significantly of concern. The total cost function (J) for the optimization is constructed as Equation (5.32) accounting for the IAQ of each zone, the thermal comfort of each zone, and total energy consumption. J_{tc} is the cost function concerning the thermal comfort of all the zones as Equation (5.33). J_{iaq} represents the cost function concerning the IAQ of all the zones as Equation (5.34). It is worthwhile to mention that the thermal comfort and IAQ of all the zones are involved in the cost functions in that the building system (including all the zones) and the air conditioning system are interrelated together and affect each other although only the temperature set point of the critical zone is optimized. J_{pow} is the cost function of total energy consumption as Equation (5.35), which includes the cooling energy consumption of the coil, the power consumptions of the supply fan and return fan.

$$J\left(T_{cz,set}\right) = \alpha_{tc} J_{tc} + \alpha_{iaq} J_{iaq} + \alpha_{pow} J_{pow} \tag{5.32}$$

$$J_{tc} = \int_0^{t=\Delta t_{pred}} \sum_{i=1}^{I} \left(PMV_i\right) dt \tag{5.33}$$

$$J_{iaq} = \int_0^{t=\Delta t_{pred}} \sum_{i=1}^{I} \left(\tan \frac{\pi C_i}{4 C_{thld}} - 1 \right) dt \tag{5.34}$$

$$J_{pow} = \int_0^{t=\Delta t_{pred}} \left(W_{fan,\sup} + W_{fan,rtn} + \frac{Q_{cooling}}{COP} \right) dt \tag{5.35}$$

where J is cost function, α is the weighting factor, C_{thld} is the threshold CO_2 concentration (950ppm was used), PMV_i is the index of PMV (i.e., predicted mean vote) of each zone and can be calculated by using Fanger's comfort equations (Fanger 1970), $Q_{cooling}$ is the cooling energy consumption of the coil, COP is the coefficient of performance including the pump and the chiller (assumed to be constant as 2.5), I is the number of zones, subscript *cz*, and *rtn* indicate critical zone and return respectively.

Searching for the optimal value of the temperature set point of critical zones is a nonlinear optimization process. There exist many methods for such optimization problems such as sequential quadratic programming (House and Smith 1991) and conjugate gradient method (Nizet et al. 1984) and Genetic algorithm (GA) (Mitchell 1997) etc. GA is a good optimization method since it can quickly find a sufficiently good solution with random initialization. This algorithm was ever used to search for global optimal solutions in HVAC fields (Wang and Wang 2002, Chang 2005, Xu

and Wang 2007b). In this study, GA is also utilized to search for the optimal value of the temperature set point of critical zones by minimizing the objective function as Equation (5.32). The fitness function (f) in the genetic algorithm is represented as Equation (5.36).

$$f\left(T_{cz,set}\right)=\frac{1}{J\left(T_{cz,set}\right)} \tag{5.36}$$

In the genetic algorithm, only one parameter (i.e., $T_{cz,set}$) constitutes the chromosome of an individual. The search scope of this parameter is between 21℃ and 24℃. 24℃ is the default set point of all the zones while 21℃ is near the cooler temperature border suggested by the standard (ASHRAE 1994). Random initialization of this parameter produces the initial population to start a GA *run*. Each set point trail (i.e., the temperature set point of the critical zone) is given to the model-based predictor to predict the responses of the system during one prediction period as show in Figure 5.2. Then the cost function estimator computes the "overall cost" (also the fitness) according to the predicted responses of the system. According to the fitness of parents and its rules for crossover and mutation, the GA optimizer generates the next generation population, and then the system responses are predicted, and the fitness is re-evaluated. This process is repeated. The criterion to stop the GA optimizer is based on the comparison of the best fitness values of two consecutive *runs*. The GA estimator stops when the relative difference between the two maximum fitness values reaches a threshold value. A GA *run* is also terminated if the number of the current generation is equal to a predefined maximum number.

The parameters of the GA driver are important for convergence speed. They are selected according to Carroll's recommendation (Carroll 2001) and also determined by simulation tests.

5.4 Performance Test and Evaluation

The multi-zone VAV air-conditioning system is also illustrated in Figure 4.3 in Chapter 4. The system serves half of a floor of a high-rise commercial building as well shown in Figure 4.4 in Chapter 4.

In this study, at high level, the system involves enthalpy control and three supervisory controls. Supply air static pressure set point can be reset by its supervisory controller according to the control status of VAV terminals to reduce the fan energy consumption. Supply air temperature also can be reset according to the control status of VAV terminals to achieve reduce of fan energy consumption and to avoid the indoor temperature out of control. DCV strategies determine an outdoor airflow set point based on estimated indoor occupancy to maintain satisfied indoor air quality and reduce energy consumption. Enthalpy control strategy determines if more outdoor air and how much outdoor air are introduced by comparing the air status of outdoor air and return air to achieve best energy saving. The outdoor airflow supervisor finally chooses the larger one of the set point from the enthalpy control strategy and the DCV strategy. In this study, the DCV strategy (i.e., the model-based optimal ventilation control strategy) was implemented.

5.5 Test Results and Analysis

The model-based optimal ventilation control strategy (i.e., optimal strategy) combines the dynamic ventilation equation scheme and the dynamic temperature set point resetting scheme of critical zones for improving energy efficiency and better indoor environmental quality. This optimal strategy was tested in the above test facility with the test conditions described in *Section 5.4.1*. In this strategy, many models are required for system performance prediction, and the performance of these models directly affects the performance of this optimal strategy. The main models of concern were evaluated in *Section 5.4.2*. The performance of the optimal strategy was evaluated in *Section 5.4.3* by comparing with that of a strategy only using dynamic ventilation equation scheme (i.e., conventional strategy thereafter). In the cost function for optimizing temperature set point of critical zones, the weighting factors relating with the indoor air quality, thermal comfort and energy consumption have obvious impacts on the performance of the optimal strategy. The choice of these factors and their effects on the strategy's performance are presented in *Section 5.4.4*.

5.5.1 Test Conditions

The test facility was built on TRANSYS platform. Many disturbances affecting building cooling load and indoor air quality are needed to be prepared as input files for TRANSYS. The internal disturbances are occupancy, lighting and equipment loads in each zone while the external disturbances are mainly the solar gains of each zone transmitted through the windows, sol-air temperature of each external wall, the outdoor air temperature, humidity and CO_2 concentration at different weather

conditions. The outdoor air CO_2 concentration was 360ppm. The generation rates of CO_2, latent and sensible loads of one person are selected to be $5*10^{-6}m^3/s$, $1.17*10^{-5}$ kg/s and 0.065kW respectively. The air-conditioning system worked from 7:50 am to 19:00 pm.

This optimal control strategy is to reduce the difference of the required outdoor air fractions of each zone, and further to reduce the total outdoor air flow rate due to the variation of the occupancies among each zones at the same time and the variation of occupancy of one zone at different time. Therefore, the occupancy profiles of each zone and the total occupancy profile are presented in Figure 5.3.

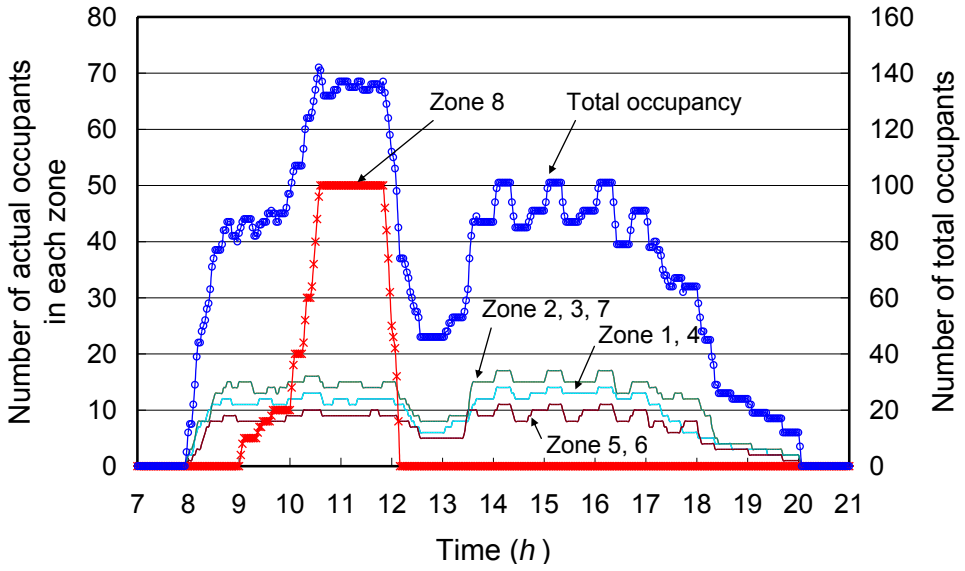

Figure 5.3 Occupancy profiles of individual zones and the total occupancy profile

A brief of the occupancies is also given bellow. The number of occupants of all the zones varied significantly. For Zone 8 as a meeting room, the occupants entered the meeting room after 9:00am gradually over a period. The number of the occupants reached the maximum about 50 persons at 10:30am, and they left the meeting room

at about 12:00am within a short period. For the zones of office usage from Zone 1 to Zone 7, the maximum density of occupancy is about $10m^2$ per person. The occupancy load varied all the day.

In out tests, we found the CO_2 concentration in the meeting room is much higher than the prescribed level (i.e., about 700*ppm* above the CO_2 concentration of outdoor air) when we used the latest standard [ASHRAE 2004]. Therefore, in this study, the following rule was used to compute the outdoor air requirement of each zone. The outdoor air requirement is compute according to the number of occupants, i.e., 10*l/s* per person for office and meeting room [ASHRAE 1999, ASHRAE 2001] while the minimum outdoor air requirement is taken according to the air-conditioning area, i.e., 0.3*l/s* per square meter for office and meeting room [ASHRAE 2004]. This rule gives consideration to not only the minimum outdoor air rate for occupant-generated pollutants but also the minimum outdoor air rate for diluting non-occupant-generated pollutants.

In the cost function as Equation (5.33), the PMV index is the function of the indoor air temperature, velocity, relative humidity, mean radiant temperature of surrounding surfaces of a zone, the mean values of the metabolic rate and clothing level of the occupants. In the absence of detailed velocity distributions, the velocity in a zone is assumed to be spatially uniform and computed by dividing the supply air volumetric flow rate to a zone by the floor area. The occupant activity level used was 1.2 *met* and the clothing insulation value was 0.8.

In our test, the sampling interval of this strategy was 60*s*. The prediction period was 300*s* while the simulation time step of the optimal control strategy was 60*s*. The weighting factors of the cost functions used are given in Table 5.1 (The detailed analysis of these factors will be delivered subsequently). Many tests were carried out to test the performance of the optimal strategy (and the conventional strategy) in different weather conditions. Only the tests in typical sunny summer day and cloudy summer day were presented in the study. Figure 5.4 shows the outdoor air dry-bulb temperature and humidity in both test days. In both test days, the weather was very humid. The set point of the outdoor air flow rate was governed by DCV control in both days.

Table 5.1 Control settings of the cost functions of the optimizer

Weighting factors of cost functions	α_{tc}	α_{iaq}	α_{pow}
Setting I	2.00	0.35	0.01
Setting II	2.00	0.50	0.01
Setting III	2.00	0.00	0.01
Setting IV	0.00	0.35	0.01
Setting V	2.00	0.50	0.00

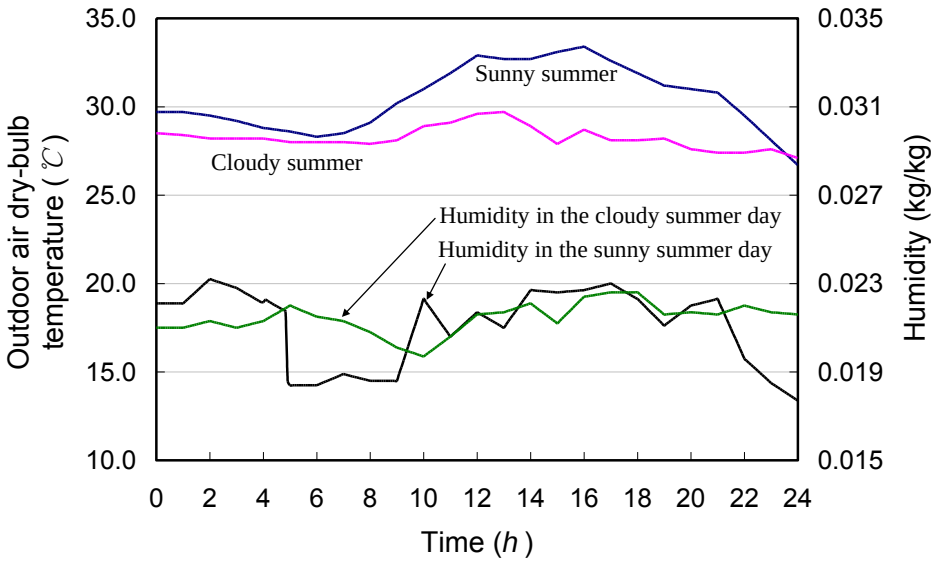

Figure 5.4 Temperature and humidity profiles of test days

5.5.2 Evaluation of the Models

In this study, many models are required for system performance prediction, and the performance of these models directly affects the performance of this optimal strategy. The main models of concern were evaluated in this section. In addition, accurate estimation of occupants of each zone is the basis of this optimal strategy for improving energy efficiency. For the performance of occupancy detection of each zone and all the space, readers are encouraged to go through the article (Xu and Wang 2007a).

The main models of concern are the cooling coil model, the models of source terms, and the models for estimating the zonal air states of each zone. All are presented next in detail. The results of the performance evaluation of these models are presented bellow when the weighting factors of *Setting I* were used.

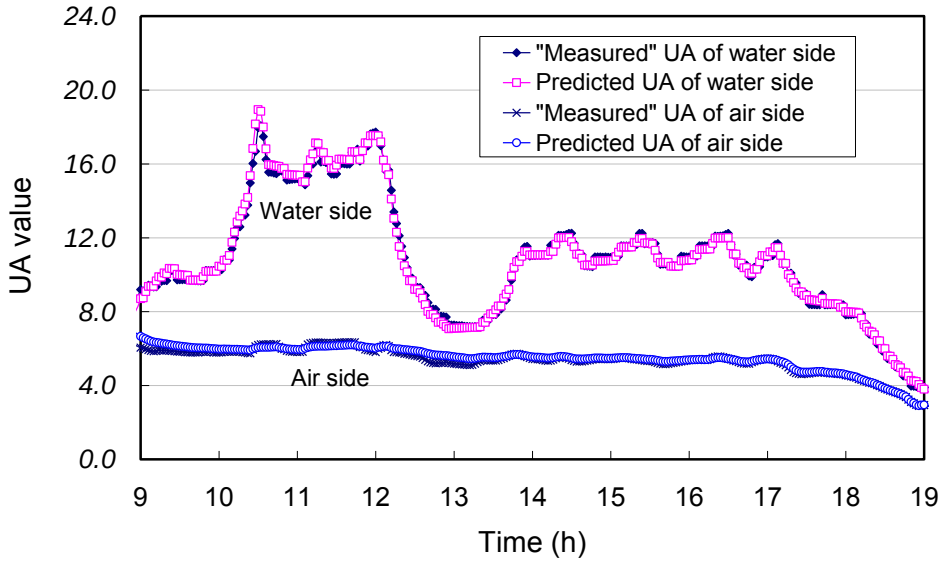

Figure 5.5 Heat transfer coefficients of the cooling coil at water side and air side

Figure 5.5 presents the "measured" and predicted heat transfer coefficients (i.e., UA values) of the cooling coil at water side and air side respectively from 9:00*am* to 7:00*pm*. The coefficients from 8:00*am* to 9:00*am* did not present since the measurements at this period were required for the initialization of *RLS* algorithm. The "measured" heat transfer coefficients were calculated using Equation (5.1-5.7) based on the measurements. The predicted heat transfer coefficients were calculated using Equation (5.8-5.9) based on the water flow rate and air flow rate while the parameters in Equation (5.8-5.9) were identified in advance. The predicted coefficients of the coil at water side and air side agreed well with the coincident "measured" coefficients. In addition, the heat transfer coefficient at water side is much larger than that at air side since water is much easier to conduct heat than air. The heat transfer coefficient at water side was much high from about 10:30*am* to 12:00*am* since much water flow rate was required for cooling when the meeting room was occupied densely.

For the source terms, i.e., sensible cooling load, latent load and pollutant load, the pollutant load (represented using CO_2) is easier to calculate based on the number of occupants than the sensible load and latent load. Therefore, the CO_2 generation rate is presented for validating the performance of models for source term identification. Figure 5.6 presents the "measured" CO_2 generation rate and the actual CO_2 generation rate of Zone 1 and Zone 8. The "measured" rate was estimated using the model as Equation (5.17) based on the measurements. The actual rate was calculated based on the actual occupants. The results show that the "measured" CO_2 generation rate matched the actual generation rate very well.

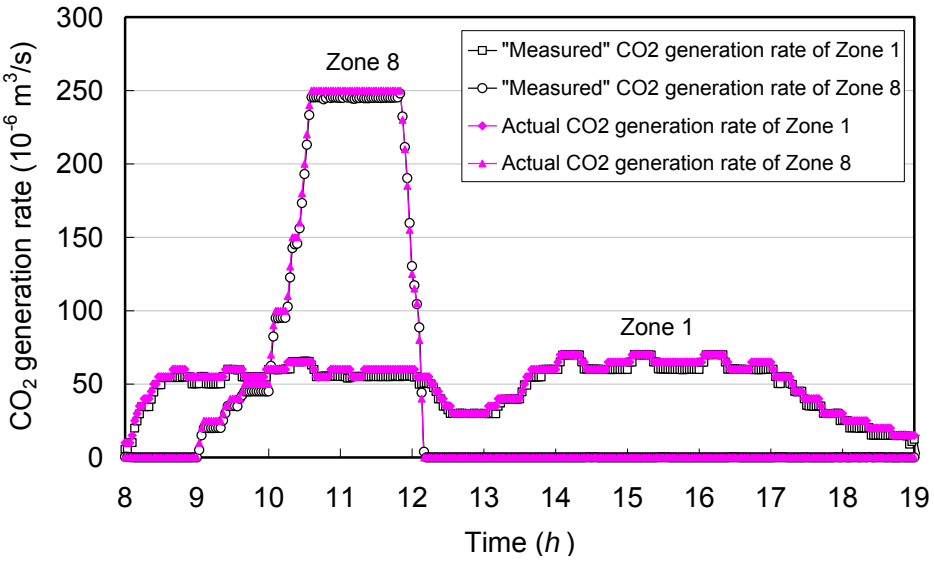

Figure 5.6 CO_2 generation rates of Zone 1 and Zone 8

For the estimation of zonal air states, only the indoor temperature of Zone 8 and the predicted temperature error are presented for performance evaluation as shown in Figure 5.7.

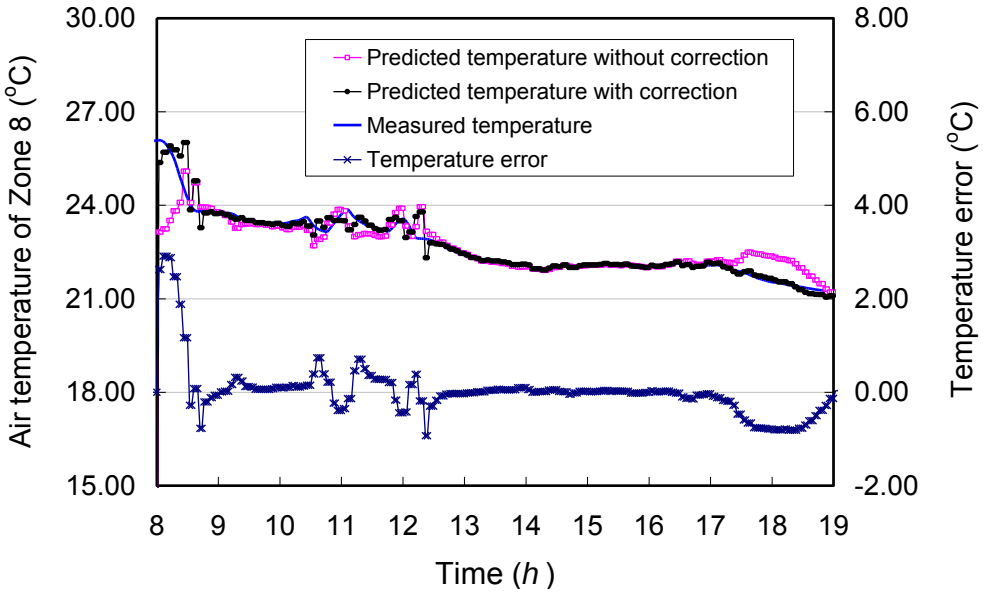

Figure 5.7 Comparison of measured and predicted air temperature of Zone 8

The results show that the predicted temperature using the model as Equation (5.20) basically agreed with the measured indoor air temperature. However, this prediction deviated from the actual measurement in some periods. When the tuning model as Equation (5.30-5.31) was used to correct the prediction, the situation was improved significantly. The tests for the prediction of the zonal moisture content and CO_2 concentration also show the model prediction matched the coincident measurement very well.

5.5.3 Evaluation of the Optimal Strategy

This model-based optimal ventilation control strategy is to establish a compromise among the indoor air quality, thermal comfort and energy consumption by the means of resetting the total outdoor air flow rate and resetting the temperature set point of critical zones. The choice of the weighting factors (i.e., coefficients) of the cost function determines the significance of the different factors when the optimal strategy decides the optimal temperature set point of critical zones. These parameters should be chosen properly according to the user's requirements and the actual system. For the performance evaluation of the optimal strategy, the performance of the conventional strategy (i.e., the strategy only using the dynamic ventilation equation scheme) is used as the benchmark. For the performance evaluation of other DCV control strategies, the previous study (Xu and Wang 2007a) has presented the relevant results.

The costs related with the thermal comfort, indoor air quality, and total energy consumption, and the total cost in the sunny summer test day are presented in Table

5.2 when different control settings of the weighting factors were used. These costs were integrated over the entire operation period. The environmental and energy performance of the optimal strategy using different control settings in the sunny summer test day are presented in Table 5.3. The environmental and energy performance of the conventional strategy are also presented in this table as the benchmark. In this section, only the performance of the optimal strategy using the control setting of *Setting I* is analyzed subsequently in detail. Table 5.2 shows that the optimal control strategy considered these three terms (i.e., thermal comfort, IAQ and power consumption) basically evenly since the weight factors are 2.00, 0.35 and 0.01 as shown in Table 5.1.

Table 5.2 Summary of the costs of the optimal strategy with different control settings in the sunny summer test day

Cost	Control settings				
	Setting I	Setting II	Setting III	Setting IV	Setting V
Cost of thermal comfort	37279	37402	37322	36944	38055
Cost of IAQ	-84229	-82567	-81404	-90234	-84007
Cost of power consumtion	2103897	2117451	2117232	2082715	2140582
Total cost	66116	54695	95816	-10755	34106

Table 5.3 Summary of the environmental and energy performance of the conventional strategy and the optimal strategy with different control settings in the sunny summer test day

Environmental and energy performance	Conventional strategy	Optimal strategy with different control settings				
		Setting I	Setting II	Setting III	Setting IV	Setting V
Environmental performance						
Average PPD of Zone 8 (%)	8.86	8.01	8.08	8.09	8.22	7.86
Maximum PPD of Zone 8 (%)	16.37	14.67	14.69	14.69	14.74	14.64
Average CO_2 concentration (ppm)	700	716	714	719	710	709
Maximum CO_2 concentration (ppm)	1009	1083	1074	1101	989	1003
Energy performance						
Fan (kWh)	224.28	227.04	227.31	227.36	227.99	226.17
Differential (%)		*-1.23*	*-1.35*	*-1.37*	*-1.65*	*-0.84*
Cooling energy consumption (MJ)	4099.07	3789.73	3810.19	3774.01	3814.34	3941.2
Differential (%)		*7.55*	*7.05*	*7.93*	*6.95*	*3.85*
Overall power consumption (kWh)	679.73	648.12	650.66	646.69	651.81	664.08
Differential (%)		*4.65*	*4.28*	*4.86*	*4.11*	*2.30*

Using the optimal strategy, the temperature set point of critical zones can be reset. Figure 5.8 presents the temperature set point of critical zones, and Figure 5.9 presents the identified critical zones for reference. In most of the office hours, the critical zone was Zone 7. From 9:10am to 12:00am, the critical zone was Zone 8 (the meeting room). Generally, the critical zone varied according to the change of cooling demand and outdoor air flow rate demand of each zone. With the identified critical zone, the optimal strategy optimized the temperature set point as shown in Figure 5.8 while the temperature set point of the other zones kept at the default value (24℃).

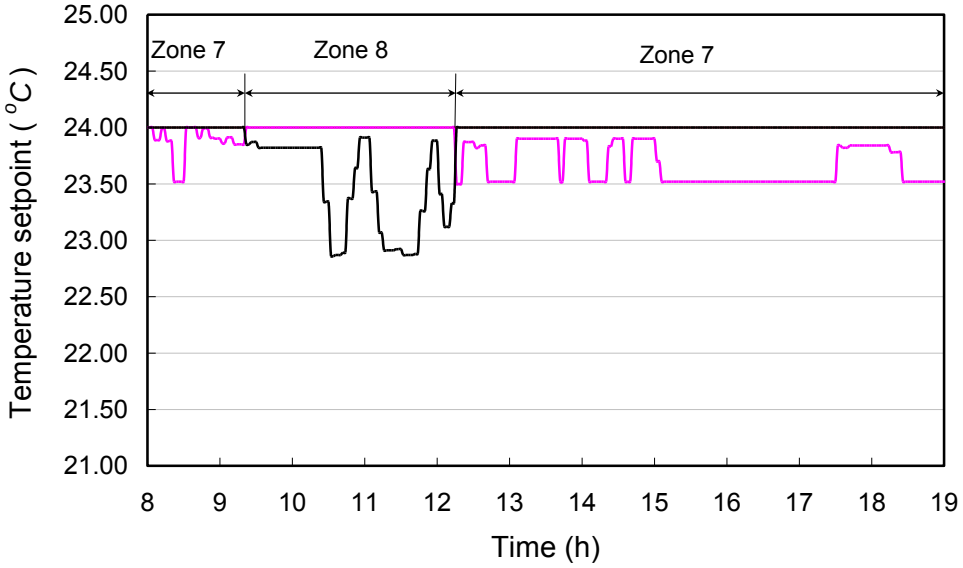

Figure 5.8 Temperature set point of critical zones using the optimal strategy (*Setting I*)

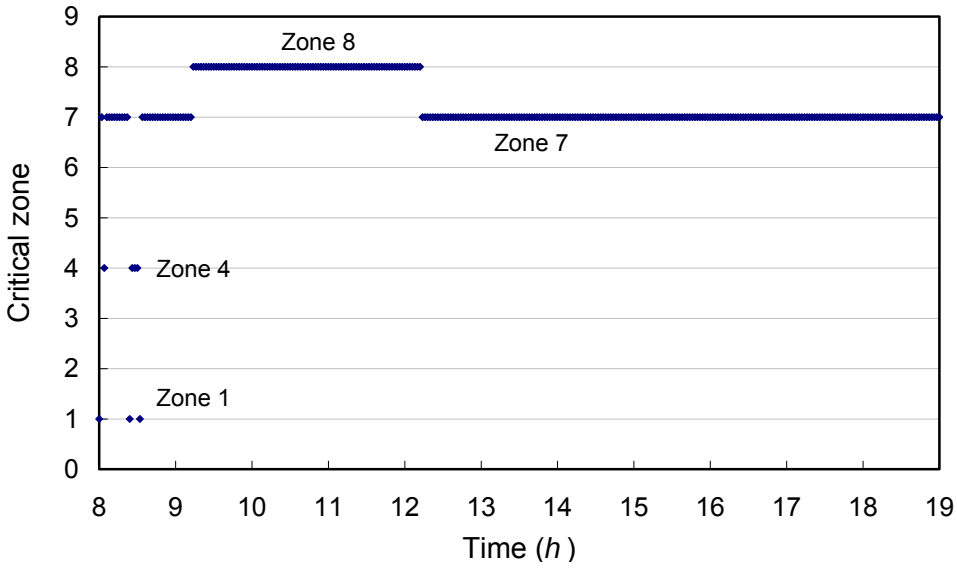

Figure 5.9 Critical zones identified

When the optimal set point of critical zone was used for the practical control, the total outdoor air flow rate reduced greatly as shown in Figure 5.10 when comparing with that using the conventional strategy as shown in Figure 5.11. From 10:30*am* to 12:00*am*, the total outdoor air flow rate using the optimal strategy is about two third

of that using the conventional strategy. It is also noticed that the total supply air flow rate increased in this period because the critical zone (Zone 8) needed more supply air flow rate to offset the sensible load due to the low temperature set point as shown in Figure 5.8. It is also worthwhile to mention that the outdoor air was controlled very well since the measured outdoor air flow rate followed the set point well.

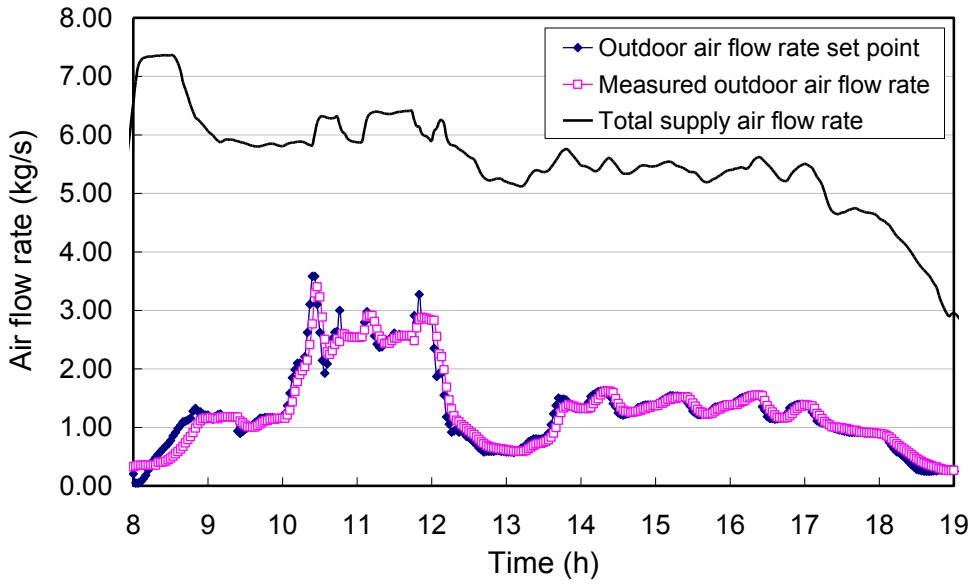

Figure 5.10 Total supply air and outdoor air flow rates using the optimal strategy (*Setting I*)

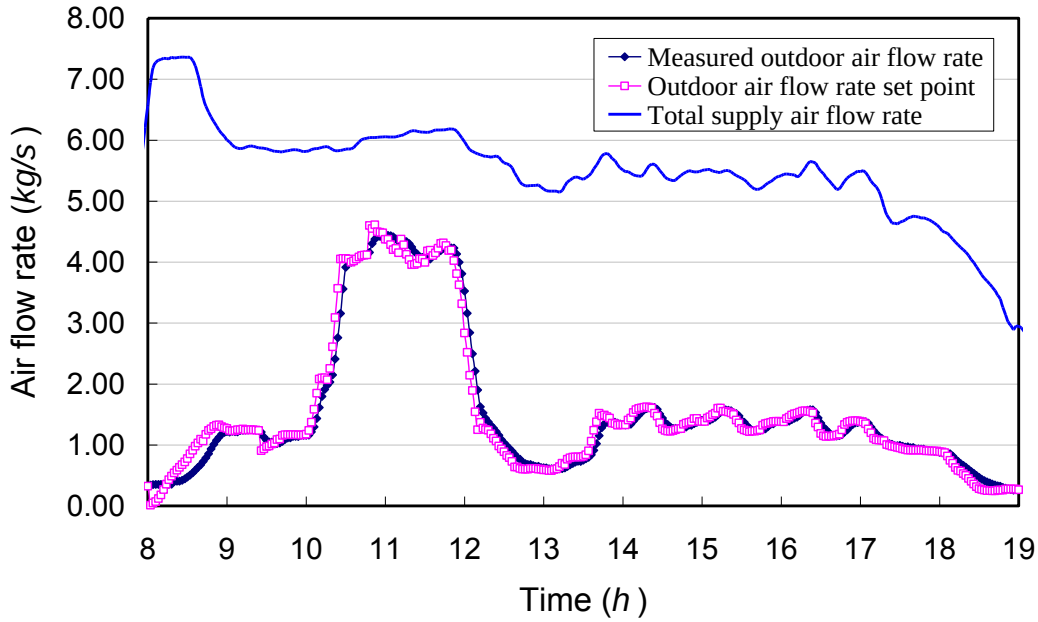

Figure 5.11 Total supply air and outdoor air flow rates using the conventional strategy

Due to the reduction of outdoor air flow rate, the cooling energy consumption also decreased. The cooling energy saving is 7.55% comparing with the benchmark using the conventional strategy. The saving of the total power consumption is 4.65% while the fan power consumption increased slightly due to the slight increase of the total supply air flow rate.

When the optimal strategy was implemented, the thermal comfort of Zone 8 increased slightly comparing with that using the conventional strategy as shown in Table 5.3 (For other zones, the average PPD using both strategies was almost the same, and does not be presented for analysis). The average PPD decreased from 8.86 to 8.01, and the maximum PPD also decreased. The maximum CO_2 concentration is 1083*ppm*, higher than the maximum value of 1009*ppm* using the conventional strategy. However, it is still acceptable since the prescribed level is 700*ppm* above

the CO_2 concentration of the outdoor air (360*ppm* in this study). The total average CO_2 concentration increased from 700*ppm* to 716*ppm*. The CO_2 concentration of each zone using the optimal strategy and the conventional strategy are presented in Figure 5.12 and Figure 5.13 for comparison.

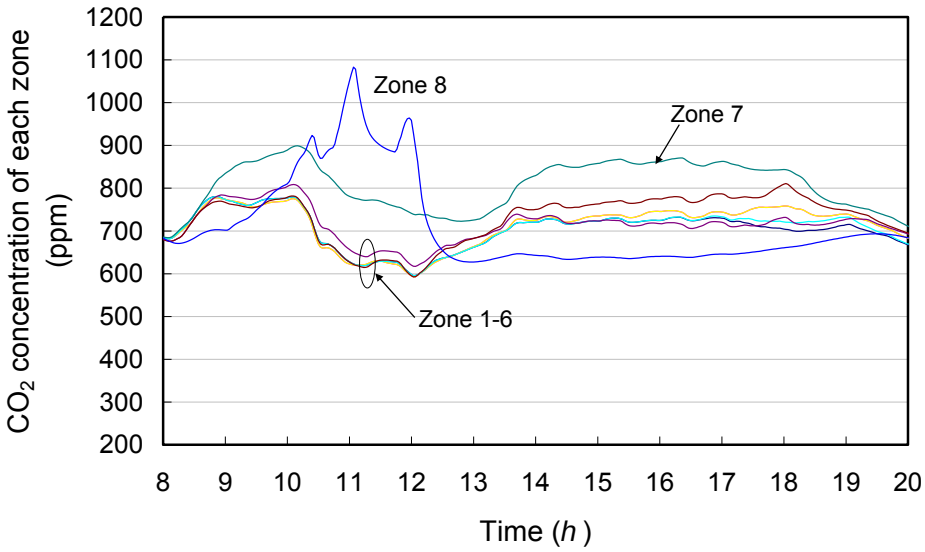

Figure 5.12 CO_2 concentration of each zone using the optimal strategy (*Setting I*)

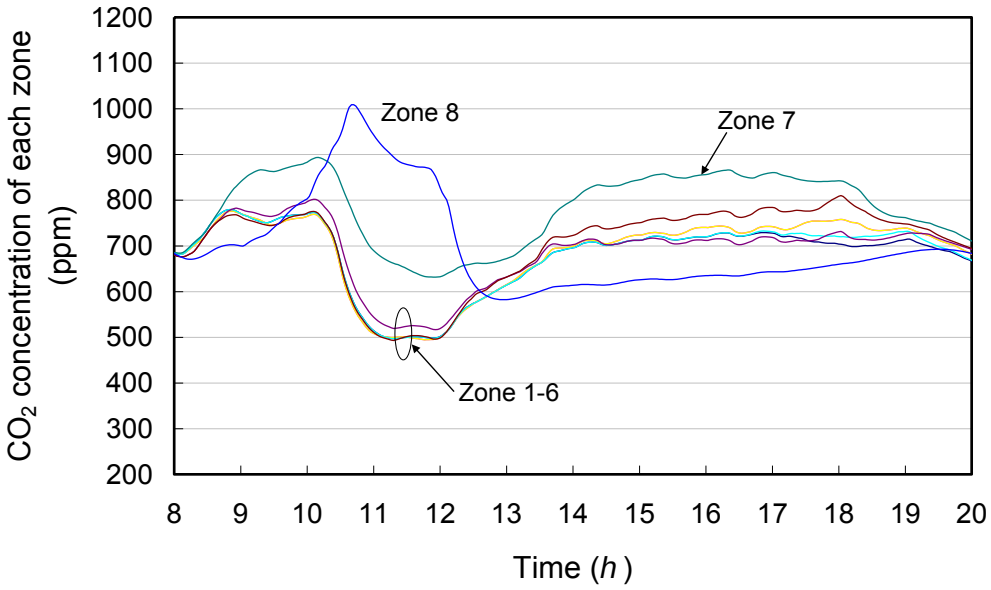

Figure 5.13 CO_2 concentration of each zone using the conventional strategy

The environmental and energy performance of the optimal strategy using different control settings in the cloudy summer day are also presented in Table 5.4 for reference. The optimal strategy using the weighting factors of *Setting I* achieved better thermal comfort and IAQ comparing with the conventional strategy. The cooling energy saving is 6.22%, and the total power consumption saving is 4.04% with fan power consumption increasing 0.77%.

Table 5.4 Summary of the environmental and energy performance of the conventional strategy and the optimal strategy with different control settings in the cloudy summer test day

Environmental and energy performance	Conventional strategy	Optimal strategy with different control settings				
		Setting I	Setting II	Setting III	Setting IV	Setting V
Environmental performance						
Average PPD of Zone 8 (%)	9.00	8.79	9.03	8.57	9.29	8.57
Maximum PPD of Zone 8 (%)	18.33	16.37	16.41	16.33	16.44	16.32
Average CO_2 concentration (ppm)	703	711	703	716	704	705
Maximum CO_2 concentration (ppm)	1070	1022	936	1098	932	1005
Energy performance						
Fan (kWh)	165.82	167.09	167.59	166.96	167.88	166.95
Differential (%)		*-0.77*	*-1.07*	*-0.69*	*-1.24*	*-0.68*
Cooling energy consumption (MJ)	3281.56	3077.34	3086.12	3056.04	3053.78	3124.09
Differential (%)		*6.22*	*5.96*	*6.87*	*6.94*	*4.80*
Overall power consumption (kWh)	530.44	509.02	510.49	506.52	507.19	514.07
Differential (%)		*4.04*	*3.76*	*4.51*	*4.38*	*3.09*

5.5.4 Evaluation of the Effects of Weighting Factors

Different settings of these weighting factors have significant effects on the thermal comfort, indoor air quality and the total energy consumption. Investigating the correlation of the total cost function and these three cost functions related with thermal comfort, IAQ and energy consumption, the suitable factors can be obtained by fine-tuning these factors according to different decision-makers. The fine-tuning

is done using the trial and error method taking into account the expected weightings of these three terms.

As presented above, the control settings of *Setting I* made the three cost function terms (i.e, thermal comfort, IAQ and power consumption) had similar contribution to the total cost function. The control parameters of *Setting II* considered the IAQ slightly more. Table 5.3 shows the IAQ improved slightly (i.e., average and maximum CO_2 concentrations) in the sunny summer test day when comparing with that using the control settings of *Setting I*. In this case, slightly more outdoor air was introduced. The total energy saving was 4.28%, 0.37% less than the saving using the control settings of *Setting I*.

Some tests were also carried out when only any two out of these three terms were considered while the third term was omitted. The control settings of *Setting III* omit the cost function related with IAQ. Therefore, the average and maximum CO_2 concentrations as shown in Table 5.3 increased obviously comparing those using *Setting I* because less outdoor air flow rate was introduced. The savings of the cooling energy consumption and the total power consumption also increased. The savings are 7.93% and 4.86%, 0.38% and 0.21% more than the counterparts of the optimal strategy using *Setting I*.

Setting *IV* only considered the cost functions related to the IAQ and power consumption while neglecting the cost function related with the thermal comfort. When it was used for the optimal strategy for the temperature set point optimization, the indoor thermal comfort was deteriorated comparing with that using *Setting I*

while the IAQ was improved as shown in Table 5.3. The average and maximum PPD of Zone 8 are 8.22 and 14.74. The cooling energy saving and the total power consumption saving are 6.95% and 4.11% respectively.

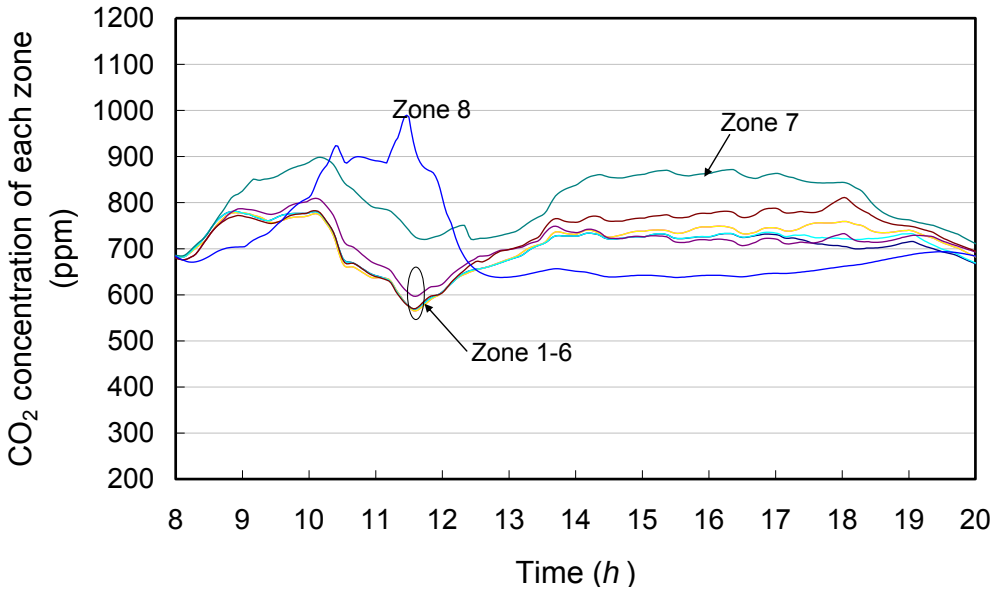

Figure 5.14 CO_2 concentration of each zone using the optimal strategy (*Setting VI*)

When the cost function of the total power consumption is neglected (i.e., the control settings of *Setting V*), the thermal comfort and IAQ had obvious improvement as shown in Table 5.3. This is due to that more outdoor air was introduced since energy is not the main issue of concern. The CO_2 concentrations of each zone using the optimal strategy with this setting are presented in Figure 5.14 for reference. The energy saving potential using *Setting V* is 2.3%, the least among those using other control settings (i.e., from *Setting I* to *Setting IV*). The energy and environmental performance of the optimal strategy using all these control settings in the cloudy summer test day is presented in Table 5.4. This table also shows the similar trends of

thermal comfort, IAQ and energy saving with those in the sunny summer test day when different control settings were used.

5.6 Summary

The model-based optimal ventilation control strategy is based on the system response predicted using simplified dynamic models to reset the indoor temperature control of critical zones to compromise the unbalance of outdoor air demands among different zones. Tests shows these incremental models can ensure the accuracy of the models and allow the models to be used conveniently on different systems and in a wide working arrange by identifying the parameters online. Tests also show that the total cost function was constructed properly by relating thermal comfort, indoor air quality and energy consumption together, and the genetic algorithm is a convenient tool for optimizing the temperature set point for online control applications by minimizing the total cost.

The evaluation of this optimal strategy shows that this strategy is capable of optimizing the system overall performance according to the chosen weighting factors. The optimal strategy was evaluated by comparing with a conventional strategy only using the multi-zone ventilation equation scheme. The results show this optimal strategy can achieve significant energy saving by comparing with the conventional strategy while maintaining acceptable thermal comfort and indoor air quality.

This optimal strategy was also evaluated by using different weighting factors (coefficients). The results show that different coefficients in the cost function have significant impacts on the performance of the optimal strategy since these coefficients determines the weightings for the optimizer to compromise the concern on different issues, such as energy and environment. The users can select or tune these weighting factors according to their concerns on different issues and according to the experiences on the operation of particular air-conditioning systems. A good choice of these weighting factors in the cost function requires more tests.

CHAPTER 6 MODEL-BASED OPTIMAL CONTROL OF OUTDOOR AIR FLOW RATE OF AIR-CONDITIONING SYSTEMS WITH PAU

This chapter presents a model-based outdoor air flow rate optimal control strategy for multi-zone VAV air-conditioning systems with the primary air-handling units (PAUs). An adaptive optimization algorithm is adopted for optimizing the set point of the outdoor air flow rate to minimize the energy cost, which compromises the energy consumption of the primary fan and the cooling energy saving by the cold outdoor air. The dynamic primary fan energy consumption is predicted using a simplified incremental fan model and the main parameters of this model is identified online. The cooling energy saving by the outdoor air is estimated online using the air side enthalpy. The lower limit of the outdoor air flow rate is determined by a CO_2-based adaptive demand-controlled ventilation (DCV) strategy using the dynamic multi-space equation to maintain the satisfied indoor air quality. Tests are conducted to evaluate the performance of the control strategy applied to a practical building system in simulation environment.

6.1 Description of the Ventilation Control System

6.1.1 Outdoor Air Flow Rate Control System with Primary Air Handling Unit

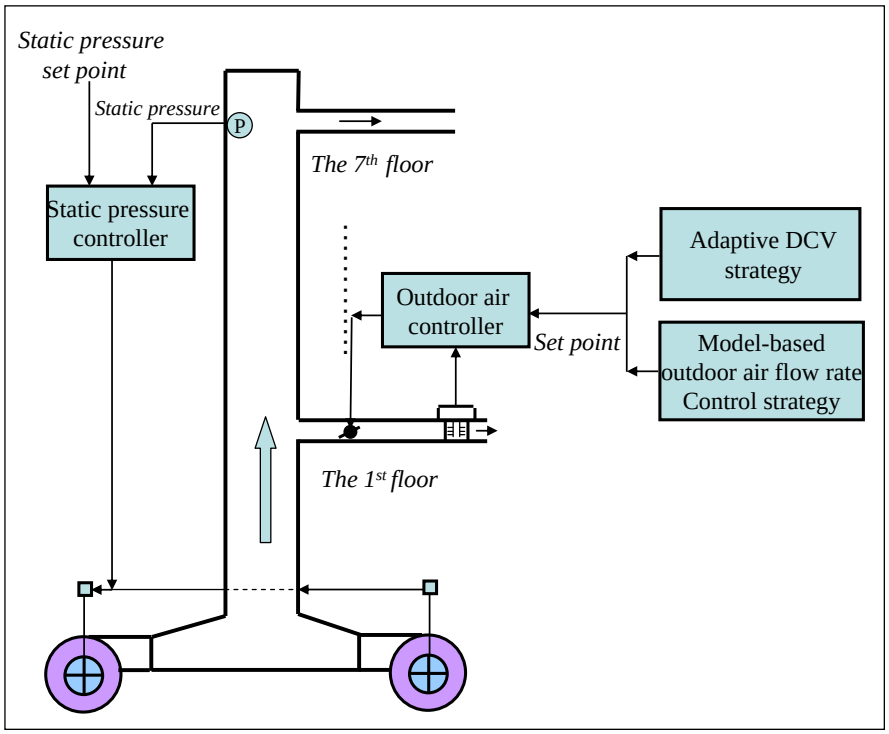

Figure 6.1 Schematics of outdoor air flow rate control system for an air-handling unit

The primary fan unit system serves total outdoor air into 7 floors in a high-rise commercial building. Each floor is divided into two parts each served by an air-handling unit. The schematic of the outdoor air flow rate control system is shown in Figure 1. The nominal motor power of primary fan is 45 kW and the design frequency is 50Hz. The design outdoor air flow rate is 17m^3/s. The pressure controller maintains the air static pressure at the sensor location at its set point by modulating the primary fan speed. The ventilation control system of each floor will be described Section 6.1.2.

6.1.2 Introduction of HVAC System

The same ventilation system described in Chapter 4 is used to serve half of each floor of a high-rise commercial building. Each floor is divided into eight zones for different usages using the partitions as shown in Figure 4.4. Zone 8 is used as a meeting room and the other zones are used as office. The ceiling height of the floor is 3.9 meters and the total floor area is 1166 m^2. All the conditioned air is delivered to the indoor space through VAV boxes. Return air is drawn back through the ceiling plenum. The design air flow rate of each floor is $6m^3/s$. The ventilation system of each floor involves three fans of variable pitch angle and a cooling coil etc. The schematic of the multi-zone VAV air-conditioning system in each floor is shown in Figure 6.2.

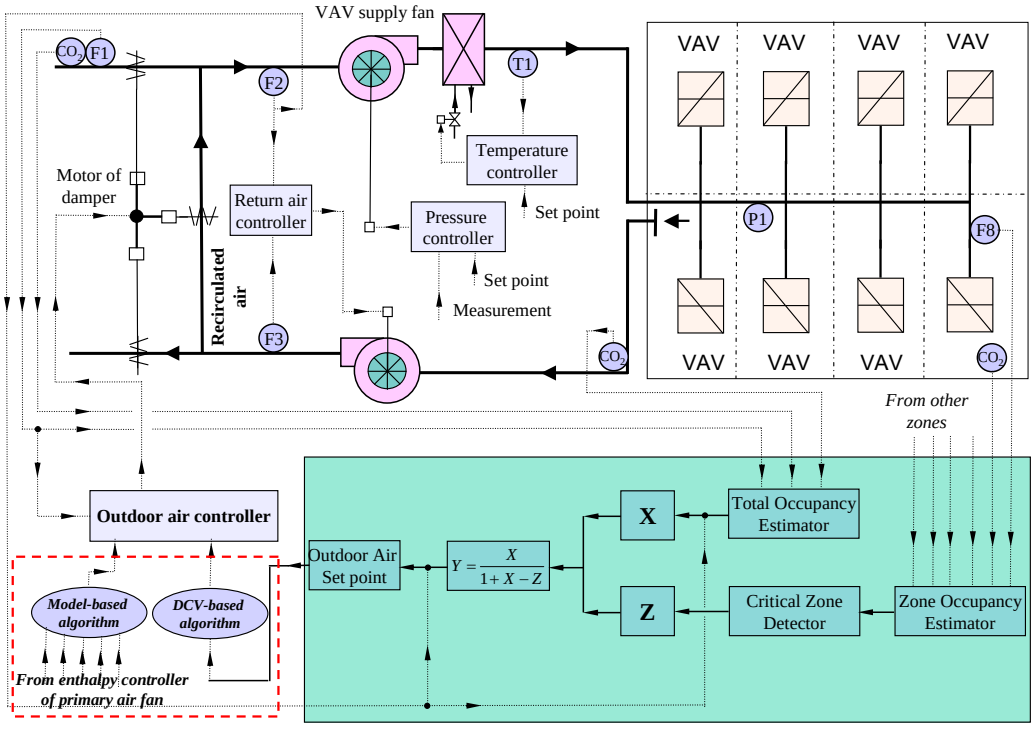

Figure 6.2 Schematics of multi-zone VAV air-conditioning system

The temperature controller controls the temperature of the supply air passing through the cooling coil. The pressure controller maintains the supply air static

pressure at its set point by modulating the supply air fan speed. The return air flow controller controls the flow rate difference between the supply air and return air. Pressure independent VAV boxes are used to control zone temperatures. All the above controllers employ the digital PID control algorithm. At the higher level, the system involves three supervisory controls. The supply air static pressure set point is reset by its supervisory controller according to the control status of VAV terminals. The supply air temperature is also reset according to the control status of VAV terminals to achieve reduced fan energy consumption and to avoid the indoor temperature out of control. The model-based outdoor air flow rate control strategy provides a preferable outdoor air set point for the whole HVAC system based on an iterative optimization method.

6.1.3 Model of Variable Speed Fan

In our research, the variable speed primary fan model developed by Clark (1985) was used to calculate the fan energy consumption and pressure rise over a wide range. Its accuracy has been validated using different air flow rate and rotation speed. The dimensionless flow coefficient and the pressure rise coefficient are calculated in Equation (6.1) and Equation (6.2) using the manufacturers' catalog data. The dimensionless coefficients of flow and pressure rise are obtained shown in Table 6.1.

$$C_f = \frac{M_a}{\rho \cdot RVS \cdot D^3} \tag{6.1}$$

$$C_h = \frac{1000 \cdot P_{rise}}{\rho \cdot RVS^2 \cdot D^2} \tag{6.2}$$

Table 6.1 Dimensionless coefficient of flow rate and pressure

C_f	C_h	C_η
0.620999	5.47272	0.72
0.745283	5.503465	0.76
0.919154	5.441974	0.79
1.093025	5.349737	0.83
1.266897	4.950044	0.8
1.440768	4.365878	0.77
1.614639	3.658728	0.72

In Table 6.1, C_f is the dimensionless flow coefficient. C_h is the dimensionless pressure coefficient. M_{out} is the outdoor air mass flow rate. *RVS* is the rotational speed. D is the diameter of fan blades. C_η is fan efficiency. ρ is air density. P_{rise} is the pressure rise of fan.

The dimensionless coefficients of fan pressure rise and fan efficiency are represented as functions of dimensionless flow coefficient shown in Equation (6.3) and Equation (6.4).

$$C_h = \sum_{i=0}^{m} a_i \cdot {C_f}^i \tag{6.3}$$

$$C_\eta = \sum_{j=0}^{n} b_j \cdot {C_f}^j \tag{6.4}$$

where i, j, a_i .and b_j are the parameters.

After the corresponding dimensionless coefficient data are generated, the parameters of Equation (6.3) and Equation (6.4) are identified using the least square fitting

method. The relationships between of dimensionless coefficients pressure rise and fan efficiency and the dimensionless flow coefficient are shown in Figure 6.4 and Figure 6.5, respectively.

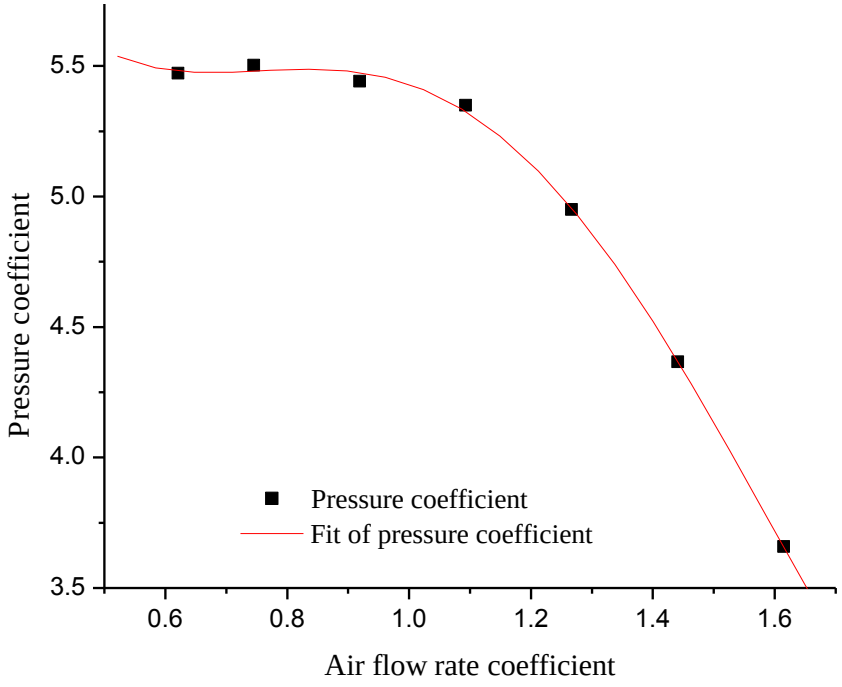

Figure 6.3 The relationship between the dimensionless pressure and the flow coefficient

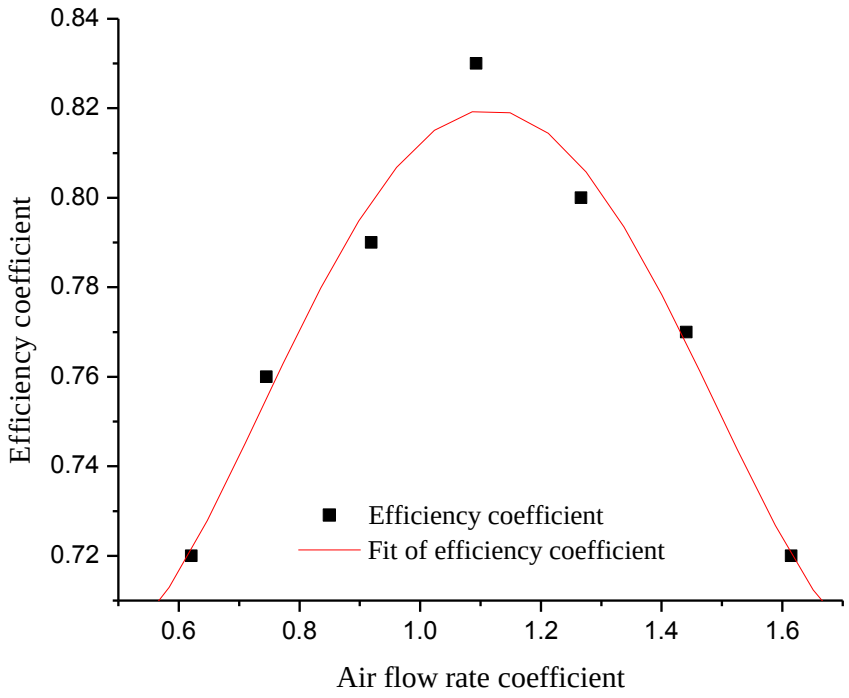

Figure 6.4 The relationship between the dimensionless efficiency and the flow coefficient

On the basis of the results of Figure 6.3 and Figure 6.4, the final format of Equation (6.3) and Equation (6.4) are rewritten in Equation (6.5) and Equation (6.6).

$$C_h = 9.213 - 16.74183 \cdot C_f + 26.68084 \cdot C_f^{\,2} - 17.46277 \cdot C_f^{\,3} + 3.74099 \cdot C_f^{\,4} \tag{6.5}$$

$$C_\eta = 1.11543 - 2.31134 \cdot C_f + 4.23314 \cdot C_f^{\,2} - 2.86883 \cdot C_f^{\,3} + 0.644 \cdot C_f^{\,4} \tag{6.6}$$

The fan power and pressure rise are thus calculated using the Equation (6.7) and Equation (6.8).

$$P_{\text{rise}} = C_h \cdot \rho \cdot RVS^2 \cdot D^2 \tag{6.7}$$

$$W_{fan} = \frac{M_a \cdot P_{rise}}{1000 \cdot C_\eta \cdot \rho} \tag{6.8}$$

where W_{fan} is the fan power.

6.2 Simplified Incremental Fan Model and Optimization Algorithm

6.2.1 Incremental Primary Fan Model and Its Parameter Identification

The power consumption of the primary fan can be modeled using a simplified incremental model as Equation (6.9), in which the energy consumption is approximately proportional to the measured outdoor air flow rate cubed when the change of the outdoor air flow rate is in a small range. The parameter C_v is assumed to be constant in the prediction period. The parameter is estimated and updated using the measured fan power and measured outdoor air flow rate at each sampling time shown in Equation (6.10).

$$W_{fan} = C_v v^3 \tag{6.9}$$

$$C_v^{\,k} = \frac{W_{fan}^{\,k}}{(v^k)^3} \tag{6.10}$$

where, v is the measured outdoor air flow rate. C_v is the parameter to be estimated. k indicates the current sampling time

6.2.2 Optimization Algorithm

The optimal outdoor air flow rate is searched by using the least square algorithm. The outdoor air flow rate set point resetting scheme is illustrated in Figure 6.5.

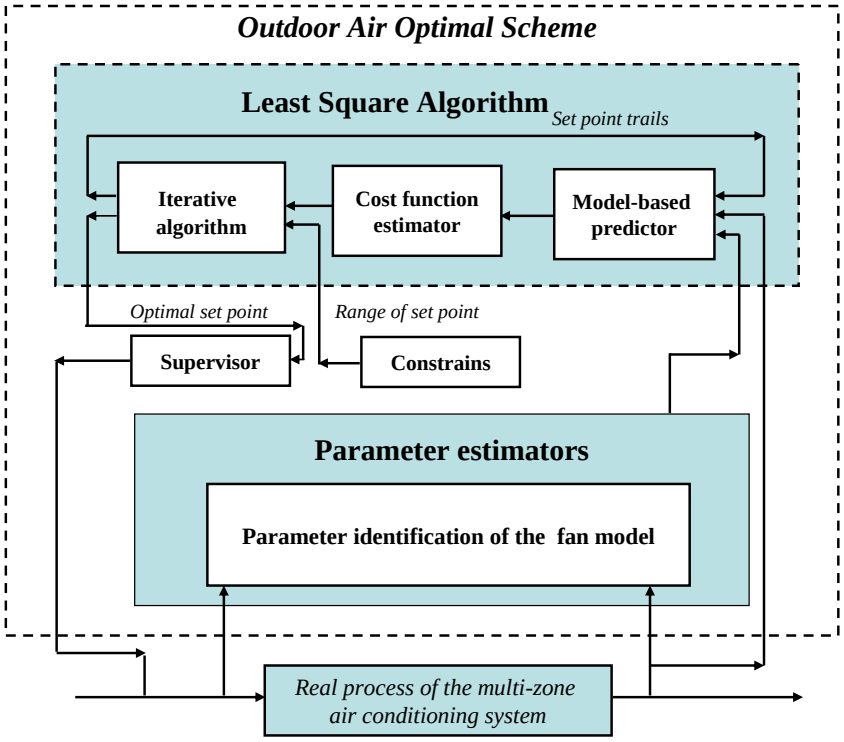

Figure 6.5 Schematic of the outdoor air flow rate set point resetting scheme

It is assumed that the energy consumptions of supply fan and return fan are not influenced by the measured outdoor air flow rate. Therefore, the cost function in a short prediction period only includes the energy consumption of the primary fan and the cooling energy saving by the outdoor air as Equation (6.11). This cost function is constructed to predict the system responses in a prediction period using the dynamic simplified incremental model.

$$W_{cost} = W_{fan} + \frac{Q_{outdoor}}{COP} = C_v^{\,k} \cdot M_{out,set}^{\,k} + \frac{M_{out,set}^{\,k} \cdot (H_{out}^{\,k} - H_{rtn}^{\,k})}{COP} \qquad (6.11)$$

where, H_{out} is the outdoor air enthalpy. H_{rtn} is the return air enthalpy. $M_{out,set}$ is the set point of the outdoor air mass flow rate. M_{dcv} is the outdoor air mass flow rate based on the DCV strategy. W_{cost} is the sum of the energy consumption of the primary fan and the heating load of the outdoor air. W_{fan} is the energy consumption of the primary fan. $Q_{outdoor}$ is the heating load of the outdoor air. COP is the coefficient of performance including the pump and the chiller (assumed to be constant as 2.5 in this research). *k* indicates the current sampling time.

When the outdoor air enthalpy is larger than or equal to the return air enthalpy ($H_{out} \geq H_{rtn}$), the outdoor air flow rate set point is set according to that determined by the adaptive DCV strategy ($M_{out,set} = M_{dcv}$). Otherwise, the cost function in Equation (6.11) will be used to optimize the outdoor air flow rate as Equation (6.12). In the optimization of each sampling step, the search range of the outdoor air flow rate is set to be [M_{dcv} , $M_{outdoor} + \Delta M$], where ΔM is a fixed increment. A supervisory decision module is developed to identify the reliability of the model-based outdoor air flow rate control strategy. When the energy consumption of the primary fan for each unit outdoor air flow rate is smaller than the provided cooling energy by each unit outdoor air flow rate, the optimal outdoor air flow rate is set to be the upper limit. Otherwise, the lower limit is used to set the optimal value in this search range. The change rate of the set point also is controlled within a given limit.

$$Min(W_{cost}) = Min(W_{fan} + \frac{Q_{outdoor}}{COP}) = Min[W(M_{out,set})] \quad (6.12)$$

In case there is a dramatic change on working condition of the system, the searched optimal value limited within a small range and limited change rate might not reach the new optimal value. However, the searched optimal value will approach the new optimal value of system after a few sampling steps, allowing stable control of the system.

6.3 Validation Tests

6.3.1 Performance of the Energy Saving Potential

Figure 6.6 presents a comparison between the outdoor air enthalpy and the return air enthalpy. It is observed that the outdoor air enthalpy was smaller than the return air enthalpy from 8:30am to 16:00pm. During this period, the model-based outdoor air flow rate control strategy may be adopted to optimize the outdoor air flow for the air-conditioning system.

To show the energy saving potential, the energy consumption of the primary fan and the cooling energy saving by using the outdoor air are presented and compared in Figure 6.7. It shows that the cooling energy saving by each unit outdoor air flow rate is larger than the energy consumption of the primary fan from about 9:30am to 12:30pm. It is concluded that this model-based outdoor air flow rate control strategy can be adopted to provide more outdoor air into the air-conditioning system during this period.

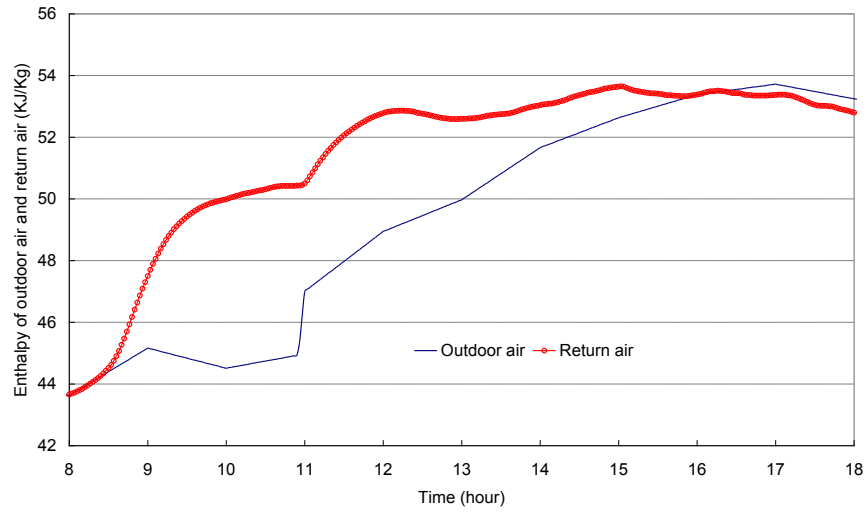

Figure 6.6 Comparison of the outdoor air enthalpy and the return air enthalpy

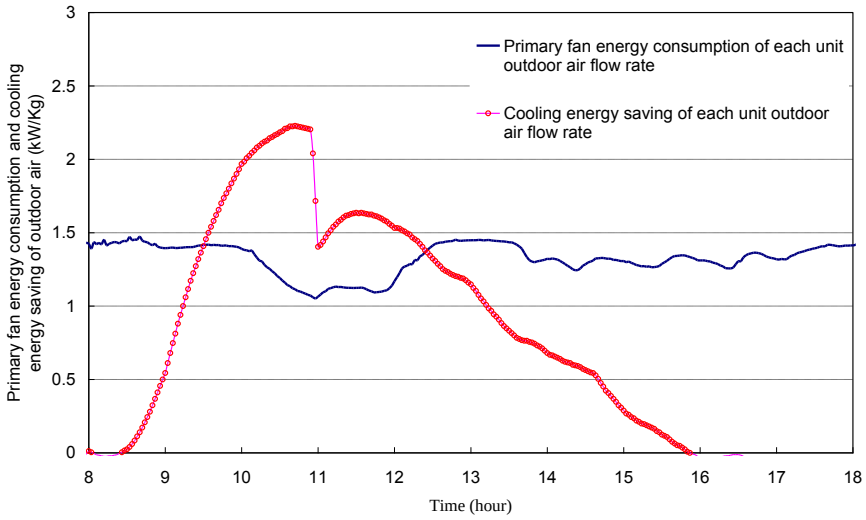

Figure 6.7 Comparison of the energy consumption of the primary fan and the cooling energy saving by the outdoor air

6.4 Overview of the Proposed and Conventional Outdoor Air Flow Rate Control Strategies

A conventional outdoor air flow rate control strategy was employed as the reference in evaluating the system operational performance of the developed new strategy. The

proposed strategy developed is the hybrid strategy integrating the DCV and the model-based outdoor air flow rate optimal control (Strategy A). The conventional strategy is the hybrid strategy integrating the DCV and the full outdoor air flow rate optimal control (Strategy B) (Wang 1999). Two simpler ventilation control strategies were also included in the test for comparison to evaluate the proposed strategy, including the strategy using DCV only and the strategy with constant outdoor air flow according the design occupancy at the floor. The adaptive DCV strategy has been introduced earlier. The constant outdoor air flow set-point used was 1.85m^3/s, which is the demanded outdoor air flow rate based current ASHRAE ventilation standard at the design occupancy.

Strategy A - When the outdoor air enthalpy is larger than the return air enthalpy, the adaptive DCV strategy is adopted to manipulate the outdoor air flow rate for ensuring a satisfactory indoor air quality. Otherwise, a supervisory decision scheme of the outdoor air flow rate control is adopted to decide the potential saving of outdoor air. In this scheme, the change of energy consumption of the primary fan when increasing or reducing the outdoor air flow rate is compared with the cooling energy saving of using outdoor air flow rate. When the energy consumption of the primary fan is smaller than the cooling energy saving by each unit outdoor air flow rate, the model-based outdoor air flow rate optimal control strategy is activated for the outdoor air flow rate control. Otherwise, the adaptive DCV strategy is actually used for outdoor air flow rate optimal control.

Strategy B - When the outdoor air enthalpy is larger than the return air enthalpy, the adaptive DCV strategy is adopted to manipulate the outdoor air flow rate. Otherwise, the outdoor air damper is set to its maximum position (full air cooling mode) for the outdoor air flow rate optimal control without considering the energy consumption of the primary fan.

6.5 Tests and Test Results

The test system was developed on the TRANSYS platform. Occupancy, lighting and equipment loads in each zone, the solar gains of each zone transmitted through the windows, sol-air temperature of each external wall, the outdoor air temperature, humidity and CO_2 concentration were used as input files. The outdoor air CO_2 concentration was 360ppm. The generation rates of CO_2, latent and sensible loads of one person are selected to be $5*10^{-6}m^3/s$, $1.17*10^{-5}$ kg/s and 0.065kW respectively. The air-conditioning system worked from 7:50 am to 19:00 pm.

6.5.1 Total Occupancy Profile and Occupancy Profiles of Individual Zones

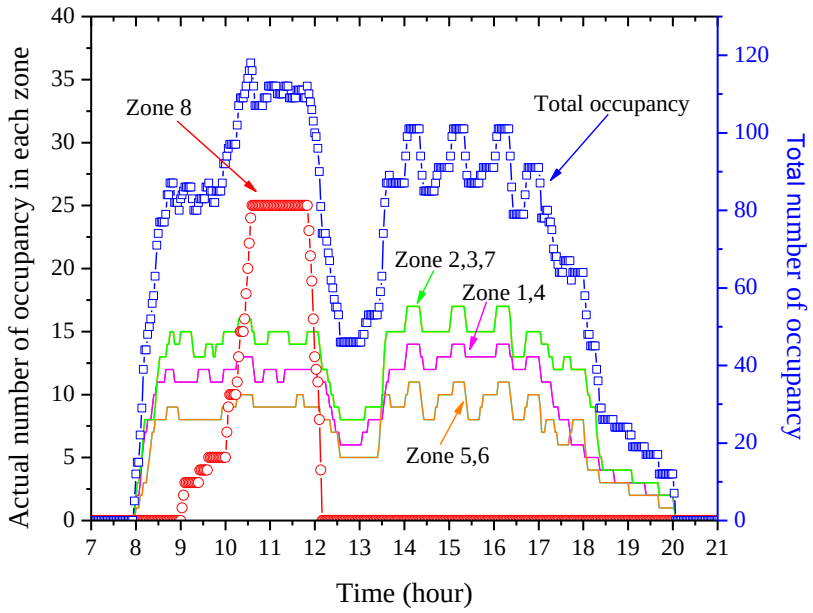

Figure 6.8 Total occupancy profile and occupancy profiles of individual zones in each floor

The occupancy profiles of each zone are presented in Figure 6.8. The number of occupancy in all the zones varied significantly. The occupants entered in the meeting room (Zone8) from 9:00am to 12:00am. The number of occupancy reached the maximum about 25 persons at 10:30am, and the occupants then left the meeting room at about 12:00am. Seven zones from zone 1 to zone 7 are used as offices. Its maximum density of occupancy is about $10m^2$ per person.

6.5.2 Predicted and Actual Total Occupancy Profiles

In order to validate the accuracy of the dynamic occupancy detection scheme presented by Wang (1998) in our air-conditioning system, the total number of occupancy in each floor is compared with the predicted total number. Figure 6.9 describes the predicted and actual total occupancy profiles of each floor. The

predicted total number of occupancy can match well with the actual total number of occupancy.

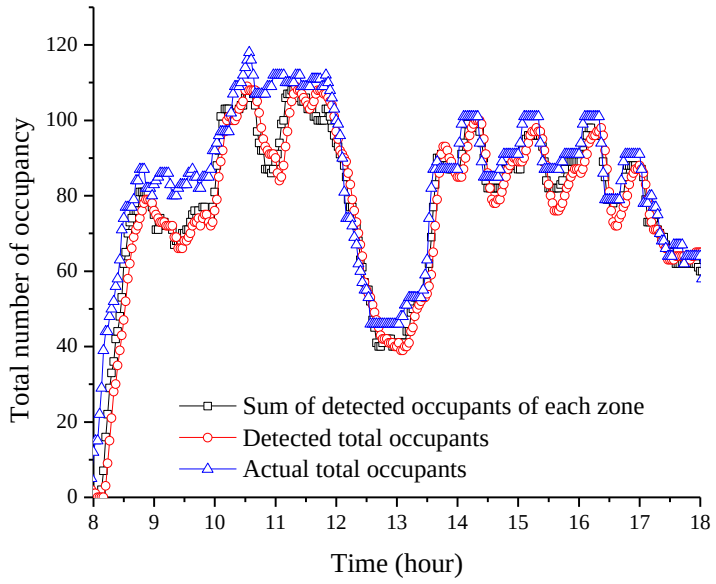

Figure 6.9 Predicted and actual total occupancy profiles in each floor

6.5.3 Predicted and Actual Occupancy Profiles of Zone 1, Zone 2 and Zone 8

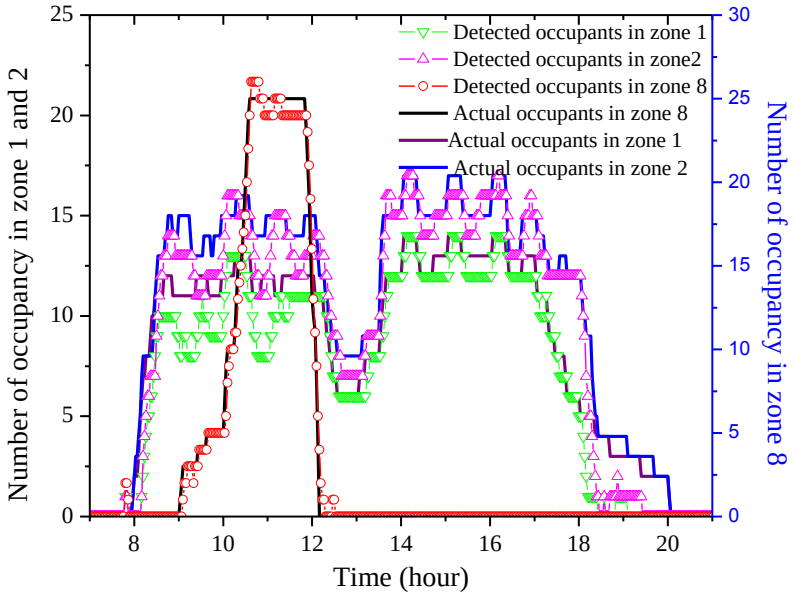

Figure 6.10 Predicted and actual occupancy profiles of Zone 1, Zone 2 and Zone 8

Meanwhile the actual number of occupancy in some zones is compared with the predicted number as well. Figure 6.10 describe the predicted occupancy profiles of Zone1, 2 and 8 respectively. Zone 8 is the meeting room in each floor. The number of occupancy in zone 8 (meeting room) changed sharply shown in Figure 6.8. In this case, the numbers of the estimated occupants in zone 1, Zone 2 and Zone 8 were compared with the actual numbers to validate the availability of the dynamic occupancy detection scheme. It is found that the predicted number agreed well with the actual ones with the error less than 10%. The occupancy prediction performances of other zones (zone 1-zone 7) were similar as the change of occupants is smooth.

6.5.4 Identifying the Critical Zone at a Floor

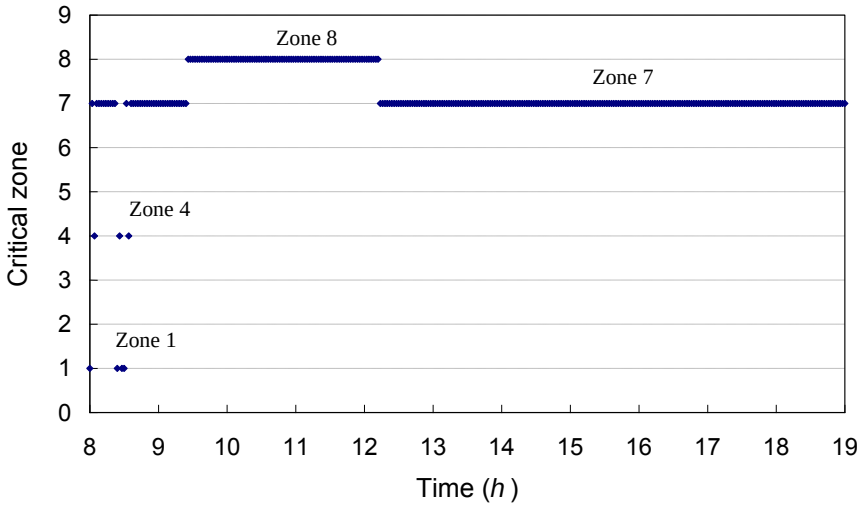

Figure 6.11 Identified critical zone in each floor

Figure 6.11 describes the detection of the critical zone in each floor. It was investigated that from 9:00am to 12:00am zone 8 was detected to be the critical zone shown in Figure 6.11, which coincided with the trend of the occupants in different zones in Figure 6.8. In addition, zone 7 was detected to be the critical zone in most

working time except the meeting periods. This result also agreed well with the trend of detected occupants in zone 7. It is also illustrated that the detection of critical zone was reasonable in our study.

6.5.5 Comparison between the Outdoor Air Flow Rate and Set Point at a Floor

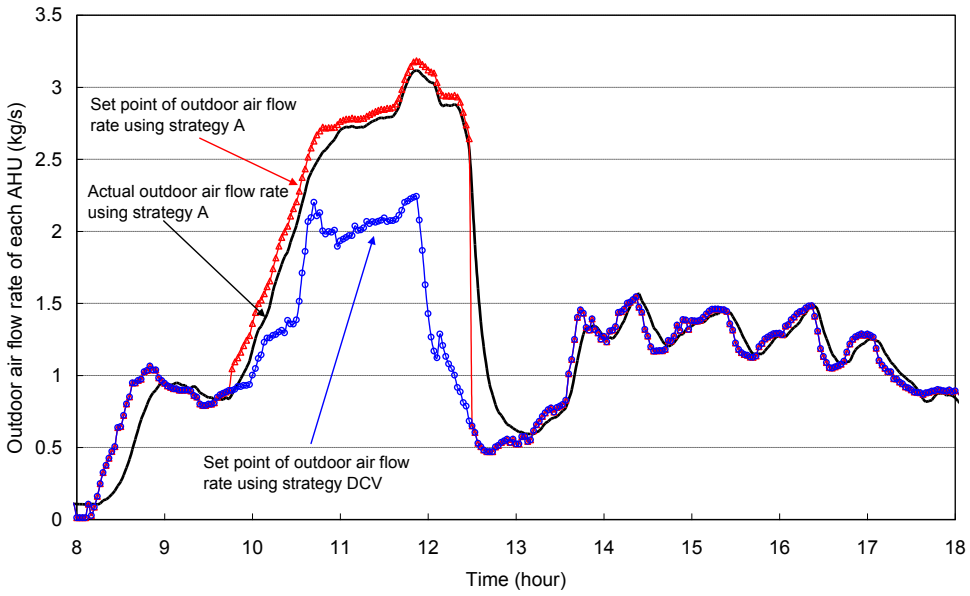

Figure 6.12 Outdoor air flow rate and set point using strategy (A) at the typical floor

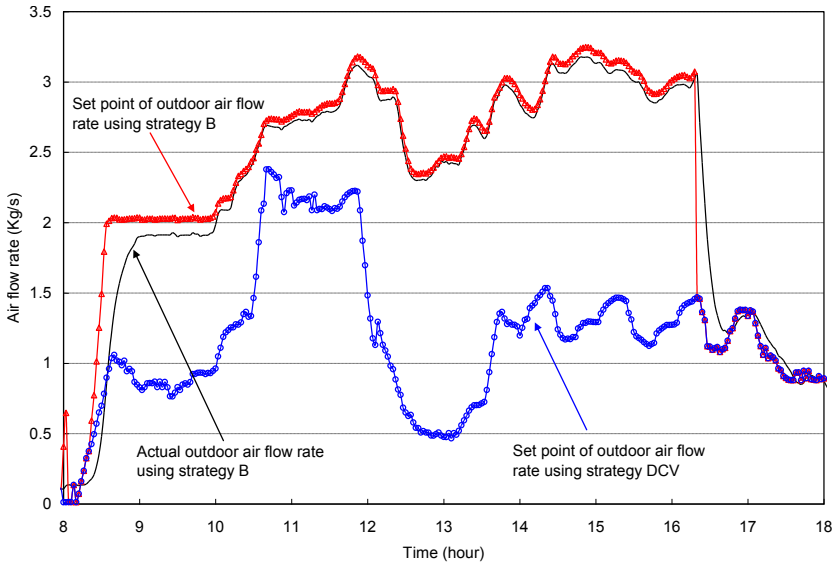

Figure 6.13 Outdoor air flow rate and set point using strategy (B) at the typical floor

Figure 6.12 and 6.13 present the actual outdoor air flow rates and the outdoor air flow rate set points when using the two outdoor air flow rate control strategies respectively. From 9:30am to 12:30am, the outdoor air flow rate using the new strategy in Figure 6.12 was larger than the set point of the DCV strategy. It is noticed that the outdoor air flow rate increased in this period because the primary fan energy consumption of each unit outdoor air flow rate is smaller than its provided cooling energy as shown in Figure 6.7. It is also worthwhile to mention that the outdoor air was controlled well since the measured outdoor air flow rate followed the set point well as Figure 6.12 and 6.13.

6.5.6 Comparison between Indoor Air CO_2 concentration of Different Zones

The indoor CO_2 concentration is an indicator of the indoor air quality. The average CO_2 concentration of each zone using the proposed strategy A was 644.0ppm, while it was about 621.8ppm using the conventional strategy B. The average CO_2 concentration of each zone using the DCV strategy and the constant outdoor air flow strategy was 724.8ppm and 520.7ppm respectively.

The CO_2 concentrations of individual zones using the proposed strategy A and conventional strategy B are presented in Figure 14 and 15 for comparison. For most of time, the CO_2 concentration using the (A) strategy was larger than that using the (B) strategy. However, it was still in the acceptable range lower than 1000ppm (ASHARE 2004). It is illustrated that the decreasing of outdoor air flow rate using the hybrid strategy of the DCV and the model-based outdoor air flow rate optimal control did not affect the IAQ.

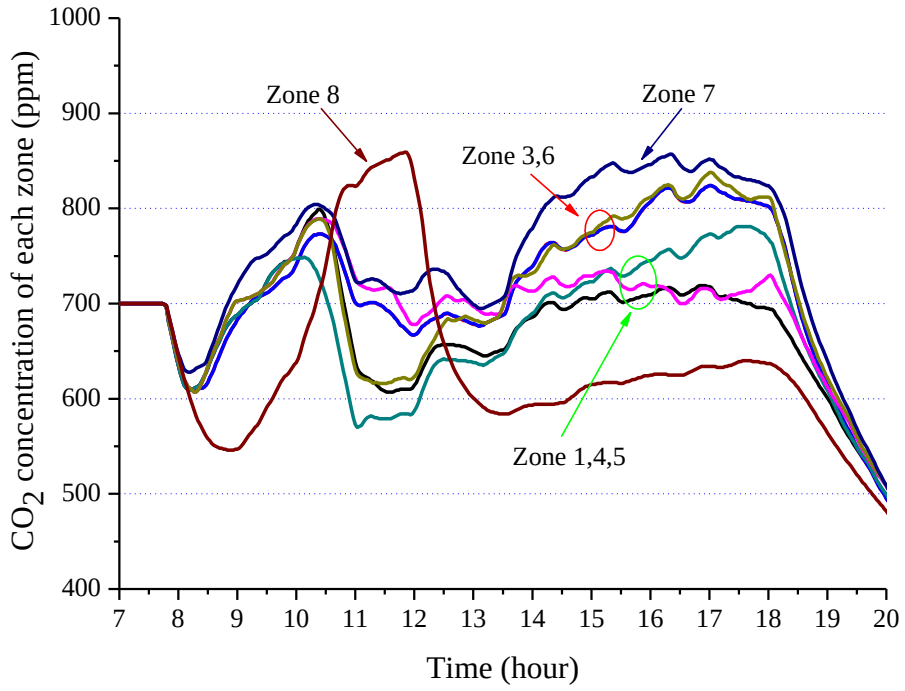

Figure 6.14 CO_2 concentration of each zone using (A) strategy

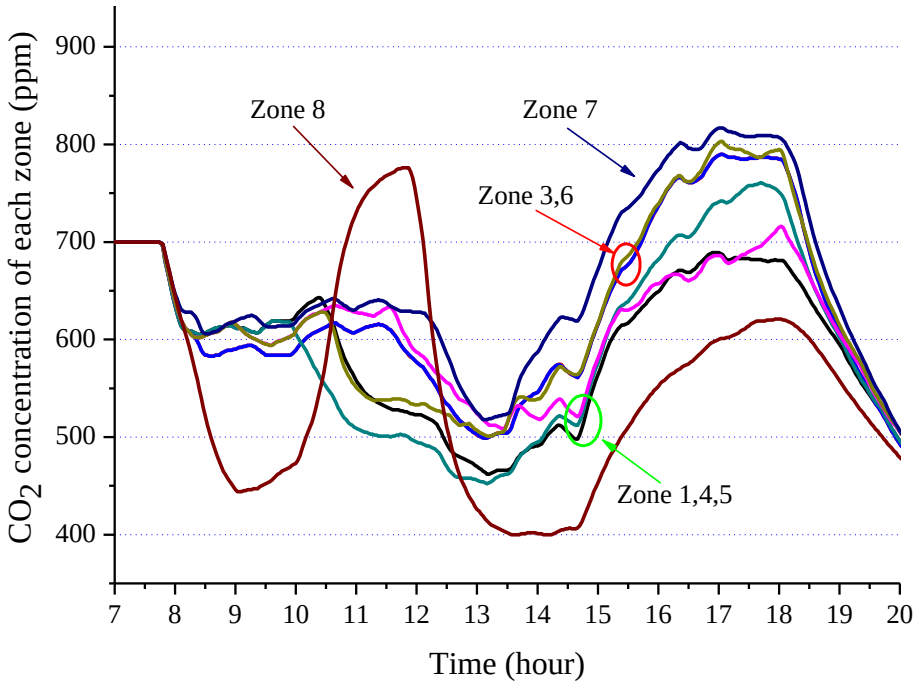

Figure 6.15 CO_2 concentration of each zone using (B) strategy

6.5.7 Effects on the Energy Consumption of the Air-conditioning System

The effects on the energy consumption of the proposed strategy A, strategy B, the adaptive DCV strategy, and the constant outdoor flow ventilation strategy are compared in Table 6.2. It shows the energy consumptions of the cooling coils and the fans, the total energy consumption of the primary fans and the cooling coils, as well as the total energy consumption of the entire air-conditioning system of the seven floors served by the same primary air-handling unit. The results show that the energy consumption of the primary fan decreased, while the energy consumption of the cooling coils increased. The energy consumptions of the supply fans and the return fans nearly remained unchanged. It indicates that the previous assumption (in Section 6.2) on the supply and return fans was suitable. The *strategy B* is used as the reference ventilation control strategy in this study. The percentage saving of the primary fan and the cooling coils energy consumption when using *strategy A* was about 5.74%. The percentage saving of the system total energy consumption was 3.35%. The percentage consuming of the primary fan and the cooling coil energy consumption when using the *adaptive DCV strategy* only was about -1.47% (more consumption), which is equivalent to -0.86% of the system total energy consumption. The percentage consumption of the primary fan and the cooling coils energy consumption when using the *constant outdoor air flow ventilation strategy* was about -5.61% (more consumption), which is equivalent to -3.26% of the system total energy consumption. Compared with the cases using the DCV strategy and constant outdoor air flow ventilation strategy, the saving of the proposed strategy was 7.21% and 11.35%.

Table 6.2 Energy consumptions when using different strategies in a typical spring day

Control Strategies	Strategy A	Strategy B	DCV strategy	Constant Flow
Supply fan consumption (kWh)	1085.22	1081.75	1085.91	1080.75
Return fan consumption (kWh)	533.01	536.16	531.83	535.89
Primary Fan consumption (kWh)	524.91	748.54	466.66	880.05
Total fan consumption (kWh)	2143.14	2366.44	2084.40	2496.68
Cooling coil consumption (MJ)	14725.34	13896.30	16736.44	13869.97
Energy consumption sum of primary fan and cooling coil system (kWh)	2161.06	2292.57	2326.26	2421.16
Percentage energy saving of primary fan and cooling coil system (%)	*5.74*	-	*-1.47*	*-5.61*
Overall energy consumption (kWh)	3779.29	3910.48	3944.00	4037.79
Overall percentage saving (%)	*3.35*	-	*-0.86*	*-3.26*

6.6 Drawbacks of Using Primary Air Handling Units in Application

The model-based outdoor air flow rate optimal control strategy can significantly reduce the system energy consumption for full air ventilation system with the primary air handling unit by optimizing the energy consumption of the primary fan and the cooling system. However, it was found that the system total energy consumption increased obviously when comparing with the system inducing outdoor air directly for ventilation. When the ventilation system inducing outdoor air directly is concerned, the total energy consumption using the hybrid strategy integrating the DCV and the enthalpy control (The same control decision will be given by the strategy A and Strategy B when without PAU) was 3161.94 kWh. The total energy consumption of the system with PAU when using the strategy A was 3779.29 kWh.

It can be found that 16.34% energy savings could be obtained if the PAU is eliminated.

Therefore the direct induction of the outdoor air is the preferable choice for the selection of the outdoor ventilation system in buildings when it is possible in practical systems. For example, in the cases the architectural constraint and local outdoor air quality do not make the use of direct fresh air induction of AHUs impossible.

6.7 Summary

A model-based outdoor air optimal control strategy is developed to optimize the outdoor air flow rate of HVAC systems with primary air units, compromising the energy consumption of the primary fan and cooling energy saving by the outdoor air based on the system performance prediction using a simplified incremental model online. Tests shows the incremental fan model can allow the models to be used conveniently on different systems and in a wide working arrange by identifying the parameter and adapting the model online.

This model-based outdoor air flow rate optimal control strategy was evaluated by comparing with different conventional ventilation control strategies. The results show this model-based outdoor air optimal strategy can achieve significant energy saving while maintaining acceptable indoor air quality for the ventilation system with a primary air handling unit.

The model-based outdoor air flow rate optimal control strategy was also evaluated by comparing with the induced outdoor ventilation system without installing a primary air unit. The results show that significant energy savings could be obtained if the primary air handling unit is eliminated.

CHAPTER 7 DEVELOPMENT AND APPLICATION OF A DATA-BASED TEMPERATURE OFFSET MODEL

The prediction of airflow, temperature, and pollution concentration distribution in ventilated rooms is important for the design as well as for the optimal control performance of efficient HVAC systems. Since experimental methods are difficult and expensive to use for parametric studies of indoor air, a preferable alternative for the prediction of such airflows is based on room modeling and mathematical calculation. A CFD-based space temperature offset model is developed in this Chapter to describe the air temperature non-uniform stratification, and to be used as a virtual temperature sensor in temperature control to compensate the temperature non-uniform stratification, and hence to improve thermal comfort in occupied rooms.

The temperature offset model is described in Section 7.1. Firstly, a CFD model is employed to emulate the air temperature non-uniform stratifications. Secondly, a temperature offset model is identified based on the data generated by the CFD model. Section 7.2 validates the accuracy and reliability of CFD model by using a practical experimental test.

7.1 CFD-Based Model and Its Parameter Identification

CFD models as a powerful tool have successfully been applied in the HVAC field (Zhang J.S. et al 1992). CFD models provide a wealth of information to detect the indoor air stratification phenomena. Meanwhile, a validated CFD model can be used to calibrate some simple empirical models to provide accurate data for system test, when the experimental measurements are difficult to carry out. In contrast to full scale ventilation performance test, the CFD method is a relatively inexpensive and alternative method. Hence, one purpose of applying CFD model in this study is to generate necessary data for the model identification and reduce the experimental costs as well.

CFD model is also selected as an alternative for representing the room as a virtual ventilated room model. Choosing a proper numerical model for CFD simulation is also necessary to obtain accurate data according to the relevant system configuration. The detailed introduction of CFD numerical models and simulation procedure for developing a data-based space temperature offset model are explained as follows.

7.1.1 CFD Theoretical Model

When the CFD simulation is used to describe the indoor thermal environment, the Navier-Stokes equations are derived based on the conservation equations of continuity, momentum, energy and mass. In three-dimensional Cartesian co-ordinates, these partial differential equations of indoor air flow, energy and mass transport are illustrated in Equations (7.4) to Equation (7.9).

Continuity equation

$$\frac{\partial}{\partial x}(\rho u)+\frac{\partial}{\partial y}(\rho v)+\frac{\partial}{\partial z}(\rho w)=0 \tag{7.4}$$

Conservation of momentum in x-direction

$$\frac{\partial}{\partial t}(\rho u)+\frac{\partial}{\partial x}(\rho uu)+\frac{\partial}{\partial y}(\rho vu)+\frac{\partial}{\partial z}(\rho wu)=-\frac{\partial p}{\partial x}+\frac{\partial}{\partial x_j}[\mu(\frac{\partial u}{\partial x_j}+\frac{\partial u_j}{\partial x})] \tag{7.5}$$

Conservation of momentum in y-direction

$$\frac{\partial}{\partial t}(\rho v)+\frac{\partial}{\partial x}(\rho uv)+\frac{\partial}{\partial y}(\rho vv)+\frac{\partial}{\partial z}(\rho wv)=-\frac{\partial p}{\partial y}+\frac{\partial}{\partial x_j}[\mu(\frac{\partial v}{\partial x_j}+\frac{\partial u_j}{\partial y})] \tag{7.6}$$

Conservation of momentum in z-direction

$$\frac{\partial}{\partial t}(\rho w)+\frac{\partial}{\partial x}(\rho uw)+\frac{\partial}{\partial y}(\rho vw)+\frac{\partial}{\partial z}(\rho ww)=-\frac{\partial p}{\partial z}+\frac{\partial}{\partial x_j}[\mu(\frac{\partial w}{\partial x_j}+\frac{\partial u_j}{\partial z})]-\rho g\beta(T_\infty-T) \tag{7.7}$$

Conservation of energy

$$\frac{\partial}{\partial t}(\rho c_p T)+\frac{\partial}{\partial x}(\rho c_p uT)+\frac{\partial}{\partial y}(\rho c_p vT)+\frac{\partial}{\partial z}(\rho c_p wT)=\frac{\alpha}{\partial x_j}(k\frac{\partial T}{\partial x_j})+q \tag{7.8}$$

Conservation of pollution transport

$$\frac{\partial C}{\partial t}+\frac{\partial}{\partial x}(uC)+\frac{\partial}{\partial y}(vC)+\frac{\partial}{\partial z}(wC)=\frac{\alpha}{\partial x_j}(D\frac{\partial C}{\partial x_j})+S \tag{7.9}$$

where u is the air velocity in the x direction (m/s), v is the air velocity in the y direction (m/s), w is the air velocity in the z direction (m/s), ρ is the air density (kg/m^3), μ is the air viscosity (Pa s), β is the thermal expansion coefficient of air (K^{-1}), g is the gravitational acceleration (m/s^2), t is the time (s), p is the pressure (Pa), T is the temperature (K), T_∞ is the reference temperature (K), C_p is the air specific heat (J/kg K), k is the air conductivity (W/m k), q is the heat within the control volume (W/m^3), C is the concentration of contaminant (kg/m^3), D is the molecular diffusion coefficient for the contaminant (m^2/s), S is the volumetric contaminant generation rate (kg/m^3 s).

Above these equations fully characterize the transient fluid flow field, heat and pollution transport throughout the air volume within a ventilated room. It can be found that six unknown parameters such as temperature, pressure, concentration of pollutions, three velocity components are existed to cope with using six equations. The problem can be closed in this case.

7.1.2 CFD Simulation and Boundary Conditions

The size of the ventilated room is 3.0 meters, 3.0 meters and 2.5 meters in length, width and height respectively. The ventilated room is geometrically built using Gambit software (Fluent 2005), which is a general-purpose preprocessor for CFD analysis. In traditional zonal modeling methods (Zhang J.S. et al 1992), the ventilated room is divided into a number of macroscopic homogeneous zones. In each zone, the air temperature, density and concentration are assumed to be

uniformly distributed. Then, equations of air continuity, momentum and energy conservation are established for these zones, which are coupled with each other. The temperature distribution in the whole room can be investigated by solving these continuity, momentum and air energy conservation equations for each zone.

Refer to this principle of traditional zonal models; the ventilated room in our study is also divided into a number of macroscopic homogeneous zones. Generally, three significant types of zones should be distinguished: one is *the measurement zones* where measurement tools, *e.g.* temperature sensors, are located; one is *the occupancy zones* where occupants usually stay; and the other is *the heat source zones* which generate heat and cooling load for this room. In most cases in application, the measurement zones are not the occupancy zones probably due to installation problems; while the thermal comfort in the occupancy zones is mainly concerned in room temperature control. As a simple example shown in Figure 7.1, the ventilated room is divided into six zones. The temperature sensor is located in Zone 6 near the exhaust air exit; while occupants always stay in Zone 2. Some times, the occupancy zones are also the heat resource zones, especially when occupants and their activities are the main heat sources.

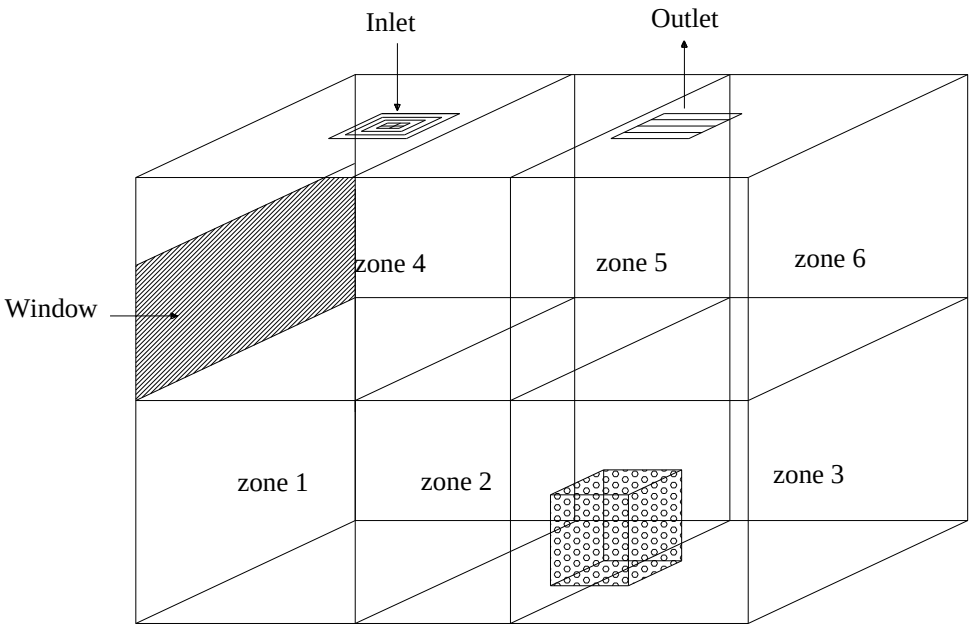

Figure 7.1 Configuration and partition of the ventilated room used CFD model

After the geometrical model of the ventilated room is established using Gambit software, CFD models can be built for numerically solving the partial differential equations that govern the conservation of air continuity, momentum and energy in the geometrical model. The indoor air is assumed to be steady state, three-dimensional, incompressible and turbulent. The mathematical equations describing the turbulent flow shown in Equation (7.4)-Equation (7.9) are unified and described in Equation (7.10).

$$\frac{\partial \rho \Phi}{\partial \tau} + div(\rho V \Phi - \Gamma_{\Phi,eff} grad \Phi) = S_{\Phi} \tag{7.10}$$

where ρ is the air density (kg m^{-3}); $\Gamma_{\Phi,eff}$ is the effective coefficient (kg m^{-1} s^{-1}); V is the air velocity vectors (m s^{-1}); S_{Φ} is the source term of the general flow property; Φ is the variable representing the air velocity, pressure and temperature individually.

Many researcher have studied the performance of different numerical models for ventilation system, especially the indoor airflow, temperature and pollution distribution. Chen (Chen 1999) compared five different k–ε models, including the standard k–ε, the LR k–ε and the RNG k–ε model. He recommended only the RNG k–ε model for simulations of indoor air-flow and noted that the performance of the other models was not stable. Rouaud et al. (Rouaud et al. 1999) showed that both the standard k–ε and the RNG k–ε model predict well the main features of the flow in clean rooms. They also claimed that the RNG k–ε seems to be more suitable, while the standard k–ε model overestimates turbulent diffusion. Cheong et al. (Cheong 2003) evaluated the current thermal comfort conditions of an air-conditioned lecture theatre, using the code Fluent (Fluent 2005) and the RNG k–ε model. Calculations of airflow characteristics and temperature gradients were in fair agreement with empirical measurements. Posner et al. (Posner 2003) have evaluated the laminar, the standard k–ε and the RNG k–ε models with respect to their performance in simulating the flow in a model room. Their simulations using the code Fluent (Fluent 2005)with the laminar and the RNG k–ε models agreed better with experimental data than calculations with the standard k–ε model.

Therefore, the RNG k–ε model is employed in our study and the coefficients of used in RNG k-ε model are shown in Table 7.1. The form of the RNG k-ε model is shown as Equation (7.11) and Equation (7.12).

$$\frac{\partial}{\partial t}(\rho\kappa)+\frac{\partial}{\partial x_i}(\rho\kappa u_i)=\frac{\partial}{\partial x_j}(\alpha_k\mu_{eff}\frac{\partial\kappa}{\partial x_j})+G_\kappa+G_b-\rho\varepsilon-Y_M+S_\kappa \qquad (7.11)$$

$$\frac{\partial}{\partial t}(\rho\varepsilon)+\frac{\partial}{\partial x_i}(\rho\varepsilon u_i)=\frac{\partial}{\partial x_j}(\alpha_\varepsilon\mu_{eff}\frac{\partial\kappa}{\partial x_j})+C_{1\varepsilon}\frac{\varepsilon}{\kappa}(G_k+C_{3\varepsilon}G_b)-C_{2\varepsilon}\rho\frac{\varepsilon^2}{\kappa}-R_\varepsilon+S_\varepsilon \quad (7.12)$$

where G_k is the generation of turbulence kinetic energy due to the mean velocity gradients, G_b is the generation of turbulence kinetic energy due to buoyancy, Y_M is the contribution of the fluctuating dilatation in compressible turbulence to the overall dissipation rate, the quantities ∂_k and ∂_ε are the inverse effective Prandtl number for k and ε respectively, S_κ and S_ε are user-defined source terms. The general used parameters for this k-ε turbulence model are listed in Table 7.1.

Table 7.1 Coefficients used in the RNG k-ε model

$C_{1\varepsilon}=1.42$	$Y_M=2\rho\varepsilon\kappa/y/RT$
$C_{2\varepsilon}$=1.68 $C_{2\varepsilon}=1.68$	$a_\kappa=a_\varepsilon=1.393$
$C_\mu=0.0845$	$\beta=0.012$
$Gh=\beta g_i\mu_i aT/\mathrm{Pr}_f/a\chi_i$	$\eta=S_k/t$
$G_k=\mu_t S^2, S=\sqrt{2S_{ij}S_{ij}}$	$\eta_0=4.38$

The continuity, momentum and energy conservation equations in steady and unsteady state are solved using the finite volume, the second-order upwind scheme and the SIMPLE algorithm. The air is assumed to be incompressible and its physical properties are assumed constant. The residuals of continuity, momentum and turbulent kinetic energy and its dissipation rate can be set by users. For example, one can use 1×10^{-4} in magnitude for convergence, and 1×10^{-7} in magnitude for the residual of energy.

No penetration and non-slip conditions are imposed at all solid wall boundaries. The constant heat flux thermal boundary condition is imposed at the solid boundaries of the local heat source. The supply air vent is defined as the velocity flow inlet. Turbulence of the supply air is specified by the hydraulic diameter of the vent and the turbulent intensity at the inlet vent. The pressure outlet boundary is imposed at the outlet vent. The window and the relevant wall are set with certain value of radiation heat flux. The other three walls, floor and ceiling are considered as adiabatic conditions. The supply air is assumed to be sent into the room with a constant air temperature, *e.g.* 17℃.

The independent grid was used in this CFD-based ventilated room model. For grid generation, the main consideration is the accuracy of numerical solver in modeling the airflow profile. More cells will lead to more accurate results, but will increase the computation burden. In this study, three different numbers of cells (about 360000, 260000, and 180000) were adopted to test the simulation performance by compromising the accuracy and computation resources. It is validated that 260000 cells are preferable for CFD-based ventilated room with higher computational accuracy and less computational time.

7.1.3 Simulation Results Based On CFD Models

In this study, some typical cases are considered in the development of the temperature offset model. The number of occupants (N_{occ}) is set from 1 to 7 with an interval of 1, and the supply air flow rate is set from 0.16m^3/s to 0.48m^3/s (or 0.72 m^3/s) with an interval of 0.08m^3/s respectively. The detailed procedure of

development of the temperature space offset model is illustrated in Section 7.3. Occupants are considered as the main heat source of the room. Occupant number changes from time to time, but occupants' activities are mainly located in the occupancy zone. In this case, the temperature difference between the measuring points and the occupancy zone is mainly determined by the supply air flow rate and the number of occupants. The former factor affects the ventilation and the hot stack of the room; while the later factor affects the amount of heat or the cooling load condition. By varying V_{sup} and N_{occ}, the indoor temperature values of different zones can be calculated accordingly.

In contrast to the conventional zonal and nodal models (Feustel H.E 1999, Ren Z., Stewart J. 2003), the effect of the heat transfer from the neighboring zones is not included in Equation (7.5). Since the inlet and indoor source conditions are responsible for the thermal characteristics of different zones, the model only creates a link among the inlet air, indoor occupants' number and individual zones. The supply air flow rate and heat flux of occupants would have created the aggregate effect of the convective flux interaction with the neighboring zones on the well-mixed zone in consideration. This is a useful assumption, because it creates a direct relationship between the actual sensor and virtual sensor without the need for modeling zonal interactions.

Table 7.2 Temperature of different zones with varying supply air flow rate (N_{occ}=1)

Supply air flow rate	Zone 1	Zone 2	Zone 3	Zone 4	Zone 5	Zone 6
0.16	19.2693	19.5989	19.735	19.8834	19.4153	19.5989
0.24	18.8682	19.0392	19.0836	19.2911	18.9321	19.0392
0.32	18.6424	18.8235	18.8455	18.9665	18.7046	18.8235
0.40	18.5023	18.6618	18.6898	18.7544	18.5486	18.6618
0.48	18.4023	18.5523	18.5893	18.6009	18.4409	18.5523
0.56	18.3316	18.6192	18.5284	18.5066	18.38	18.4884
0.64	18.3288	18.5704	18.4597	18.4608	18.365	18.4215
0.72	18.2962	18.4993	18.3759	18.441	18.3272	18.3738

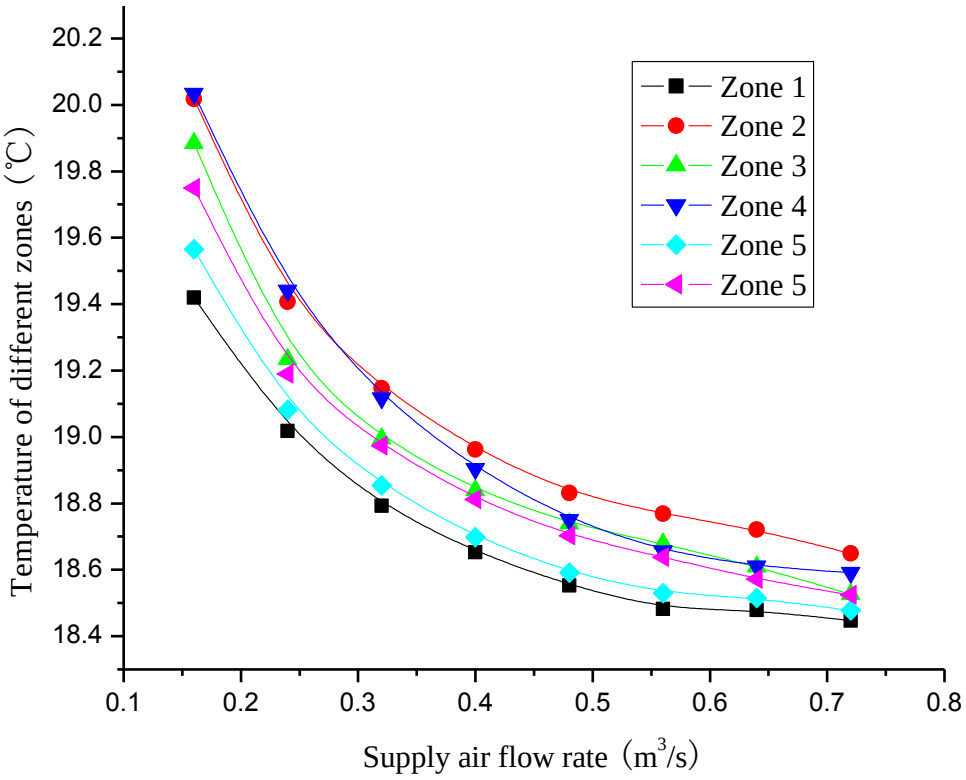

Figure 7.2 Relationship between supply air and temperature of zones with 1 occupant

Figure 7.2 shows the relationship of temperature values of different zones within this ventilated room with the supply air flow rate when the number of occupants is set to be 1. The actual temperature sensor is located in zone 6 near the duct of exhaust air and the zone 2 is set to be occupied zone where the occupants located mainly. It is found that the temperature of all zones decreased with the increasing of supply air flow rate with constant temperature, while the number of occupants is constant. As for each zone, the temperature decreased with the increasing of supply air flow rate as well. The temperature differences among different zones are obvious.

When the number of occupant is one, the temperature difference between the zone 2 and zone 6 is detected in Figure 7.2 based on the results of Figure 7.3. The

data-based temperature offset model in this case is shown in Equation (7.13).The R-Square is 0.99828. It can be found the simplified model with the identified parameters is with high accuracy to express the relationship between the actual temperature sensor and occupied zone,

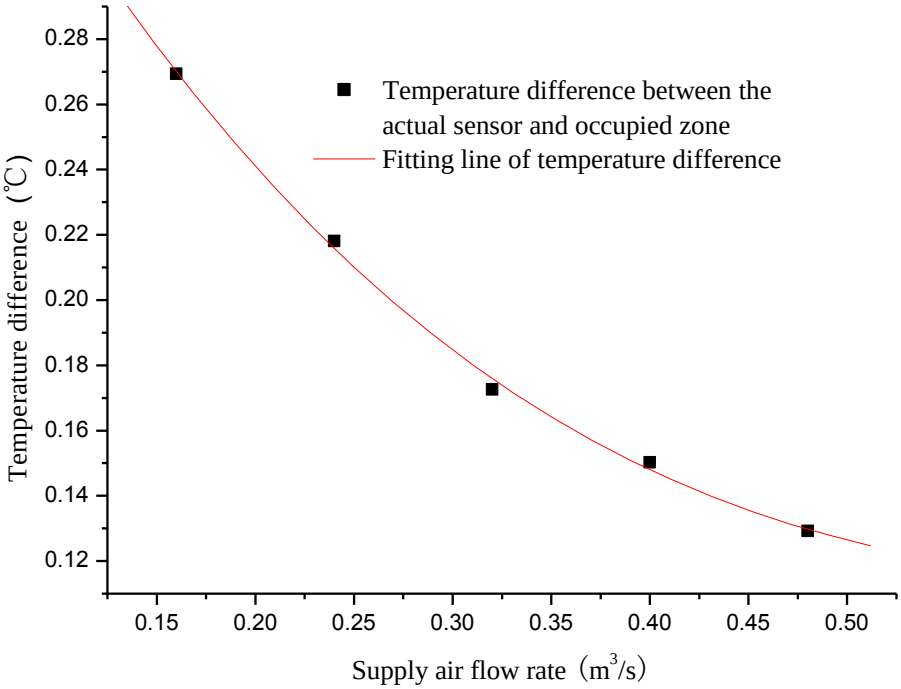

Figure 7.3 Temperature difference between actual and virtual sensor at different supply air flow rates (1 occupant)

$$T_{Virtual} = -1.509 * V_{Sup}{}^{3} + 2.757 * V_{Sup}{}^{2} - 1.684 * V_{Sup} + T_{Sensor} + 0.478 \qquad (7.13)$$

Using the same approach, the temperature values of actual temperature sensor and occupied zone with varying V_{sup} and N_{occ} are obtained accordingly and its results are shown in Table 7.3.

Table 7.3 Temperature values of actual temperature sensor and occupied zone with varying V_{sup} and N_{occ}

	Number of occupants	Temperature of actual sensor (℃)	Temperature of occupied zone (℃)
V_{sup}=0.16	1	19.5989	19.87191
	2	19.74615	20.05544
	3	20.05905	20.89782
	4	20.41927	21.42868
	5	20.7149	21.99772
	6	21.01446	22.41423
	7	21.36727	23.06554
V_{sup}=0.24	1	19.0392	19.25102
	2	19.10137	19.47058
	3	19.32659	19.68687
	4	19.52535	20.12447
	5	19.75851	20.43641
	6	19.96255	20.83488
	7	20.19787	21.21541
V_{sup}=0.32	1	18.8235	18.9955
	2	18.75	18.75
	3	18.85	19.05
	4	19.05	19.35
	5	19.15	19.55
	6	19.45	19.95
	7	19.75	20.05

V_{sup}=0.4	1	18.6618	18.81073
	2	18.60571	18.81616
	3	18.74294	19.02219
	4	18.85446	19.18679
	5	19.01226	19.41839
	6	19.1163	19.58497
	7	19.26742	19.79235
V_{sup}=0.48	1	18.5523	18.69027
	2	18.48446	18.66142
	3	18.59603	18.82438
	4	18.70919	18.98112
	5	18.81939	19.1514
	6	18.90814	19.30251
	7	19.01849	19.47333

To detect the decision parameters (supply air flow rate and number of occupants) which are relevant to the temperature difference between actual temperature sensor and the occupied zone, it necessary to identify the empirical model accurately using the results of CFD numerical simulations. Temperature difference with different supply air flow rate and occupants are illustrated in Table 7.4 accordingly.

Table 7.4 Temperature difference with different supply air flow rate and occupants

Flow rate (m^3/s)	N_{occ}=1	N_{occ} =2	N_{occ} =3	N_{occ} =4	N_{occ} =5	N_{occ} =6	N_{occ} =7
0.16	0.27301	0.36921	0.83877	1.00941	1.28282	1.39977	1.69827
0.24	0.21182	0.306	0.428	0.59912	0.6779	0.87233	1.01754
0.32	0.172	0.26	0.31	0.45	0.54	0.62	0.7
0.4	0.14893	0.21045	0.2525	0.33233	0.40613	0.46867	0.52493
0.48	0.13797	0.17696	0.22835	0.27193	0.33201	0.39437	0.45484

Figure 7.4 describes that temperature difference between actual sensor and the occupied zone with different supply air flow rate with constant number of occupants. And the fitting relationships are identified as well. It can be investigated that the temperature difference are obviously different with the different supply air flow rate and number occupants. The temperature difference can be calculated based on varying supply air flow rate when the number of occupants is known. This idea can be adopted for indoor ventilation control system to consider the indoor air stratification phenomena.

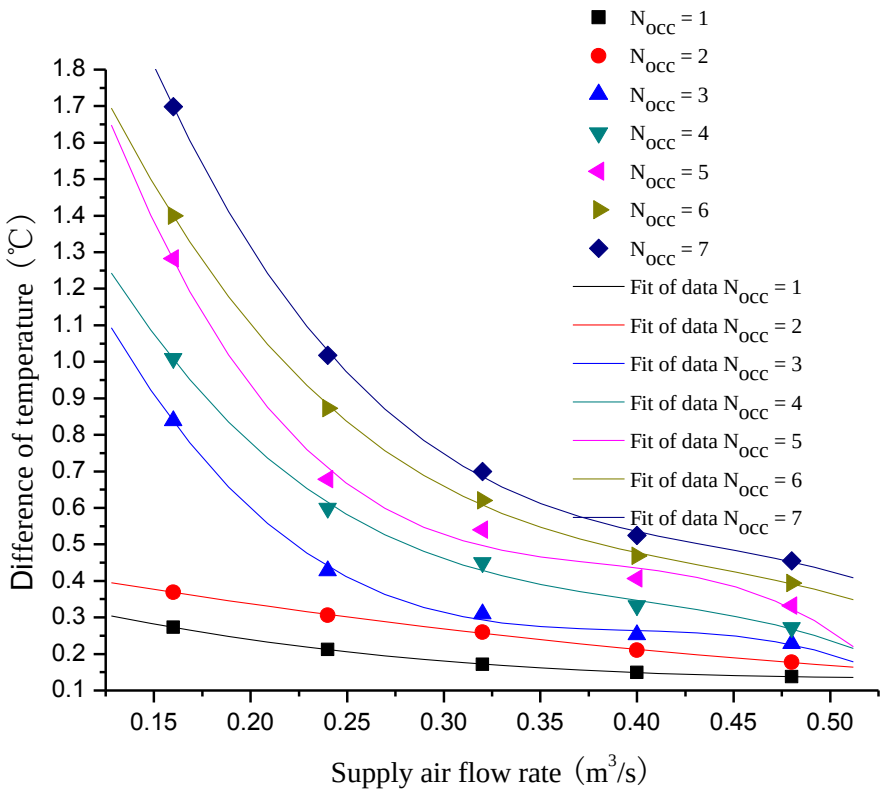

Figure 7.4 Relationship between supply air and temperature of zones with different occupants

CFD modeling can generate a temperature offset contour map. As an example, Figure 7.5 shows the temperature offset varies with the occupant number and the

supply air flow rate. It can be investigated that the temperature difference increases with the increasing number of occupants when the supply air flow rate is constant. Meanwhile, the temperature difference decreases with the increasing supply air flow rate when the number of occupants is constant.

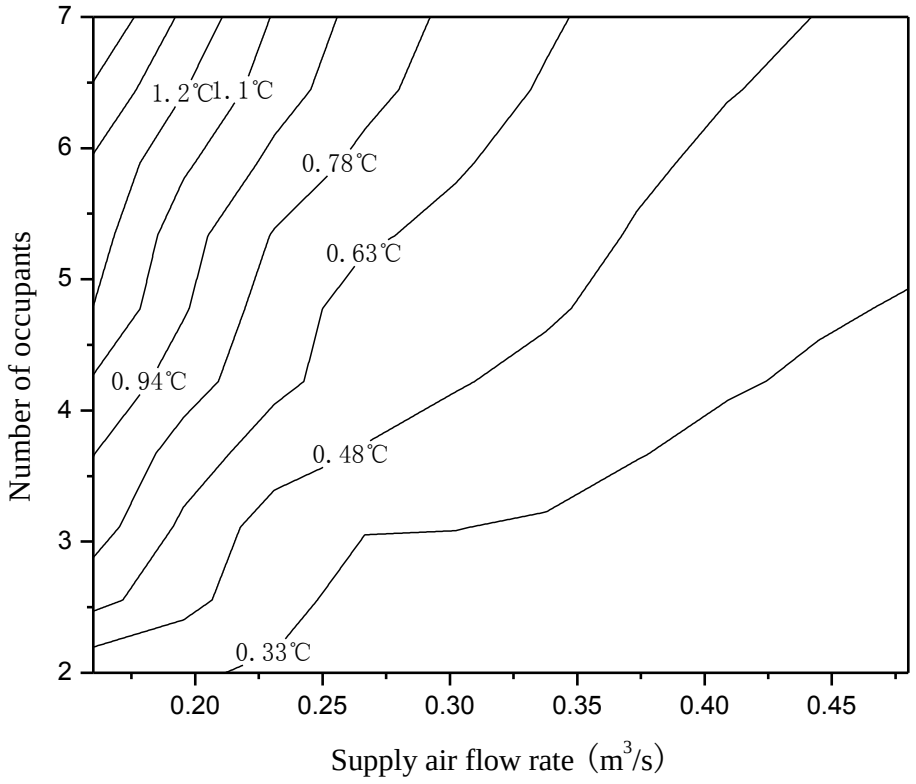

Figure 7.5 Temperature difference between Zone 2 and Zone 6 relative to supply air flow rate and number of occupants

7.1.4 Development of a Space Temperature Offset Model

Given the number of occupants and the supply air flow rate, the temperature offset contour map can be used as a look-up table for finding the temperature difference between the temperature measurement and the temperature which is concerned in control. In order to reduce the requirement for data storage, a simplified method

should be used to replace the contour map. The general expression of a space temperature offset model has the form as Equation (7.14).

$$\Delta T_{off} = f_{off}(V_{\sup}, N_{occ}) \tag{7.14}$$

where ΔT_{of} is the temperature offset (℃); $V_{\sup}$ is the supply air flow rate; N_{occ} is the occupant number; f_{off} is usually a nonlinear function.

It is sometimes difficult to obtain the explicit form of the nonlinear function f_{off} *w.r.t.* V_{sup} and N_{occ}. A simple method to solve this problem is to rewrite the nonlinear function as Equation (7.15).

$$\Delta T_{off} = \sum_{i=1}^{N} C_i\left(N_{occ}\right) V_{\sup}^{i-1} \tag{7.15}$$

where the nonlinear function f_{off} is written in the form of a polynomial of V_{sup}; and the parameters C_i, i = 1 - N are N_{occ}-dependent.

The space temperature offset model in the form of Equation (7.15) was given in Table 7.5, where different sub-models corresponded to different numbers of occupants and the polynomial order N = 3 was used. These coefficients were identified using the least square method.

Table 7.5 The identified coefficients and order of the space temperature offset model

Coefficient / N_{occ}	C_1	C_2	C_3	$C4$	N

1	0.478	-1.684	2.757	-1.509	3
2	0.517	-1.053	0.803	-0.187	3
3	2.893	-19.753	49.839	-42.223	3
4	2.817	-16.873	40.020	-33.187	3
5	4.293	-29.249	75.529	-66.287	3
6	3.556	-19.415	42.192	-32.239	3
7	4.519	-25.461	55.566	-42.026	3

The space temperature offset model is developed to use virtual temperature sensor to compensate temperature non-uniform distribution in ventilated room for maintaining satisfied indoor air thermal environment. CFD simulation is applied to describe the temperature stratification in an occupied room and generate essential data. Based on these data, a simple space temperature offset model is developed, which establishes a simple relationship between the measured temperature and the temperature which is concerned in the control of room temperature.

The temperature offset model shown in Figure 7.6 is identified using the data generated from the CFD simulation of the air temperature non-uniform stratifications. Many significant factors, which will affect the structure of the offset model, such as variations in the supply air flow rate and the strength of heat sources, are taken into account in CFD modeling. After the corresponding training data are generated and the structure of the offset model is determined, the least square fitting method is used to identify the parameters of the offset model. This temperature offset model is used as a virtual temperature sensor in a zone temperature control system to compensate the temperature non-uniform stratification and to improve thermal comfort in occupied rooms.

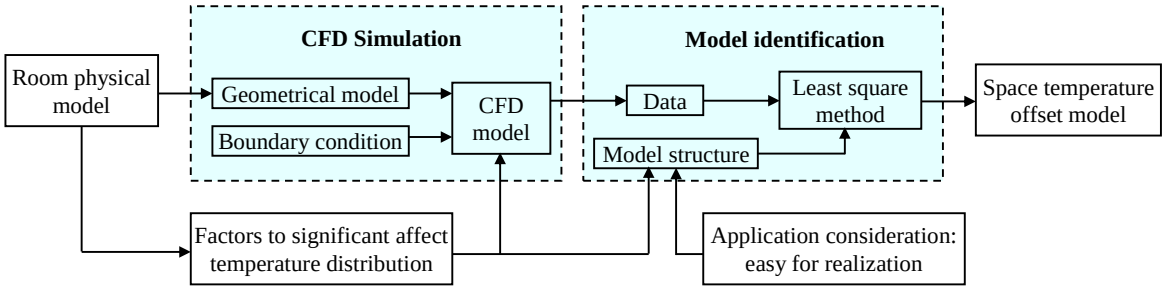

Figure 7.6 Strategy of developing practical space temperature offset model

The space temperature offset model (7.15) can be used in the temperature control system of a conditioned space to improve the thermal comfort. Figure 7.7 shows how to use the space temperature offset model (7.15) in a typical pressure-dependent VAV system. In this system, the supply air temperature is usually maintained to be a constant and the indoor air temperature is controlled to a predefined set point by changing the supply air flow rate. The manipulation of the supply air flow rate is done through a VAV box according to the control signal given by a PI controller.

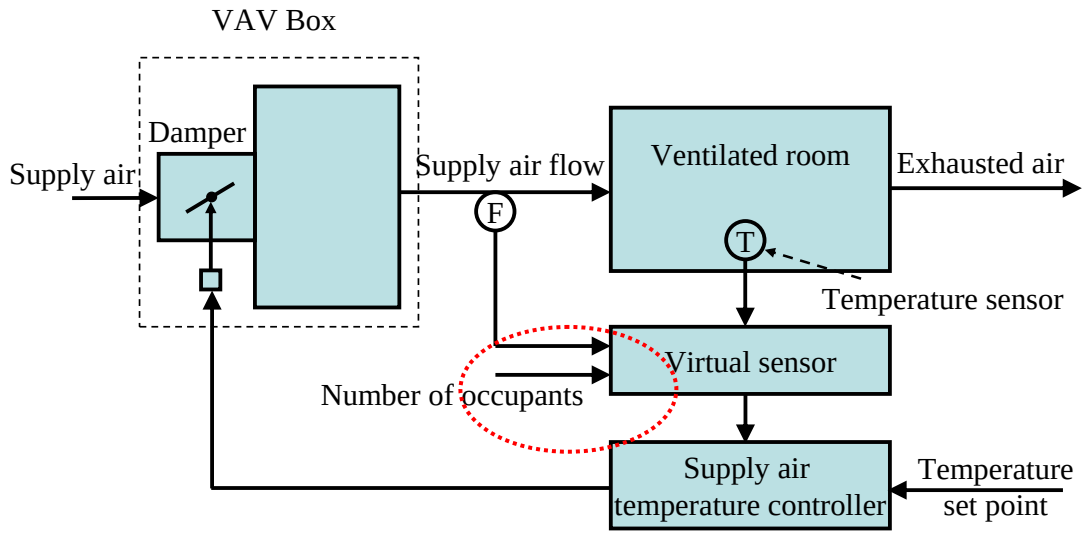

Figure 7.7 The control system of pressure-dependent VAV box

7.1.5 Simplified Space Temperature Offset Model

The virtual temperature sensor has the form of Equation (7.16)

$$T_{virt} = T_{sens} + \Delta T_{off} \tag{7.16}$$

Where, T_{virt} is the output of the virtual temperature sensor; T_{sens} is the temperature measurement from the actual temperature sensor; ΔT_{off} is calculated by Equation (7.15). The virtual sensor is placed between the actual temperature sensor and the controller. The inputs of the virtual sensor include the temperature measurement from the actual sensor, the supply air flow measurement and the number of occupants. When the three inputs are available, the virtual sensor calculates the temperature difference between the measuring point and the place where zone occupants actually stay, and send the calculated temperature measurement to the controller.

The supply air-flow measurement can be obtained using a flow meter. However, it is difficult for the virtual sensor in application to know exactly the number of occupants. To solve this problem, it is possible to design the virtual sensor to allow the occupants to manually reset the occupancy number; but this is not convenient in application especially when the number of occupants varies frequently.

To simplify the application of the models in Table 7.5, the simplified modeling method introduced next. The basic idea is that the number of occupants is divided into different modes with a small number, for example, small level medium level and large level. Then, the space temperature offset model of (7.15) becomes Equation (7.17). Table 7.6 listed the coefficients of these simplified sub-models. The

temperature difference between the space temperature offset model (7.15) and the simplified version (7.17) can be calculated using the results of Table 7.5 and Table 7.6. It should be noted that the introduced relative errors were less than 8.0%. Therefore, the dominant modal behavior of the temperature process can be captured well.

$$\text{Mode } j\text{:}\quad \Delta T_{off} = \sum_{i=1}^{N_s} C_{i,j} V_{\text{sup}}^{i-1} \tag{7.17}$$

where j indicates the j^{th} mode; N_s is a total number of modes which should be much smaller than N. In application, users need only to choose the operating mode, not to change the occupant number frequently. It is described in the red circle part of Figure 7.9. Although the model accuracy will be reduced, the operation of the virtual sensor becomes much simple and convenient.

Table 7.6 The identified coefficients and order of the simplified model

Coefficient / Level (N_{Occ})	C_1	C_2	C_3	C_4	N
Small (*1*-*2*)	0.497	-1.368	1.780	-0.848	3
Medium (*3*-*4*)	2.855	-18.313	44.929	-37.705	3
Large (*5*-*7*)	4.123	-24.709	57.762	-46.851	3

7.2 Experimental Validation of the CFD-based room model

7.2.1 General Description of Set-up

A real ventilation room was used to test the indoor air temperature distribution using temperature data logger to validate the accuracy of CFD-based room model. The

size of real ventilated room is 3.0m×3.0m×2.5m (L×M×H), and its size is the same as the simulated room shown in Figure 7.1. Two dry bulb air temperature sensors were used to measure the indoor air temperatures in the occupied zone and near the inlet of the return air duct. Its accuracy is ±0.2℃ and the working range is from 0℃ to 50℃. The response time of sensor is 360 seconds. It was found that the indoor air temperature take around 20 minutes to reach the stable condition indicating the room thermal constant of around 20minutes.

One sensor was located in the occupied zone which was 1.25 m from the front wall, 1.5 m from the front left wall and at a height of 0.8 m above the floor. The other was located near the return duct which was 0.1 m under the ceiling (below the louver). The temperature of supply air was kept at 18℃. The measurements of two temperature sensors were recorded with a sampling interval of 1 min. The supply air flow rate was set to be 0.16m^3/s, 0.24m^3/s, 0.32m^3/s,0.4m^3/s, and 0.48m^3/s and the number of occupants was 1 and 4 respectively. The internal heat gain was the generation of occupants. Totally 8 tests were conducted with different combination of the supply air flow rate and the number of occupants. After the indoor air temperature became stable, the average of the temperature measurement over a period of 20 min was taken as the temperature of the sensors to reduce effects of the noises and disturbances in the experiment. The temperature profiles of the sensors with different supply air flow rates and occupant numbers were shown in Figure 7.8 and Figure 7.9.

7.2.2 Comparison of Experimental and Simulation Results

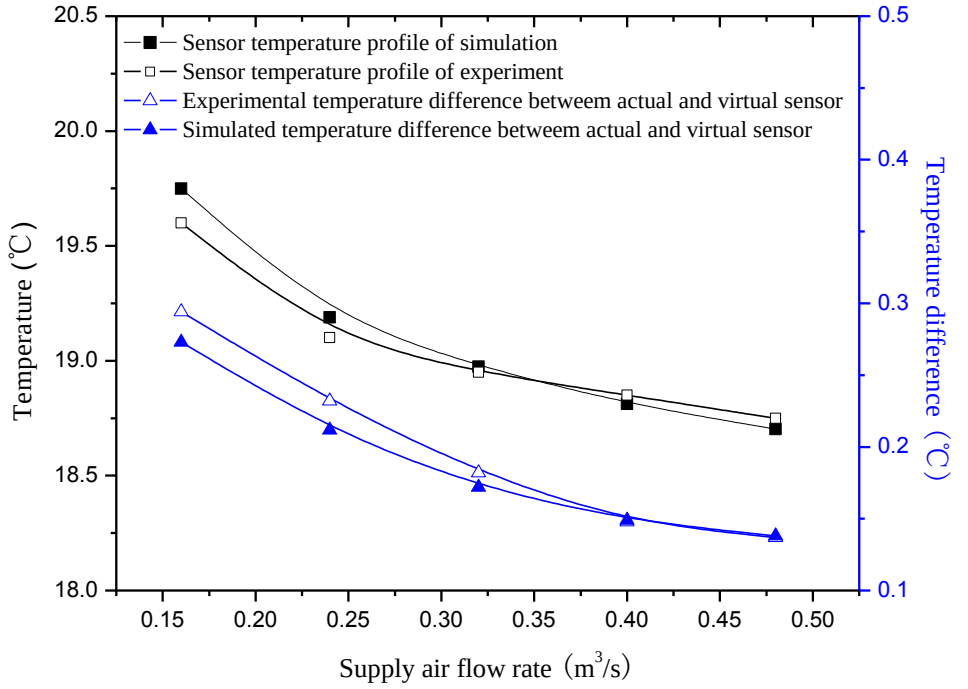

Figure 7.8 Temperature profiles of actual sensor and temperature difference (Number of occupants is 1)

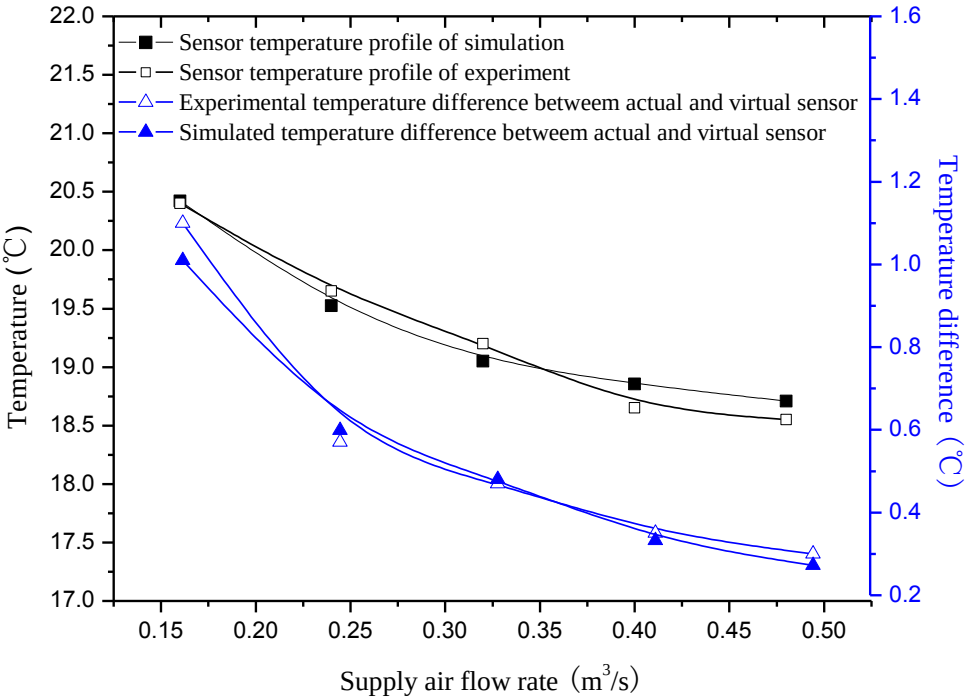

Figure 7.9 Temperature profiles of actual sensor and temperature difference (Number of occupants is 4)

The air temperature measurements at two sensor positions with different supply air flow rate and occupants were used to evaluate the accuracy of the CFD model. Figure 7.8 and Figure 7.9 present the comparisons of the actual temperature measurements and its difference with the virtual (CFD) sensor measurements. There were noticeable differences between the virtual and real sensor measurements due to the heat flux through walls, windows, and indoor heat generation. But acceptable agreement can be found between them. The comparison shows that there was significant difference between the air temperatures at different locations with practical air-conditioned space and the accuracy of presented CFD-based room model was acceptable for the application in this study.

7.3 Summary

A virtual temperature sensor has been developed to compensate the non-uniform air temperature stratification and improve the accuracy of the temperature control in occupied zone. Experimental tests have been carried out to validate the accuracy of the CFD room model. Fair agreement was found between the simulated and measured results. The result verified that the use of the virtual temperature sensor can efficiently compensate the influence of the temperature non-unified stratification on temperature control systems, and hence improve the thermal comfort in the occupied zone.

CHAPTER 8 DEVELOPMENT AND EVALUATION OF A VIRTUAL VENTILATION CONTROL TEST SYSTEM

The traditional complete-mixing air model fails to consider the impact of non-uniform air temperature stratifications. This chapter presents a CFD-based virtual test method for control and optimization of indoor environment by combining a ventilated room with a ventilation control system. The ventilated room and its dynamic ventilation control system are represented by a Computational Fluid Dynamics (CFD) model and dynamic models of the temperature sensor, PID controller and actuator and VAV damper model respectively. A space temperature offset model developed in Chapter 7 is used to improve the accuracy of temperature measurement and control at the occupied zone as a virtual sensor. The control strategy adopted by the ventilation test system, model components of the test system, typical case studies are introduced in detail in Section 8.2 and Section 8.3.

8.1 Introduction of Indoor Ventilation Test Systems

8.1.1 Overview of Well-Mixed Based Ventilation Control and Test Systems

The operation and control of heating, ventilating and air conditioning (HVAC) system are essential for ensuring satisfactory indoor comfort and indoor air quality (IAQ). Over the last decades, there have been increasing interests in studying how to maintain appropriate indoor comfort level. Proper ventilation of buildings can create

thermally comfortable environment by controlling indoor air parameters, such as air temperature. A low ventilation rate may cause deficiencies of the system performance such as poor mixing of supply and room air, poor indoor thermal comfort. To improve the indoor ventilation performance, it is essential to have a suitable tool to predict and test ventilation performance in buildings. Many local and supervisory control approaches of air-conditioning systems for the last twenty years are presented to evaluate and improve the ventilation performance.

Wang (Wang 1999) developed several dynamic models of building and variable air volume (VAV) air-conditioning systems, which incorporate the thermal (i.e. indoor air temperature), hydraulic, environmental and mechanic characteristics as well as energy performance. These models can simulate the system using a model-based program to maintain satisfied indoor thermal comfort. Kwok (Kwok 2003) presented an adaptive interface relationship of indoor comfort temperature with outdoor air temperature in order to preset the indoor air temperature as a function of outdoor air temperature. This algorithm can improve the occupants' acceptance of thermal comfort. Feriadi (Feriadi 2003) developed a thermal comfort prediction chart and fuzzy thermal comfort model suitable for naturally ventilated buildings in the tropics based on data collected through field surveys in Singapore and Indonesia. Wang and Jin (Wang et al 2000) presented a supervisory ventilation control strategy to predict indoor air thermal condition and evaluate the ventilation performance of HVAC system based on TRNSYS simulation platform. Yuan (Yuan 2006) developed a model predictive strategy to access multiple-zone ventilation and temperature control performance of a single-duct VAV system. Chao (Chao 2004)

established a dual-mode demand control ventilation strategy targeting at use in buildings where the number of occupants varies frequently. Natasa (2007) presented an approach to improve building thermal comfort by use of computer-based tools.

All these simulation systems have taken the indoor air as "perfectly mixed" into consideration. Since the indoor dynamic property is simplified, these simulation systems can not precisely feedback the spatial variation of the controlled variable. Such an assumption can be unrealistic in applications where controlled variables vary considerably over distances.

8.1.2 Feasibility of CFD Models for the Building Ventilated Room

CFD model as a powerful tool have successfully been applied in the HVAC field (Pappas A. 2008). Many researches on predicting detailed room airflow patterns, indoor temperature distributions, and pollutant transportation indoors have been studied (Zhai et al 2005; Chung 1998; Aganda 2000; Sinha 2000, Alamdari 1994). Meantime, CFD is a useful tool in design practice for the verification and comparison of tentative building design alternatives (Taeyeon 2007). In contrast to full scale ventilation performance test, the CFD method is a relatively inexpensive and alternative method. It is applicable to provide complete information concerning indoor environment and space ventilation control performance of a new developed control strategy before it is constructed.

It would be a significant step forward to integrate the simulation of the space ventilation and the indoor thermal stratification phenomena to a real-time ventilation control strategy for ventilation performance test purposes. This Chapter presents a CFD-based test method combining a ventilated room with a dynamic ventilation and control system. The ventilated room is built using the CFD models. The ventilation and control system is programmed using user defined function program (UDF) interfaced with the CFD model. The UDF program is compiled using C^{++} code. This approach of merging the traditional ventilation and control system with CFD simulation to test indoor ventilation performance is very challenging, but if it is successfully achieved, it will undoubtedly provide new possibilities for testing and evaluating the ventilation control processes in applications.

8.2 Development of the CFD-Based Ventilation Test System

8.2.1 Overview of the Ventilation Test Method

In the design of ventilation test system, evaluating the indoor air environment has been the main target of the analysis from the start of CFD application. Based on our experiences in applying CFD to HVAC system, we have refined the following two major components which are indispensable for indoor ventilation performance test: (1) simulated ventilation room, (2) ventilation and control system. Both of these have become essential tools in the analysis of indoor environments and space ventilation.

1) Simulated ventilation room

Experimental measurements are reliable for providing sufficient data to test ventilation performance but need large labor-effort and time. In the proposed ventilation test method, the CFD simulation is used to represent the room as a virtual ventilated room model (Fluent 2005).

2) Ventilation and control system

The next critical step in applying CFD for ventilation and control test is the development of a ventilation and control system. The components of the ventilation and control system in this study include a temperature sensor model, a space temperature offset model, a PID controller model, an actuator model and a VAV damper model, which are programmed using user defined function program (UDF) and interfaced with the CFD model.

At this stage, the CFD-based online ventilation control test technique combined CFD simulation with the ventilation and control system has developed into a preferable test tool. The schematic diagram of the virtual online ventilation control test method is shown in Figure 8.1.

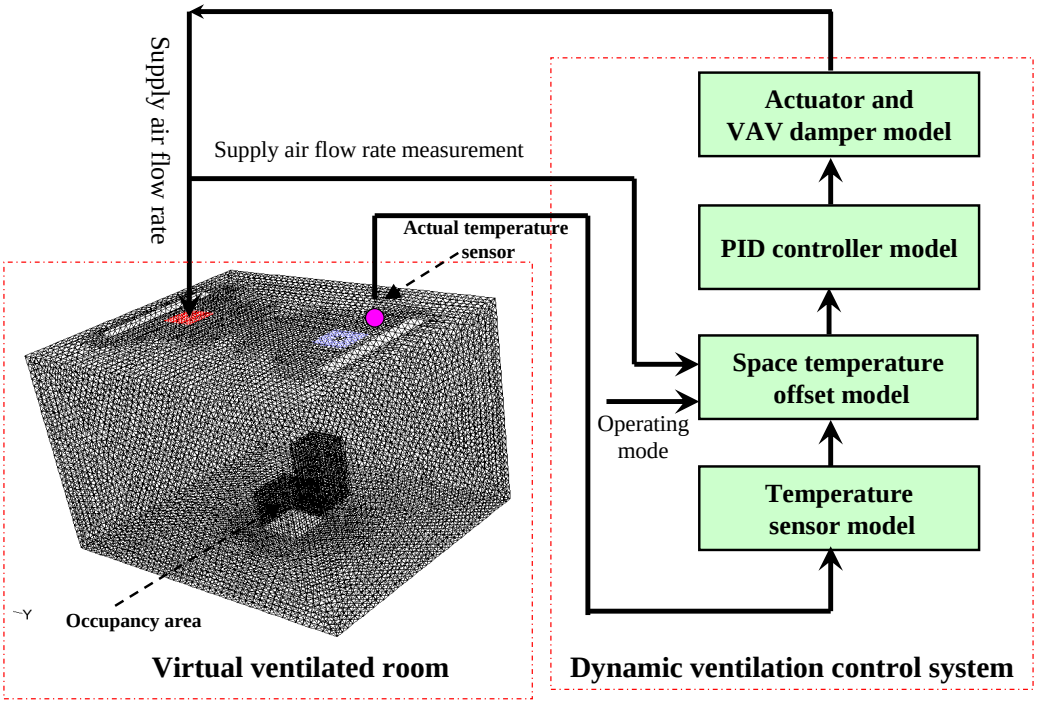

Figure 8.1 Configuration of virtual online ventilation control test system

The indoor air temperature near exhaust air is monitored by a temperature sensor as the actual indoor air temperature measurement. Figure 8.2 describes the typical pressure-dependent VAV ventilation control system used in this study, in which the supply air temperature was set as constant and the indoor temperature is controlled to a predefined set point. The manipulation of the supply air flow rate is done through a VAV damper according to the control signal given by a PID controller.

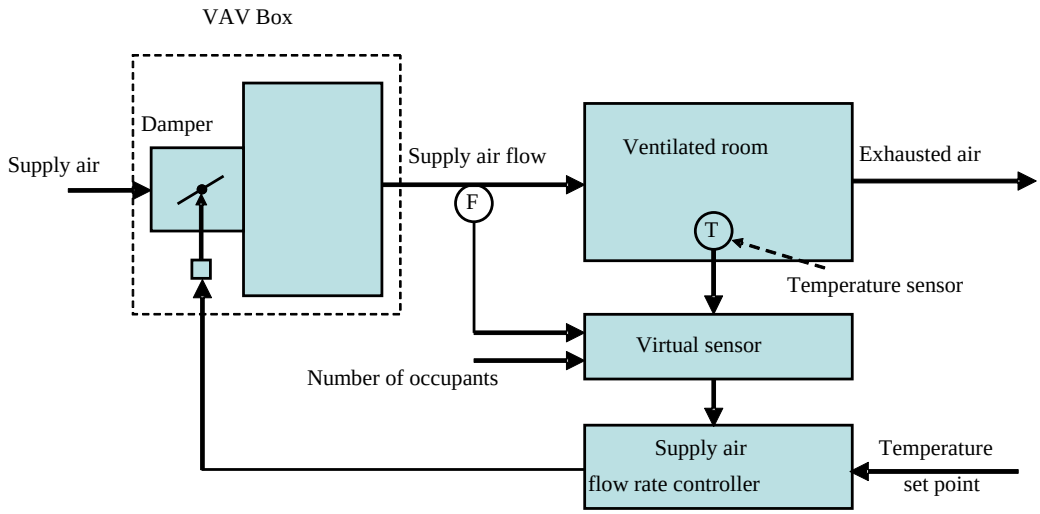

Figure 8.2 Control schematics of pressure-dependent VAV system

8.2.2 Ventilated Room Model

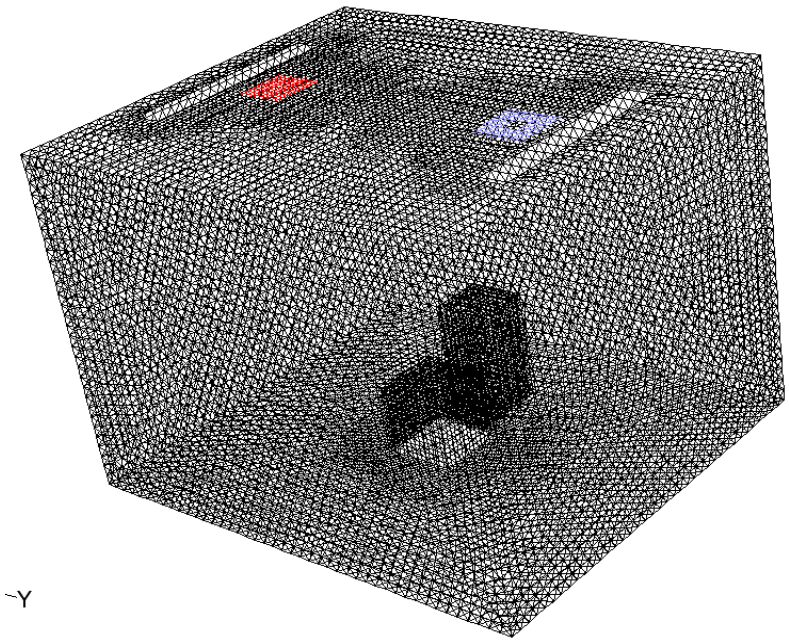

Figure 8.3 Ventilated room configuration

Assume the size of the room is X meters, Y meters and Z meters in length, width and height respectively. The ventilated room is geometrically built using Gambit software, which is a general-purpose preprocessor for CFD analysis. After the

geometrical model of the ventilated room is established using Gambit software, CFD models can be built for numerically solving the partial differential equations that govern the conservation of air continuity, momentum and energy in the geometrical model. The flow is assumed to be steady state, three-dimensional, incompressible and turbulent. The mathematical equations describing the turbulent flow are described by the following time-averaged Navier-Stokes equation. As a commonly used and popular CFD model, the renormalization group (RNG) k-ε turbulence model is adopted in this study because it is reliable for assessing indoor thermal environment. The detailed introduction of the CFD room model, RNG k-ε turbulent model, boundary conditions, and grids are illustrated in Section 7.1 of Chapter 7.

8.2.3 Temperature Sensor Model

The dynamics of the temperature sensor (Wang, S.W. 1999) was simulated by using the time constant method. One first-order differential equation (Equation (8.1)) represents the dynamic characteristics of a sensor:

$$\frac{dy'}{d\tau} = \frac{y - y'}{T_c} \tag{8.1}$$

where y is the true value of the measured temperature, y' is the measured value of the variable, and T_c is the time constant.

8.2.4 PID Controller Model

A typical PID controller model (Wang, S.W. 1999) is adopted in this study. The controller function used in dynamic ventilation control loops uses the ISA algorithm, which has the discrete form as shown by Equation (8.2) and (8.3). The handling of the proportional term, integral term and derivative term follows the algorithm implemented in ventilation control system.

$$U_k = K_p e_k + [I_{k-1} + \frac{K_p \Delta T}{2T_i}(e_{k-1} + e_k)] + K_p T_d \frac{e_k + e_{k-1}}{\Delta T} \tag{8.2}$$

$$I_{k-1} + \frac{K_p \Delta T}{2T_i}(e_{k-1} + e_k) = I_k \tag{8.3}$$

where e_k, e_{k-1} the error signals at current sampling and previous sampling, K_p is the proportional gain, T_i is the integral time, T_d is the derivative time, ΔT is the sampling interval, I_k and I_{k-1} is the integral time at the current and previous time steps, U_k is the output of PID controller.

8.2.5 Actuator Model and VAV Damper Model

The actuator model was used to represent the characteristics of actuators (Haves 1989). The actuator is assumed to accelerate very quickly and then turn at constant speed. A minimum change (e.g. the sensitivity of the actuator defined as a parameter of the model) in a demanded position is required to restart the actuator. The model includes the hysteresis in the linkage between actuators and dampers. The damper stem is driven by a rotary actuator; the speed of the damper stem varies with the position of the crank. The actuator model also counts the number of "start/stop or

reversals" of an actuator and the value of "travelled distance" of the valve (counted as one unit when the valve moves from its minimum position to its maximum position).

8.3 Test and Evaluate the Ventilation Performance

8.3.1 Performance Indices of the Developed Ventilation Test System

To check the ability of the CFD-based test method in testing the control stability, the parameters of the controller were tuned to investigate their effects in system control response. The proportional gain of the controller was set to be -0.1, -0.3 and -10.0 in the tests respectively. The integral time value was selected to 65. The results of these tests illustrated in Figure 8.4.

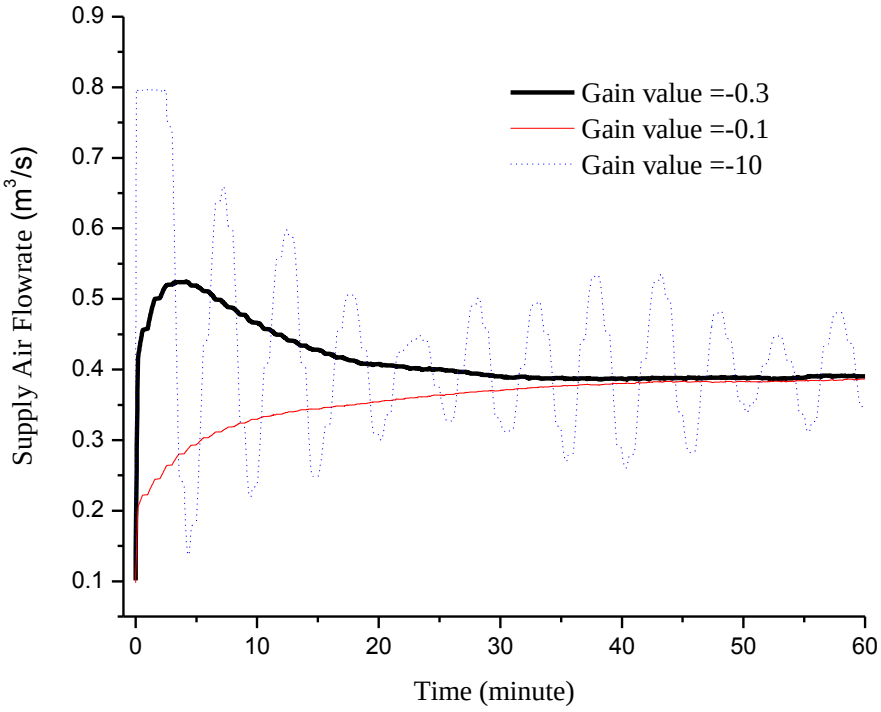

Figure 8.4 System responses in tests with different proportional gains

Figure 8.4 shows the comparison of the actual supply air flow rate with different proportional gains of the PID controller. It can be found that the actual control of the supply air flow rate was stable when the gain was -0.3. When the gain was -0.1, the system response was too slow in reaching the control reference value. The supply air flow rate was oscillating obviously when the gain value was -10.0. It can be observed that the unstable control performance was caused by using the irrational parameters of PID controller.

8.3.2 Control Error Analysis

An increased amount of emphasis on the mathematical and measurement of control system performance can be studied on automatic control. A performance index is a quantitative measure of the performance of a system and is chosen so that emphasis is given to the important system specifications. Modern control theory assumes that he systems engineer can specify quantitatively the required system performance. Then a performance index can be calculated or measured and used to evaluate the system performance. A quantitative measure of the performance of a system is necessary for automatic parameters optimization of a control system, and for the design of optimum systems.

The system is considered an optimum control system when the system parameters are adjusted so that the index reaches an extreme value, commonly a minimum value. A performance index, in order to be useful, must be a number that is always positive or zero. Then the best system is defined as the system that minimizes this index. The summary of the system control errors with different gains is presented in Table 8.1

using the averaged error analysis method. This method is an error analysis method analyzing the averaged absolute magnitude of the errors. It is written in Equation (8.4). The relative errors of different gain value with time are shown in Figure 8.5.

$$I_{error} = \frac{\int_0^T |e(t)|dt}{n} \tag{8.4}$$

where T is a finite time when this averaged value approaches a steady-state; I_{error} is the performance index; $e(t)$ is the relative system error.

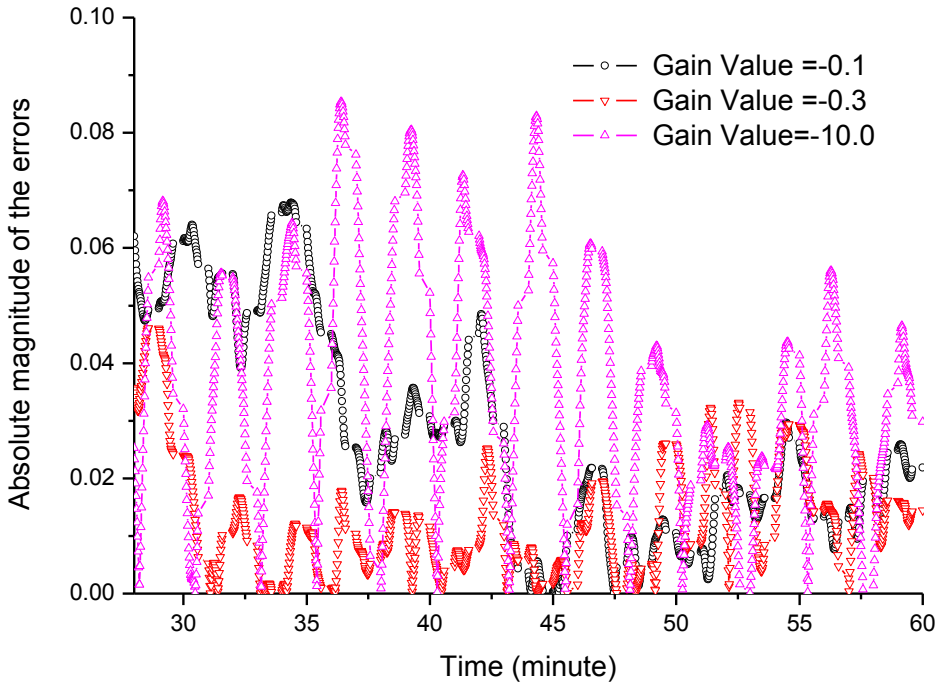

Figure 8.5 The absolute magnitude of the relative error with time

Table 8.1 Averaged absolute magnitude of the error

Gain value	-0.1	-0.3	-10.0
Error	0.0273	0.0129	0.0363

Based on the results of Figure 8.5 and Table 8.1, it can be seen that the average system control error was smallest when the gain value was -0.3. It shows that -0.3 is preferable for the temperature controller to improve the dynamic control performance based on the test using the system developed in this study. From these results, it can found that the tuning test of the controller can be conducted to test the stability of different control strategies.

8.3.3 Constant Temperature Set Point of Indoor Air

Firstly, the indoor air temperature set point is set to be 18℃. The indoor number of occupants is set to be 1.

A typical pressure-dependent VAV ventilation and control system was constructed on this virtual ventilation test platform with 2 seconds sampling time. First, one hundred time steps with a time difference of 0.2 seconds was simulated. Internal iterations are set to 70 which make sure the system is converged in initial each time step. Then, nine time steps with a time difference of 2 seconds was simulated. For each time step 70 internal iterations were found to be adequate for mass and energy convergence criteria as well.

In this dynamic ventilation control process, the measured temperature near exhaust air of room was used as the input of temperature controller. The supply air flow rate is manipulated by the VAV damper based on a pressure-dependent ventilation control system.

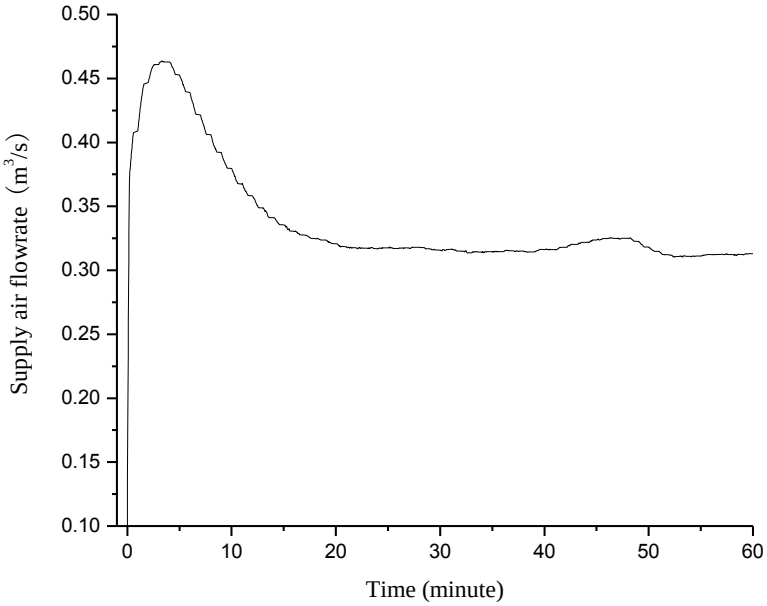

Figure 8.6 Supply air flow rate response of ventilation system

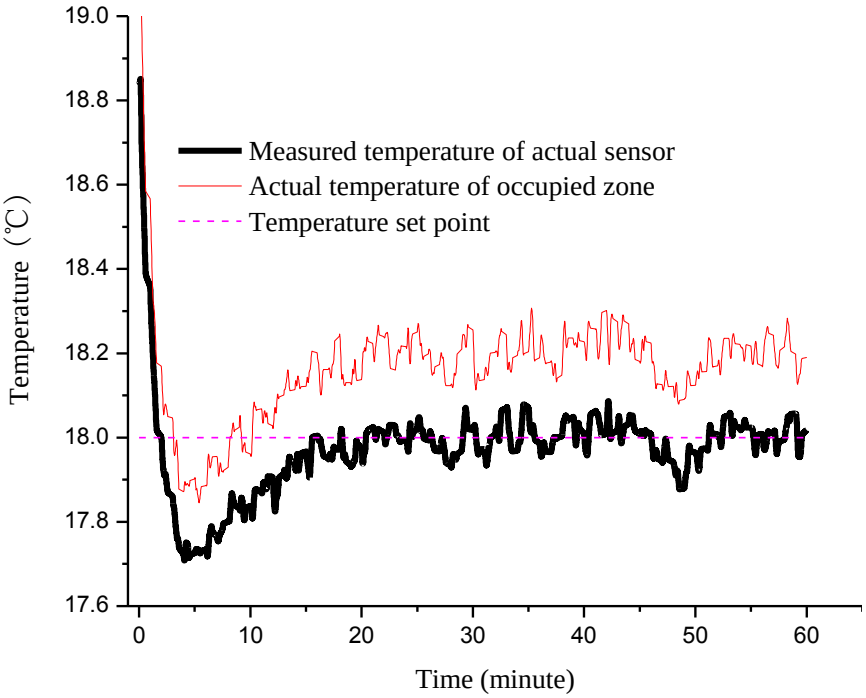

Figure 8.7 Comparison between temperature profiles at different locations

Figure 8.6 presents the dynamic supply air flow rate trend of the ventilation system. Figure 8.7 presents the temperature profiles at different locations, i.e., the temperature of actual sensor, temperature control set point and temperature of

occupied zone. The indoor air temperature near exhaust air was calculated using CFD model as the actual sensor value. This temperature value was monitored by a temperature sensor. In addition, the temperature of occupied zone in the ventilated room was calculated based on a volume weighted temperature value using CFD simulation. The supply air temperature was also set to be 17℃, and the temperature set point was set to be 18℃. Both control strategy stabilized the closed-loop system. However, there was a significant offset between the room temperature and its set point in the conventional control strategy, which may cause thermal comfort for occupancy. It can be found that the sensor value reached the temperature set point with less deviation when the supply air flow was 0.328m^3/s. This ventilation control reached a stability condition after about 20 minutes. It is observed that the proposed CFD-based test method is a feasible way to evaluate a ventilation control strategy.

In order to improve the accuracy of temperature measurement and control at the occupied zone, a virtual sensor is developed by using a space temperature offset model as in Chapter 7. The general expression of this space temperature offset model can be written as Equation (8.5).

$$T_{Virtual} = f(V_{Sup}) + N_{Occupant} * Q_{heat,per} + T_{Sensor} \tag{8.5}$$

where V_{Sup} is supply air velocity through a damper, T_{Sensor} is the measured temperature using an actual sensor; $T_{Virtual}$ is the predictive temperature using a virtual sensor, N_{Occ} t is the number of occupants $Q_{heat,per}$ is the heat generation of each occupant indoor.

In contrast to the traditional zonal and nodal models (Feustel 1999, Ren 2003), the effect of the heat transfer from the neighboring zones is not included in Equation (8.3). Since the inlet and indoor source conditions are responsible for the thermal characteristics of different zones. The model only creates a link among the inlet air, indoor occupants' number and individual zones. The supply air flow rate and heat flux of occupants would have created the aggregate effect of the convective flux interaction with the neighboring zones on the well-mixed zone in consideration. This is a very useful assumption, because it creates a direct relationship between the actual sensor and virtual sensor without the need for modeling zonal interactions.

For example, when the indoor number of occupants is set to be 1, the coefficients and orders of the Equation (8.5) are identified by the least square algorithm using the simulated data. A third-order temperature offset model obtained in Chapter 7 is mentioned again as shown in Equation (8.6).

$$T_{Virtual} = -1.509 * V_{Sup}{}^{3} + 2.757 * V_{Sup}{}^{2} - 1.684 * V_{Sup} + T_{Sensor} + 0.478 \qquad (8.6)$$

Based on the developed space temperature offset model, the temperature difference between actual and virtual temperature sensor with varying supply air velocity is fitted in Figure 7.3 of Chapter 7.

When the indoor number of occupants is changed to be 7, the relevant space temperature offset model shown in Equation (8.7) can be obtained using the same estimation approach.

$$T_{Virtual} = -0.1721 * V_{Sup}{}^{3} + 1.4225 * V_{Sup}{}^{2} - 4.0738 * V_{Sup} + T_{Sensor} + 4.5191 \qquad (8.7)$$

The temperature of occupied zone was higher than the actual sensor value. Obvious indoor thermal stratification might be caused by indoor thermal plume of heat sources and poor mixing between supply and indoor air. It is significant to interoperate a space temperature offset model with this ventilation test method to estimate indoor thermal stratification in the room tested. A space temperature offset model in Equation (8.6) was adopted to compensate the indoor air temperature stratification for improving the ventilation control.

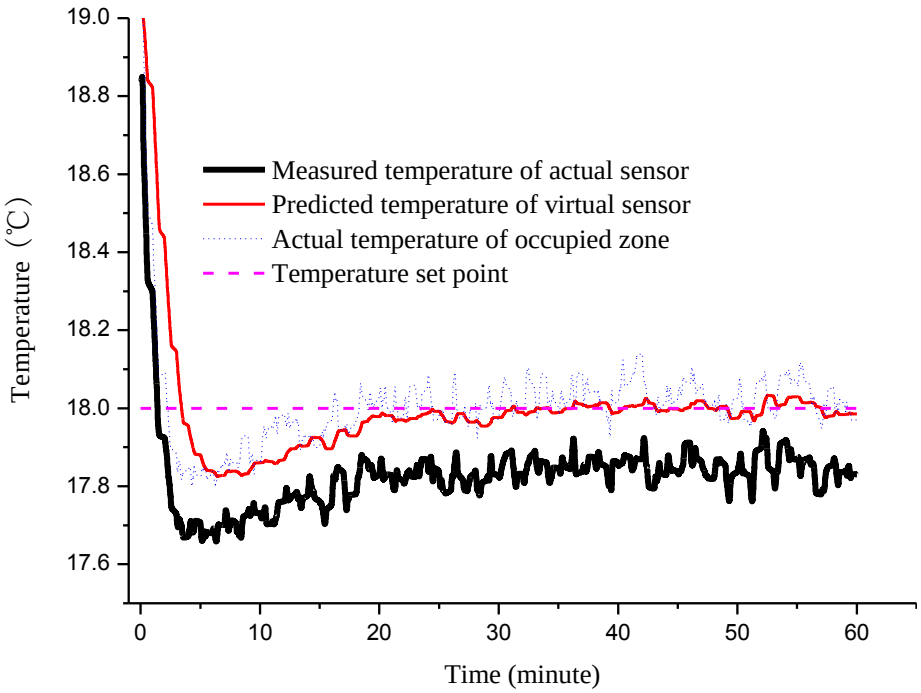

Figure 8.8 Temperature profiles of the actual & virtual sensor

The virtual sensor located in occupied zone represents the indoor air temperature, which was alternatively used as the input value of PID controller to control the space temperature in the room tested.

Figure 8.8 presents the actual sensor and virtual sensor temperatures. The indoor air temperature set point was set to 18℃. Without using a space temperature offset model, the temperature of occupied zone was much higher than its actual sensor temperature as shown in Figure 8.7. When the space temperature offset model was used, the temperature of the occupied zone represented by the virtual sensor was used by the controller. The indoor temperature control performance after adopting the space temperature offset model was evaluated on the simulation platform. The temperature of occupied zone extracted using CFD simulation in Figure 8.8 is also used as a reference value to validate the accuracy of the control strategy. The profiles of the actual temperature at the occupied zone and the temperature measurement of virtual sensor agreed very well. The results show that the use of the virtual sensor improved the accuracy of the ventilation control process significantly.

It can also seen that there were obvious difference between the actual temperature profiles in the occupied zone without and with using the space temperature offset model in the control strategy in the cases the same temperature control set point was used. The actual sensor temperature measurement shown in Figure 8.7 was higher than 0.25℃ than that virtual sensor measurement in Figure 8.8. The temperature difference when using the actual sensor measurements for control directly resulted in a deviation of about 0.2℃ in the occupied zone.

Figure 8.8 presents the temperature given by the actual sensor and the virtual sensor in the closed-loop control system, in which the supply air temperature was set to be 17℃, and the indoor air temperature set point was still set to be 18℃. The dotted

line describes the actual temperature variations of the occupied zone. It can be seen that the actual temperature of the occupied zone and the temperature measurement of the virtual sensor agreed very well, which shows that the temperature offset model can achieve acceptable accuracy in presenting the temperature of the occupied zone. There were obvious differences between the temperature given by the virtual sensor and the actual one. Therefore, when they were used as the input of the PI controller separately, the performance of the control of the occupied zone temperature was different, as shown in the studies below.

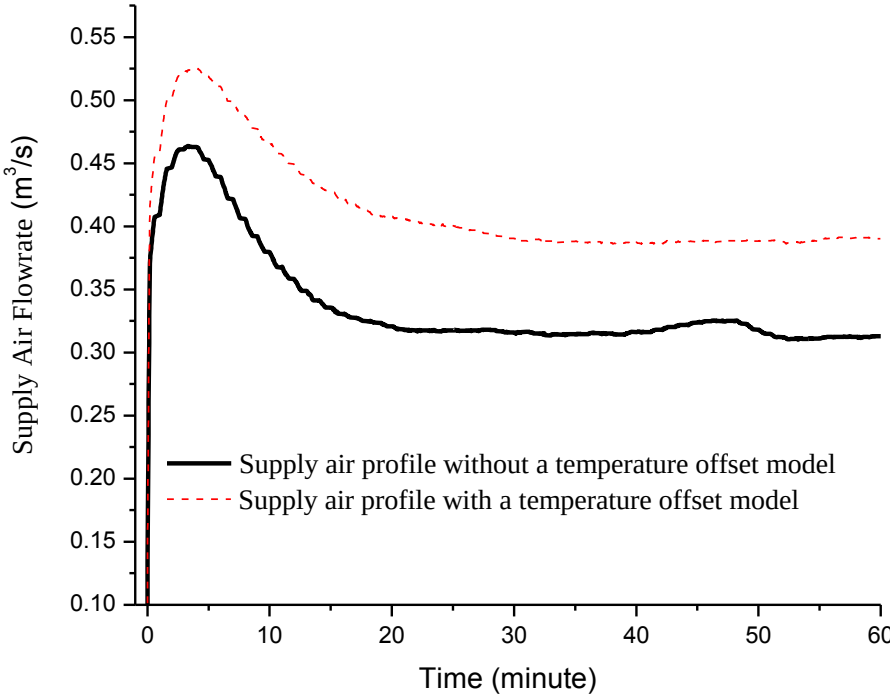

Figure 8.9 Supply air flow rates at tests with and without adopting temperature offset model

Figure 8.9 presents the supply air flow rate profiles at the tests with and without adopting temperature offset model. It is found that the supply air flow rate determined by ventilation control strategy when adopting the temperature offset

model was 20% higher than that controlled by the strategy without adopting the offset model. The reason was that more supply air flow rates were needed to dilute the indoor heat plume in the occupied zone.

The conclusion can be drawn in other operating modes. For example, Figure 8.10 compares the control performance of the proposed strategy with the conventional one when the medium level mode was used in the virtual sensor. In this case, the temperate difference was about 0.4℃, and this difference was compensated efficiently by the virtual sensor. Therefore, the thermal comfort was certainly improved.

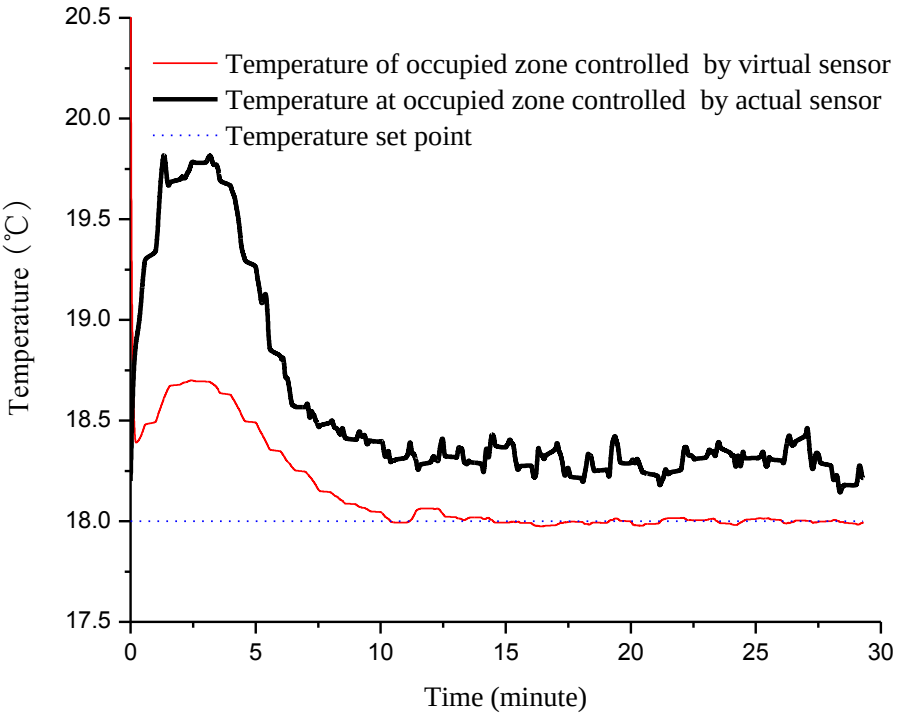

Figure 8.10 The temperature of occupied zone with the use of the actual & virtual sensor

8.3.4 Incremental Reset of Indoor Air Temperature Set Point

The indoor thermal environment is affected when varying the indoor or outdoor conditions, such as supply air flow rate, supply air temperature, indoor heat source radiation and heat flux through the exterior walls and windows. In this section, simulation test is conducted to evaluate the control performance of the virtual sensor for ventilation control system at different working conditions using varying indoor occupants' number. Referring to the space temperature offset models as Equation (7.14) developed in Chapter 7, experimental tests were also carried out to investigate the control performance when the operating mode was switched from the small-level (one occupant) to the medium-level (five occupants).

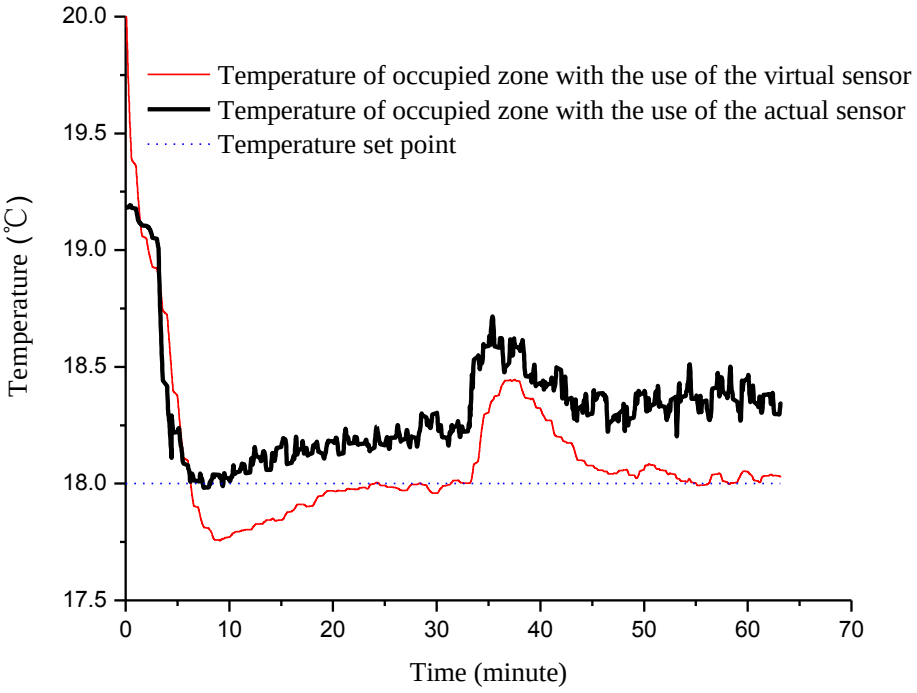

Figure 8.11 The temperature profile with varied control mode of occupants

Figure 8.11 illustrates the test results. At the moment when the time was 33 minutes, the operating mode was switched from the small-lever mode to the medium-level because the number of occupants was changed from 1 to 5. It can be seen that the closed-loop system was stable in both operating modes. The room temperature was manipulated back to its set point in around 10 minutes. Therefore, the switch of operating modes did not affect the system stability seriously. However, the time consumed to reach to the steady condition obviously decreased comparing with the initial status when the number of occupant was one. Some initial values of system boundary condition might not be reasonable. To improve the control system responses to the varying indoor heat loads quickly, it's necessary to select the preferable initial values for this virtual test system.

When the operating mode was switched from the small-lever mode to the high-level, which are the number of occupants was changed from 1 to 5, the indoor air temperature response of occupied zone with different number of occupants were illustrated in Figure 8.12.

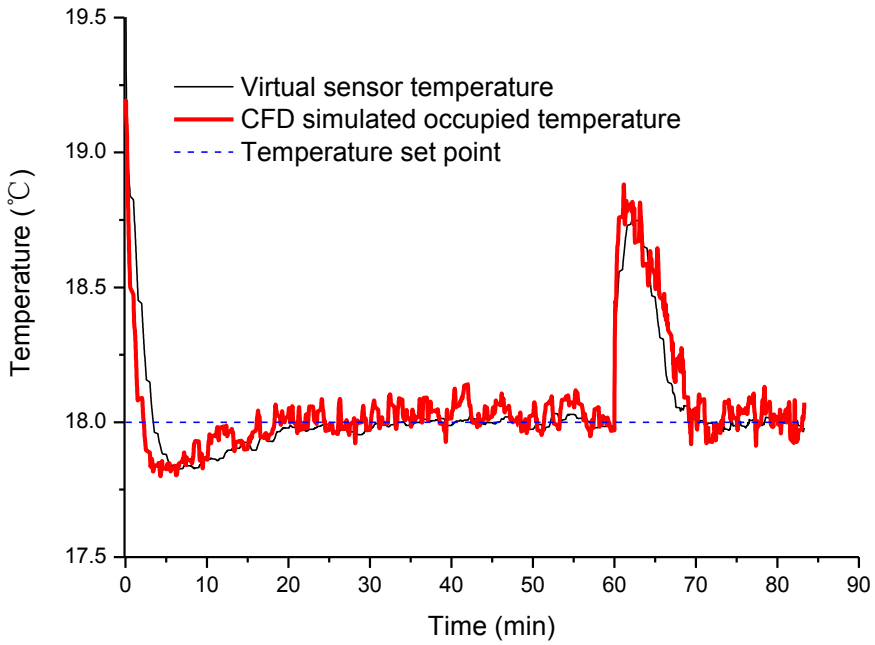

Figure 8.12 The temperature of occupied zone with different number of occupants

The virtual sensor temperature was estimated based on a space temperature offset model. The CFD simulated occupied temperature and the actual temperatures of occupied zone were obtained using CFD simulation. The virtual sensor temperature values in the test can agree well with the CFD simulated occupied temperature with the minor averaged error. It can be concluded that the virtual sensor can efficiently compensate the effect of non-uniform distribution on the temperature control in a simulated environment for developing optimal control strategy in advance.

8.4 Computation Speed and Practical Constraints in Applications

The CFD-based feedback ventilation test method was carried out successfully in this study. An important restriction for the use of this type of CFD simulation for room model is that the time taken for solving the numerical equations of room model. Computing time consumed by the simulation includes two parts: the time spent by

calculation of the ventilation system and control strategy and the time spent for the CFD calculation (CFD internal iterations). CFD internal iterations take most of the total computing time. The actual ventilation control strategy was tested for one hour, while the computing time taken by the coupled ventilation control system running the CFD model was about 10 hours on a Pentium 2 3.16 GHz PC.

With improving the processor and the simplification of the traditional turbulent model for CFD simulation, the presented CFD-based ventilation test method could be a test tool suitable for practical use in testing and evaluating the ventilation and control performance of spaces served by their ventilation systems and control strategies.

8.5 Summary

A CFD-based ventilation test method is presented by integrating a conditioned room model into its ventilation system and control strategy to evaluate the ventilation performance. This test method is demonstrated to be a feasible way for investigating ventilation control performance in a simulated environment as an evaluation tool for the ventilation systems and control strategies. However, the current typical mean of CFD simulation of the ventilated space is still too slow in computing on today's personal computers while the computing time for the ventilation system and control strategy simulation is negligible. To bring this test method for practical application, more effective CFD simulation, such as simplified numerical models, or more powerful computers is needed.

CHAPTER 9 IMPLEMENTATION OF CO_2-BASED ADAPTIVE DCV STRATEGY AND ENTHALPY CONTROL IN A SUPER HIGH-RISE BUILDING

This chapter presents the site implementation and validation of a CO_2-based adaptive DCV strategy in a super high-rise building in Hong Kong. An intelligent building management and integration platform (IBmanager) and the online control software packages of the optimal control strategies for implementing these technologies/tools are presented. The IBmanager can communicate with the control stations of the Building Management System (BMS) through a proper communication protocol and interface. The performance of this DCV strategy is practically tested and validated by comparing with that of the original used fixed outdoor air flow rate control strategy, which was implemented in the BMS. The enthalpy-based outdoor air optimal control strategy in this high-rise building is also tested and the total annual potential energy saving in Region 2 is estimated as well.

9.1 An Outline on the Management and Communication Platform

The management and communication platform was developed based on IBmanager. IBmanager was developed in Prof. Wang's team in The Hong Kong Polytechnic University. IBmanager is an open IBMS integration and management platform based on middleware and web services technologies to support the integration and

management of building automation systems from different vendors as well as remote monitoring and management services. It provides a convenient platform for integrating full scale building automation and industrial automation (IA) systems. IBmanager integrates various subsystems, involving data acquisition, network communication, automation and information management, and provides relevant software platforms for the supervision, management and customized development. IBmanager supports the customized development of various IB subsystems.

Figure 9.1 presents the interface connection and function blocks of IBmanager, which is actually a middleware platform. This platform can be divided into several parts, i.e., OPC (OLE for Process Control) servers, historical database, BMS function components, BMS HMI (human machine interface) based on the LAN (Local Area Network) version, web services server and building management web server. The OPC servers are distributed on various PCs in the LAN. The BMS function components execute the tasks of real-time data access, alarms & events process, historical data access, scheduling, parameter optimization of control strategies, performance/fault diagnosis of HVAC systems, etc. The BMS HMI based on the LAN version realizes the full BAS functions in the LAN applications. The web services server converts the COM/DCOM interfaces to web services interfaces. The Active Service Pages (ASP) and dynamic link library (DLL) files are deployed in the building management web server to communicate with the web services server and provide the user access interface (web pages) to users. There are several important functions that should be implemented in BASs, such as real-time data sharing, alarm/event, historical data and trending, scheduling and network

management. The real-time data access is accomplished by OPC DA (Data Access). The historical data access is accomplished by OPC HDA (historical data access) and the alarms & events are accomplished by OPC AE (Alarm & Event). These functions are wrapped as public web services interfaces for the communication and integration on Internet.

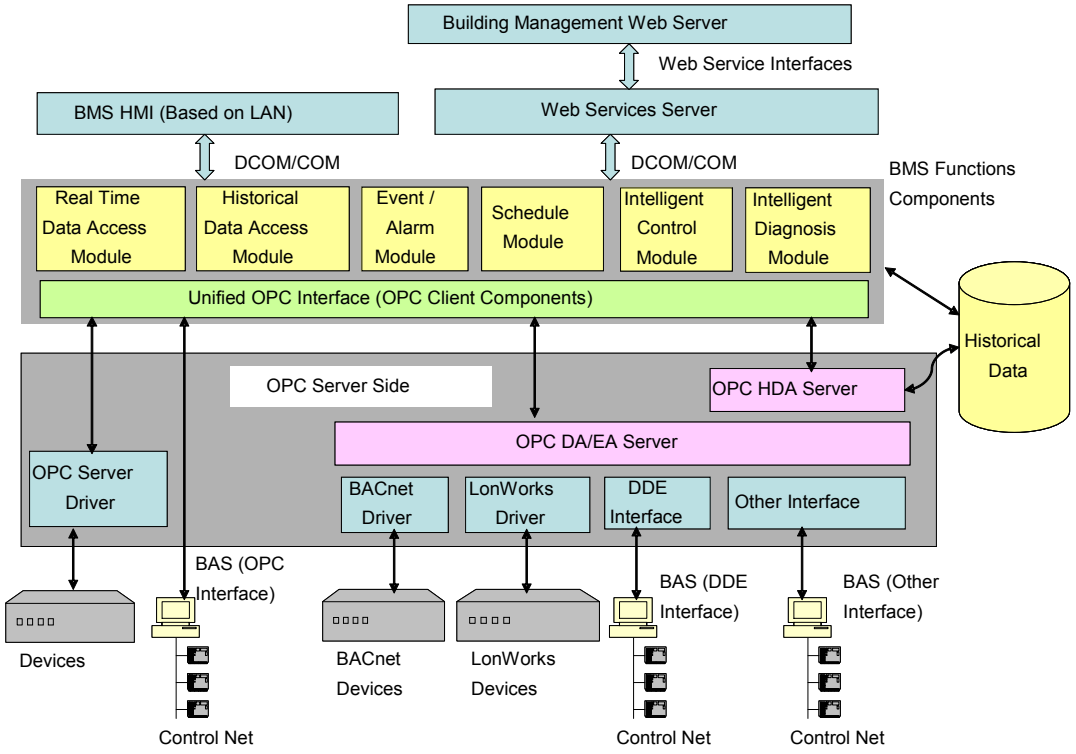

Figure 9.1 Interface connection and function blocks of IBmanager

Typical applications of IBmanager are listed as follows:

- *Internet-based centralized management platform integrating multiple (vendor) systems:* support centralized services and management on Intranet/Internet;
- *Supervision, integration and development platform for BA and IA systems:* integrate field control stations of different vendors (protocols);
- *Supporting and management platform for independent online applications:*add

third-party or complicated application programs of added-value services to BA systems.

9.2 Online Optimal Control Software Packages and Their Implementation Architectures

Figure 9.2 shows the in-situ implementation architectures of the DCV strategy, in which an Intelligent Building Management and Integration platform (IBmanager) was used as the communication platform for implementing the DCV strategy presented in Chapter 4. The DCV strategy was programmed by using the application program of Matlab and complied as a dynamic link library (DLL) module and integrated into IBmanager. IBmanager and integrated DCV strategy are operated on a separate Personal Computer (PC) connected with the main station of the BMS through a BACnet protocol and interface. IBmanager can receive the system operation data and also can send the optimal control settings to the BMS for practical control. A decision supervisor is designed for the operator to set whether the set point from the DCV strategy can be used or ignored. This implementation approach provides adequate spaces and freedoms for further improving the performance of the DCV strategy to make it have satisfactory performance and be convenient used in practice.

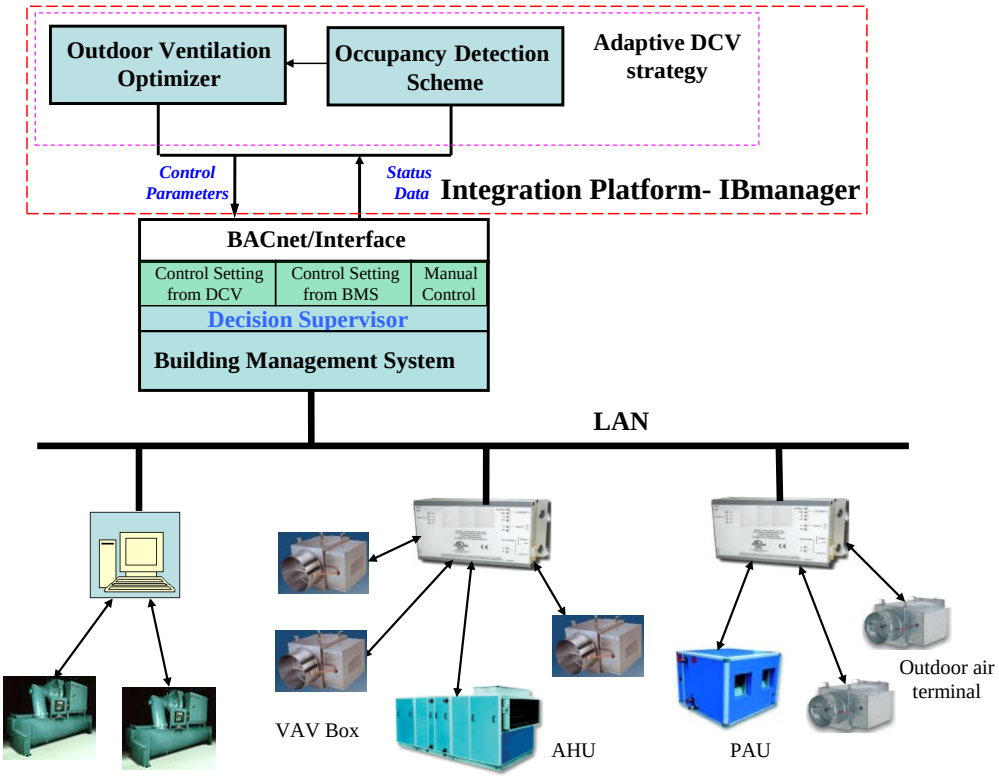

Figure 9.2 In-situ implementation architectures of the DCV strategy

The interface is used for the interoperation of the management and communication platform based on IBmanger and ATC (Automatic Temperature Control) system. This interface was developed based on a trial version of the BACnet SDK (Software Development Kit) since the network of the BMS system was based on the BACnet protocol. IBmanager can receive the system operation data through a NAE connecting with local controllers, and BA outstations connecting with sensors, actuators, etc. At the meantime, IBmanager can send the optimal control settings to the ATC systems through the NAE for the practical control of the building services systems to improve their operating efficiency.

9.3 Overview of the Intelligent Building Management System

The IBMS (intelligent building management system) for the application of the online control software packages to achieve reliable and energy efficient control and operation of the ventilation control system in the super high-rise building presented in Chapter 4, is shown in Figure 9.3. This platform includes six main functions, i.e., Access Management, History Data, System Setting, System Configuration, System Maintenance and Real-Time Monitoring.

Figure 9.3 Front page of the IBMS

Access Management is to control the authorities of different users including supervisory user, advanced users (including programming) and usual operators. The supervisory user has the highest authority and can manage the access of all other

users. *History Data* is to record the system operation data into the database. The recorded operation data can be used for many purposes, i.e., modeling training, fault detection and diagnosis, etc. *System Setting* is to configure this system in terms of the protocols used in building automation systems and/or the building management systems. *System Configuration* is to configure the data points of IBmanager based on the field installation information provided by the MVAC&BMS contractors. It can also set the parameters for different control strategies. *System Maintenance* is to provide the log services. *Real-Time Monitoring* is to monitor the system operation, component operation, etc. It has friendly human machine interface (HMI). Some operation data can be monitored with visualization while some can be monitored in the form of tables. Figures 9.4 to Figure 9.7 show the monitoring interfaces of the real-time operation data with visualization for the ventilation system, respectively. The main operation data (i.e., flow rate, CO_2 concentration and temperature of supply air; flow rate, CO_2 concentration and temperature of return air; flow rate, CO_2 concentration and temperature of outdoor air; CO_2 concentration of different zones, etc.) can be displayed on these monitoring interfaces to allow the operators to know whether or not the system/corresponding components are operated properly.

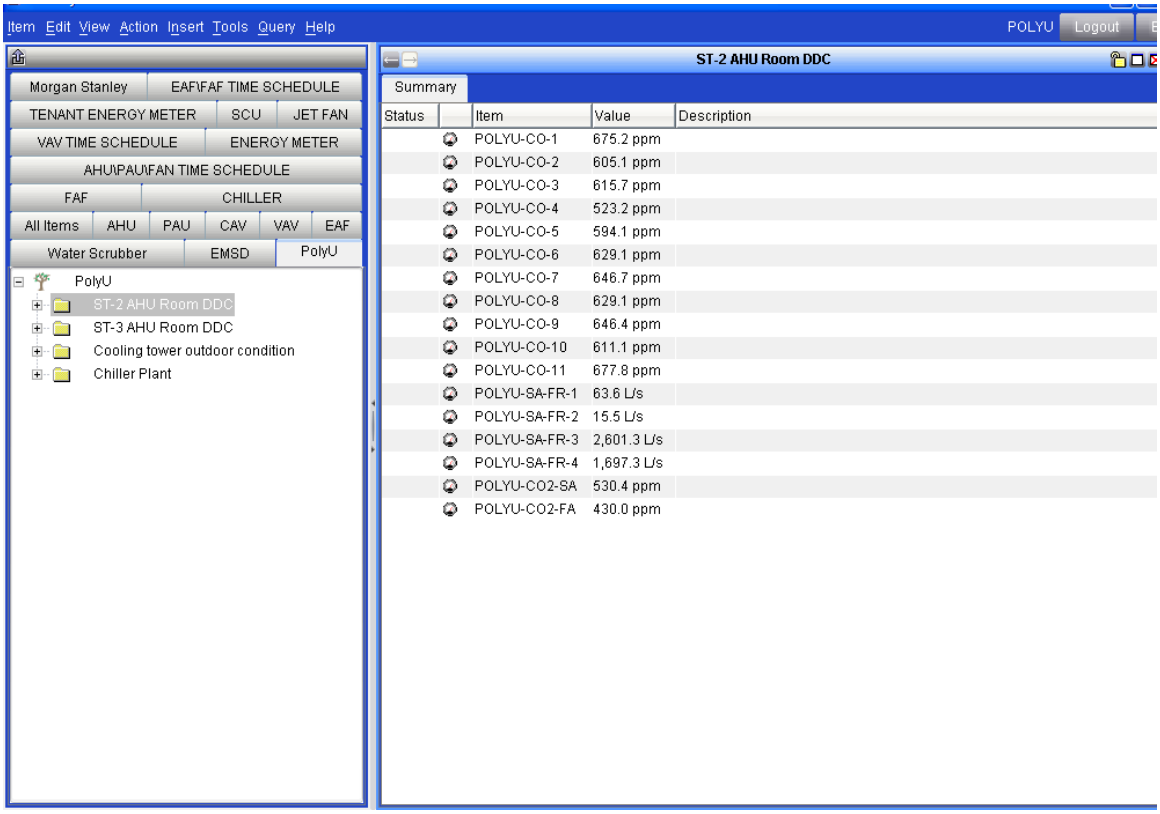

Figure 9.4 Monitoring interface of the CO_2 sensors status in AHU1 system

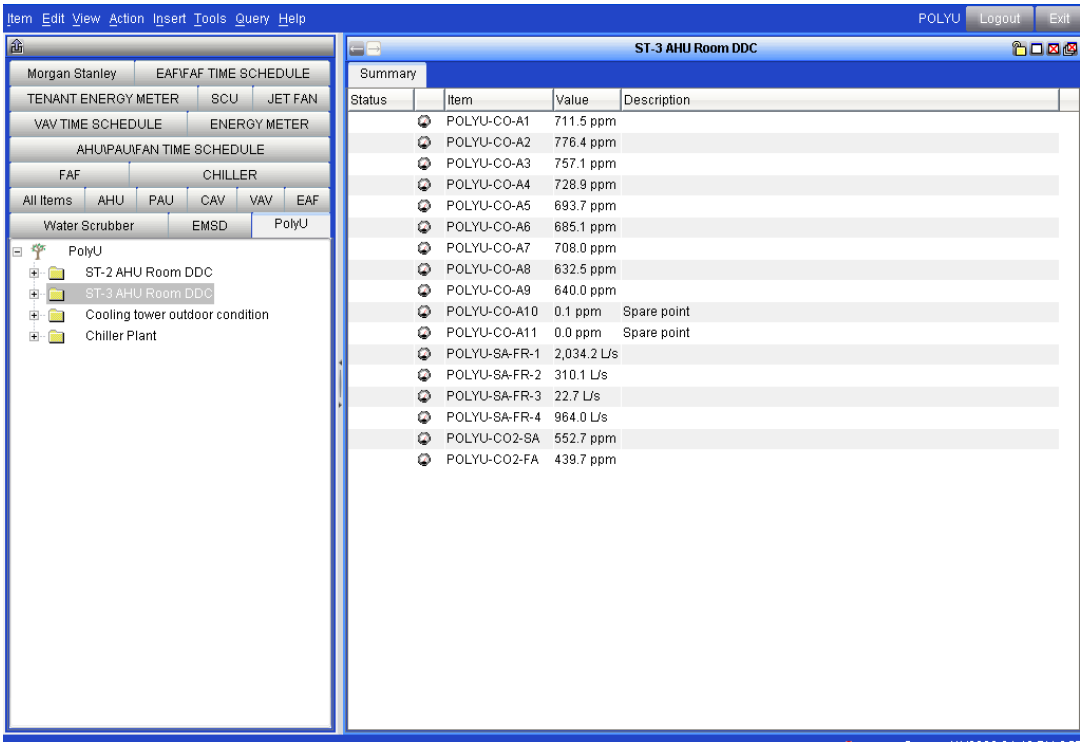

Figure 9.5 Monitoring interface of the CO_2 sensors status in AHU2 system

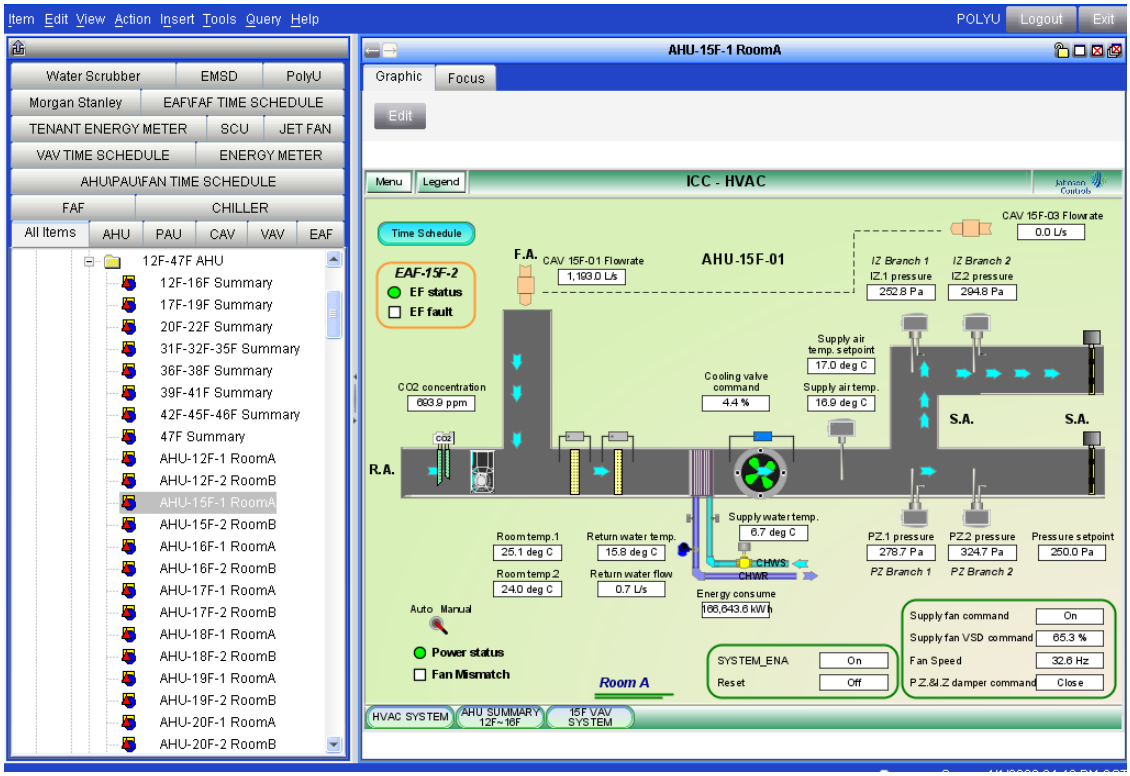

Figure 9.6 Monitoring interface of AHU1 system operation status

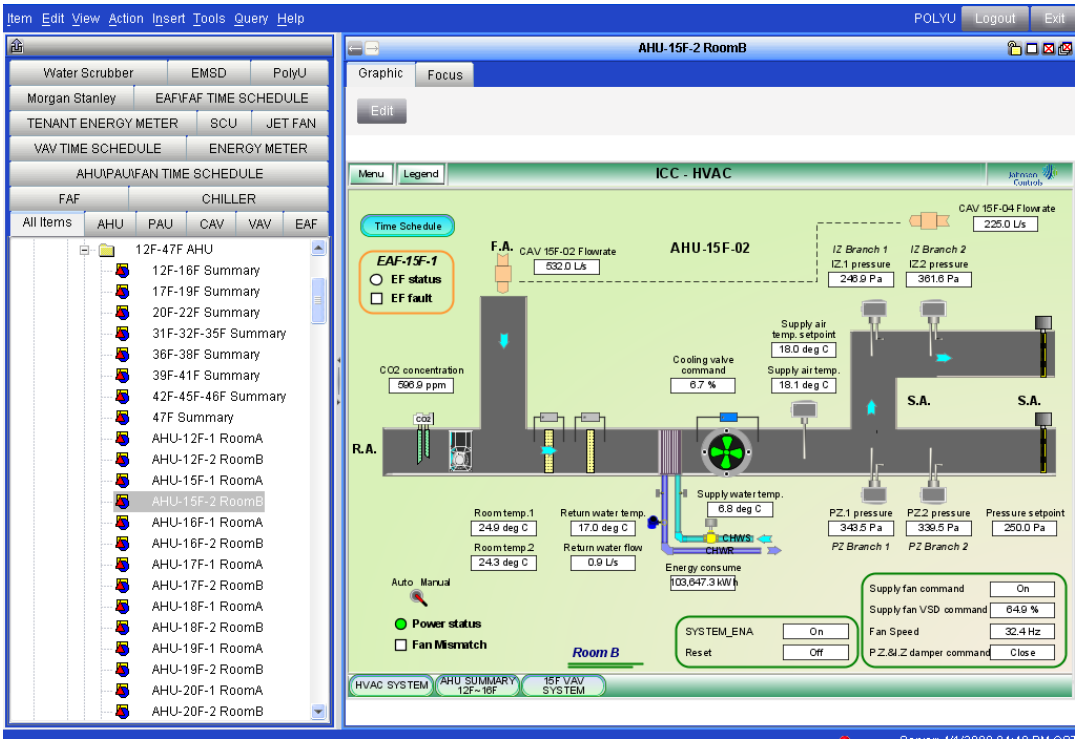

Figure 9.7 Monitoring interface of AHU2 system operation status

9.4 Building System Description and the DCV Strategy Implementation

9.4.1 Building and Ventilation System Description

The building concerned in this study currently is the tallest building in Hong Kong. It is approximately 490 meter height and about 321,000 m^2 floor area. It involves a basement of 4 floors, a block building of 6 floors and a tower building of 98 floors. The basement is mainly used for car parking. The block building from the ground floor to the fifth floor mainly serves as the commercial center involving hotel ballrooms, shopping arcades and arrival lobbies. The tower building is mainly used for commercial offices and a six-star hotel on the upmost zone. Each office floor has a floor area of 3600 m^2 and is served by two air-handling units (named AHU1 and AHU2, respectively).

The building is divided into five regions and the 15^{th} floor in Region 2 (from the 15^{th} floor to 47^{th} floor) is selected as the typical floor and is mainly concerned in this research. Figure 9.8 is the schematics of the multi-zone ventilation system in this typical floor. This typical floor is divided into 7 zones for multi-zone ventilation control. Zones 4, 5, 6 and 7 are served by the AHU1 ventilation system, and Zones 1, 2 and 3 are served by the AHU2 ventilation system. Required supply air into the whole typical floor is firstly supplied through four separate supply air ducts, and then mixed in the main supply air duct. VAV dampers are installed to connect the main supply air ducts to deliver supply air into ventilated zones with diffusers. Return air is drawn back through the ceiling plenum.

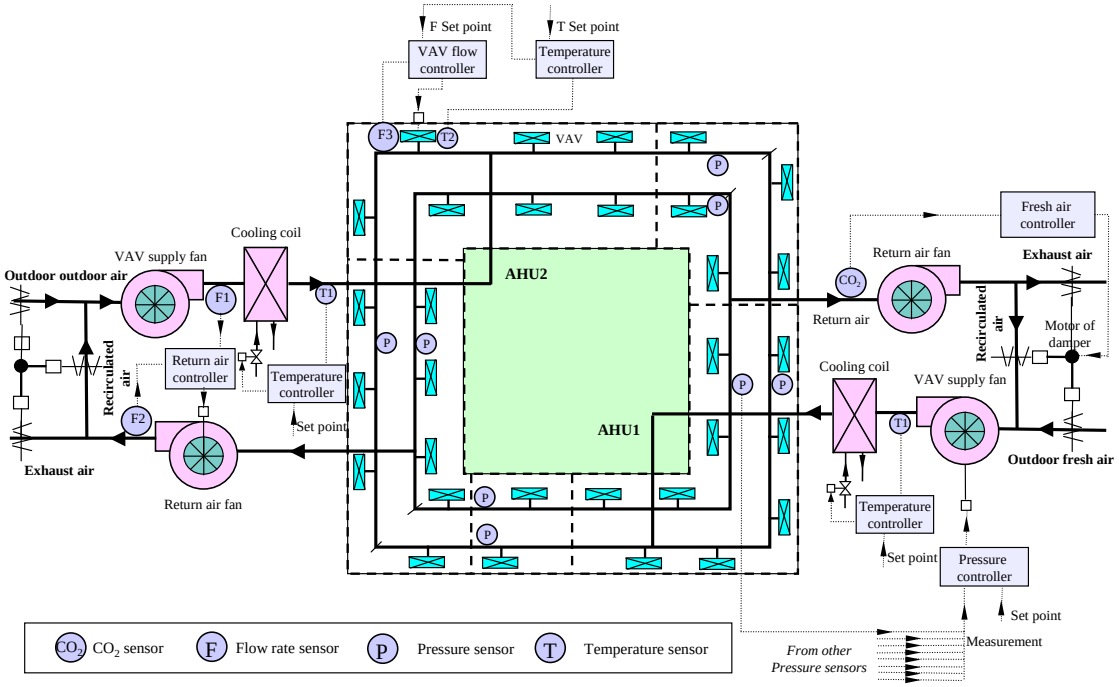

Figure 9.8 Schematic of the multi-zone ventilation system in the typical floor

To fully study the performance of the proposed DCV strategy, this typical floor was fully instrumented. The major instrumentations installed include the air flow meters of AHU systems, CO_2 sensors of AHU systems, CO_2 sensors located in different zones, and fan power meters, etc. For each AHU system, the outdoor air is supplied through four separate supply air ducts. The locations of the air flow meters for each AHU systems are illustrated in Figure 9.9.

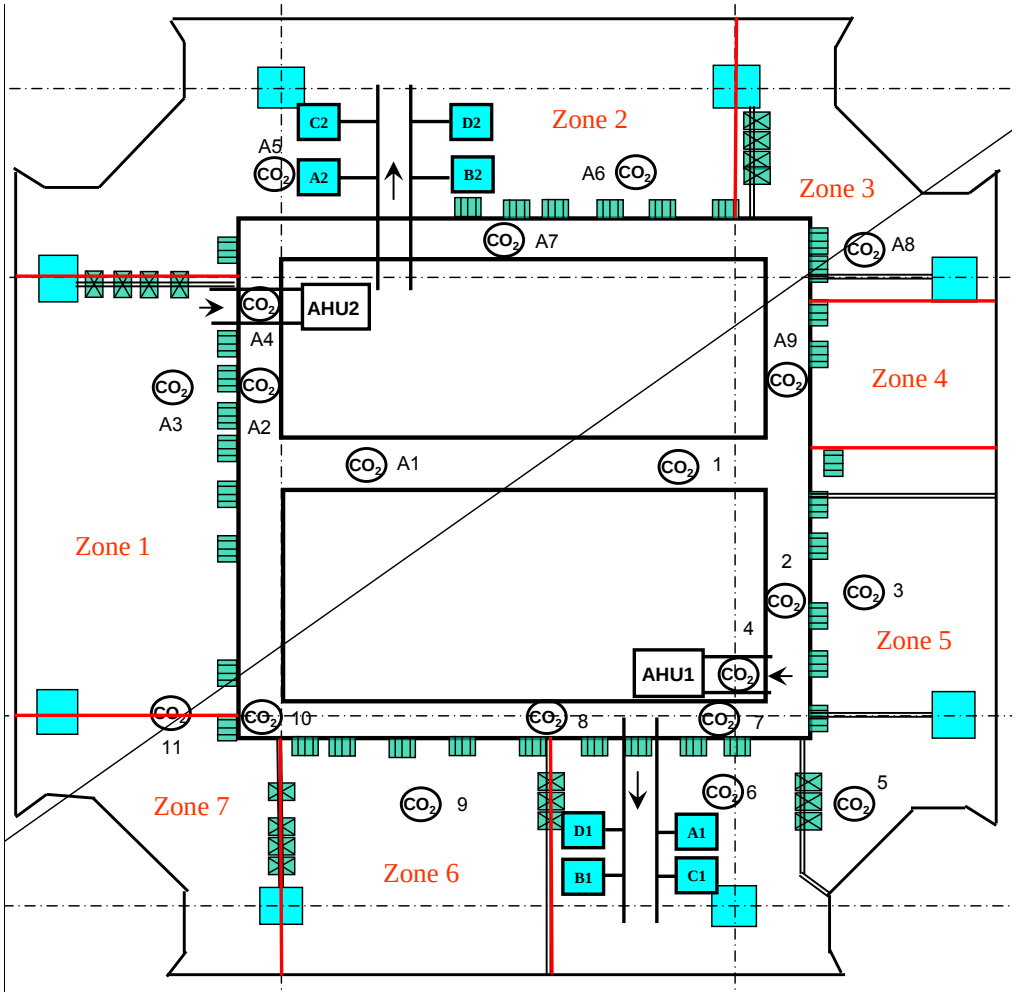

Figure 9.9 Schematic of the location of CO_2 sensors in the typical floor

The outdoor air for the whole Region 2 is centrally supplied by four primary air units (PAUs). Two of them serve for AHU1 systems and two of them serve for AHU2 systems in all floors in Region 2. Figure 9.10 presents the schematic of the outdoor ventilation control for each AHU system. The DCV strategy provides the outdoor air flow rate set point for the outdoor air controller of each floor. The outdoor air flow rate is then controlled through adjusting the position of the outdoor air damper to maintain the actual air flow rate of each AHU system at the desired set point. The static pressure in the 36th floor is used for the fan speed control. The static

pressure set point can be maintained constant or can be reset down at part-load conditions.

The sub-processes in this ventilation system are controlled by the local digital controllers. The air temperature in each zone is controlled by a pressure-independent VAV controller. The positions of VAV dampers are controlled by maintaining the supply air flow rate at the intended set point. The supply air temperature is controlled by adjusting the chilled water flow rate through the AHU systems.

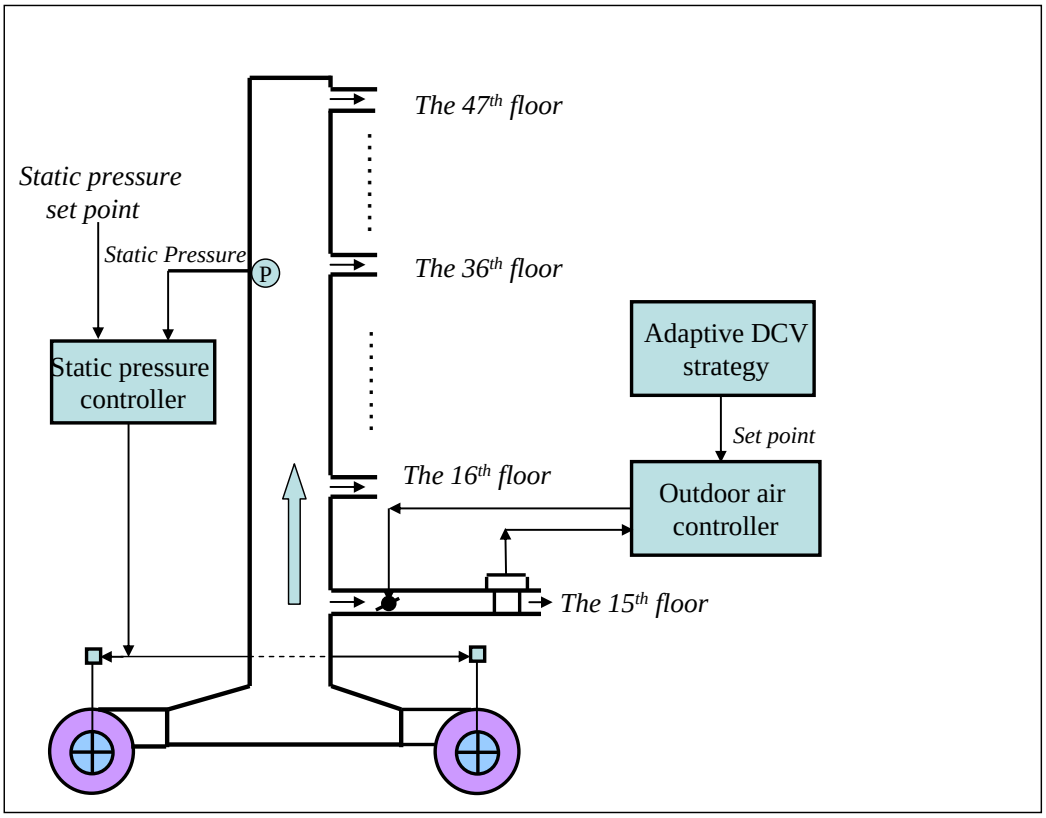

Figure 9.10 Schematics of the outdoor ventilation control system for each AHU system

The CO_2 sensor product eSENSE is selected to measure indoor air CO_2 concentration in the ventilated rooms. The eSENSE-d is a display model with a LCD.

Both are available for wall mounting as well as for duct mounting. The unit is designed for connecting to direct digital control. The linear output functions are pre-programmed as CO_2 transmitters with the outputs 0-10V. The measuring ranges can be modified form a PC and use of the software UIP (version 4.0 or higher) together with the communication cable. The configuration of the CO_2 sensor installed in practical ventilation system is shown in Figure 9.11.

Figure 9.11 The configuration of the CO_2 sensor

9.4.2 Implementation of Two Ventilation Strategies

The online control software packages of the ventilation control strategy for implementing technologies are integrated with BAS system with the support of the management and communication platform to achieve energy efficient and indoor air

quality control. The control packages of control strategies are developed in the application program of Matlab. The occupancy detection strategy and multi-zone ventilation control strategy complied as control packages are programmed as a form of subroutines, and are complied as a DLL module for the convenient implementation in IBmanager. All developed online control packages operate on a separate computer connected with the main station of ventilation control system (BMS). All control packages can run in parallel with ventilation program developed by the BMS system. A decision supervisor in the ventilation control system is designed for the operator to set whether the set point of outdoor air flow rate or occupancy profiles generated by the developed control packages are used or ignored as the reset value of BMS system.

IBmanager can receive the system operation data through a network automation engine (NAE) connecting with local controllers and BA outstations connecting with sensors, actuators, etc. At the meantime, IBmanager can send the optimal control settings to the automatic temperature control (ATC) system through the NAE for the practical control of the building services systems efficiently.

The performance of the DCV strategy was practically tested and compared with that of the original implemented fixed outdoor air flow rate control strategy. Figure 9.12 illustrates the flow chart of the original outdoor fixed air flow rate control strategy, in which the return air CO_2 concentration was used to reset the outdoor air flow rate set point. When the measured return air CO_2 concentration was equal to or larger

than the set point of 800ppm, the outdoor air flow rate was set to 1200L/s. Otherwise, the outdoor air flow rate set point was set to 960L/s.

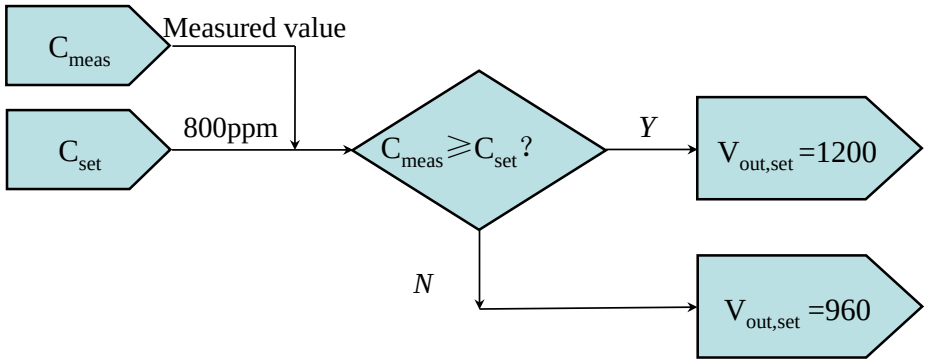

Figure 9.12 Control flow diagram of the existing fixed outdoor air flow rate control strategy

where C_{mea} is the measured CO_2 concentration of return air, C_{set} is the CO_2 set point of return air, $V_{out,set}$ is the outdoor air flow rate set point.

Secondly, the dynamic adaptive DCV strategy presented in Chapter 4 was also compiled as a DLL module as a control package operating in the IBmanager system. The control logic of DCV strategy is shown in Figure 9.13. The control package of this strategy is determined by the decision supervisor to be the set point of outdoor air flow rate of BMS system accordingly.

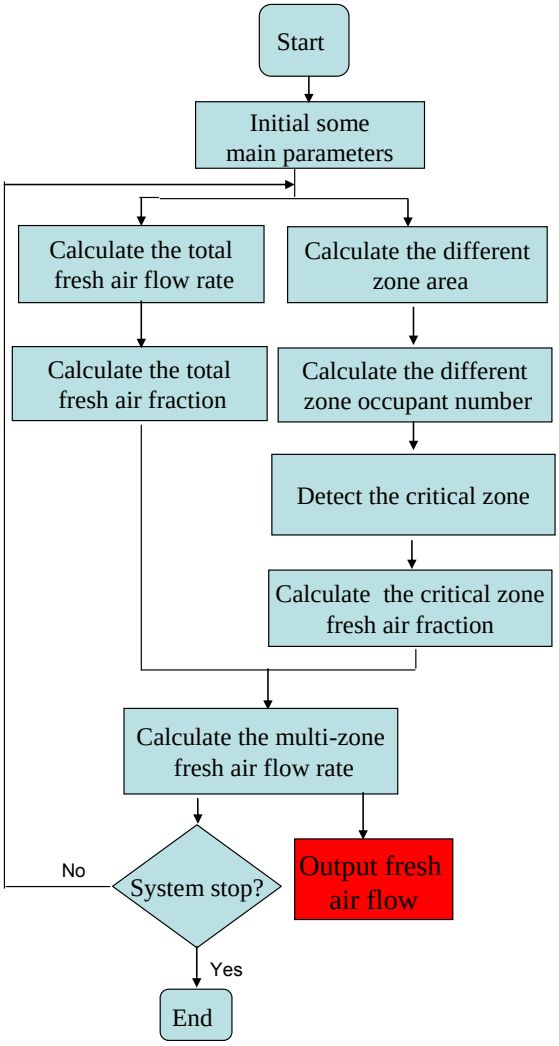

Figure 9.13 Flow chart of the adaptive DCV strategy

In this strategy, the occupancy of each zone and the total occupancy need to be determined for calculating the required outdoor air flow rate, and the critical zone is identified using the measured supply air flow rates of each zone together with the calculated coincident outdoor air flow rates. Based on the identified occupancies and critical zones as well as other measurements, the demanded outdoor air flow rate directly from outdoors can be estimated as presented subsequently.

9.4.3 Commissioning and Calibration of Measurement Instrumentations

Various aspects may affect the measurement accuracy of instrumentations. To ensure the system to operate as desired, all measurement instrumentations should be calibrated and commissioned properly to make them have capability of providing reasonable and reliable measurements. Considering that the air flow meters and CO_2 sensors of the AHU systems play significant roles in the implementation of the DCV strategy, their commissioning and calibration are presented hereafter.

Figure 9.14 describes the AHU system schematics of 15th floor in ICC building. The outdoor air flow rate, supply air flow rate and return air flow rate are measured by the air flow stations. The CO_2 concentration of outdoor air, return air and supply air are measured using CO_2 sensors located in the main ducts of AHU system. The measured air flow rate and CO_2 concentration are all saved in the IBserver data base.

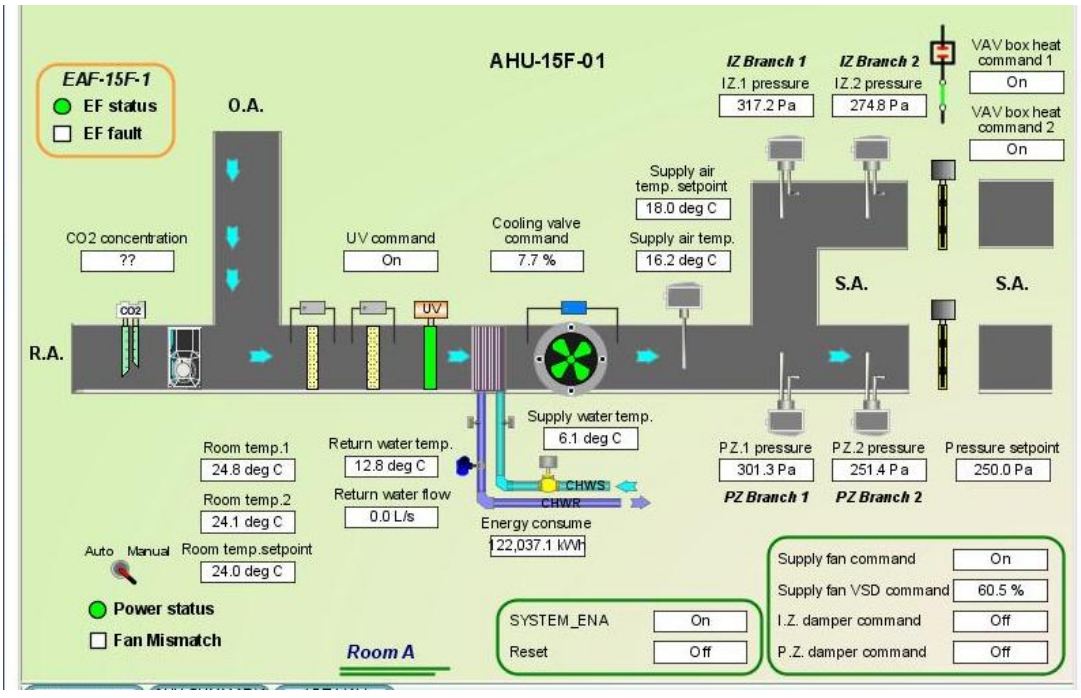

Figure 9.14 The monitored AHU1 system of 15th typical floor of ICC building

9.4.3.1 Calibration of AHU air flow rate

There are four air flow meters are installed in the four separate supply air ducts to measure the supply air flow rates in four supply air ducts. The actual total supply air flow rate of each AHU system is the sum of the measurements of the four air flow meters. To calibrate their accuracies, a portable air flow meter was used to measure the air flow rates of the four separate supply air ducts and the measurement results are named '*manual measured'*. In the meanwhile, the measurements of the four air flow meters installed in these four ducts were recorded by the BMS and the measurements results are called '*BMS recorded*'. Table 9.1 summarizes the comparison results between the two sets of measurements.

Table 9.1 The calibration results of the AHU air flow meters

AHU	Measurement locations	BMS recorded (L/s)	Manual measured (L/s)	Relative deviation (%)
AHU1	*A1*	1512.9	1525.5	0.8
	B1	2968.0	3120.0	4.9
	C1	1567.6	1642.2	4.5
	D1	3061.0	2917.0	4.9
	Total flow rate of four meters	9109.5	9204.7	1.05
AHU2	*A2*	2946.0	3070.0	4.0
	B2	1577.9	1665.0	5.2
	C2	2880.0	2791.3	3.2
	D2	2159.0	2030.0	6.4
	Total flow rate of four meters	9562.9	9556.3	0.1

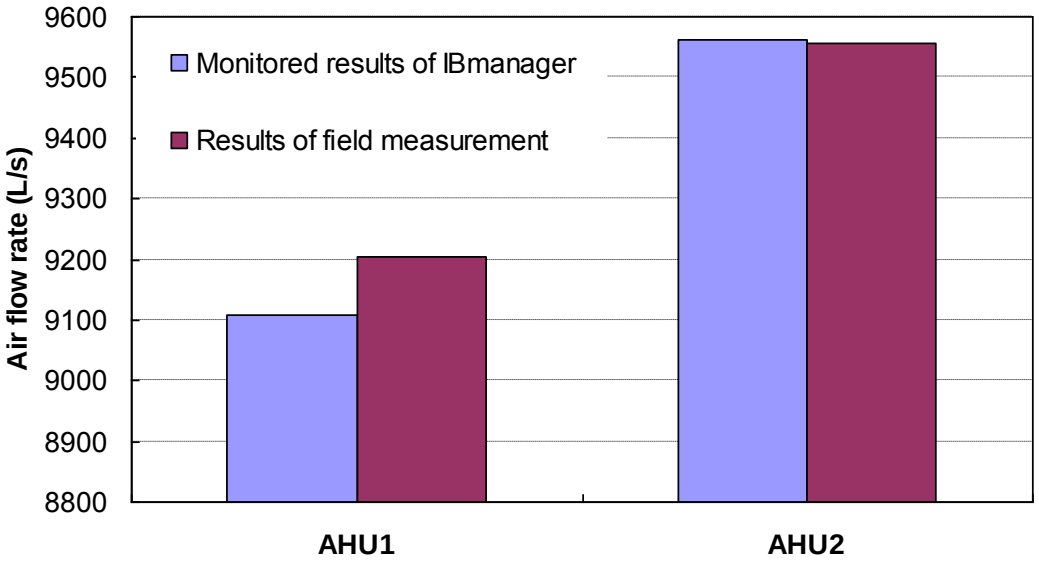

Figure 9.15 The comparison of air flow rates of each AHU system between the recorded result using the BMS and field measurement

Figure 9.15 presents the comparison of total supply air flow rate between the recorded result using the BMS and field measurement. It can be found that the air flow rate of each meter recorded by the BMS agreed well with the measured data by using the portable flow meter. The relative deviations between the two sets of measurements were less than 7.0%. The relative deviations of the total air flow rate of each AHU system between them were less than 1.05%. It can therefore be concluded that all these air flow meters can provide the reliable measurements.

9.4.3.2 Effects of sensor locations

The air flow rate sensors of AHU system are located in the main ducts of two AHU systems to measure the practical air flow rate values. Meantime CO_2 sensors are installed as well to monitor the field CO_2 values of total supply air, outdoor air, return air, and different zones. The locations of sensors in each AHU system are

shown in Figure 9.16. The return air CO_2 value was often less than the supply air CO_2 value or equal to the outdoor air CO_2 value during the working time. According to the field observation, it was noticed that the return air CO_2 sensors were installed near the mixing region of outdoor air and return air. On the basis of the field installing experience, it can be concluded that the CO_2 sensors values of return and outdoor air were influenced by the intensive turbulent flow field in the main mixing region. To solve this problem, the return air sensors were relocated into another position which was outside of the mixing zone shown in Figure 9.17. After the relocation, the return air CO_2 value was investigated to be higher than the CO_2 values of the supply air and outdoor air during the whole working time.

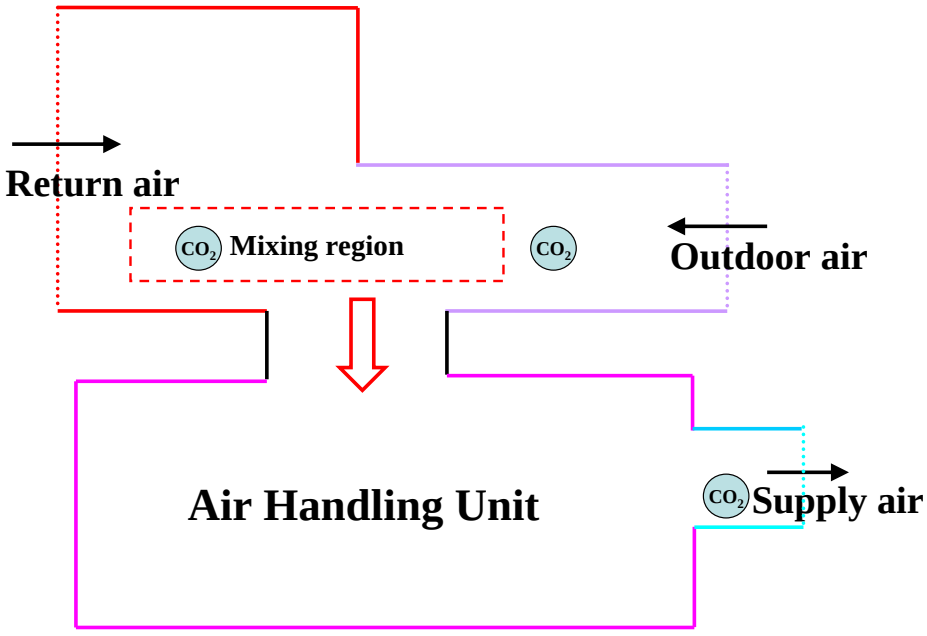

Figure 9.16 Schematics of locations of CO_2 sensors of the AHU system

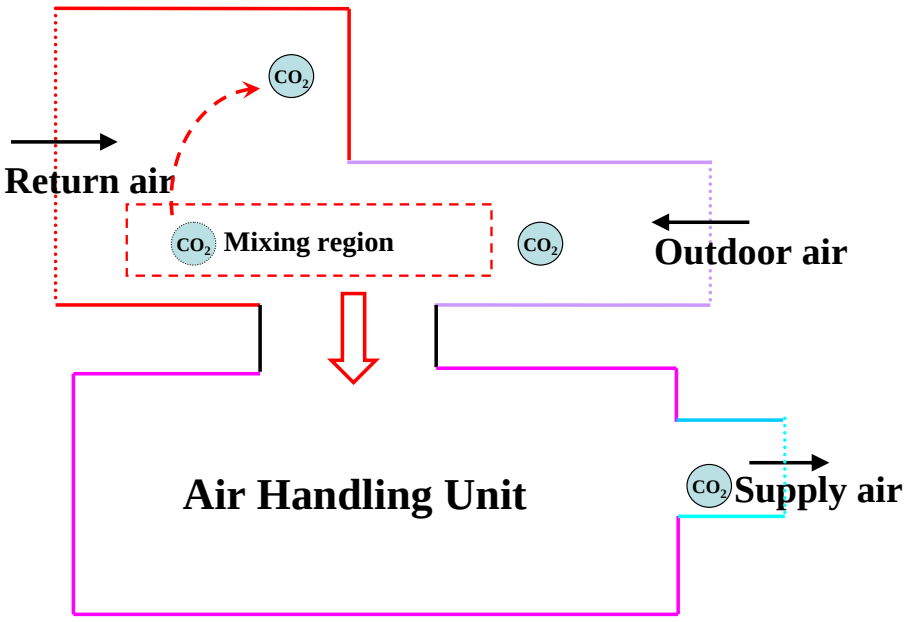

Figure 9.17 Schematics of relocations of CO_2 sensors of the AHU system

9.4.3.3 Calibration of CO_2 sensors

Because the accuracy of CO_2 sensors directly affects the performance of the occupancy detection scheme, the CO_2 sensors installed in the AHU systems were calibrated as well. The CO_2 sensors were calibrated using the volume concentration conservation method based on the measurements of air flow meters. In principle, the CO_2 sensors of the AHU system should satisfy the CO_2 volume concentration conservation equation, as described in Equation (9.1), if the measurements of all related CO_2 sensors are accurate. Since the recorded CO_2 values of the outdoor air sensors were in the range of 350ppm - 400ppm, it is concluded that the outdoor air CO_2 sensors are accurate (ASHRAE 2004). To verify the measurement accuracy of the return air and supply air CO_2 sensors, the measurement of the return air CO_2 sensors was firstly assumed to be accurate. The supply air CO_2 concentration can

therefore be calculated using Equation (9.2), based on the CO_2 concentrations of the outdoor air and return air as well as the measured air flow rates of the AHU systems.

$$V_{out} * C_{out} + V_{rtn} * C_{rtn} - V_s * C_s = 0 \tag{9.1}$$

$$C_s = (V_{out} * C_{out} + V_{rtn} * C_{rtn}) / V_s \tag{9.2}$$

where C_{rtn} is the CO_2 concentration of return air, V_s is the supply air flow rate, V_{out} is the outdoor air flow rate, and V_{rtn} is the return air flow rate.

Figure 9.18 and Figure 9.19 present the comparisons between the actual measured supply air CO_2 concentrations and calculated ones for the AHU1 system and AHU2 system, respectively. It can be observed that the obvious deviations were existed between the two sets of values. Therefore, the measurements of CO_2 sensors of supply air or/and CO_2 sensors of the return air might be inaccurate.

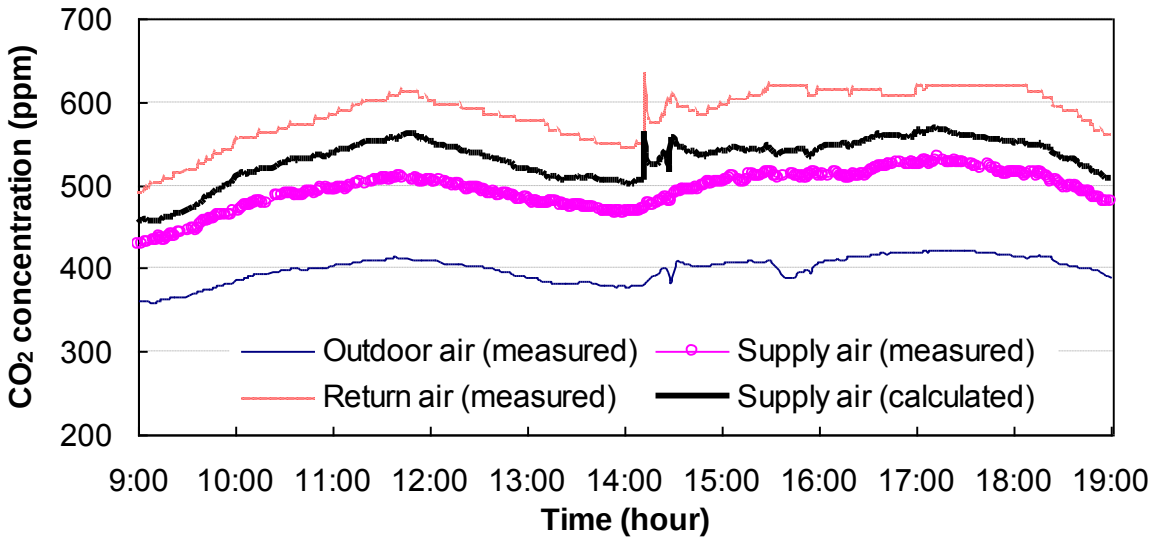

Figure 9.18 CO_2 concentrations of sensors in AHU1 system before calibration

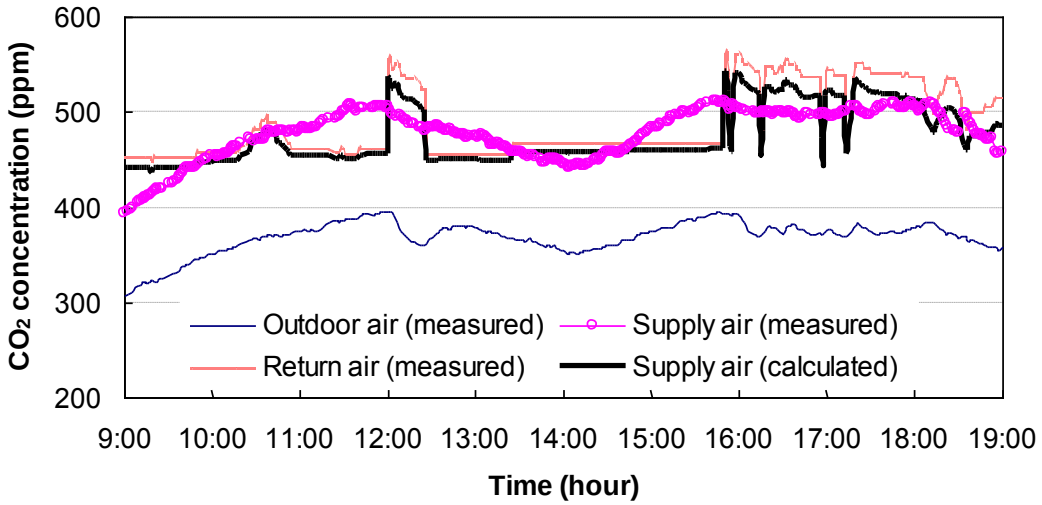

Figure 9.19 CO_2 concentrations of sensors in AHU2 system before calibration

To improve the measurement accuracy of CO_2 sensors of the return air and supply air, both sets of sensors were calibrated in the typical atmospheric conditions (around 400ppm). Their measurements were compared with the measured values using an accurate CO_2 sensor. If the relative deviation was larger than 5%, the settings of sensors will be adjusted using the method presented in Ref. (Ogura et. al. 2000). Otherwise, it can be validated that the calibrated sensor is accurate.

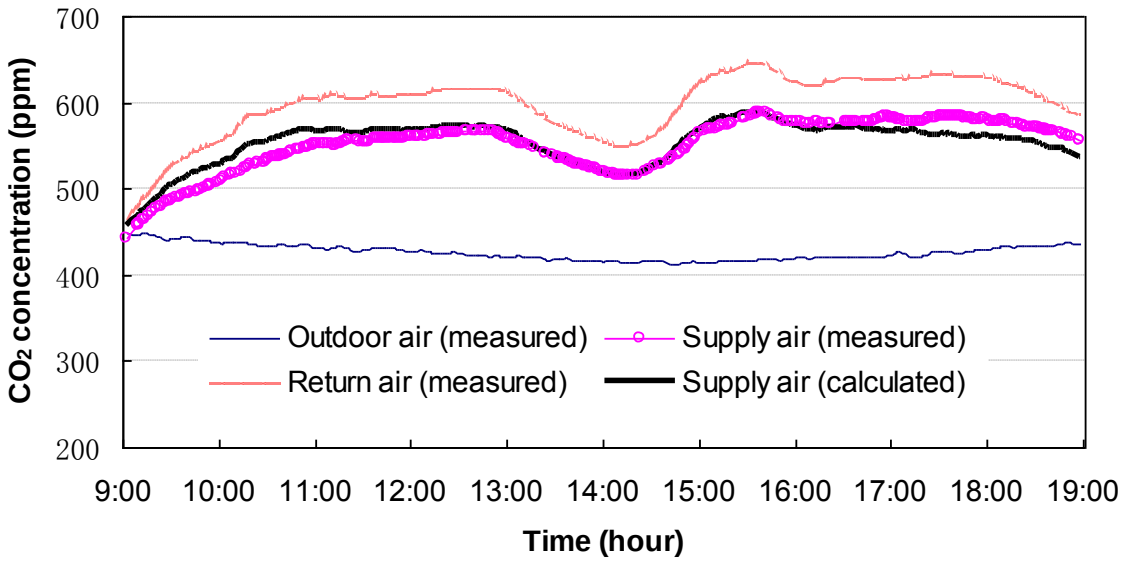

Figure 9.20 CO_2 concentrations of sensors in AHU1 system after calibration

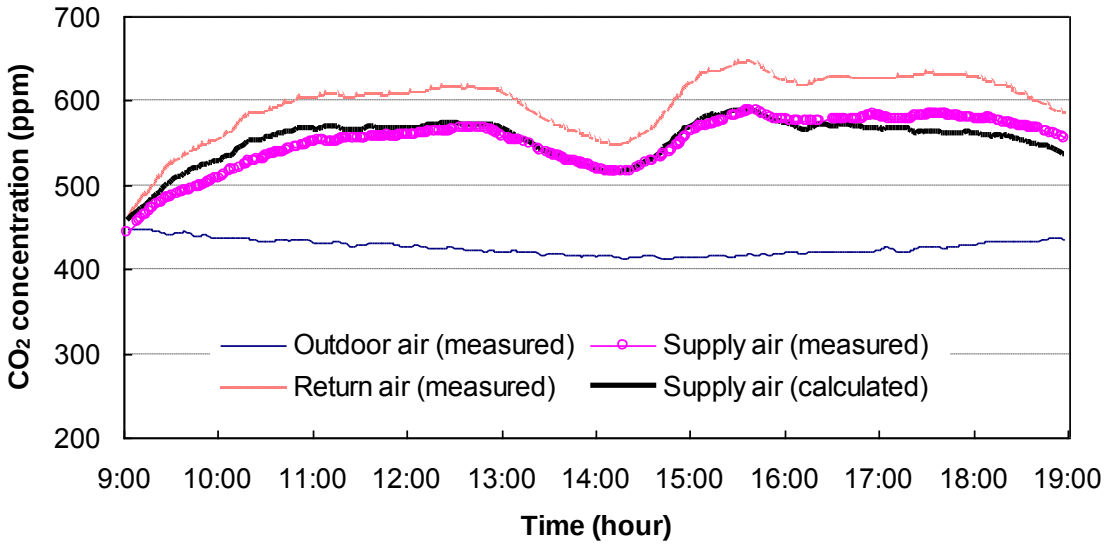

Figure 9.21 CO_2 concentrations of sensors in AHU2 system after calibration

After the field calibration, the measured supply air CO_2 values were compared with the calculated supply air CO_2 values using Equation (9.2). The comparison results for the two AHU systems are presented in Figure 9.20 and Figure 9.21. From both figures, it can be found that the measured supply air CO_2 values agreed will wit the calculated ones. It worthy noticing that all CO_2 sensors located in AHU systems in the typical floor were calibrated using the same method.

9.5 Validation and Performance Evaluation

Since the CO_2-based occupancy detection scheme plays a significant role in the DCV strategy, the performance of the CO_2-based occupancy detection scheme is firstly validated in 9.4.1 while the performance of the DCV strategy is validated in Section 9.4.2.

9.5.1 CO_2-based Occupancy Detection Scheme

To validate the effectiveness of the CO_2-based occupancy detection scheme, the actual occupancy in the typical floor was counted by observing the number of office occupants going and leaving the offices through the monitor of the central CCTV, as shown in Figure 9.22. The counted number of occupants was compared with that coincident predicted value by using the occupancy detection scheme of the DCV strategy based on the online measurements. Figure 9.23 and Figure 9.24 show the comparison results. It can be found that the predicted number of occupancy can agree well with the counted number of occupancy. This demonstrated that this CO_2-based occupancy detection scheme can provide the reliable estimates under dynamic working conditions.

Figure 9.22 Schematic of site counting the occupancy in the typical floor

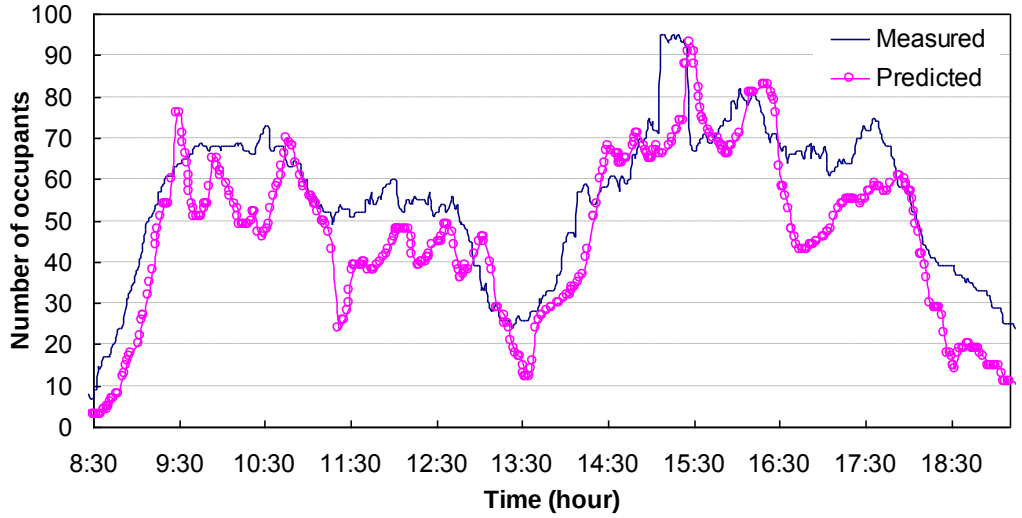

Figure 9.23 Comparison of measured and predicted occupancy profile of typical floor

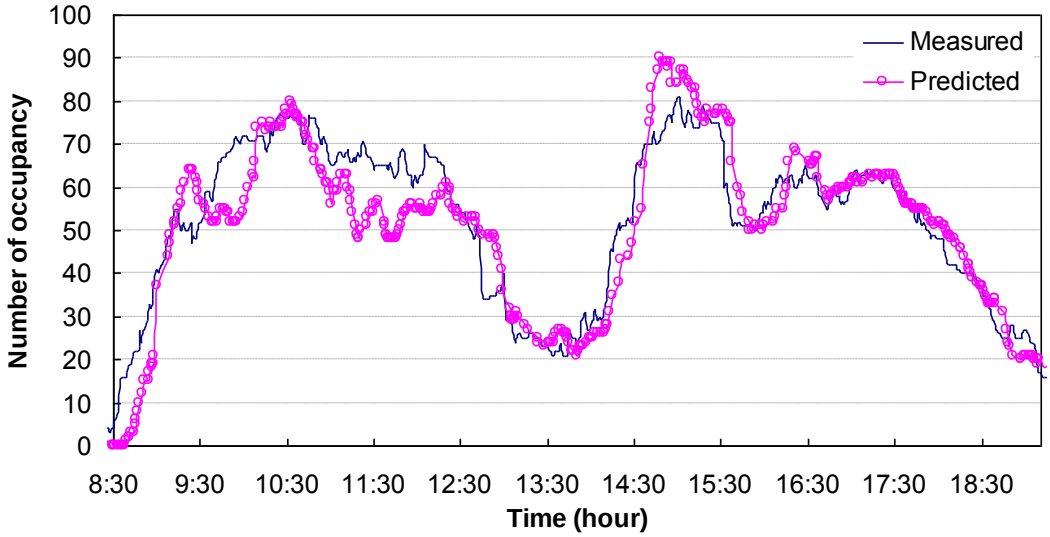

Figure 9.24 Comparison of measured and predicted occupancy profile of typical floor

Deviations still existed in several particular time periods; it might be caused by the detecting delay of CO_2 sensors happened in some special sites of this complicated and huge ventilation system.

9.5.2 Adaptive DCV Strategy

Many field tests were carried out in winter periods and the results of a typical winter day are presented herein. To further demonstrate the performance of the DCV strategy, the simulation test in summer working conditions was also conducted. The simulation test was carried out using the actual historical data recorded by the BMS. The only difference between the site test in winter period and simulate test in summer conditions is that the set point in the winter period is actually used for practical control. In the simulation test, the recorded data from the BMS were used. It is worthwhile to point out that, during the test, the primary air fan operating frequency was constant (i.e., 45Hz) since the current operation of the primary fan in site is the fixed speed operation.

The performance of the DCV strategy is evaluated by comparing with that of the fixed outdoor air flow rate control strategy in terms of the outdoor air flow rate and indoor air CO_2 concentration as well as the energy performance.

Figure 9.25 illustrates the outdoor air flow rate set points provided by the two ventilation strategies. It can be observed that the outdoor air flow rate set point optimized by the DCV strategy was much less than that provided by the fixed outdoor air flow rate control strategy during the whole test period.

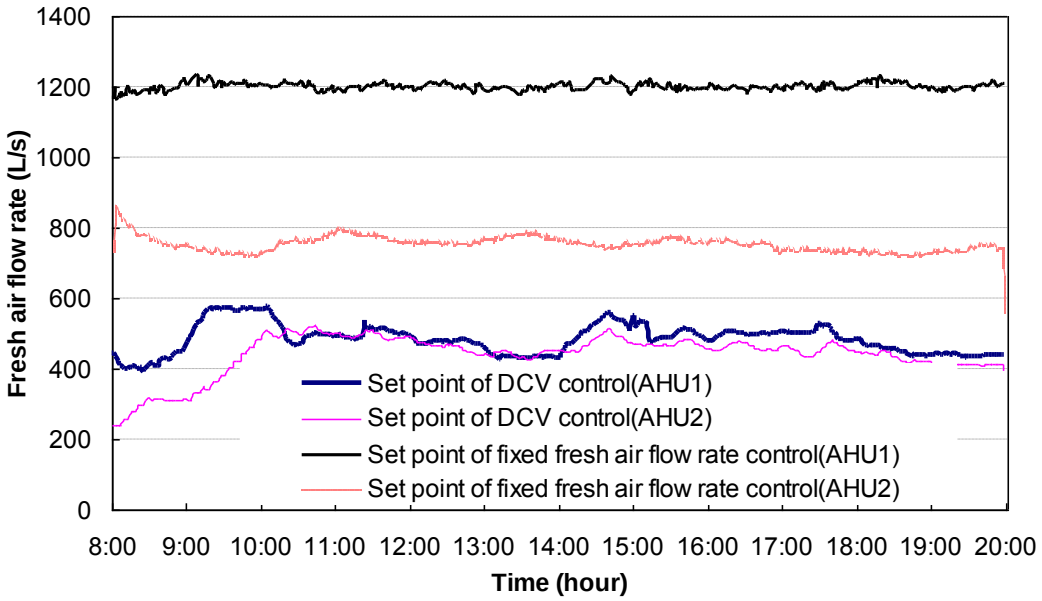

Figure 9.25 Comparison of outdoor air flow rate using two ventilation control strategies

Meanwhile, the outdoor air is a main parameter to affect the indoor air quality (CO_2 concentration) in the ventilation control system. Therefore it will be significant to analyze the energy consumption and indoor air quality of these two control strategies.

Figure 26 and Figure 27 present the indoor air CO_2 concentration of each zone when using the fixed outdoor air flow rate control strategy. Where $C_{zone,i}$ is the CO_2 concentration of *zone i*. i = 1,...,*7*. The average CO_2 concentration of each zone in the AHU1 and AHU2 system were 580.7ppm and 540.5ppm, respectively. Figure 9.28 and Figure 9.29 present the indoor air CO_2 concentration of each zone when using the DCV strategy. The average CO_2 concentration of each zone in the AHU1 and AHU2 system were 623.8ppm and 570.6ppm, individually. It is clearly showed that, in most of test period, the CO_2 levels using the DCV strategy were larger than

that using the fixed outdoor air flow rate control strategy. The maximum CO_2 concentration using the DCV strategy in the AHU1 system was 815.2ppm, which is some higher than the maximum value of 755.0ppm associated with the use of the fixed outdoor air flow rate control strategy, while the maximum CO_2 concentration using the DCV strategy in the AHU2 system was 700.5ppm, which was also some higher than the maximum value of 625.5ppm related to the use of the outdoor air flow rate control strategy. However, these maximum CO_2 value was still significant less than 1000.0ppm, which therefore still is in the acceptable range described in the ASHRAE standard (2004).

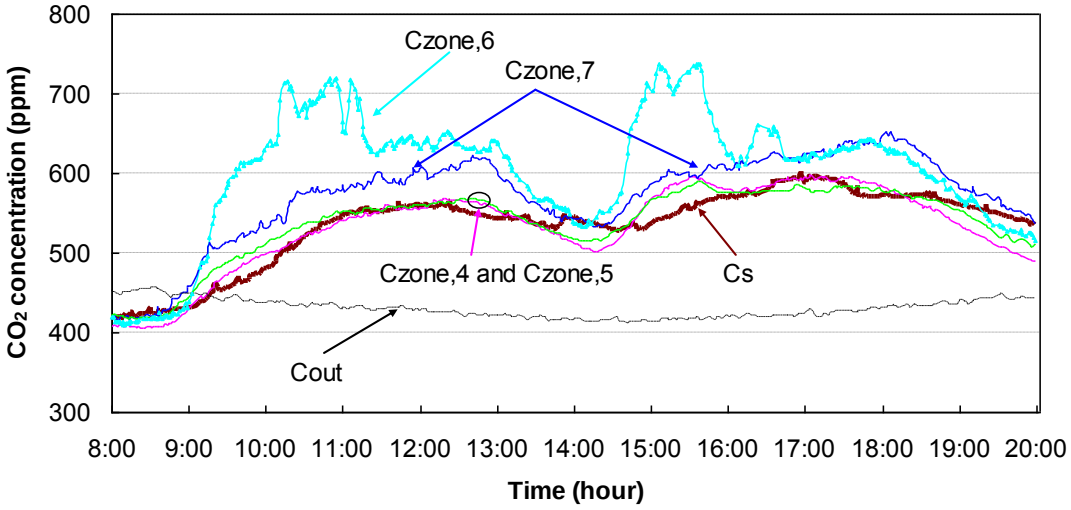

Figure 9.26 Indoor air CO_2 concentrations of individual zones in AHU1 system using the fixed flow control strategy

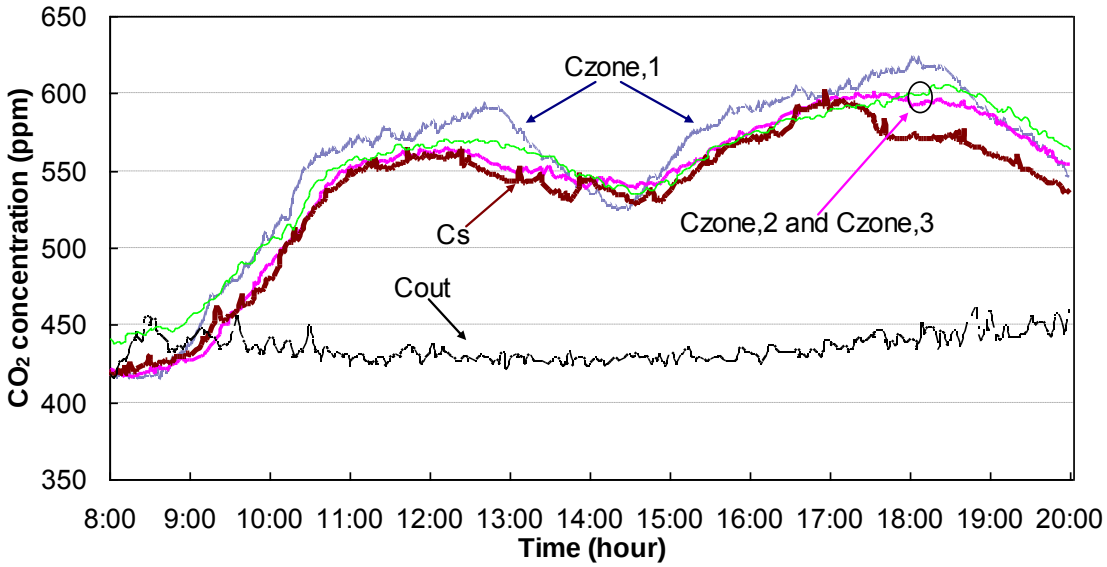

Figure 9.27 Indoor air CO_2 concentrations of individual zones in AHU2 system using the fixed flow control strategy

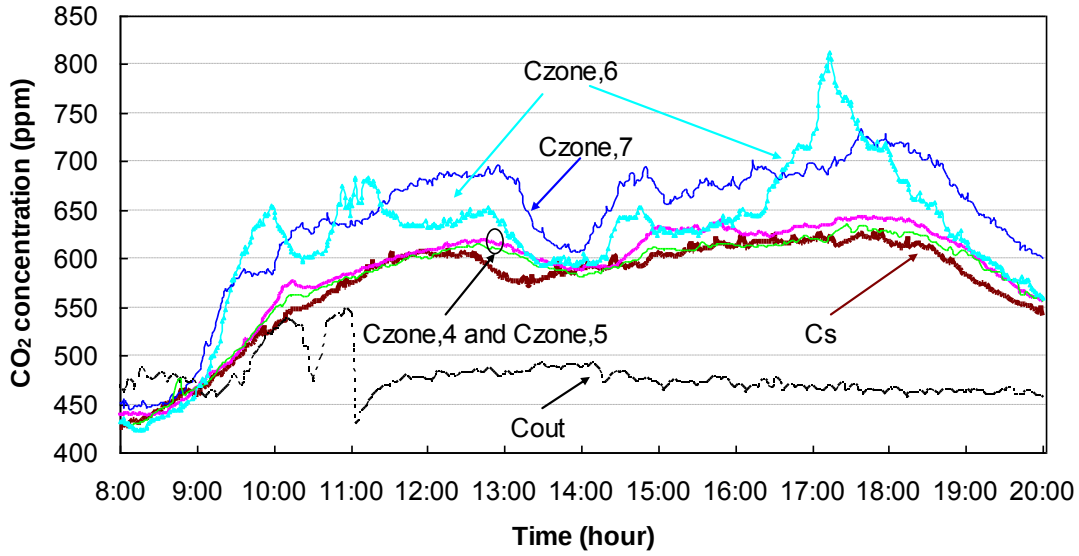

Figure 9.28 Indoor air CO_2 concentrations of individual zones in AHU1 system using the DCV strategy

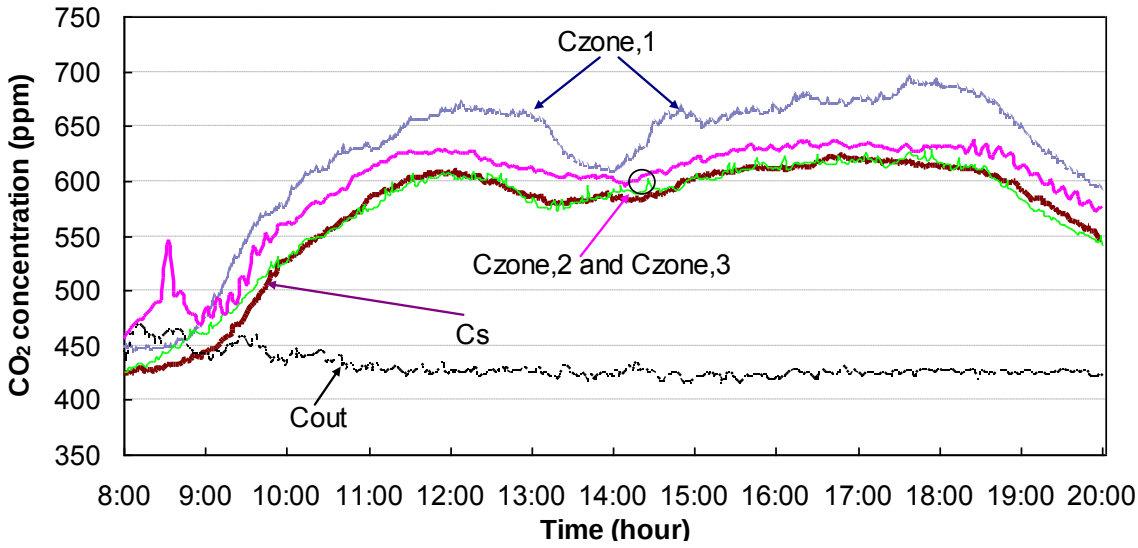

Figure 9.29 Indoor air CO_2 concentrations of individual zones in AHU2 system using the DCV strategy

The energy consumptions of both the tested data in the winter periods and simulated data in the summer and spring periods due to the use of the two ventilation strategies were also compared. The energy consumption for cooling outdoor air was calculated using the outdoor air enthalpy, the return air enthalpy and the coefficient of performance (*COP*) including chillers and pumps (COP of 2.5 was used). Table 9.2 summarizes the energy consumptions of the primary fan and the energy consumption for cooling outdoor air in the typical floor when the DCV strategy is only used to control the outdoor air for the typical floor. It can be found that, in the winter and spring test days, the cool outdoor air provided free cooling (marked as negative consumption), which therefore helped to reduce the energy consumption of the water side system (as the system was still running in cooling mode). The more cool outdoor air, the more cooling energy will be saved and DCV strategy therefore should not be used in winter and cool spring days. However, in the hot days in

summer and middle seasons, the hot outdoor air needs to be cooled down. The more hot outdoor air is used, the more cooling energy will be consumed. Compared with the use of the fixed outdoor air flow rate control strategy, the primary fan energy consumption was reduced when the DCV strategy was used, due to the use of less outdoor air.

Table 9.2 Energy performance comparisons between two reference ventilation strategies in spring, winter and summer test days (Typical floor)

Test cases	Strategies used	AHU1		AHU2	
		Fixed flow	DCV	Fixed flow	DCV
Spring case (simulated)	Primary fan energy consumption (kWh)	612.3	608.0	794.6	761.9
	Energy consumption for cooling outdoor air (kWh)	-7.9	-3.0	-5.0	-2.8
Summer case (simulated)	Primary fan energy consumption (kWh)	612.3	608.0	794.6	761.9
	Energy consumption for cooling outdoor air (kWh)	198.1	79.8	124.4	71.9
Winter case (site tested)	Primary fan energy consumption (kWh)	612.3	608.0	794.6	761.9
	Energy consumption for cooling outdoor air (kWh)	-110.0	-38.3	-69.1	-31.8

As mentioned earlier, there are four primary fans were used to provide the outdoor air for all floors in Region 2. To demonstrate the energy benefits due to the use of the DCV strategy for all floors in whole Region 2, the data in the three typical days are presented. The mechanical cooling was needed in the air-conditioning system in the spring, summer and winter periods, although the outdoor air temperature may be relatively cool in the winter period. In the simulation study, the actual historical data recorded by the BMS were used as the working conditions. When the fixed outdoor air flow rate control strategy was implemented, the primary fan was operated using

the current operation strategy in site (i.e., maintaining the fan operating frequency at 45Hz). The DCV strategy was used only when it is beneficial in saving energy. When the DCV strategy was used, a simplified variable frequency primary fan model was used to optimize the fan operating speed. The dimensionless air flow rate coefficient, pressure coefficient and fan efficiency in the fan model were fitted using the manufacture catalogue date of the actual fan used in the real building. The pressure controller maintained the air static pressure of sensor at its set-point by modulating the primary air fan operating frequency. Table 9.3 summarizes the test results by using the DCV strategy and the fixed outdoor air flow rate control strategy in the three selected typical working days, when the set-points provided by the both strategies were used to control the outdoor air of all floors in Region 2.

Table 9.3 Comparisons of the energy consumption performance related to the use of the two ventilation strategies in the three typical working days

Cases	Control mode	AHU1		AHU2	
		Fixed flow	DCV	Fixed flow	DCV
Cool Spring day	Primary fan energy consumption (kWh)	612.3	288.3	794.6	324.5
	Primary fan energy saving (%)	-	52.9	-	59.2
	Energy consumption for cooling outdoor air (kWh)	-189.6	-73.0	-119.0	-67.4
	Energy saving for cooling outdoor air (%)	-	-61.5	-	-43.4
Summer day	Primary fan energy consumption (kWh)	612.3	288.3	794.6	324.5
	Primary fan energy saving (%)	-	52.9	-	59.2
	Energy consumption for cooling outdoor air (kWh)	4754.4	1915.2	2985.6	1725.6
	Energy saving for cooling outdoor air	-	59.7	-	42.2

	(%)				
Winter day	Primary fan energy consumption (kWh)	612.3	288.3	794.6	324.5
	Primary fan energy saving (%)	-	52.9	-	59.2
	Energy consumption for cooling outdoor air (kWh)	-2640.2	-919.7	-1657.8	-763.5
	Energy saving for cooling outdoor air (%)	-	-65.2	-	-53.9

The results showed that the primary fan energy consumption was decreased while the energy consumption for cooling outdoor air was increased significantly when the DCV strategy was used, as compared with the use of the fixed outdoor air flow rate control strategy in the spring and winter test day. However, both the primary fan energy consumption and the energy consumption for cooling outdoor air were decreased obviously related to the use of the DCV strategy in the summer test day. On the basis of the energy consumptions of the three typical test days, the annual energy consumptions for outdoor air ventilation in Region 2 (i.e., including PAU fan energy consumption and the energy consumption for cooling outdoor air) by using the DCV strategy (only when it provides energy benefit) was about 523,766 kWh. When using the fixed outdoor air flow rate control strategy, it was about 1,186,058 kWh. Compared with the original fixed outdoor air flow rate control strategy, about 662,292 kWh (55.8%) of outdoor air ventilation energy was saved by using the DCV strategy in Region 2 of the building whilst the ventilation requirement was fulfilled.

9.6 Energy Savings of the Enthalpy-based Ventilation Strategy

The adaptive DCV strategy can provide significant energy savings in summer season. However, additional energy will wasted in cold winter seasons. Because the enthalpy of outdoor air is much lower than the enthalpy of return air. Conventional studies (Park 1984, Wang 2000, ASHRAE 2004, Spitler 1987) have validated that enthalpy-based ventilation control is a satisfied approach to save system energy consumption during a cold winter season. Therefore, the enthalpy-based ventilation control is recommended to be used in the high-rise during the cold winter seasons. When the outdoor air enthalpy is smaller than the return air enthalpy, the enthalpy-based ventilation control strategy is used to provide the outdoor air flow rate set point. Due to the installation of the PAU systems in this high-rise building, the power consumption of PAU systems are not neglected when enthalpy control strategy is adopted. Two operation schemes are included in the enthalpy ventilation control strategy. One is the full outdoor air control scheme; the other one is the model-based outdoor air flow rate optimal control scheme, presented in Chapter 6. In this case, a supervisory strategy will be used to determine which operation mode to be used. In the very cold winter test days, it was found that the cooling energy saving by the outdoor air were much larger than the energy consumption of the PAU fan system. Therefore the full outdoor air cooling scheme is set to provide the outdoor air flow rate set point. In this case, more outdoor air provided, more energy be achieved.

In middle seasons, the power consumption of the PAU fan system might be larger or smaller than the cooling energy saving by the outdoor air up to the outdoor air temperature, outdoor air relative humidity, return air temperature and return air

relative humidity and so on. In this case, the developed model-based outdoor air flow rate optimal control scheme can be used to reset the outdoor air flow rate set point. Figure 9.10 presents the schematic of the outdoor ventilation control for each AHU system. During the implementation of the enthalpy control strategy, the energy consumption of the PAU fan system are measured using the power meters, and the enthalpy of outdoor air and return air are measured by using the enthalpy sensors, which can be calculated based on the measured return air parameters (i.e., temperature, RH, etc.). However, there are no RH sensors and no temperature sensors (except that in the typical floor) for measuring the return air status in. To test and evaluate the performance of the enthalpy-based control strategy in practice, it is necessary to install the enthalpy sensors in Region 2 of the high-rise building. This section briefly estimated the potential energy savings due to the use of enthalpy-based ventilation control strategy in Region 2 in advance.

9.6.1 Estimation of Additional Energy Savings

In very cold winter days, the full air cooling scheme will be used about 480 hours. Otherwise, the model-based outdoor air flow rate optimal control scheme (partial air cooling mode) will be used to reset the outdoor air flow rate set point for about 360 hours. The full air cooling control scheme was tested in field and the energy consumption of the air-conditioning system was measured and calculated accordingly. As far as the partial air cooling mode is concerned, the system energy consumption was estimated with the historical recorded field data. Next part is the brief illustrations of the estimated procedure of annual total energy saving of

air-conditioning system in Region 2 of the high-rise building by using the enthalpy-based ventilation control strategy.

Firstly, the original fixed outdoor air flow rate control strategy introduced in Section 9.4.2 can maintain the outdoor air flow rate of each primary air fan in AHU1 and AHU2 are 10.5m^3/s and 9.5m^3/s, respectively. The power of the primary fan is near 30Kw, and the frequency is 45Hz. According to the manufacturer data, the design flow rate of each primary air fan is 17m^3/s; the design frequency is 50Hz. Because the cooling energy saving by the outdoor air is larger than power consumption of the PAU systems, the full air cooling control scheme is use to provide more cold outdoor air into the ventilation system to reduce the cooling energy consumption. Therefore, the maximum outdoor air flow rate and frequency were all set to be the design values. The energy consumptions between these two outdoor air flow rate control strategies are measured and calculated. Table 9.4 summarizes the additional energy savings of Region 2, which are estimated based on the current operation of PAU systems in Region 2 of this high-rise building. It is estimated that about 179020.8 kWh cooling energy can be saved by using the enthalpy-based control (from the use of full air cooling concept and model-based outdoor air optimal control) with a cost of 50400 kWh PAU energy consumption. However, the total energy saving is still obvious, about 12.8000 kWh.

Table 9.4 Annual total energy savings of Region 2 due to the use of enthalpy control

Items	Outdoor air cooling energy saving (kWh)	Additional PAU fan power consumption (kWh)	Total energy saving (kWh)
Value	179020.8	50400	128620.8

Remarks: the above estimation is based on the overall COP of water system is 2.5.

9.7 Summary

The performance of adaptive DCV was in-situ implemented and tested by comparing with that of the original implemented fixed outdoor air flow rate control strategy. The results from the site test and simulation study showed that this DCV strategy can help to reduce the system running cost while still maintaining the satisfied indoor air quality. Test results show that the annual total energy consumption in Region 2 when using the DCV strategy can be significantly reduced by compared with that with the use of the fixed outdoor air flow rate control strategy.

The results also showed that the DCV strategy can help to reduce the overall energy consumption significantly in the hot summer and middle seasons in Hong Kong, but it may not be the proper method for outdoor air control in winter conditions. In the winter periods, the enthalpy control strategy should be a better choice instead of using DCV strategy. The enthalpy-based outdoor air flow rate control strategy is evaluated by compared with the original fixed outdoor air flow rate control strategy. Its potential energy savings due to the use of enthalpy control in Region 2 in this building are also validated on the basis of the simulation accordingly.

Chapter 10 CONCLUSIONS AND RECOMMENDATIONS

Firstly, the ventilation optimal control strategies for multi-zone air-conditioning systems have been developed. They include: (1) a CO_2-based adaptive Demand Controlled Ventilation (DCV) strategy, (2) an indoor air temperature set point reset strategy for critical zones, (3) a model-based indoor air temperature set point resetting strategy for critical zones, and (4) a model-based outdoor air flow rate optimal control strategy for a full air system with primary air handling units. There four ventilation control strategies were tested in a simulated environment. Meanwhile, the CO_2-based adaptive DCV strategy was practically implemented and validated in a super high-rise building in Hong Kong. The performance test and evaluation of these strategies showed that all these optimal control strategies can maintain satisfactory indoor air quality provide acceptable indoor thermal comfort with less energy inputs.

Secondly, a CFD-based ventilation test method has been proposed for the control and optimization of indoor environment by combining a ventilated room with a ventilation control system. This test method can provide new possibilities for testing and evaluating the ventilation control processes in real systems. In this method, a data-based space temperature offset model was used to describe the complex indoor thermal non-uniform distribution. This offset model can effectively describe the

difference between the temperature in actual sensor location and in the occupied zone in the CFD-based ventilation test method.

10.1 The Main Contributions of This Thesis

1) Conclusive Remarks on CO_2-Based Adaptive DCV strategy and Indoor Air Temperature Set Point Reset Strategy for Critical Zones

The CO_2-based adaptive DCV strategy using the dynamic multi-zone ventilation equation has been proposed for the multi-zone air-conditioning systems. The performance of this strategy was evaluated by comparing with that of three conventional DCV strategies in summer conditions in Hong Kong. The three conventional DCV strategies include: *Strategy A – it uses the detected total occupancy load to determine the outdoor air flow rate; Strategy B – it uses the required fresh air fraction of the critical zone to determine the outdoor fresh air flow rate; Strategy C - it uses the dynamic multi-zone ventilation equation to determine the required outdoor air fraction of the identified critical zone.* The CO_2-based adaptive DCV strategy can achieve satisfied indoor environment with slightly more energy consumption about 5.4% -5.7% by comparing with the strategy A. The strategy B consumed 25.3% - 32.2% more energy to satisfy the needs of ventilation in critical zones. The strategy C consumed 13.6%-14.5% more electricity to satisfy the needs of ventilation in critical zones. However, the energy saving of the CO_2-based adaptive DCV strategy was up to 11.7%-17.7%.

The indoor air temperature set point reset strategy for critical zones has been developed to reset the temperature set point of the identified critical zone. This strategy can adjust the demanded outdoor airflow rate, while keeping the critical zones supplied with sufficient fresh air. It will result in less total outdoor airflow demand eventually. This indoor air temperature set point reset strategy is combined with the adaptive DCV strategy to evaluate its performance by comparing with the DCV strategy which determines the outdoor air flow rate according to total occupancy load. When adopting the indoor air temperature set point reset strategy for critical zones separately, the electrical energy consumption can be further reduced by 5.4-5.7%. This adaptive DCV strategy using dynamic multi-zone ventilation equation and critical zone temperature set point reset can achieve satisfied indoor environment with slightly more energy consumption about 7.8% - 9%.

2) Conclusive Remarks on Model-Based Indoor Air Temperature Set Point Resetting Strategy for Critical Zones

The model-based indoor air temperature set point resetting strategy for critical zones has been developed and evaluated in selected summer conditions in Hong Kong. The system response predicted using simplified incremental models to optimize the indoor temperature set point of critical zones to improve the unbalance of fresh air requirements among different zones. Validation tests allow the models to be used conveniently and accurately on different systems and in a wide working arrange by identifying the parameters online.

The evaluation tests of this optimal strategy show that this strategy is capable of optimizing the system overall performance according to the chosen weighting factors. The optimal strategy was evaluated by comparing with a conventional DCV strategy. The maximum CO_2 concentration using this optimal strategy is 1083ppm, slightly higher than the maximum value of 1009ppm using the conventional DCV strategy. However, it is still acceptable since the prescribed level is 700ppm above the CO_2 concentration of the outdoor air (360ppm in this study). The maximum PPD value is 14.74 lower than the maximum value 16.37 when using the conventional DCV strategy. The results show this optimal strategy can achieve significant energy saving (about 3.09%-4.51%) by comparing with the conventional DCV strategy, while maintaining acceptable thermal comfort and indoor air quality.

3) *Conclusive Remarks on Model-Based Outdoor Air Flow Rate Optimal Control Strategy*

The model-based outdoor air flow rate optimal control strategy has been developed to optimize the outdoor air flow rate of HVAC systems with primary air-handling units. A cost function is constructed by compromising the power consumption of primary air fan and the energy consumption for cooling outdoor air. The system response can be predicted by using a simplified incremental primary air fan model. A hybrid strategy of the DCV and the model-based outdoor air flow rate optimal control and a conventional hybrid strategy of the DCV and the full outdoor air flow rate optimal control are proposed and compared in the tested spring conditions in Hong Kong. The averaged CO_2 concentration using the hybrid strategy of the DCV

and the model-based outdoor air flow rate optimal control is 644.2ppm, slightly higher than the maximum value of 621.8ppm using the conventional strategy. The percentage savings of primary fan and cooling coil power consumption is about 1.93%. The total power saving of the whole system is 1.01%.The results show this outdoor air optimal strategy can achieve noticeable energy saving while maintaining acceptable indoor air quality for the ventilation systems with primary air-handling units.

However, it was found that the system total energy consumption increased obviously by comparing with the induced outdoor ventilation system. As the ventilation system with a primary air unit in our study is concerned, the total energy consumption using the hybrid strategy of the DCV and the model-based outdoor air flow rate optimal control was 1563.68 kWh, and the total energy consumption using hybrid strategy of the DCV and the full outdoor air optimal control with the induced outdoor air unit was 1413.71 kWh. It is investigated that about 9.59 % energy savings could be obtained without installing the primary air handling unit. Therefore the induced outdoor air unit is the preferable choice for the installation of the outdoor ventilation system in the modern building when it is feasible in practical system construction.

4) *Conclusive Remarks on CFD-Based Virtual Ventilation Control Test Method*

The CFD-based virtual ventilation test method has been presented by integrating a conditioned room model into its ventilation system and control strategy to evaluate the ventilation performance. This test method was demonstrated to be a feasible way

for investigating ventilation control performance in a simulated environment as an evaluation tool for the ventilation systems and control strategies. Complex indoor thermal conditions, especially the difference between the temperature in actual sensor location and in the occupied zone, were compensated using a data-based space temperature offset model. Experimental tests have been carried out to validate the accuracy of the CFD room model. Fair agreement is found between the simulated and measured results. The experience shows that the use of the virtual temperature sensor can efficiently compensate the influence of the temperature non-unified stratification on temperature control systems, and hence improve the accuracy of the ventilation control process significantly.

5) *Conclusive Remarks on In-situ Implementation of the Ventilation Control Strategies*

The site implementation and validation of the adaptive DCV strategy in a super high-rise building in Hong Kong is presented. The performance of this strategy was validated by comparing with that of the original implemented fixed outdoor air flow rate control strategy. The results from the site tests and simulation studies show that this DCV strategy can help to reduce the system energy cost while still maintaining the satisfied indoor air quality. When the DCV strategy was used in the typical floor, both the primary fan energy and the energy consumption for cooling the outdoor air were decreased in the hot days in the summer and middle seasons. However, the primary fan energy consumption was decreased while the energy consumption for cooling outdoor air was increased in the cool days in winter and middle seasons.

Test results show that the annual total energy consumption when using the DCV strategy can be significantly reduced by comparing with the fixed outdoor air flow rate control strategy.

The results also show that the DCV strategy can help to reduce the overall energy consumption significantly in the hot summer and middle seasons in Hong Kong, but it may not be the proper method for outdoor air control in winter conditions. In the winter periods, the enthalpy control strategy should be a better choice instead of using DCV strategy.

In addition, the enthalpy-based outdoor air flow rate control strategy is evaluated by compared with the original fixed outdoor air flow rate control strategy in the cold winter periods in the high-rise building. It is estimated that about 179020.8 kWh cooling energy can be provided by using the enthalpy-based outdoor air control strategy (from the use of full air cooling concept and model-based outdoor air optimal control) with a cost of 50400 kWh PAU energy consumption in the Region 2 (totally 24 floors). However, the total energy saving is still obvious, i.e. about 128,000 kWh per year.

10.2 Recommendations for Future Work

1) Site implementation and commission of ventilation control strategies

The implementation and evaluation of the CO_2-based adaptive DCV strategy have been operated in a super high-rise building using the IBmanager system. Results show that this DCV strategy can obtain the acceptable indoor environment quality with less energy by comparing with the conventional ventilation strategy with fixed flow. To further improve the ventilation performance in this building, the proposed model-based indoor air temperature optimal control strategy for temperature resetting and the model-based optimal control of outdoor air flow rate of full air system with primary air-handling unit in field should be implemented and validated on the ventilation performance in the practical high-rise building. Many problems may arise with the in-situ implementation of these developed ventilation strategies and extra efforts are therefore needed to test these ventilation strategies to achieve satisfactory control performance.

2) The CFD-based ventilation test method

On the space temperature offset model, it is currently developed for a single zone system. Since the inlet and indoor source conditions are mainly responsible for the thermal characteristics of different zones, the model only creates a link among the inlet air, indoor occupants' number and individual zones. It is assumed that the supply air flow rate and heat flux of occupants would have created the aggregate effect of the convective flux interaction with the neighboring zones on the well-mixed zone in consideration. It creates a direct relationship between the actual sensor and virtual sensor without the need for modeling zonal interactions. In fact, the effect of the heat transfer from the neighboring zones should be included into the

space temperature offset model. To improving the accuracy of the model, it is therefore necessary to extend the method for considering the interaction among different zones in the future.

The CFD-based feedback ventilation test method was carried out successfully in this research. However, the current CFD simulation of the ventilated space was still too slow using today's personal computers while the computing time for the ventilation system and control strategy simulation is negligible. To bring this test method for practical application, a simplified numerical model will be needed to develop for more effective CFD simulation in future.

REFERENCES

A. Abbassi and L. Bahar. 2005. Application of neural network for the modeling and control of evaporative condenser cooling load. Applied Thermal Engineering 25(17-18): 3176-3186.

A. Pappas and Z. Zhai. 2008. Numerical investigation on thermal performance and correlations of double skin façade with buoyancy-driven airflow. Energy and Buildings 40: 466-475.

A. Persily. 1993. Ventilation, carbon dioxide and ASHRAE Standard 62-1989. ASHRAE Journal 35 (7): 40-44.

A.A. Aganda, J.E.R. Coney and C.G.W. Sheppard. 2000. Airflow malt distribution and the performance of a packaged air-conditioning unit evaporator. Applied Thermal Engineering 20: 515-528.

A.H. Land and A G. 1960. Doig. An automatic method of solving discrete programming problems. Econometrica 28(3): 497-520.

A.J. Katz and P.R. Thrift. 1994. Generating image filters for target recognition by genetic learning, IEF, E Trans. on Pattern Analysis and Machine Intelligence 16: 906.

A.M Bassily and G.M. Colver. 2005. Cost optimization of a conical electric heater.

Alamdari F., K.M. Bennett and P.M. Rose. 1994. Airflow and temperature distribution within an open-plan building space using a displacement ventilation system. Proceeding of Room vent.

ASHRAE. 1994. Addendum 55a. ANSI/ASHRAE Standard 55..

ASHRAE. 1996. ASHRAE Standard 62-1989R. Ventilation for acceptable indoor quality (Public review draft), Atlanta.

ASHRAE. 1999. ASHRAE Standard 62-1999. Ventilation for acceptable indoor quality, Atlanta.

ASHRAE. 2001. ASHRAE Standard 62-2001. Ventilation for acceptable indoor quality, Atlanta.

ASHRAE. 2003. ASHRAE looking at demand control ventilation requirements. Indoor environment quality strategies. 16(2): 14-15.

ASHRAE. 2004. ASHRAE Standard 62.1-2004. Ventilation for acceptable indoor quality, Atlanta.

ASHRAE. 2004. Energy standard for buildings except low-rise residential buildings, ANSI/ASHRAE/IESNA standard 90.1-2004, American Society of Heating, Refrigerating and Air-Conditioning Engineers, Inc., 1791 Tullie Circle NE, Atlanta, GA 30329.

B. Davidge. 1991. Demand controlled ventilation system in office buildings, Proceeding of the 12th AIVC conference air movement and ventilation control within building pp: 151-171.

B. Degw and Tekinibank. 1995. The intelligent building in Europe, British Council of Offices, The College of Estate Management.

B. Fleury. 1992. Demand controlled ventilation: A case study. Proceedings of the 13th AIVC Conference Ventilation for Energy Efficiency and Optimum Indoor Air Quality. Conventry, UK. 343-346.

B. Griffith and Q. Chen. 2003. A momentum-zonal model for predicting zone airflow and temperature distributions to enhance building load and energy simulations. HVAC&R Research 9(3): 309-325.

Back, T., D.B. Fogel, and Z. Michalewicz. 2000. Evolutionary Computation 1: Basic Algorithm and Operators, Institute of Physics Publishing, Bristol and Philadelphia.

C. Inard, H. Bouia and P. Dalicieux. 1996. Prediction of air temperature distribution in buildings with a zonal model. Energy and Buildings 24: 125-132.

C. Park, G.F. Kelly and J.Y. Kao. 1984. Economizer algorithms for energy management and control system. Nat Bur (US) NBSIR 84-2832.

C. Topp. 1999. Diffusion and evaporation-controlled emission in ventilated rooms. Ph.D. Thesis, Alborg University, Denmark.

C.Y.H. Chao and J.S.Hu 2004. Development of a dual-mode demand control ventilation strategy for indoor air quality control and energy saving, Building and Environment 39: 385-397.

C.Y.H. Chao and J.S.Hu. 2004. Development of an enthalpy and carbon dioxide based demand control ventilation for indoor air quality and energy saving with neural network control. Indoor and Built Environment 13(6): 463-475.

CONTAM. Indoor Air-International Journal of Indoor Air Quality and Climate, 6: 278-288.

D. Chan and K.W.Horace Mui. 2003. Adaptive comfort temperature model of air-conditioned building in Hong Kong, Building and Environment 38: 837-852.

D. Elovitz. 1995. Minimum outside air control methods for VAV systems. ASHRAE Transactions 101(2): 613-618.

D. Sodergren. 1982. A controlled ventilation system. Environment international 8: 483-386.

D.B. Fogel. 1994. Applying evolutionary programming to selected control problems. Computers and Mathematics with Applications 27 (11): 89-104.

D.L. Carroll. 2001. FORTRAN Genetic algorithm (GA) driver. Version 1.7a. http://cuaerospace.com/carroll/ga.html, http://cuaerospace.com/carroll/gatips.html

D.R. Clark. 1985. Building Systems and Equipment Simulation Program HVACSIM^{+} - User's Manual, National Bureau of Standards and Technology, Washington, DC.

E. Aggelogiannaki, H. Sarimveis and D. Koubogiannis. 2007. Model predictive temperature control in long ducts by means of a neural network approximation tool. Applied Thermal Engineering 27(14-15): 2363-2369.

E. David. Goldberg. 1989. Genetic Algorithms in Search, Optimization, and Machine Learning, Addison-Wesley, Reading, MA.

E. HUTTER. 1981. Thermal study of behavior of the galleries covered by simulation in mode varied with taking into account of the stratification of air. Ph.D. Thesis, Univeristy of Paris VII, 207P.

E.A. Koeppel, S.A. Klein, J.W. Mitchell and B.A. Flake. 1995. Optimal supervisory control of an absorption chiller system. HVAC&R Research 1(4): 325-42.

Ed Kidd et al. 2001. DOE-2 Program Documentation, Energy Science &Technology Software Center, Oak Ridge, http://gundog.lbl.gov/dirsoft/d2getdoc.html

F. Haghighar, J. Jiang, J.C.Y. Wang, and F. Allard. 1992. Air movement in building using computational fluid dynamics. Transactions of ASME Journal of Solar Energy Engineering 114: 84-92.

F. Haghighat and A.C. Megri. 1996. A Comprehensive Validation of Two Airflow Models - COMIS and CONTAM.

F. Haghighat and G. Donnimi. 1992. IAQ and energy management by demand controlled ventilation. Environmental technology 13:351-359.

F. Haghighat, J. Jiang and Y. Zhang. 1999. The impact of ventilation rate and partition layout on the VOC emission rate: time dependent contaminant removal. Indoor Air 276-283.

F. Haghighat, Y. Li and A.C. Megri. 2001. Development and validation of a zonal model – POMA. Building and Environment 36 (9): 1039-1047.

F. Zhao. 1998. Operation strategies for economizer control in an air conditioning system. Concordia University, Montreal.

F.W. Yu and K.T. Chan. 2006. Advanced control of heat rejection airflow for improving the coefficient of performance of air-cooled chillers. Applied Thermal Engineering 26(1): 97-110.

Fluent Inc. 1998. Fluent user's guide. Version 5.0, Fluent Inc., Lebanon, NH, USA.

Fluent Inc.2005. FLUENT User's Guide, Version 6.2.

G. Donnini, F. Haghighat and V. Hguyen. 1991. Ventilation control of indoor air quality, thermal comfort, and energy conservation by CO_2 measurement.

Proceedings of the 12th AIVX conference air movement and ventilation control within buildings. pp: 311-331.

G. Golub and D. Oleary. 1989. Some history of the conjugate gradient and Lanczos methods, SIAM Rev. 31: 50-102.

G. Walton. 1997. CONTAM '96 Users Manual. NISTIR 6055, National Institute of standards and Technology, USA.

G.F. Franklin, G.D. Powell and H.L. Workman. 1990. Digital control of dynamic system. New York: Addison-Wesley Publishing Co.

G.J. Raw, M.S. Roys and A. Leaman. 1990. Further findings from the office environment survey: productivity. Proc. of 5th International Conference on Indoor Air Quality and Climate, Toronto, 231-236.

G.V. Reklaitis, A. Ravindran and K.M. Ragsdell. 1983. Engineering optimization: methods and applications. New York: Wiley.

GSA. 2003. Facilities standards for the public buildings service - mechanical engineering. Tech. rep. 5, US General Services Administration.

H. Arkin and M. Paciuk. 1997. Evaluating intelligent building according to level of service system integration, Automation in Construction 6(5): 471-479.

H. Beyer. 2001. The Theory of Evolution Strategies, Springer-Verlag, Berlin Heidelberg.

H. During. 1994. Energertic consumption and thermal comfort of the heated buildings: approach by the zonal models. Ph.D. Thesis, INSA Lyon.

H. Feriadi. 2003. Thermal comfort for natural ventilated residential buildings in the tropical climate, PhD. dissertation, National University of Singapore, Singapore.

H.B Awbi. 1996. A CFD study of the air quality at the breathing zone. Indoor Air 1996, 2.

H.E. Feustel. 1992. A Special Issue Devoted to the COMIS (Conjunction of Multizone Infiltration Specialists Model) - Foreword. Energy and Buildings 18: 77.

H.E. Feustel. 1999. COMIS – an international multizone air-flow and contaminant transport model. Energy and Buildings 30: 3-18.

H.J. Park and D. Holland. 2001. The effect of location of a convective heat source on displacement ventilation: CFD study. Building and Environment 36: 883-889.

H.N. Lain. 1995. Intelligent computer control of air conditioning systems based on genetic algorithm and classifier system, Proc. Building Simulation '95 Conf, 4th Int. Conf. Int. Building Performance Simulation Association, Madison, WI. 151-157.

H.S. Brightman, S.E. Womble, J.R. Girman, W.K. Sieber, J.F. McCarthy, and J.D.Spengler. 1997. Preliminary comparison of questionnaire data from two IAQ studies: occupant and workspace characteristics of randomly selected buildings and 'complaint' buildings. Proc. Health Buildings/IAQ'97, 2: 453-458.

I.P. Chung and D. Dunn-Rankin. 1998. Using numerical simulation to predict ventilation efficiency in a model room, Energy and Buildings 28: 43-50.

J. Fehlmann, H. Wanner, and Zamboni. 1993. Indoor air quality and energy consumption with demand controlled ventilation in an auditorium. Proceedings of the 6th International Conference on Indoor Air Quality and Climate. 5: 45-50.

J. House and T. Smith. 1991. Optimal control of a thermal system. ASHRAE Transactions 97(2):991-1001.

J. Janssen, T. Hill and J. Woods. 1982. Ventilation for control of indoor air quality: A case study. Environment International 8:487-496.

J. Jones and D. Meyers et al. 1997. Performance analysis for commercial available CO_2 sensors. Journal of architectural engineering 3 (1): 25-31.

J. Kettler. 2003. Standard 62's multiple spaces equation: For design, not control. ASHRAE Journal 45(8): 20-22.

J. Liu and G.Q. Liu. 2005. Some indoor air quality problems and measures to control them in China. INDOOR AND BUILT ENVIRONMENT 14(1): 75-81.

J. Nizet, L. Lecomte and F. Litt. 1984. Optimal control applied to air conditioning in building. ASHRAE Transactions 90(1B): 587-600.

J. Spitler, D. Hittle, D. Johnson, and C. Pederson. A comparative study of the performance of temperature-based and enthalpy-based economy cycles, ASHRAE Trans 93(2): 13-22.

J. Sun and A. Reddy. 2005. Optimal control of building HVAC&R systems using complete simulation-based sequential quadratic programming (CSB-SQP). Building and Environment 40(5): 657-69.

J.D. Posner, C.R. Buchanan and D. Dunn-Rankin. 2003. Measurement and prediction of indoor air flow in a model room, Energy and Building 35(5): 515-526.

J.E. Seem. 2009. Development and evaluation of optimization-based air economizer strategies. International Journal of Energy Research 29(4): 359-76.

J.H. Holland. 1975. Adaptation in Natural and Artificial Systems. The University of Michigan Press, Ann Arbor, MI.

J.J.K. Jaakkola. 1994. Sick building syndrome in relation to indoor air temperature, relative humidity and air change. Proc. Thermal Comfort: past, present and future, Garston, United Kingdom, 168-181.

J.M. Samet. 1993. Indoor air pollution: a health perspective. Indoor Air: 3: 219-226.

J.P. Nordvik and J.M. Renders. 1991. Genetic algorithms and their potential for use in process control: a case study, Proc. 4th Int, Conf on Genetic Algorithms, San Diego, CA, 480-486.

J.R. Nielsen. 1998. The influence of office furniture on the air movements in a mixing ventilation room. Ph.D. Thesis, Aalborg Unversity, Denmark.

J.S. Zhang, L.L. Christianson, G.J. Wu and R.H. Zhang. An experimental evaluation of a numerical simulation model for prediction room air motion. Proceedings of Indoor Air Quality, Ventilation and Conservation Conference, Montreal, Canada, 360-371.

K. Ogura, H. Shiigi, T. Oho and T. J. Tonosaki. 2000 Electrochem. Soc. 147: 4351.

K. Taeyeon, et al. 2007. Two-step optimal design method using genetic algorithms and CFD-coupled simulation for indoor thermal environments. Applied Thermal Engineering 27: 3-11.

K.A. Papakonstantinou, C.T. Kiranoudis and N.C. Markatos. 2003. Mathematical modeling of environmental conditions inside historical buildings. The case of the archaeological museum of Athens. Energy and Buildings 31: 211-220.

K.F. Fong, V.I. Hanby and T.T. Chow. 2008. A robust evolutionary algorithm for HVAC engineering optimization. HVAC&R Research 14 (5): 683-705.

K.F. Fong. 2006. HVAC system optimization for energy management by evolutionary programming. Energy and Buildings 38 (3): 220-231.

K.I. Krakow, F. Zhao and A.E. Muhsin. 2000. Economizer control. ASHRAE Transactions 106: 13-25.

K.J. Astrom and B. Wittenmark. 1989. Adaptive control. New York: Addison-Wesley Publishing Co.

K.W. Lee and H.N. Lain. 1995. Optimizing neural network weights using genetic algorithms: a case study, Proc. IEEE Int. Conf. on Neural Networks, Perth, Australia 3: 1384-1388.

K.W. Mui, L.T. Wong and P.S. Hui. 2006. A new sampling approach for assessing indoor air quality. Indoor and Built Environment 15(2): 165-172.

K.W.D. Cheong, E. Djunaedy, Y.L. Chua, K.W. Tham, S.C. Sekhar, N.H. Wong and M.B. 2003. Ullah, Thermal comfort study of an air-conditioned lecture theatre in the tropics, Building and Environment 38(1): 63-73.

L. Davis. 1995. Handbook of Genetic Algorithms, Van Nostrand Reinhold, New York.

L. Mora, J. Gadgil and E.Wurtz. 2003. Comparing zonal and CFD model predictions of isothermal indoor airflows to experimental data. Indoor air 13: 77-85.

L. Mora. 2002. Comparing zonal and CFD model predictions of indoor airflows under mixed convection conditions to experimental data. EPIC conference.

Laret. 1980. Contribution to the development of mathematical models of the transitory thermal behavior of structures of dwelling. Ph.D. Thesis, Univeristy of Liege.

M. Giraud and Lafon. 2002. A comparison of evolutionary algorithms for mechanical design components. Engineering Optimization 34: 307-322.

M. Hydeman, S. Taylor, J. Stein, E. Kolderup and T. Hong. 2003.Advanced variable air volume system design guide. Tech. rep., California Energy Commission.

M. Mbaye, Z. Aidoun and V. Valkov et al. 1998. Analysis of chemical heat pumps (CHPs): Basic concepts and numerical model description. Applied Thermal Engineering 18(3-4): 131-146.

M. Mitchell. 1997. An introduction to genetic algorithm. The MIT Press.

M. Musy, E. Wurtz, F. Winkelmann and F. Allard. 2001. Generation of a zonal model to simulate natural convection in a room with a radiative/convective heater. Building and Environment 36(5): 589-596.

M. Zaheer-uddin and G.R. Zheng. 2000. Optimal control of time-scheduled heat, ventilating and air conditioning process in building. Energy Conversion Manage 41(1): 49-60.

M. Zamboni, O. Berchtold and C. Filleux. 1991. Demand controlled ventilation: An application to auditoria. Proceedings of the 12th AIVC Conference Air Movement & Ventilation Control within Buildings, Conventry, UK. 143-155.

M.J. Mendell. 1993. Non-specific symptoms in office workers: a review and summary of the epidemiologic literature. Indoor Air 3: 227-236.

M.M. Ardehali and T.F. Smith. 1997. Evaluation of HVAC system operational strategies for commercial buildings. Energy Conversion Manage 38(3): 225-236.

M.Y. Chan. 2005. Commuters' exposure to carbon monoxide and carbon dioxide in air-conditioned buses in Hong Kong. Indoor and Built Environment 14(5): 397-403.

March 17-19, 1997 Tokyo, Asia Pacific Energy Reserch Center, Japan.

N. Djuric, V. Novakovic, J. Holst and Z. Mitrovic. 2007. Optimization of energy consumption in buildings with hydronic heating systems considering thermal comfort by use of computer-based tools. Energy and Buildings 39: 471-477.

N. Nassif, S. Kajl and R. Sabourin. 2005. Ventilation control strategy using the supply CO_2 concentration set point. HVAC&R Research 11(2): 239-262.

N.N. Kota, J.M. House, J.S. Arora and T.F. Smith. 1996. Optimal control of HVAC systems using DDP and NLP techniques. Optimal Control Applications & Methods 17(1):71-78.

O. Rouaud and M.Havet. 2002. Computation of the airflow in a pilot scale clean room using k–ε turbulence models. International Journal of Refrigeration 25(3): 351-361.

Overview of the DOE-2 program, Version 2.1D. 1989. Simulation Research Group, Lawrence Berkeley Laboratory, LBL-19735.

P. Haves and A.L. Dexter. 1989. Simulation of local loop controls. Proc. Building, IBPSA. Vancouver.

P. Haves and A.L.Dexter. 1989. Simulation of local loop controls. In Proceedings of Building 89, IBPSA, Vancouver.

P. Vitalijus. 2004. Demand controlled ventilation: A case study for existing Swedish multifamily buildings. Energy and Buildings 36: 1029-1034.

P. Wolkoff. 1995. Volatile organic compounds - source, measurements, emissions, and the impact on indoor air quality. Indoor Air 3.

P.O. Fanger. 1970. Thermal comfort. New York:McGraw-Hill.

Q. Chen and W. Xu. 1998. A zero-equation turbulence model for indoor air simulation. Energy and buildings 28: 137-144.

Q. Chen. 1999. Comparison of different k–ε models for indoor airflow computations. Part B, Fundamentals, Numerical Heat Transfer 28(3): 353–369.

R. Hooke and T.A. Jeeves. 1961. Direct search solution of numerical and statistical problems. Journal of the Association for Computing Machinery, 8: 212-229.

R. Kohonen, S.W. Wang and H. Peitsman. 1993. Development of emulation method. IEA Annex 17, Final Report, Helsinki, Finland.

R.C. Legg. 1986. Characteristics of single and multi-blade dampers for duct air systems. Building Services Engineering Research and Technology 7(4): 129-135.

R.G. Echert. 1959. Heat and mass transfer. New York: McGraw-Hill.

R.T. Olson and S. Liebman. 1990. Optimization of a chilled water plant using sequential quadratic programming. Engineering Optimization 15:171–91.

S. Gabel, J.J. Janssen, J. Christoffel and S. Scarborough. 1986. Carbon dioxide-based ventilation control system demonstration. United States Department of Energy.

S. Mumma and R. Bolin. 1994. Real-time, on-line optimization of VAV system control to minimize the energy consumption rate and to satisfy ASHRAE Standard 62-1989 for all occupied zones. ASHRAE Transactions 100 (1): 168-179.

S. Wang, Z. Xu , H. Li , J. Hong and W.Z. Shi. 2004. Investigation on intelligent building standard communication protocols and application of IT technologies. Automation in Construction 13 (5): 607-619.

S. Wang, Z. Xu, J. Cao and J. Zhang. 2007. A middleware for web service-enabled integration and interoperation of intelligent building systems. Automation in Construction 16 (1): 112-121.

S. Yuan and R.Perez. 2006. Multiple-zone ventilation and temperature control of a single-duct VAV system using model predictive strategy. Energy and Buildings 38: 1248-1261.

S.L. Sinha, R.C. Aroraand and S. Roy. 2000. Numerical simulation of two-dimensional room air flow with and without buoyancy, Energy and Buildings 32: 121-129.

S.W. Wan. 1999. Dynamic simulation evaluation of building VAV air-conditioning system and of EMCS on-line control strategies. Building and Environment 34: 681-705.

S.W. Wang and J.B. Wang. 2002. Robust sensor fault diagnosis and validation in HVAC systems. Transactions of the Institute of Measurement and Control 24(3),: 231-262.

S.W. Wang and L. Zheng. 2001. Dynamic and real-time simulation of BMS and air-conditioning system as a "living" environment for learning/training. Automation in Construction 10: 487-505.

S.W. Wang and X.Q. Jin. 1998. CO_2-based occupancy detection for on-line outdoor air flow control. Indoor and Built Environment 7: 165-181.

S.W. Wang and X.Q. Jin. 2000. Model-based optimal control of VAV air-conditioning system using genetic algorithm. Building and Environment 35: 471- 487.

S.W. Wang, J. Burnett and H. Chong. 1999. Experimental Validation of CO_2-based occupancy detection for demand-controlled ventilation. Indoor and built environment 8: 377-391.

S.W. Wang. 2006. Dynamic simulation of building VAV air-conditioning system and evaluation of EMCS on-line control. Build Environment 34: 681-705.

S.W. Wang. 2006. Enhancing the applications of building automation systems for better building energy and environmental performance. HVAC&R Research 12(2): 197-199.

T. Kusuda. 1976. Control of ventilation to conserve energy while maintaining acceptable indoor air quality. ASHRAE Transactions 82(1): 1169-1181.

T.Y. Chen. 2002. Application of adaptive predictive control to afloor heating system with a large thermal lag. Energy and Building 34: 43-51.

TRNSYS. 1996. A transient Simulation Program. Solar Energy laboratory of the University of Wisconsin; Madison, USA.

W. Wurtz, M. Musy and L. Mora. 1999a. Introduction of specific laws in zonal model to describe temperature fields and air flow patters in mixed ventilated buildings. Journal of the Human-Environment system 3(1): 43-59.

W. Xu and Q. Chen. 2001a. A two-layer turbulence model for simulating indoor airflow-Part I. Model development. Energy and Buildings 33: 613-625.

W. Xu and Q. Chen. 2001b. A two-layer turbulence model for simulating indoor airflow-Part II. Applications. Energy and Buildings 33: 627-639.

W.H. Yik. 1997. Survey of energy end-use in commercial buildings in Hong Kong.

W.M. Kroner. 1997. An intelligent and responsive architecture. Automation in Construction 6: 381-393.

Wolfram Mathworld. 2006. Conjugate Gradient Method. Available at: http://mathworld. wolfram.com/FibonacciNumber.html.

Workshop on methodologies and data for energy demand and supply outlook,

X. Jin, Z. Du and X. Xiao. 2007. Energy evaluation of optimal control strategies for central VWV chiller systems. Applied Thermal Engineering 27(5-6): 934-941.

X.H. Xu and S.W. Wang. 2007a. An Adaptive Demand-controlled Ventilation Strategy with Zone Temperature Reset for Multi-zone Air-conditioning Systems. Indoor and Built Environment 16(5): 426-437.

X.H. Xu and S.W. Wang. 2007b. Optimal Simplified Thermal Models of Building Envelope Based on Frequency Domain Regression Using Genetic Algorithm. Energy and Building 39(5): 525-536.

X.H. Xu, S.W. Wang and W.Z. Shi. 2004. A robust sequencing control strategy for air-handling units. Building Services Engineering Research and Technology 25(2): 141-158.

Y. Ke and S. Mumma. 1997. Using carbon dioxide measurements to determine occupancy for ventilation controls. ASHRAE Transactions 103(2):364-374.

Y. Yao, Z.W. Lian and Z.J. Hou. 2004. Optimal operation of a large cooling system based on empirical model. Applied Thermal Engineering 24(16): 2303-2321.

Y.C. Chang. 2004. A novel energy conservation method--Optimal chiller loading. Electric Power Systems Research 69(2): 221-26.

Y.C. Chang. 2005. Genetic algorithm based optimal chiller loading for energy conservation. Applied Thermal Engineering 25(17-18): 2800-2815.

Z. Bien, W.C. Bang, D.Y. Kim and J.S. Han. 2002. Machine intelligent quotient: its measurements and applications. Fuzzy Sets and Systems 127 (1): 3-16.

Z. Ren and J. Stewart. 2003. Simulating air flow and temperature distribution inside buildings using a modified version of COMIS with sub-zonal divisions. Energy and Buildings 35: 257-271.

Z.J. Zhai and Q.Y. Chen. 2005. Performance of coupled building energy and CFD simulations, Energy and Buildings 37: 333-344.